PL-TR--
94-1014

PRECISION POINTING EXPERIMENT

Richard C. Smith et al.

Lockheed Missiles & Space Co.
6400 Uptown Blvd NE
Albuquerque, NM 87109

October 1994

Final Report

PHILLIPS LABORATORY
Space and Missiles Technology Directorate
AIR FORCE MATERIEL COMMAND
KIRTLAND AIR FORCE BASE, NM 87117-5776

PL-TR--94-1014

This final report was prepared by Lockheed Missiles & Space Co., Albuquerque, New Mexico, under Contract F29601-89-C-0015, Job Order 2864TMAA, with the Phillips Laboratory, Kirtland Air Force Base, New Mexico. Mr. Jack M. Richardson (VTSS) was the Laboratory Project Officer-in-Charge.

When Government drawings, specifications, or other data are used for any purpose other than in connection with a definitely Government-related procurement, the United States Government incurs no responsibility or any obligation whatsoever. The fact that the Government may have formulated or in any way supplied the said drawings, specifications, or other data, is not to be regarded by implication, or otherwise in any manner construed, as licensing the holder, or any other person or corporation; or as conveying any rights or permission to manufacture, use, or sell any patented invention that may in any way be related thereto.

This report has been authored by a contractor of the United States Government. Accordingly, the United States Government retains a nonexclusive royalty-free license to publish or reproduce the material contained herein, or allow others to do so, for the United States Government purposes.

This report has been reviewed by the Public Affairs Office and is releasable to the National Technical Information Service (NTIS). At NTIS, it will be available to the general public, including foreign nationals.

If your address has changed, if you wish to be removed from the mailing list, or if your organization no longer employs the addressee, please notify PL/VTSS, Kirtland AFB, NM 87117-5776 to help maintain a current mailing list.

This technical report has been reviewed and is approved for publication

RONALD R. NINNEMAN
SPICE Program Manager
Precision Structures Branch

FOR THE COMMANDER

L. KEVIN SLIMAK
Chief, Structure and Controls Division

HENRY L. PUGH, JR, Colonel, USAF
Director, Space and Missiles Technology Directorate

DO NOT RETURN COPIES OF THIS REPORT UNLESS CONTRACTUAL OBLIGATIONS OR NOTICE ON A SPECIFIC DOCUMENT REQUIRES THAT IT BE RETURNED.

REPORT DOCUMENTATION PAGE

Form Approved
OMB No. 0704-0188

1. AGENCY USE ONLY *(Leave blank)*	2. REPORT DATE	3. REPORT TYPE AND DATES COVERED
	October 1994	Final 23 Feb 89 - 30 Sep 94

4. TITLE AND SUBTITLE

PRECISION POINTING EXPERIMENT

5. FUNDING NUMBERS

C: F29601-89-C-0015
PE: 63218C
PR: 2864
TA: TM
WU: AA

6. AUTHOR(S)

Richard C. Smith,* Ross Blankinship,* Marshall Edwards,*
Ed Weston,* Brian Hamilton**

7. PERFORMING ORGANIZATION NAME(S) AND ADDRESS(ES)

Lockheed Missiles & Space Co.
6400 Uptown Blvd NE
Albuquerque, NM 87109

8. PERFORMING ORGANIZATION REPORT NUMBER

9. SPONSORING/MONITORING AGENCY NAME(S) AND ADDRESS(ES)

Phillips Laboratory
3550 Aberdeen Avenue SE
Kirtland AFB, NM 87117-5776

10. SPONSORING/MONITORING AGENCY REPORT NUMBER

PL-TR--94-1014

11. SUPPLEMENTARY NOTES

*Lockheed **Honeywell

12a. DISTRIBUTION/AVAILABILITY STATEMENT

Approved for public release; Distribution is unlimited.

12b. DISTRIBUTION CODE

13. ABSTRACT *(Maximum 200 words)*

The objective of the Spice Program was to demonstrate improvement in precision pointing, tracking, and retargeting by integration of active isolation, active and passive structural control, advanced materials, active optics, and adaptive control. Experiments were carried out on a full-size and well-characterized precision test-bed that represented a space laser structure. In the Precision Pointing Experiment, an active control system that combined low authority local rate feedback and high authority global control was designed with the goal of achieving 50:1 attenuation of line-of-sight jitter in the 5- to 500-Hz band. The jitter was due to disturbances input at the base of the structure and at the simulated secondary mirror. A custom suite of optical sensors allowed determination of the line of sight of the structure. Proof mass actuators of unprecedented force and linearity were developed during this and preceding subtasks. A series of tests culminated with the attainment of repeatable attenuation of line-of-sight jitter by 75:1 in the band 5 to 500 Hz with little spillover into unmodeled structural modes or unregulated degrees of freedom. The control system proved to be robust, with gain margin ≥1.75 demonstrated. Comparison of measure transfer functions with those calculated from the structural model used in the control system design showed that high controller performance does not require unreasonable structural model accuracy.

14. SUBJECT TERMS	15. NUMBER OF PAGES
SPICE, Structural Control, Proof Mass Actuator, Optical Sensors	192
	16. PRICE CODE

17. SECURITY CLASSIFICATION OF REPORT	18. SECURITY CLASSIFICATION OF THIS PAGE	19. SECURITY CLASSIFICATION OF ABSTRACT	20. LIMITATION OF ABSTRACT
Unclassified	Unclassified	Unclassified	SAR

CONTENTS

Section		Page
1.0	OVERVIEW	1
	1.1 THE SPICE PROGRAM	1
	1.2 THE SPICE STRUCTURE	1
	1.2.1 Hardware	1
	1.2.2 Control and Data Acquisition System	3
	1.3 THE PRECISION POINTING EXPERIMENT, PHASE 1	4
	1.3.1 Overview	4
	1.3.2 The Open-Loop Test Sequence	6
	1.3.3 The FRF/LAC Test Sequence	6
	1.3.4 The HAC/LAC Test Sequence	8
	1.4 HIGHLIGHTS OF PHASE 1 OF THE PRECISION POINTING EXPERIMENT	8
	1.4.1 Validation of the OSS Design	8
	1.4.2 Integration of PMAs into the Structure	9
	1.4.3 Demonstration of LAC Attenuation	9
	1.4.4 Demonstration of HAC/LAC Attenuation	10
2.0	SUBTASK 02-09: THE PRECISION POINTING EXPERIMENT, PHASE I	11
	2.1 TASK 1 - PMAs	11
	2.2 TASK 2 - LABORATORY OPERATIONS	18
	2.3 TASK 3 - PRECISION POINTING EXPERIMENT CONTROLS DESIGN	20
	2.4 TASK 4 - PRECISION POINTING EXPERIMENT CONTROLS SUPPORT	22
	2.5 TASK 5 - SIMULATION	24
	2.6 TASK 6 - TESTING	24
	2.7 TASK 7 - SYSTEM ENGINEERING	27
	2.8 TASK 8 - OPTICAL SENSING SYSTEM	28
	2.9 TASK 9 - SOFTWARE	29
	2.10 TASK 10 - STRUCTURAL MODELING	31
3.0	THE HAC/LAC TEST SEQUENCE	34
	3.1 INTRODUCTION	34
	3.2 PRELIMINARY TESTS	34
	3.2.1 Disturbance Attenuation by a Preliminary HAC System	34
	3.2.2 Tests of Preliminary HAC Model 5A11	35
	3.2.3 Sine Wave Attenuation Tests with Final HAC Version	36

CONTENTS (Concluded)

Section		Page
	3.3 THE FINAL HAC	39
	3.3.1 The HAC Design Concept	39
	3.3.2 Structural Modal Model Used in HAC	41
	3.3.3 Disturbance Models	44
	3.3.4 Sensor Noise Models	47
	3.3.5 Model of Local-Loop Rate Damping and LAC Used in HAC	48
	3.3.6 Stinger Cross-Axis Stiffness Model	48
	3.3.7 The SAVI Controller Model	49
	3.3.8 Regulator Design Process	53
	3.3.9 Estimator Design Process	58
	3.3.10 The HAC Implementation as Single Matrix Multiplication	60
	3.3.11 Addition of Low-Frequency High-Pass Filters	63
	3.3.12 Packaging for Implementation in Star Array Processor	64
	3.3.13 Summary Of Closed-Loop System Design	66
	3.4 MAIN HAC TESTS	66
	3.4.1 Chronology of Final HAC Tests	71
	3.4.2 Performance Test Results	73
	3.4.3 Gain Margin Test Results	111
	3.4.4 Transfer Function Test Results	112
	3.4.5 Conclusion	115
4.0	LESSONS LEARNED	120
	4.1 TEAMWORK	120
	4.2 ELECTRONICS	120
	4.3 CONVENTIONS AND COORDINATES	121
	4.4 CALIBRATION	121
	4.5 TEST PLANNING	121
	4.6 SUBTASK PLANNING	122
	4.7 NONPRECISION HARDWARE ON A PRECISION STRUCTURE	122
	4.8 DATA MANAGEMENT PLANNING	122
	4.9 SIMULATION	122
	4.10 PROOF MASS ACTUATORS	123
	4.11 DIFFICULTY WITH ADSs	123
5.0	CONCLUSION	125
	REFERENCES	126
	APPENDIX - GRAPHS	129
	ACRONYMS	182

FIGURES

Figure		Page
1.	The SPICE structure.	2
2.	The SPICE control and data acquisition computer system.	4
3.	The SPICE test sequences with their objectives and goals.	6
4.	Average OSS noise breakout.	9
5.	Decrease in LOS x- and y-PSDs as LAC and HAC loops are activated.	10
6.	The SPICE PMA.	13
7.	Pair of PMAs mounted on a tripod leg of the SPICE structure.	15
8.	Force output from PMA voice coil is proportional to current.	16
9.	Example of PMA frequency response (unit 001).	17
10.	The SPICE digital control system hardware.	30
11.	Summary of predicted attenuation data including the 20:1 HAC.	36
12.	Residual PSDs after attenuation of 100-μrad disturbances by 5A11 HAC.	37
13.	Attenuation of a 7.8-Hz sine wave disturbance by the final HAC (5A19).	38
14.	Model of disturbances.	46
15.	Model of interaction of SAVI with the SPICE structure.	49
16.	Global and SMTS local coordinates.	55
17.	Integral feedback on output forces.	64
18.	Implementation of HAC system in the Star VP-3 array processor.	65
19.	MATRIXx command file with added comments.	67
20.	The HAC closed-loop system model.	70
21.	Effect of change in shaker stinger threads on LOS-x.	75
22.	Effect of change in shaker stinger threads on LOS-y.	76
23.	Calculated and measured RMS PMA rates - 100-μrad disturbances.	92
24.	Calculated and measured RMS PMRS outputs - 100-μrad disturbances.	93
25.	Calculated and measured RMS SMTS outputs - 100-μrad disturbances.	94

FIGURES (Continued)

Figure		Page
26.	Calculated and measured RMS SMRS and LOS outputs - 100-μrad disturbances.	95
27.	Calculated and measured LVDT outputs - 100-μrad disturbances.	96
28.	Calculated and measured RMS PMA rates - quiescent.	97
29.	Calculated and measured RMS PMRS outputs - quiescent.	98
30.	Calculated and measured RMS SMTS outputs - quiescent.	99
31.	Calculated and measured RMS SMRS and LOS outputs - quiescent.	100
41.	Modification of HAC for gain margin tests.	111
42.	Configuration for measurement of HAC regulator open-loop transfer function.	113
43.	Predicted singular values of the regulator in the final (5A19) HAC design.	114
44.	Open-loop transfer functions from PMA 1 to PMA 1.	116
45.	Attenuation of a 6.3-Hz sine wave disturbance by the final HAC (5A19).	117
46.	The LOS in the 6.3-Hz sine wave test	118
A-1.	Spectra of PMA 1 rate - quiescent conditions.	130
A-2.	Spectra of PMA 2 rate - quiescent conditions.	131
A-3.	Spectra of PMA 3 rate - quiescent conditions.	132
A-4.	Spectra of PMA 4 rate - quiescent conditions.	133
A-5.	Spectra of PMA 9 rate - quiescent conditions.	134
A-6.	Spectra of PMA 10 rate - quiescent conditions.	135
A-7.	Spectra of PMA 11 rate - quiescent conditions.	136
A-8.	Spectra of PMA 12 rate - quiescent conditions.	137
A-9.	Spectra of PMA 13 rate - quiescent conditions.	138
A-10.	Spectra of PMA 14 rate - quiescent conditions.	139
A-11.	Spectra of PMA 16 rate - quiescent conditions.	140

FIGURES (Continued)

Figure		Page
A-12.	Spectra of local x-axis signal for PMRS 1 - quiescent conditions.	141
A-13.	Spectra of local y-axis signal for PMRS 1 - quiescent conditions.	142
A-14.	Spectra of local x-axis signal for PMRS 2 - quiescent conditions.	143
A-15.	Spectra of local y-axis signal for PMRS 2 - quiescent conditions.	144
A-16.	Spectra of local x-axis signal for PMRS 6 - quiescent conditions.	145
A-17.	Spectra of local y-axis signal for PMRS 6 - quiescent conditions.	146
A-18.	Spectra of local x-axis signal for SMRS - quiescent conditions.	147
A-19.	Spectra of local y-axis signal for SMRS - quiescent conditions.	148
A-20.	Spectra of local x-axis signal for SMTS 8 - quiescent conditions.	149
A-21.	Spectra of local y-axis signal for SMTS 8 - quiescent conditions.	150
A-22.	Spectra of local x-axis signal for SMTS 9 - quiescent conditions.	151
A-23.	Spectra of local y-axis signal for SMTS 9 - quiescent conditions.	152
A-24.	Spectra of LOS-x signal - quiescent conditions.	153
A-25.	Spectra of LOS-y signal - quiescent conditions.	154
A-26.	Spectra of LOS-x - 100-μrad caged-target LOS disturbances.	155
A-27.	Spectra of LOS-y - 100-μrad caged-target LOS disturbances.	156
A-28.	Spectra of PMA 2 rate - 100-μrad caged-target LOS disturbances.	157
A-29.	Spectra of PMA 3 rate - 100-μrad caged-target LOS disturbances.	158
A-30.	Spectra of PMA 4 rate - 100-μrad caged-target LOS disturbances.	159
A-31.	Spectra of PMA 9 rate - 100-μrad caged-target LOS disturbances.	160
A-32.	Spectra of PMA 10 rate - 100-μrad caged-target LOS disturbances.	161
A-33.	Spectra of PMA 11 rate - 100-μrad caged-target LOS disturbances.	162
A-34.	Spectra of PMA 12 rate - 100-μrad caged-target LOS disturbances.	163
A-35.	Spectra of PMA 13 rate - 100-μrad caged-target LOS disturbances.	164

TABLES

Table		Page
1.	The open-loop test sequence and test objectives.	7
2.	The FRF/LAC test sequence and test objectives.	7
3.	The HAC/LAC test sequence and test objectives.	8
4.	Tasks summary of the Precision Pointing Experiment.	11
5.	The SPICE PMA specifications.	12
6.	Comparison of SPICE5 finite element model and modal test.	32
7.	Input disturbance and caged-target LOS levels.	35
8.	Summary of disturbance response data.	35
9.	The HAC modal model summary.	42
10.	The HAC design degrees of freedom - input forces (N).	44
11.	The HAC design degrees of freedom - outputs.	45
12.	Selected estimator measurement noise.	47
13.	Modes retained from combined SAVI/structural model.	52
14.	Quiescent test PSDs.	77
15.	Shaker-driven test PSDs.	78
16.	Residual RMS performance test results.	80
17.	Summary of residual LOS jitter performance results	90
18.	List of summary performance graphs.	91
19.	List of LOS performance figures.	101

1.0 OVERVIEW

This document is the Final Report on subtask 02-09 of the Space Integrated Controls Experiment (SPICE) program. The subtask is known as Phase I of the Precision Pointing Experiment. This section discusses the SPICE program, the SPICE structure, and the function of Phase I of the Precision Pointing Experiment in SPICE. Later sections present a task by task description of the subtask (Section 2.0), the analysis and test results from the High Authority Control (HAC) / Low Authority Control (LAC) test sequence (Section 3.0), and lessons learned (Section 4.0) in the performance of Phase I of the Precision Pointing Experiment.

1.1 THE SPICE PROGRAM

The SPICE is a 67-month (2/23/89 - 9/30/94) cost-plus award fee task-ordered program. Its objective is to demonstrate improvement in directed energy weapon precision pointing, tracking, and re-targeting by integration of:

- Active isolation,
- Active structural control,
- Passive structural control,
- Advanced structural materials,
- Active optics, and
- Adaptive control.

1.2 THE SPICE STRUCTURE

1.2.1 Hardware

The SPICE team integrated these technologies on a representative space laser structure, a significant portion of which was inherited from the Space Active Vibration Isolation (SAVI) program. Figure 1 shows the structure as it is at present. Most of its major subsystems are visible in the figure:

- Beam Expander - Simulates an M = 10 Cassegrain telescope with:
  - 7-segment, 5.6-m average diameter hexagonal primary mirror
  - Secondary mirror mass simulator
  - Mirror mass simulators rigid to >130 Hz
- Tripod Legs - 8-m-long graphite-epoxy composite

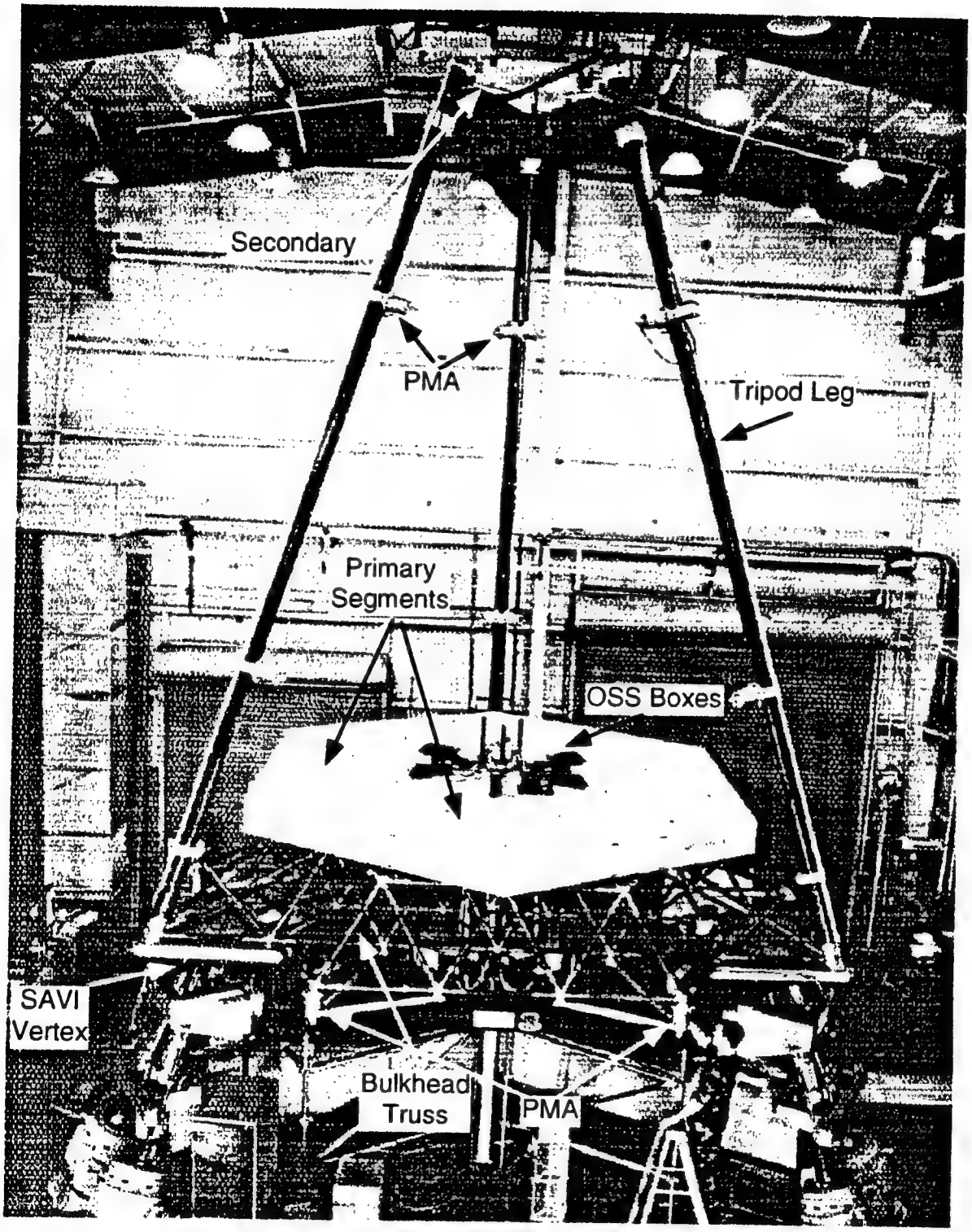

Figure 1. The SPICE structure.

- Bulkhead Truss:
  - 264 ~1-m-long graphite-epoxy struts connected by 64 node balls into a polyhedral shape with hexagonal upper and lower decks. Stiffness variation from strut to strut ≤10 per cent
  - Linear connectors or "joints" at strut ends
- SAVI - Isolates forward body from aft body disturbances:
  - Magnetic actuators - for rigid body control and disturbance input
  - Linear actuators - for ± 2 deg retargeting (not yet used by SPICE)
- Optical Sensing System (OSS) - Suite of sensors that enables calculation of line of sight (LOS) from measurements of:
  - Primary mirror mass simulator segment tilt
  - Secondary mirror mass simulator tilt
  - Secondary mirror mass simulator translation
- Proof Mass Actuators (PMAs):
  - 18 actuators that enable attenuation of the effects of input structural disturbances
  - Accelerometers that provide local structure rates and relative velocity of proof mass to housing

Above the secondary in an enclosure on the roof of the SPICE laboratory (and attached to the upper end of the load rod) is the device that simulates space weightless conditions.

- Gravity Offload:
  - Zero spring rate mechanism (see Ref. 1 for a description)
  - ~3000-kg capacity (limited by strength of building 765 roof)

The SPICE structure is a full-scale test-bed for integration of directed energy weapon technologies. It is a precision structure equipped with sensors that allow accurate determination of the simulated telescope LOS and actuators that are commanded by the HAC/LAC system to stabilize the LOS. The structure has been well characterized by a modal test to which the finite element model used in designing the control system is correlated.

1.2.2 Control and Data Acquisition System

The SPICE program has assembled the formidable collection of computer hardware and software required to handle the high data rates and large quantity of data required for the Precision Pointing Experiment. The "modal system" consists of a HP3565 front-end computer and a HP9000/380 that runs the CADA-X Fourier Monitor software package which performs the frequency domain analyses. The CADA-X package is a product of LMS International. The

elements within the shaded area in Figure 2 are collectively called the real-time system. The Aptec Computer Systems IOC-24 computer functions as the front end to the Star Technologies VP-3 array processor that runs the controller in real time in closed loop tests. In running the controller, the STAR performs a 198 by 266 matrix multiply every 0.001 s. The C51 disk can store about 20 min of time records for the full set of 199 (including the time stamp) 32-bit variables and 38 16-bit variables at that data rate. The real-time system calculates the LOS components from the OSS measurements and returns them to the modal system where they were treated like another pair of sensor signals.

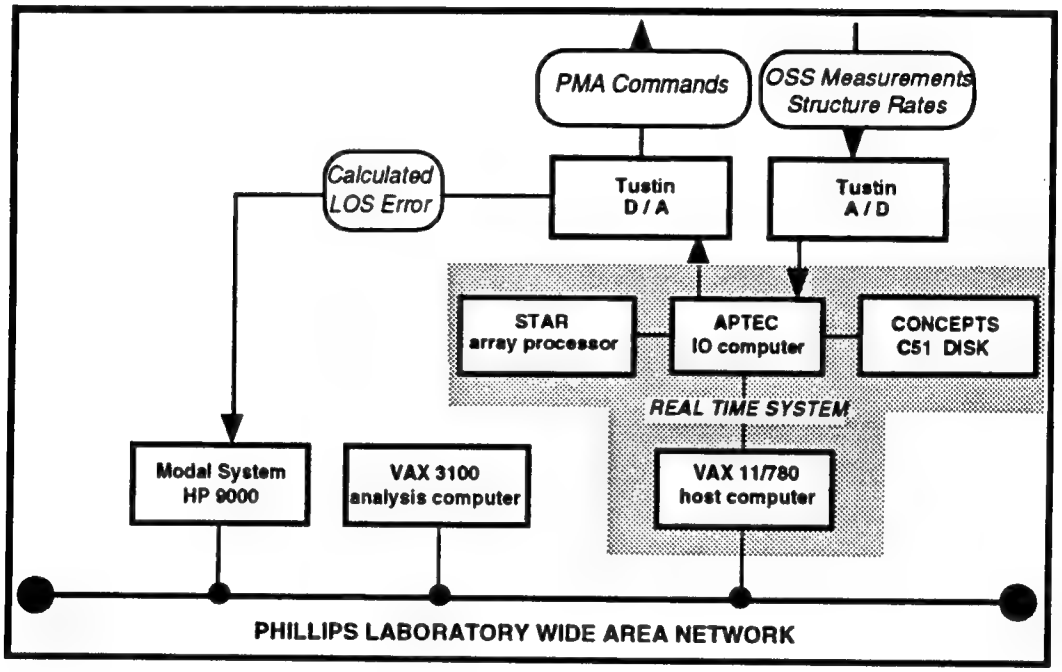

Figure 2. The SPICE control and data acquisition computer system.

1.3 THE PRECISION POINTING EXPERIMENT, PHASE 1

1.3.1 Overview

The full Precision Pointing Experiment will demonstrate attenuation of root-mean-square (RMS) LOS jitter by active control and passive damping of the structure. These technologies will work as a single system with passive techniques providing structural damping of modes outside the HAC band that can be amplified by the HAC. With the passive damping in place, higher HAC gains are possible without causing instability of the control system.

Phase 1 of the Precision Pointing Experiment demonstrated attenuation of RMS LOS by active control alone. A low authority controller, which provided rate feedback damping at the sites of

the PMA attachments to the SPICE structure, produced some of the attenuation of the RMS LOS directly and also enabled a distributed high authority controller to attenuate it further without becoming unstable.

The goal of Phase 1 of the Precision Pointing Experiment was to attenuate the RMS LOS by an unprecedented factor of 50. Accomplishing this on the large (~3000-kg) SPICE structure, in a laboratory space that had somewhat less environmental control than a typical living room, required development of several technologies:

- An OSS that can measure LOS <1 μrad accurately,
- Proof mass actuators with stroke and force capability beyond the state of the art,
- A controller to effect the unprecedented LOS attenuation,
- A finite element model of the structure of exceptional fidelity - so the effectiveness of the HAC designed using it is not compromised,
- A high-fidelity time-domain nonlinear simulation to provide insight into potential difficulties from nonlinear effects,
- Custom software to handle an experiment that requires high-speed (1-kHz) data rates and a large number of structure states in the controller, and
- Interface electronics to allow signals to be transmitted without such problems as ground loops or 60-Hz contamination.

Design and prototyping activities were performed in earlier SPICE subtasks and the final steps of the development efforts were achieved in Phase 1 of the Precision Pointing Experiment.

A series of test sequences was planned and executed on the structure as subsystems were integrated into SPICE. Figure 3 indicates the SPICE test sequences and the goals of each, with the tests performed in Phase 1 of the Precision Pointing Experiment shaded. The first modal test indicated in the lower left of the figure was performed before the Precision Pointing Experiment and before the full OSS and the PMAs were incorporated into the structure. The OSS concept was demonstrated in this test through the inclusion of the prototype secondary mirror rotation sensor (SMRS), one prototype primary mirror rotation sensor (PMRS), and mass simulators for each of the other five PMRSs. Reference 2 discusses development of the OSS. Results from the first modal test guided further development of the OSS, preliminary HAC design, and the design of the modal test that was performed on the current structure. That second modal test was a part of the Frequency Response Function (FRF)/LAC test sequence. The two test sequences involving passive damping will be part of Phase 2 of the Precision Pointing Experiment. Later sections of this report contain discussion of the Phase 1 test sequences.

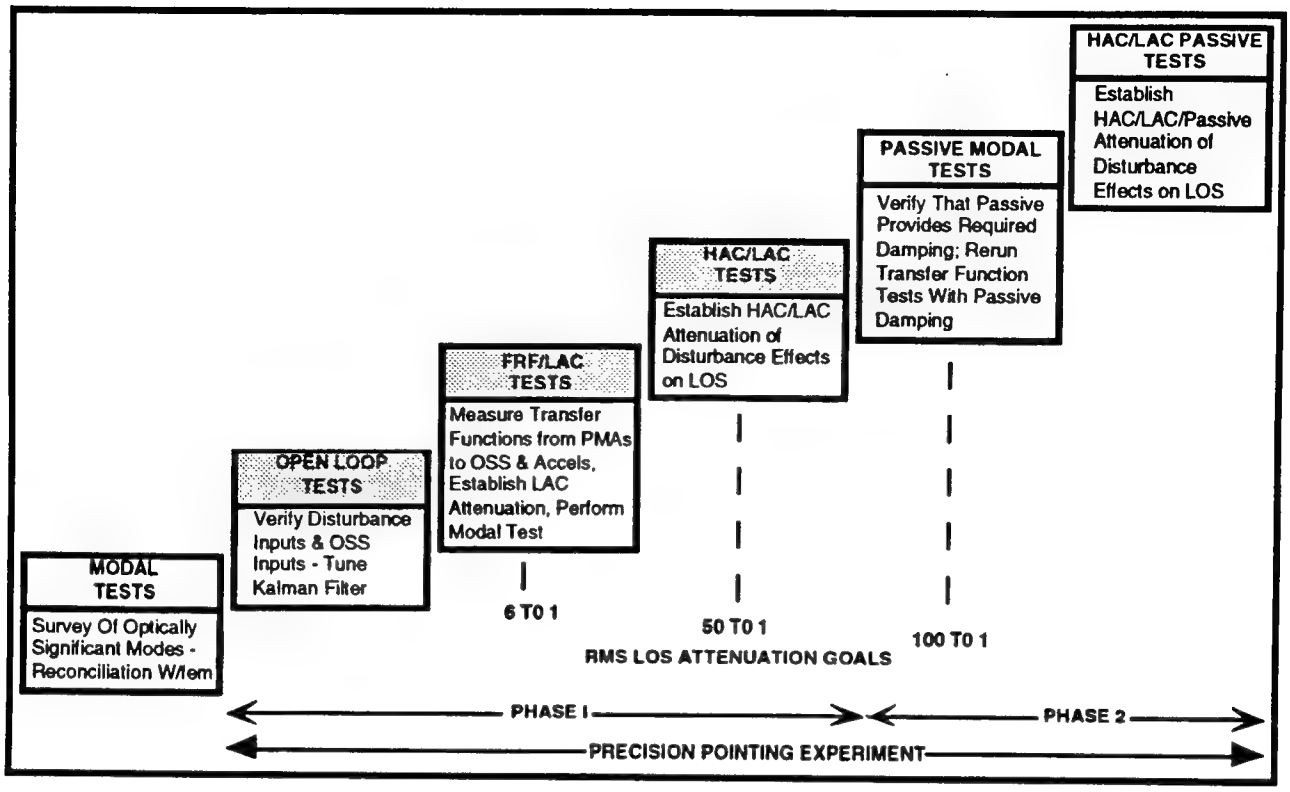

Figure 3. The SPICE test sequences with their objectives and goals.

1.3.2 The Open-Loop Test Sequence

The open-loop test sequence was the first of the three test sequences of the Precision Pointing Experiment. The most important accomplishment of the open-loop tests was the successful characterization of the OSS and its integration into the SPICE structure. These tests also included the first attempt to determine the relationship between input force levels and RMS LOS (called the disturbance filter tuning tests), and the first checkout of the real-time system. Table 1 summarizes the four test series that comprised the open-loop test sequence and the objectives of each. The third of these, the disturbance filter tuning, proved to be unexpectedly balky. Two additional attempts were required to identify and deal with the apparently nonlinear effects encountered. References 3 through 5 discuss the problems with these tests and their final resolution during the FRF/LAC test sequence. The real-time system performed well in a brief checkout. For further discussion of the open-loop test sequence see Reference 6.

1.3.3 The FRF/LAC Test Sequence

The major achievements of the FRF/LAC tests included integration of the PMAs into the SPICE structure and a full modal test of the structure in its final Precision Pointing Experiment Phase 1

configuration. This test sequence also included measurement of the end-to-end FRFs required for HAC design and the completion of the disturbance filter tuning test series that was left over from the open-loop tests. The last series of tests in the sequence provided a direct verification of attenuation of the effect of input disturbance forces by the LAC. Table 2 summarizes these tests and their objectives. Reference 5 presents a more detailed discussion of the FRF/LAC tests.

Table 1. The open-loop test sequence and test objectives.

Test Series	Objectives
OSS and surrogate PMA accelerometer noise tests	• Determine the OSS noise floor, characterize the noise spectrum within the bandwidth critical to control system performance, and characterize the components that comprise the OSS noise. • Determine the noise floor of the surrogate control accelerometers available from the SPICE instrumentation inventory. • Determine, by experiment, the effects of environmental parameters on sensor noise to establish if bounds must be placed on conditions during data acquisition.
OSS and surrogate PMA accelerometer frequency response function tests	• Provide measurements of OSS response that will be used to perform baseline comparisons with the finite element predictions. • Identify frequency ranges and specific optically critical modes to be measured with high accuracy during the modal test as part of the Precision Pointing Experiment. • Demonstrate the structure's load linearity through OSS and surrogate control accelerometer measurements. • Predict stability of closed-loop HAC design using singular-value analysis.
Disturbance filter tuning tests	• Establish, by experiment, the disturbance levels that yield 100 μrad of LOS jitter per axis (x and y).
Kalman filter tuning tests	• Provide "first-light" data for tuning the control system Kalman filter. • Debug and check out the Kalman filter and real-time control computer hardware and software.

Table 2. The FRF/LAC test sequence and test objectives.

Test Series	Objectives
Conclusion of the open-loop disturbance tuning tests	• Establish by experiment the input disturbance levels that yield 100 μrad LOS jitter per axis in the SPICE structure
Open-loop characterization of LAC stability and gain	• Verify the circuitry prior to loop closure • Compare results to predictions and determine maximum safe loop gain
Modal test of the structure with the PMAs installed	• Characterize the SPICE structural modes with the PMAs and all relevant mounting brackets, electronics, and harnessing in place to allow precise updating of the structural model
Open-loop FRF measurements	• Establish the structural response from the PMAs to the sensors for comparison with the structural model
Closed-loop characterization of the LAC	• Complete checkout of local analog loops • Verify correct closed loop operation of the LAC
Digital system frequency response tests	• Provide frequency response data for design of the HAC
FRF measurements with LAC loops closed	• Provide frequency response data for design of the HAC
OSS power spectral density (PSD) measurements with Precision Pointing Experiment disturbance set	• Establish the sensitivity of the OSS LOS to modal excitation of the SPICE structure with the PMAs in place

1.3.4 The HAC/LAC Test Sequence

The HAC/LAC test sequence concluded Phase I of the Precision Pointing Experiment with a demonstration of attenuation by the HAC/LAC system of the effect of input disturbances on the LOS. Table 3 summarizes the HAC/LAC tests and their objectives. Attenuation of LOS jitter by 75:1 in the band 5 to 500 Hz was achieved. This exceeds the Phase I goal of 50:1 attenuation in that band. For an extensive discussion of the HAC/LAC tests and the analysis leading to the final design of the HAC/LAC system, see Section 3.0 of this report.

Table 3. The HAC/LAC test sequence and test objectives.

Test Series	Objectives
Test of preliminary HAC design	• Demonstrate attenuation by HAC/LAC system • Identify areas in which HAC needs to be tuned further
Sine wave attenuation tests with final HAC design	• Directly verify HAC attenuation at dominant structural mode
Power spectra measurements with final HAC design	• Demonstrate attenuation of disturbance effects by full HAC/LAC system
Gain margin tests of final HAC design	• Establish gain stability margins of HAC
HAC/LAC closed-loop FRF tests	• Examine effects of controller on modes outside the HAC bandwidth

1.4 HIGHLIGHTS OF PHASE 1 OF THE PRECISION POINTING EXPERIMENT

The achievements of subtask 02-09 were based upon success in design and development of the OSS, the PMAs, the custom software that ran the experiment, the finite element model, the simulation, the interface electronics, and the controller itself. Each of these is a highlight of the program in its own right. Those selected for mention here have the additional virtue of being among the more quantifiable:

- Design and fabrication of an OSS that meets optical measurement sensitivity requirements,
- Successful integration into the structure of 18 PMAs that meet all specifications,
- Demonstration of RMS LOS jitter attenuation by the LAC, and
- Demonstration of >50:1 RMS LOS attenuation by the HAC/LAC system.

1.4.1 Validation of the OSS Design

In tests of the full HAC/LAC controller, the effects of input disturbances on the RMS LOS are attenuated to <1 μrad per axis. Therefore the OSS must be able to measure 1 μrad with good

signal-to-noise ratio. This was flowed down to a requirement that total LOS noise due to the OSS must be ≤200 nrad. As Figure 4 indicates, the OSS, which was designed and fabricated by the SPICE team, met that stringent requirement. Details of the design, fabrication, and calibration of the OSS may be found in References 2 and 7. Most of the noise in OSS measurements is due to turbulence in the long unshielded air paths of the beams associated with the OSS secondary tilt and translation sensors. The noise contributions by the sensors themselves are negligible.

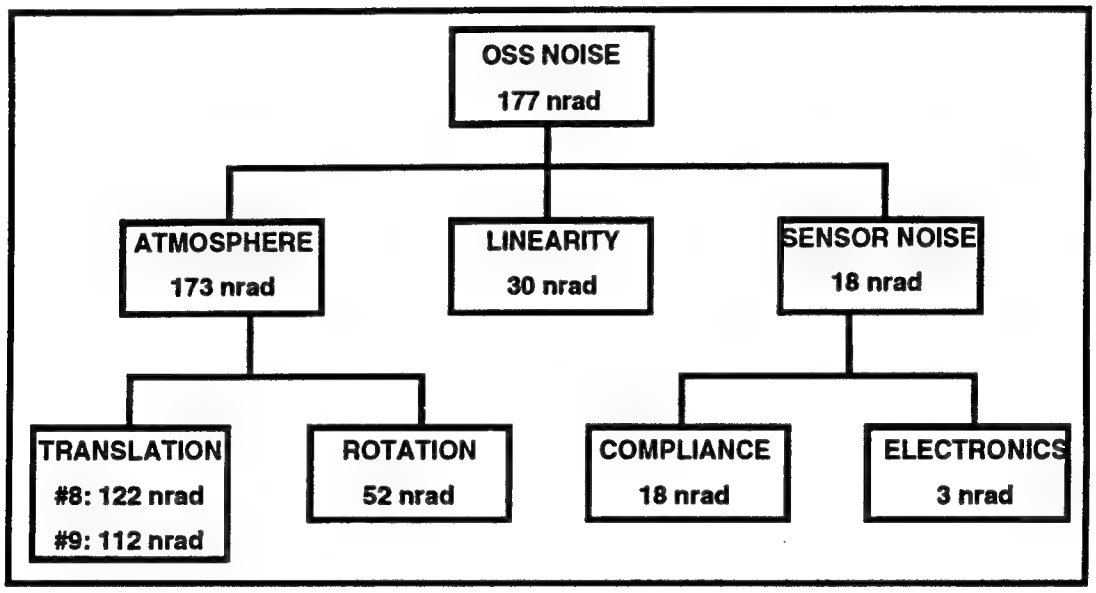

Figure 4. Average OSS noise breakout.

1.4.2 Integration of PMAs into the Structure

The SPICE PMAs are a significant extension of the state of the art in force and stroke capability. The stringent specifications on cross-axis modes and force accuracy required for full realization of the HAC/LAC system performance goals were met in the final design. Reference 8 provides a complete list of these specifications. The extensive effort required to design, fabricate, and integrate these PMAs into the SPICE structure was brought to a successful conclusion when all control loops were closed and the PMAs performed as modeled to attenuate LOS jitter.

1.4.3 Demonstration of LAC Attenuation

The LAC loops that are incorporated into the PMAs can function as a stand-alone rate feedback attenuating subsystem. During Phase 1 of the Precision Pointing Experiment, the LAC loops

attenuated the RMS LOS jitter due to input disturbance forces by a factor of nine from its open-loop value.

1.4.4 Demonstration of HAC/LAC Attenuation

The SPICE program surpassed the Phase 1 goal of 50:1 attenuation of RMS LOS jitter. The team had adopted that goal, which exceeds anything previously achieved by a factor of five, even before the sensors and actuators were built. Figure 5 shows attenuation by LAC and HAC/LAC in one of the HAC/LAC tests.

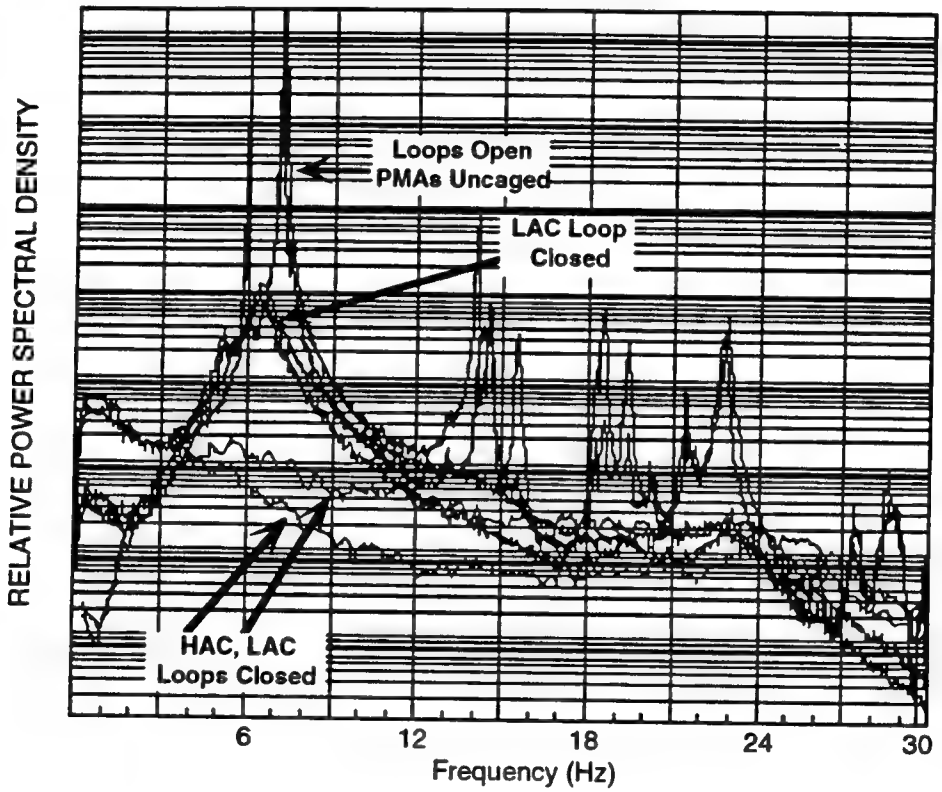

Figure 5. Decrease in LOS x- and y-PSDs as LAC and HAC loops are activated.

2.0 SUBTASK 02-09: THE PRECISION POINTING EXPERIMENT, PHASE I

While the most visible aspect of the Precision Pointing Experiment subtask was the test results, this subtask also encompassed significant behind-the-scenes effort in hardware, software, modeling, and controls design. Table 4 summarizes the 10 tasks that comprised subtask 02-09. In the subsections which follow, the results of each task are discussed and references are provided to the wealth of documentation that has been generated during the past 2 yr.

Table 4. Tasks summary of the Precision Pointing Experiment.

Task No.	Task Area	Task Description
1	PMAs	Resolve technical issues remaining after subtask 02-08, update specifications, procure and install PMAs.
2	Laboratory Operations	Coordinate team efforts, direct integration of Precision Pointing Experiment equipment, address needs for spares, address safety issues, perform calibration and checkout of equipment.
3	Controls Design	Update the control system design developed under the subtasks 02-03 and 02-08 using SPICE 4 structural model.
4	Controls Support	Update the HAC system design, as required, after each phase of integration and testing.
5	Simulation	Maintain a detailed nonlinear time-domain computer simulation of the integrated SPICE Experiment.
6	Testing	Perform and report on three test sequences: the open-loop tests, the FRF/LAC tests, and the HAC/LAC tests.
7	System Engineering	Maintain requirements flowed down from top level to subsystems, generate test requirements, maintain subsystem interface requirements and specifications.
8	OSS	Fabricate, test, install, and align the OSS.
9	Software	Develop, implement, and support the integration and test of the real-time control system software; develop postprocessing software and procedures required to support postrun data analysis
10	Structural Modeling	Develop and maintain a structural model of the SPICE test article.

2.1 TASK 1 - PMAs

One of the most critical elements leading to the successful demonstration of the HAC/LAC control system was the development of the force actuators used by the control system. The control actions in this experiment are provided by 18 identical linear inertial force actuators, the PMAs. The PMA task of SPICE Subtask 02-09 called for the contractor to:

- Resolve all technical issues remaining after subtask 02-08,
- Update component specifications,
- Procure the PMAs,
- Plan and perform acceptance testing,

- Design, fabricate, and install hardware to mount the PMAs to the structure, and
- Design, fabricate, and install PMA electronics.

The development of the SPICE PMAs spanned three major subtasks of the SPICE task-order contract, namely:

- Precision Pointing Experiment Design (02-03),
- Investigation of Critical Technologies for Active Structural Control (02-08), and
- Precision Pointing Experiment, Phase I (02-09).

The PMA development effort is discussed extensively in the PMA Final Report (Ref. 9) and its bibliographic references. Realization of the SPICE PMA was a significant technology development effort, not simply a procurement. Its specifications for force and stroke (Table 5), the fundamental sizing parameters, represented extensions beyond the state of the art for such a device. Moreover, cross-axis and parasitic performance parameters, which are often left uncontrolled, were recognized as crucial to the success of the Precision Pointing Experiment and were therefore specified precisely as well.

Table 5. The SPICE PMA specifications.

Force	40 N zero to peak
Stroke	82 kg-mm peak-to-peak stroke proof mass product
Accuracy	5% nominal gain, 3% linearity
Dynamics	1000-Hz force response with <60 deg phase loss
Mechanical	• In-axis mode frequency = 5 Hz ± 20% • All other suspension mode frequencies >90 Hz • Housing mode frequencies (between actuator and sensor) >1 kHz • No stiction sources
Gravity	No bias power required in any orientation
Sensors	• Proof mass stroke position • Housing acceleration • Proof mass acceleration • Bobbin temperature

Figure 6 shows a cutaway view of the SPICE PMA. The PMA is capable of applying an inertial force to a body, which is particularly useful for the active control of flexible structures. Inside the device, a heavy mass (called the "proof mass") is weakly suspended from the housing in one degree of freedom. A voice coil force actuator pushes on the proof mass when electric current is applied to its coil. While pushing on the proof mass, the voice coil also reacts against the housing, and thus anything to which the housing is attached, i.e., the SPICE beam expander structure.

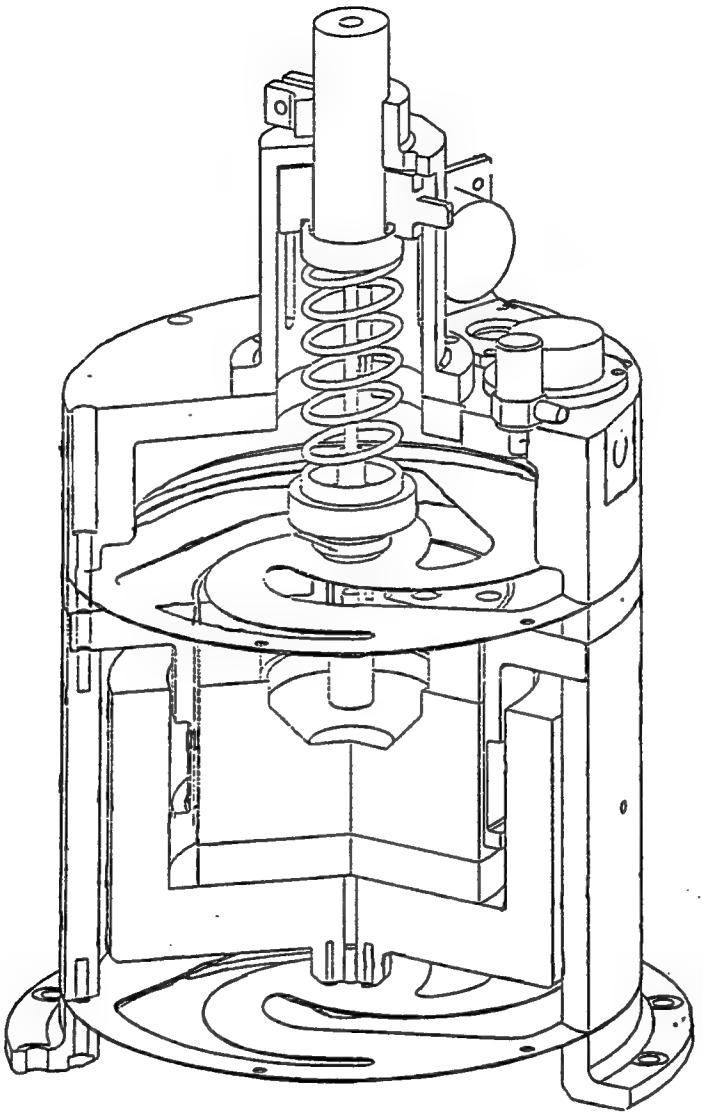

Figure 6. The SPICE PMA.

At the outset of the subtask 02-09 effort, the major technical difficulty centered around the design of the flexures that suspend the proof mass from the housing. This suspension must be very compliant in one degree of freedom, very stiff in the other five degrees of freedom, linear and elastic over a large stroke, and able to support the proof mass against gravity. These conflicting specifications had led to failure in the previous subtask. After several more iterations, the conclusion was that the development of a flexure that could meet all of the specifications would require more program resources than were readily available and therefore it was necessary to make some concessions. Analyses showed that the system-level objectives could still be met with reductions in the PMA requirements for both flexure linearity and cross-axis stiffness. With these modifications to the specification, a final flexure design was developed that is similar to the original flexure geometry devised by the Harris Company, Melbourne, Florida, but with modified web shape and thickness. In addition, a coil spring was added to the design to carry the gravity bias, instead of making the flexures do it as originally conceived by Harris.

A prototype of the final design was built and tested extensively in the SPICE facility in a joint effort of Harris and Honeywell Inc., Glendale, Arizona, engineering. When the last of the remaining technical issues were resolved, 20 additional units were purchased. The Harris Company fabricated the PMAs and 18 were installed onto the SPICE structure. Figure 7 shows a pair of PMAs mounted on a leg of the structure. The locations of the PMAs on the structure can be seen in Figure 1. Honeywell designed and built the required electronics which have been integrated, tested, and calibrated. The SPICE Program purchased three spare PMAs, one of which is the prototype which has been retrofitted to match the exact configuration of the others and renamed "production unit 1". The motivation for procuring three spares is not so much to protect against anticipated failure of the installed units as it is to allow for expansion of the SPICE baseline control system design. If a decision is ever made to increase the number of actuators on the structure, it will probably be done in multiples of three due to the symmetry of the structure.

Figures 8 and 9 show, respectively, the linearity (2.2%) and bandwidth (<2 deg phase loss at 1 kHz) achieved by the actuator. Reference 9 includes data in many other categories, showing the PMA to be fully compliant with the final specification.

In summary, despite technical and programmatic difficulties experienced along the way, the SPICE PMAs have been successfully reduced to practice. These devices meet a set of specifications that is much more stringent than the industry norm and that allows full realization of the HAC/LAC system performance goals in the system-level tests.

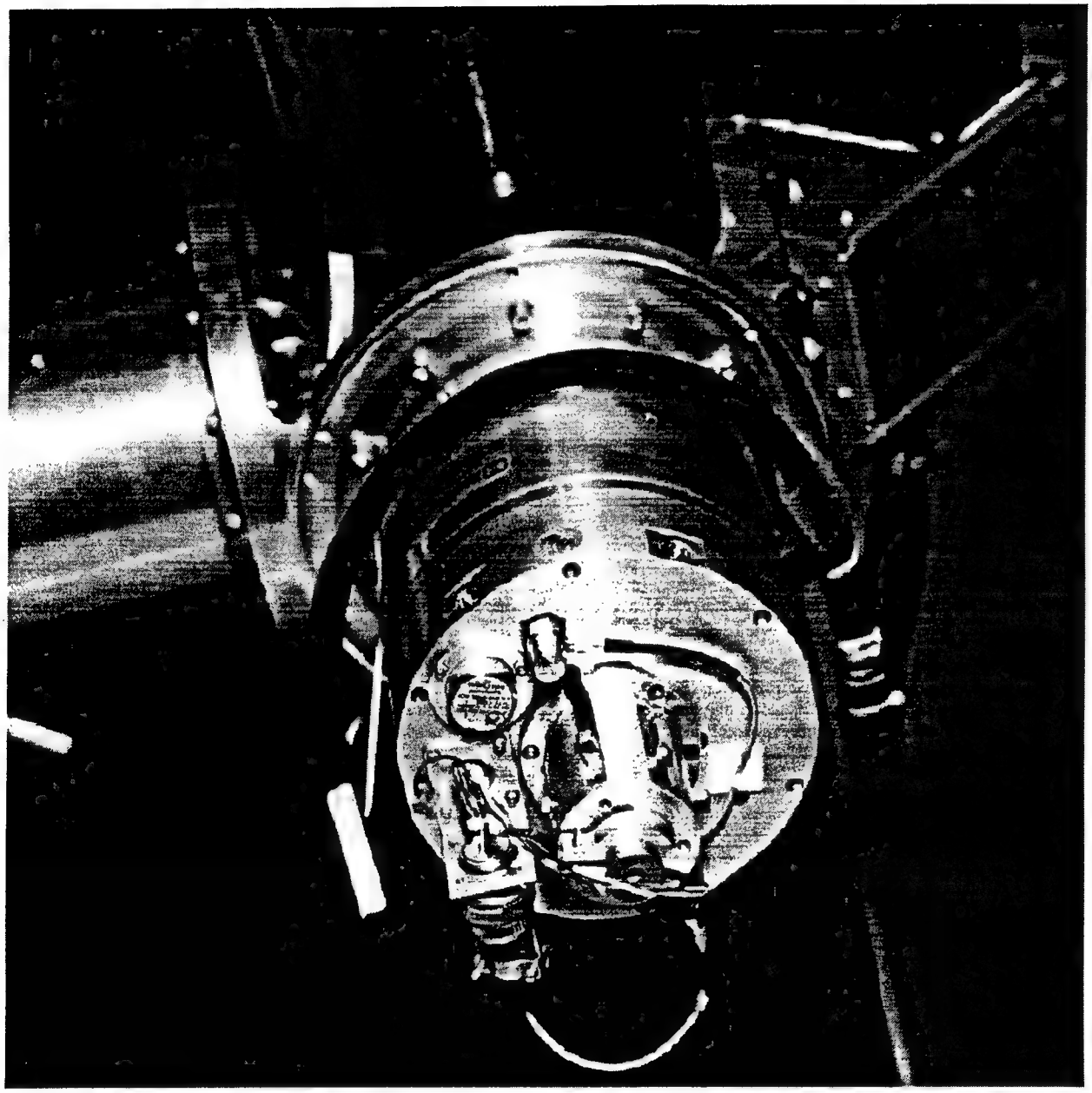

Figure 7. A pair of PMAs mounted on a tripod leg of the SPICE structure.

- **Curves below are taken at several different stroke positions.**
- **Linearity of 2.2 percent over entire operating range achieved.**

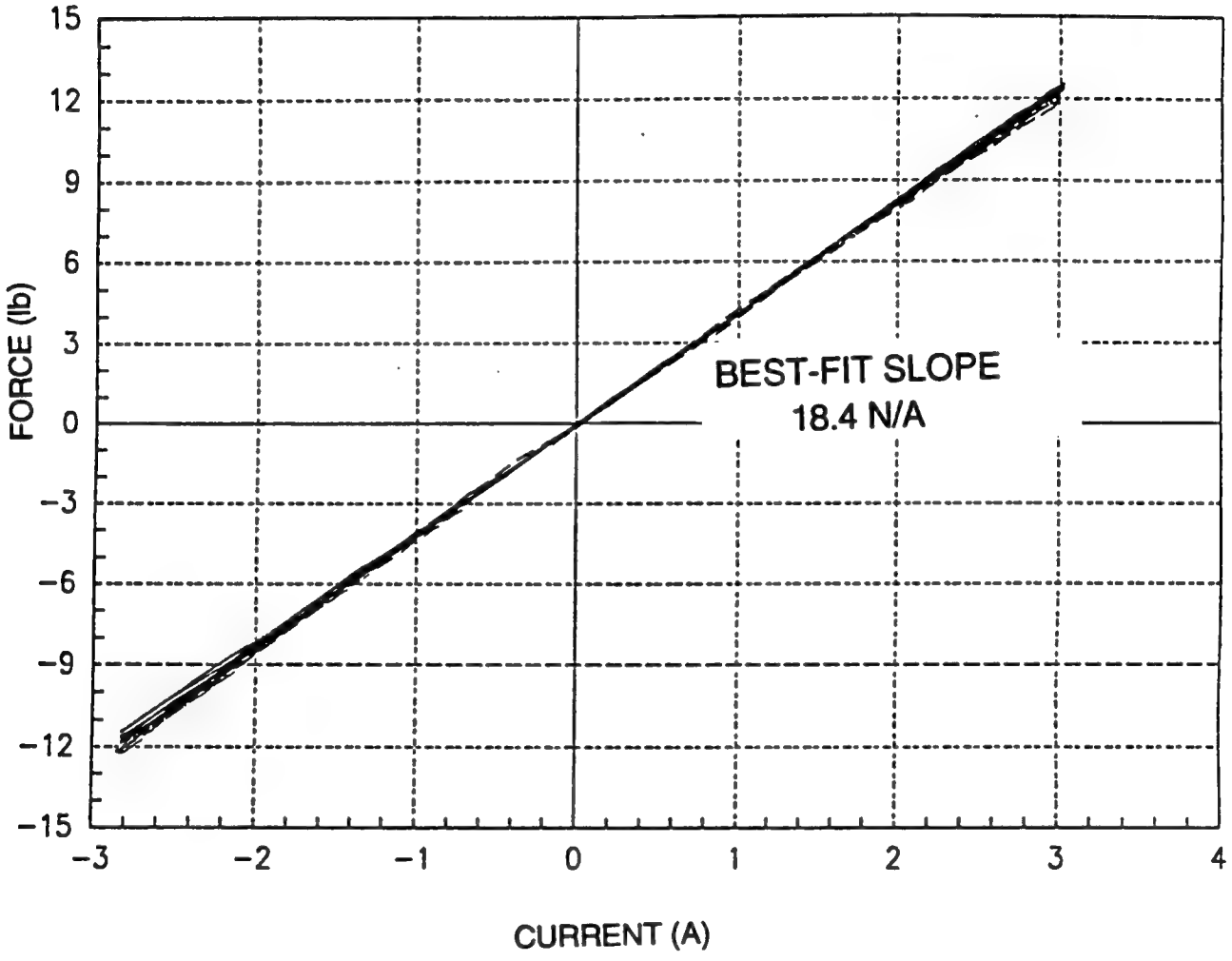

Figure 8. Force output from PMA voice coil is proportional to current.

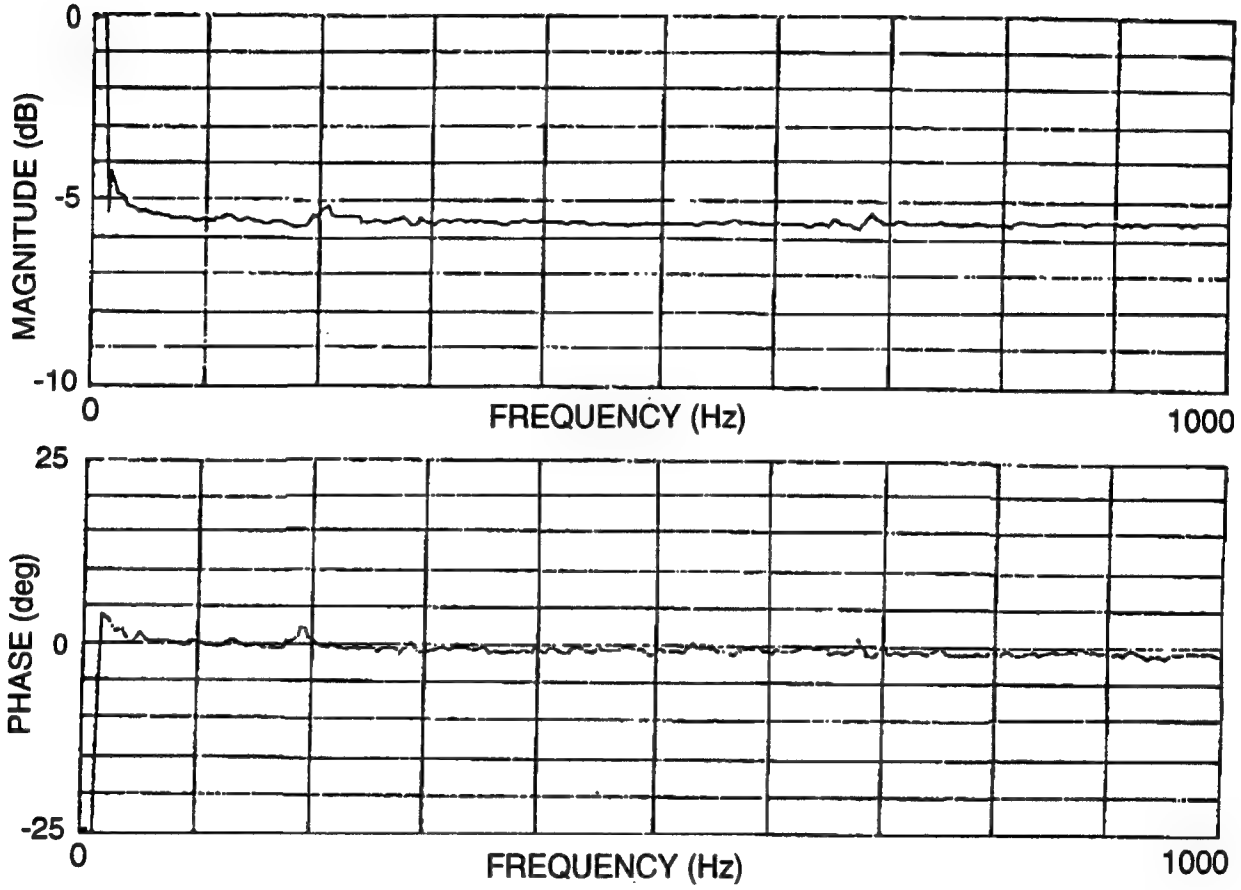

Figure 9. Example of PMA frequency response (unit 001).

2.2 TASK 2 - LABORATORY OPERATIONS

This part of subtask 02-09, while perhaps the least well-defined task at the time of the program plan, became one of the largest efforts in the subtask. The laboratory operations effort is often underestimated or ignored when planning an experiment. Despite very thorough planning, laboratory cost was slightly underestimated in this subtask.

Other tasks throughout SPICE had already dealt with the design of the system, and even the reduction to hardware of the major subassemblies such as the PMA and the OSS. Nevertheless, in any hardware experiment, the reduction to practice of a large integrated test facility is an enormous undertaking. The laboratory operations effort was, for SPICE, the "glue" which bound together the various disciplines of the program. The types of efforts that were included in laboratory operations are discussed next.

- Interdisciplinary Coordination. The success of a hardware integration like SPICE often depends upon having an individual deliberately tasked with understanding in detail what others in various disciplines are doing. If everyone assigned to the program has a full-time commitment to their own discipline, they cannot take the time to follow what others are doing in sufficient detail to unearth potential problems. Even the most careful interface documentation can fall short if people are too busy to read it, and the tendency of documents to become obsolete as time passes can make them a source of error. Medium-scale programs like SPICE that have many engineers, but cannot afford the high costs of rigid document control, must fill the gap with vigilance. It must be recognized that vigilance does take some engineering time.

- Hardware Conventions. With many engineers performing design and analysis functions in different locations in different states, it was essential that SPICE find a way to make sure everyone adopted the same conventions. In this context, conventions are names, numbering sequences, signal scaling and polarity, coordinate frames, filtering, and other such parameters. To communicate this information to the various members of the team, a conventions diagram was generated which includes all this information on a single E-size page. Each engineer on SPICE has one on his wall for easy reference (Ref. 10).

- Configuration Control. Drawings of the as-built SPICE hardware have been kept up to date and are controlled in the SPICE files. A plan for a configuration control board (Ref. 11) was generated to control changes to the SPICE structure.

- Interface Electronics. The design, fabrication, integration, and testing of cabling and electronics to interconnect, power, and control the various parts of the system were major elements of the laboratory operations task. This effort involved >2 mi of cable, almost 10,000 electronic parts, hundreds of connectors, and more than 100 pages of drawings for documentation. The handling of control, telemetry, and fault monitoring functions required a dedicated computer interfaced to 20 other distributed microprocessors and various analog multiplexers, and the development of appropriate software. The development of the SPICE electronics is documented in the SPICE Electronics Final Report (Ref. 12) and its bibliographic references.

  Since the ultimate goal of the SPICE Precision Pointing Experiment was to demonstrate significant reductions in measured analog signals from the system sensors, it was of paramount importance that the noise-free transfer of analog signals throughout the system be given as much attention as the development of the sensors and actuators themselves. This is often overlooked, and many otherwise well-conceived experiments have failed due to such factors as poor grounding and shielding. This type of mistake, once made, is usually prohibitively expensive to correct and results in low signal-to-noise ratios and generally poor data throughout the experiment. Furthermore, when an active control system with bandwidth near 60 Hz is involved, the huge spectral peaks at 60 Hz so often explained away by experimentalists can be amplified, resulting in signal clipping and even instability. The 60-Hz energy cannot be filtered without degrading the phase of the loop, which high bandwidth loops will not tolerate.

  The SPICE program dealt with these issues from the beginning, ensuring by design that no sensor or component anywhere in the system was allowed to have a direct connection from signal to chassis ground. In a large distributed system like SPICE, in which many cables are more than 100 ft long, this is the first step toward avoiding "ground loops." A single-point grounding philosophy was established early and rigidly maintained. In the SPICE system:

- Every command/telemetry signal was transmitted using balanced differential line drivers and receivers with three-conductor "twin-ax" cables,
- No 60-Hz power was distributed anywhere on the structure (a direct current [DC] power bus drove local DC-to-DC converters for electronics supplies where needed), and
- All differential signals were buffered into a signal interface console where they are available to the Tustin analog-to-digital converters and to front panel access through appropriate anti-aliasing and isolation circuitry - the interface console also hosted the system's single point ground connection, and this ground was tied via heavy braid to the HP3565, the front-end computer of the modal system, located adjacent to it.

Extremely clean analog signals throughout the system resulted from these efforts. Electronic noise was ~1 to 2 mv RMS, and no 60-Hz spikes were observed on measured PSDs in any of the system-level tests.

- Mechanical Integration. Integration of the major subassemblies onto the structure and their subsequent alignment, along with the design and fabrication of mounting brackets, special test equipment, and other peripheral hardware, also were part of the laboratory operations task.

- Maintenance. Routine maintenance of the hardware was another operations function. Failures in the SAVI battery chargers and stacks were repaired with no impact to the program schedule. One of the tripod legs came into contact with the overhead crane, resulting in a crack in the epoxy-graphite composite material. A custom patch was constructed and applied to the crack. Several minor difficulties with various computers and equipment were also diagnosed and corrected.

- Calibration. Routine calibration, particularly of the OSS, was performed regularly, sometimes as often as twice daily. Calibration procedures were generated and filed.

2.3 TASK 3 - PRECISION POINTING EXPERIMENT CONTROLS DESIGN

The purpose of this task was to develop the control system to Conceptual Design Review (CDR) level. The goal of the CDR system was a reduction of RMS LOS jitter by a factor of 50. The

progress of this task was reported in Technical Interchange Meeting (TIM) briefings and is documented in the reports of those meetings. At the May 7, 1992, TIM, progress reported in task 3 included:

- Moving the analysis software from the Lockheed VAX cluster in Sunnyvale, California, to the SPICE VAX Workstation. Development on the control system during subtask 02-08 had been done on the VAX cluster. At the beginning of subtask 02-09, it was decided to consolidate design and analysis at the test site.
- Converting the control system from FORTRAN to MATRIXx. Much of the design and analysis on the VAX cluster had used FORTRAN routines. Once resident on the VAX Workstation, these routines were converted into MATRIXx command files. After this effort all design and analysis were done using MATRIXx.
- Redesign of the control system to the newly released SPICE4 structural model, which had been reconciled with the results of the first modal test. In subtask 02-08, control system design efforts used the SPICE3 structural model.

Reference 13 contains further discussion of these areas.

At the next TIM, held on June 24, 1992, the following control system developments were briefed:

- Demonstration by analysis that the baseline LAC design was stable. The singular values of the open-loop LAC system were shown to have less than unity gain, even assuming low structural damping values, beyond 300 Hz. The measured phase loss of the PMAs would result in >30 deg of phase margin below 1000 Hz. The LAC was consequently shown to be gain stable at high frequencies and phase stable at low frequencies.
- Analysis of the effects of measurement noise. Actual OSS and accelerometer sensor noises were shown to be well within the values used to tune the HAC Kalman filter.
- Analysis indicating that neither stability nor performance would be degraded due to the transverse modes of the flexure. There had been significant concern about PMA flexure cross-axis modes. A 100:1 system was designed for this analysis.
- Modification of the Phase 1 HAC design to a near-final version. This version, designed to the SPICE4 model, resulted in 77:1 attenuation in simulation.

Reference 14 has further discussions of these topics.

The final TIM in which task 3 results were briefed took place August 26, 1992 (Ref. 15), by which time the control system design included the rigid-body modes of the structure. All subsequent design updates were done under task 4.

2.4 TASK 4 - PRECISION POINTING EXPERIMENT CONTROLS SUPPORT

The purposes of this task were to provide analytical support for the subtask 02-09 test series and to upgrade the control system design as testing progressed to reflect the results of that testing. The progress of the task is best summarized by referring to the TIM briefings at which progress reports were made.

Some task 4 results were reported at the August 26, 1992, TIM (Ref. 15), namely:

- Development and testing of a LOS matrix for real-time implementation in the Star VP-3. The 2 by 18 matrix mapped the 18 OSS signals into LOS x and y. This matrix was imbedded in the full 186 by 222 Star controls matrix, with proper scaling. All open-loop and FRF/LAC tests were done using this matrix.
- Development and software testing of a set of algorithms for separating atmospheric noise from structural and sensor noise on the OSS sensors using a set of two 3-axis Angular Differential Sensor (ADS) cubes. The algorithm was never implemented in hardware due to limitations in the ADS cubes.
- Development of an algorithm for testing HAC robustness using measured versus predicted FRF data. The technique employed singular value theory. Although the approach was conservative, it was expected to be useful nonetheless. In fact, the approach was too conservative to be of practical use. One exception is that it did predict stability of the control system in the vicinity of 11 Hz, where there are suspension modes not modeled in the HAC system. It was therefore unnecessary to include these modes in the 50:1 HAC design.
- Development of an algorithm for using the measured FRFs (with LAC loops closed) to tune the HAC estimator where instability was indicated. This algorithm was never used during HAC testing.

At the October 21, 1992, TIM (Ref. 16), the task 4 progress reported included:

- Development of the Kalman filter test plan. In this test, only the Kalman filter would be running in real time. The test was to have verified proper implementation of the controller (proper channel assignments, scale factors, etc.), as well as to have measured the accuracy of the structural model, by comparing actual measurements with predicted measurements from the estimator. The differences, called innovations, should have statistics consistent with predictions of those statistics. This test was run during the open-loop test series, but with poor results due to adverse interaction between SAVI and the flexible modes of the structure. The Kalman filter test was

never repeated after the SAVI controller was modified to eliminate that interaction. In its place, an open-loop test was run to verify proper implementation. Model accuracy was ascertained by comparison of test and model FRFs.

- Analytical verification that the LAC system would be stable, even though it was not pure colocated rate feedback. Only local-loop damping, in which the PMA force commands (which are relative between housing and proof mass) are proportional to relative rate between housing and proof mass, is certain to be stable. In LAC, force is proportional to housing rate only. The analysis corroborated results which indicated that it is necessary to have local-loop damping just to keep LAC stable. If there were no local-loop damping, LAC would be unstable as predicted. This analysis concluded that the baseline design of local-loop damping was ample to stabilize the LAC.
- Analytical determination of the best mix of sensors to be used in local-loop and LAC damping. The three sensors included in the trade were the Linear Variable Differential Transducer (LVDT), which measures relative displacement between the housing and proof-mass, the Sundstrand QA700 accelerometer, and the Wilcoxon 736 accelerometer. The LVDT, because its measurement of displacement is differentiated to yield rate, is best used at low frequencies only (<15 Hz). The Wilcoxon is a high frequency sensor with poor dynamics and noise at low frequencies, while the QA700 is a good low-frequency sensor. The noise analysis resulted in a recommended set of filters to be used to combine the three sensor types. The outputs of the filters are housing rate for LAC and relative rate for local-loop damping. These recommendations resulted in a set of specifications for the electronics design.
- Determination of the high-frequency modes in the HAC spillover region that require passive damping, and the degree of damping required per mode, to obtain 100:1 HAC performance with gain margin of 2. These requirements were to be flowed down to hardware requirements on passive damping elements. Due to a lack of funding, the effort was halted at this meeting.

The results of the open-loop test sequence were briefed at the next TIM on January 27, 1993 (Ref. 17). The primary task 4 area of interest concerned results of a new algorithm used to separate the statistics of atmospheric turbulence from background structural motion. The analysis was based on covariance analysis applied to the x-axes of the two secondary mirror translation sensors (SMTSs) and the y-axis of the SMRS. The important result from this work was the conclusion that RMS LOS jitter due to OSS sensor noise, including atmospheric turbulence, was <200 nrad RMS above 1 Hz. An analysis of harmonic distortion observed in the OSS was also presented at this meeting.

The remaining control systems effort was done as part of the HAC/LAC tests. It is discussed in Section 3.0.

2.5 TASK 5 - SIMULATION

This task supported the maintenance and use of a high fidelity, nonlinear time-domain computer model of the SPICE hardware. The computer model, in its latest form, resides on a DecStation 5000/125 workstation (node name "SPEEDY") as a MATRIXx SYSTEM BUILD model. The model includes 1457 states and takes ~5 hr on the DecStation 5000 to model 1 s of real time. The simulation is self-documented, with extensive comment text in the files that prepare the parameters and clear labeling on all signals in the SYSTEM BUILD blocks. In addition, it is documented through numerous reports contained in the Honeywell SPICE files under file numbers 0329.13.x-x.

The high-fidelity model is a lineal descendant of the SAVI nonlinear simulation, which included detailed modeling of the SAVI magnetic suspension and large angle rigid body modeling using quaternion mathematics. For SPICE, which did not use the SAVI coarse followup system, sections of the SAVI model were removed. The SPICE models of the beam expander flexibility were added, as were detailed models of the SPICE sensors, actuators, and discrete-time control system. The nonlinear SPICE simulation is very large and turnaround time for simulation runs was correspondingly large, but it served a vital purpose. The day-to-day analyses in support of the system design efforts were performed using reduced-order linear models to get faster turnaround times. However, at intervals throughout the program, the full model was exercised to verify system stability and performance when sampling, quantization, nonlinearities, hardware high and low pass filters, etc., were introduced. Furthermore, since the high-fidelity model was developed and maintained by a different individual than the one who did the linear analysis, a valuable cross-check against errors was provided.

Due to constraints of program funding, the simulation effort was terminated prematurely. As a result, the current version does not include the results of the SPICE5 finite element model, or any of the latest designs of the HAC controller.

2.6 TASK 6 - TESTING

The SPICE Precision Pointing Experiment was one of the most ambitious active control experiments ever attempted in controls-structures interaction, as attested to by the extensive

efforts put forth in the areas of controls, modeling, hardware, and software. But no matter how good the quality of the test article, an experiment of this magnitude would have been doomed to failure if test methodology had been poor. The SPICE Precision Pointing Experiment test sequences spanned nearly a year and were the subject of planning and documentation efforts at least as thorough as those undertaken for the design of the hardware itself.

The SPICE tests were broken into three sequences: the open-loop tests, the FRF/LAC tests, and the HAC/LAC tests. The objectives of the open-loop tests centered around characterization of the structure, the system sensors, and the laboratory environment. Emphasis in the sensor and environment area was on establishing the noise floor and dynamic range of the instrumentation, especially the SPICE OSS. For the structure, detailed FRFs were taken from the disturbance sources to the system sensors. These tests were performed while the PMAs were still being built and provided validation of the open-loop models that supported the final design of the control system. The open-loop tests are documented extensively in Reference 6.

The next test sequence was called the FRF/LAC tests because it combined the functions of two test sequences from an earlier plan. The 18 PMAs were installed on the structure at the beginning of these tests. The tests covered detailed characterization and calibration of the PMAs as subassemblies, including closure of the local loops. With the loops closed, FRFs were taken from the actuators to the sensors. These FRFs were the last vital piece of data to be used in verifying the design of the HAC system. In addition, to quantify the effect that the installation of the PMAs had on the structure, a new modal test was performed on the structure to provide data for correlation with the final NASTRAN model. The FRF/LAC tests are documented extensively in the final report of the FRF/LAC tests (Ref. 5).

In the final test sequence, the HAC/LAC tests, the system was characterized with all loops closed. This included not only studies of global stability and performance, but also closed-loop FRFs which allow visibility into the inner workings of the system and detailed comparison to analytical models. The final design of the HAC system and the results of the HAC testing are presented in Section 3.0 of this document.

Months before testing began, an executive test plan (Ref. 18) was generated which described the SPICE approach to testing and test planning. The guidelines set forth in this document were followed throughout the testing. As each test sequence approached, a planning meeting was conducted with all disciplines represented and the objectives of the test sequence were established. In SPICE, all tests were planned to support specific requirements for data, such as to

compare to a particular analysis or to fill in a certain box in the system performance chart. Once these requirements for data were established, a plan for collecting the data was written. The resulting draft was reviewed by all disciplines prior to release. Test plans for each of the three test sequences are available in the SPICE library (Refs. 19-21).

The heavy emphasis on system engineering in SPICE led to an early detailed understanding of the goals and requirements for testing and data reduction. This led to the acquisition of equipment such as a 104-channel analog front end for the modal test computer, an increase in the number of accelerometers in the laboratory inventory, and various computer resources for data manipulation and reduction. Acquisitions of this type take substantial amounts of time to complete. Early visibility into the required number of channels of instrumentation, dynamic ranges, data file sizes, and other such parameters helped avoid the sort of test practices which evolve from making do with whatever is on hand at the last minute.

Most of the data collected was in the frequency domain, either PSDs or FRFs. Therefore the primary tool for data acquisition was the modal test system, which is optimized for collecting frequency-domain data on many channels simultaneously. The SPICE modal test system consists of an HP9000/380 computer (network node name "TAZ") running the LMS Fourier Monitor software package, with an HP3565 front end configured for 104 channels of analog input and two source outputs. This system provides the means for orderly naming and archiving of the data collected. In addition, for each test performed, the system saves the entire setup on disk, including all engineering scale factors that were applied. The conditions of each test run were entered in the log book, allowing easy data identification months after the test for comparisons. For major tests, spreadsheets were created showing the connections to the various patch panels. The actual patching was then done in accordance with the spreadsheet and checked against it, leaving a clear audit trail of what signals were actually analyzed.

Data were reduced in a variety of ways, depending upon the specific test. Modal data were reduced using the LMS software to mode shapes, frequencies, and dampings, and transmitted over the network to the finite element analyst in Sunnyvale, California. The PSDs were converted by LMS to universal file format and then transferred via the network to node "SLOPOK", the controls design VAX. On "SLOPOK", data were passed through a program converting it to MATRIXx format, and it was then processed on MATRIXx by the controls designer. The FRF data were also converted through universal files to MATRIXx, but ended up on "SPEEDY", the local DecStation 5000 which hosts the system nonlinear simulation. This

platform was the only one locally available that was big enough to perform the comparisons against the analytical predictions as described in the next paragraph.

The number of FRFs taken in a test depended on the number of inputs and outputs being studied. The largest number of FRFs in any of the tests was 912. In addition, the FRFs often had to be taken in more than one frequency band to obtain the desired resolution. This resulted in thousands of FRFs, each consisting of as many as 2048 complex data points, coming from a single test. This enormous volume of data had to be compared to the analytical predictions in a systematic manner in a short period of time. The only solution was to automate the function. An algorithm was devised (Ref. 5) that assigns a numerical score between 0.0 to 1.0 to each FRF that expresses the degree of agreement between measurement and analytical prediction for that FRF. These scores can then be sorted and plotted in a variety of ways to lend insight into the results of the tests. Of particular importance is the fact that only the worst scoring FRFs needed to be studied by eye and, if their comparisons to prediction were considered acceptable, it could be confidently assumed that the rest of the FRFs matched at least as well. This reduced the time necessary for data review to an acceptable level. It would otherwise have taken days just to plot out all the data from a single test, let alone to review it.

2.7 TASK 7 - SYSTEM ENGINEERING

The function of the system engineering task was to provide top-level technical direction to the Precision Pointing Experiment, i.e., to make sure that the goals were kept firmly in mind. This involved monitoring the interfaces between various disciplines and subsystems in the interest of overall performance. There was an ongoing need to develop and maintain requirements and to ensure that the effects of any subsystem requirements modification were analyzed, flowed down to other subsystems, and flowed back up to the top level to assess the effects on system performance.

Guided by the system engineer, the SPICE program integrated analysis and hardware. For example, the original specifications for the PMAs could not be met and modifications that brought the units closer to one of the specifications often entailed losing ground in another area. The decision on what specification changes would be made was done with a coordinated series of analyses that emphasized retaining system performance goals.

It is also necessary that the results and methodology of analyses and tests be documented for them to be useful. The system engineering function oversaw the documentation effort and outlined a series of test plans, quick look reports, and test final reports to fill this need.

2.8 TASK 8 - OPTICAL SENSING SYSTEM

The SPICE HAC system is a global (noncolocated) control system designed using modern control methods. The development of the cost function to be minimized is central to the ultimate performance of the system and should represent the actual parameter of interest at the system level. In the case of SPICE, this parameter is the optical RMS LOS jitter of the telescope mounted on the beam expander structure. It was recognized early that it would be necessary to measure and score the actual LOS. An innovative approach was developed for avoiding the high cost of real optics and the associated clean room environment. This involved designing a custom sensor that would make measurements of the relative motions of mass-model mirror segments and derive from those measurements what the LOS of a real telescope would be if it were mounted on the same structure.

The OSS, consisting of nine separate devices mounted on the center petal of the segmented primary mirror, performs this function. Each of these devices measured the motion of another petal in two degrees of freedom with respect to the center petal. Six of the devices, the PMRSs, measured tilts of the outer primary petals, the SMRS measured tilts of the secondary, and the two SMTSs measured translations of the secondary at two different points. These 18 measurements were then combined to calculate the LOS of the simulated telescope through an equation that includes its f-number and magnification. Implicit in this approach is the assumption that the mirror petals are rigid in the frequency band of interest, since the OSS measures motion of only small patches on each petal. The petals were designed with this in mind, and component testing showed no petal modes below 100 Hz.

The same approach could have been used to make an estimate of wavefront quality by adding extra sensors to measure relative translations of the primary segments, but this was deferred during the Precision Pointing Experiment to cut costs. The main objection to deferring these extra measurements is that the control system might redirect energy into combinations of motions that would result in reduced RMS LOS jitter but that would degrade wavefront quality. Testing has shown that the action of the control system reduces the jitter on all system sensors, so this is very unlikely.

The OSS is documented in detail in two final reports (Refs. 2 and 7). The devices performed exceptionally well, achieving the full dynamic range on LOS required. They can measure LOS jitter >100 μrad RMS and have a measured noise floor <200 nrad RMS. The full-scale range of the individual sensors is ±240 μrad for the PMRS, ±1400 μrad for the SMRS, and ±4.2 mm for the SMTS.

2.9 TASK 9 - SOFTWARE

Under SPICE Subtask 02-09, it was necessary to develop and implement control system software to support the Precision Pointing Experiment. This specialized software enables the following computer hardware and associated critical components to perform their function in real time:

- VAX 11/780
- Star VP-3 Array Processor
- Aptec IOC-24 Input/Output Computer (6 Input/Output Processors)
- TUSTIN System 2100 Digital-to-Analog Converter
- TUSTIN System 2100 Analog-to-Digital Converter
- Concepts C-51 High Speed Disk Drive (2.5 Gbyte)

These components are configured as detailed in Figure 10. There are two Aptec Input/Output Processors connected to the Star to support the relatively large data rate requirements and the Input/Output overhead penalty associated with the Star.

The real-time control system software is comprised of the following executable codes:

- VAX 11/780 Real-Time Control System Master Control Software:
  - •• HOST and STARTUP VMS DCL Command Procedures
  - •• HOST Executable Program
- Star VP-3 Array Processor Software:
  - •• RADDR to download buffer pooling addresses
  - •• SKF, the master Star routine
- Aptec IOC-24 Software:
  - •• Master Input/Output Processor Software
  - •• Slave Input/Output Processor Software
  - •• A2D Input/Output Processor Software
  - •• D2A Input/Output Processor Software
  - •• Concepts C-51 Disk Drive Input/Output Processor Software

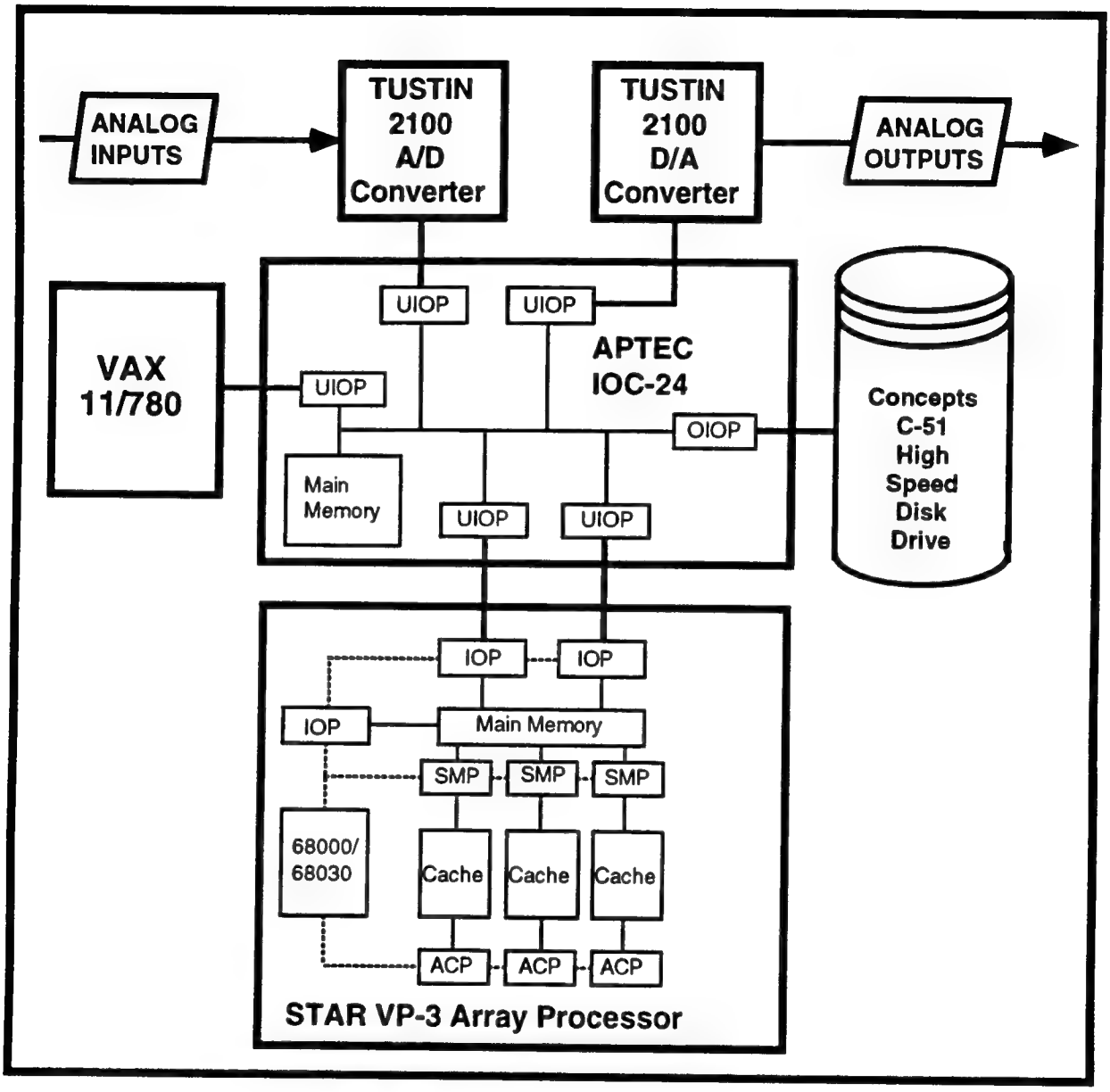

Figure 10. The SPICE digital control system hardware.

Additional postprocessing software and procedures were required to support postrun data analysis of telemetry data acquired (and stored on the Concepts C-51 High Speed Disk Drive) during integration testing and experiment execution. Consequently, the following data analysis utilities were implemented to extract and translate data to a format usable by commercial analysis programs (such as MATRIXx, IDEAS, etc.).

- UNPACK: VAX 11/780 Data Extraction Routine
- XLATE: VAX 11/780 Data Conversion Routine

For complete documentation of the real-time control system software and the data analysis utilities refer to References 22 through 25.

2.10 TASK 10 - STRUCTURAL MODELING

The final design of the HAC depended strongly upon the accuracy of the finite element model of the SPICE structure. The SPICE finite element modeling began with SAVI1, inherited from the SAVI program. The next version, SPICE1, included improved models of the rigid segments that were to make up the telescope simulator. Successive upgrades resulted in models of increasing fidelity until, at SPICE4, a finite element model was developed that was actually reconciled with the first SPICE modal test. Variants of SPICE3 and SPICE4 were developed in which models of hardware not yet on the structure (e.g., the PMAs) were added. Discussions of the earlier models may be found in References 26 and 27. The reconciliation of the SPICE4 models with the modal test is discussed in Reference 28.

The latest SPICE finite element models, the SPICE5 models, were reconciled to a full modal test of the structure in its final Precision Pointing Experiment, Phase 1 configuration. The SPICE5 models are evolutionary models derived from the SPICE4 model series corresponding to the HAC/LAC hardware test configuration. Two SPICE5 models, SPICE5A and SPICE5G, were developed (Ref. 29). The SPICE5A model considers the SPICE beam expander structure to be fully free-free with no connection to ground (i.e., the same boundary conditions considered in the previous SPICE models). The SPICE5G model is identical to the SPICE5A model with the exception of

- Inclusion of the gravity off-load suspension rod/zero spring rate suspension mechanism representation (connected to ground), and
- Inclusion of stiffness effects of the secondary mirror disturbance shaker stingers (connected to ground).

This summary pertains to development of the SPICE5A model and its correlation to the test results. The SPICE5G model is discussed in Appendix A of Reference 29.

The basis for the SPICE5 models is the SPICE4X model (Ref. 28). SPICE4X was developed for open-loop testing prior to the installation of the PMAs. As the most current of the SPICE4 models with respect to mass properties and OSS and LOS equation implementation, it was modified to include the PMAs and other structural and mass property updates. The result of the modification, designated SPICE4Y, was used for preliminary control system design and system checkout purposes. SPICE4Y (which was not formally documented) was then "tuned" to the results of the modal test that was performed during the FRF/LAC test sequence (Ref. 20) to obtain the SPICE5A model. Table 6 summarizes the model/test modal frequency comparisons.

Table 6. Comparison of SPICE5 finite element model and modal test.

Test Mode	Freq (Hz)	Analysis Mode	Freq (Hz)	Percent Diff
1	6.823	25	6.796	-0.40
4	7.799	26	7.824	0.32
5	7.875	27	7.880	0.06
10	15.297	28	15.517	1.42
11	15.835	29	16.054	1.36
12	16.838	30	16.917	0.47
13	19.443	31	19.347	-0.50
14	19.706	32	19.950	1.22
16	20.762	33	21.013	1.19
18	23.025	34	22.185	-3.79
19	23.940	35	24.142	0.84
20	24.104	36	24.223	0.49
23	30.740	37	31.038	0.96
24	32.646	38	32.629	-0.05
25	33.564	39	33.695	0.39
26	33.841	41	35.221	3.92
27	35.317	40	35.042	-0.78
28	36.256	42	36.330	0.20
29	39.298	43	39.378	0.20
30	41.651	44	41.588	-0.15
31	42.234	45	42.108	-0.30
32	45.380	46	44.451	-2.09
33	47.081	47	46.404	????
35	51.010	48	46.791	????
36	51.447	49	49.706	????
37	53.439	50	50.304	????
		51	51.669	????
		52	51.830	????
		53	51.934	????
38	58.523	54	58.465	-0.10
39	60.600	56	61.763	-1.88
40	61.501	55	61.042	-0.75

The shaded area in Table 6 denotes a region of poor cross-orthogonality corresponding to complicated bulkhead modes. It is not clear which analysis modes should be matched with which test modes in this region. The problem with modeling modes in which bulkhead motion predominates did not translate into a difficulty for the HAC/LAC system. The excellent fidelity of the SPICE5 models out to almost 50 Hz was vital to the demonstration of disturbance attenuation by HAC/LAC.

3.0 THE HAC/LAC TEST SEQUENCE

3.1 INTRODUCTION

In the HAC/LAC test sequence, the culmination of Phase 1 of the Precision Pointing Experiment, a HAC/LAC system successfully attenuated LOS jitter in the 5- to 500-Hz band due to input disturbance forces by more than 75:1. Earlier test sequences have been documented (Refs. 5, 6) but the results of the HAC/LAC tests have not. Therefore this section is the final report of the HAC/LAC tests. Some tests performed as preliminaries to the main test sequence are briefly discussed in Subsection 3.2. Subsection 3.3 discusses the design of the final Precision Pointing Experiment HAC system. Subsection 3.4 provides the results of the tests in which the effectiveness of the HAC/LAC system was demonstrated.

3.2 PRELIMINARY TESTS

3.2.1 Disturbance Attenuation by a Preliminary HAC System

This test was done during a "window of opportunity" in the FRF/LAC tests and its results were briefly discussed in Reference 30. It corresponds to the test of a system designed to produce 20:1 attenuation of LOS jitter (Subsection 4.2.4 of Ref. 21). This first attempt to close a HAC loop resulted in stable operation of the controller and demonstrated attenuation of RMS LOS jitter by 26:1.

The determination of the set of input disturbance forces required to produce 100 μrad RMS of LOS jitter per axis was revisited twice before it was fully resolved (Refs. 3-5). After resolution of the problems, the six forces were input singly with the PMAs caged and the resulting RMS LOS was recorded for each. It was then assumed that the relationship between an input disturbance force level and the resulting jitter is linear and that the effect of applying several forces at once is the root-sum-square of the individual effects. Sets of force levels were then calculated that should, on these assumptions, produce certain desired RMS LOS jitter levels or, as they came to be called, caged-target LOS levels. These calculated force sets are shown in Table 7. Table 8 shows the measured RMS LOS results from tests in which the calculated disturbance sets, now characterized by their caged-target LOS levels, were input to the structure. Tests were run with PMAs caged and all control loops open, with PMAs uncaged and all control loops open, with the inner and LAC loops closed, and with all control loops closed. The same data are presented in graphical form in Figure 11. The average attenuation goal of 20:1 for the preliminary HAC was exceeded in this test.

Table 7. Input disturbance and caged-target LOS levels.

Caged Target LOS Level (μrad)	RMS Input Disturbance Levels (N) at:					
	SAVI Vertex Actuator #:			Secondary Mirror Shaker:		
	1	2	3	X	Y	Z
0	0	0	0	0	0	0
10	2.4	3.8	4.5	4	2	2
20	4.9	7.6	9.1	8	4	4
30	7.3	11.3	13.6	12	6	6
38	9.6	14.8	17.7	8	4	4
40	9.8	15.1	18.2	16	8	8
60	14.7	22.5	27.3	24	12	12
80	19.6	30.0	36.4	32	16	16
100	24.5	37.8	45.5	40	20	20

Table 8. Summary of disturbance response data.

Caged Target LOS Level (μrad)	RMS LOS Response (μrad)							
	PMAs Caged		PMAs Uncaged		LAC Closed		20:1 HAC Closed	
	X	Y	X	Y	X	Y	X	Y
0					0.6	0.6		
10		9.3	4.0	5.4				
20	21.8	20.8	9.9	11.9	2.5	2.9		
30	32.5	32.3						
38	40.5	39.0						
40			20.7	25.6				
60			31.4	43.1	6.5	8.0	2.5	2.7
80			43.6	60.3				
100			44.1	47.0	10.4	12.9	4.1	4.2

3.2.2 Tests of Preliminary HAC Model 5A11

Several preliminary models of the HAC system were tested during the HAC/LAC tests. In one of these tests, the 100-μrad caged-target LOS level disturbances (Table 7) were input to the structure and the preliminary HAC (designated 5A11) was activated to attenuate the LOS jitter. Frequency domain data were taken using the modal system LMS software in the band 0 to 256 Hz. The band is a lot wider than the effective band of the HAC (~5-50 Hz); it was used to ensure that the HAC was not amplifying any modes above that band.

Figure 12 shows the residual PSDs of the x and y components of the LOS jitter. Their RMS values are 1.84 and 1.96 μrad, respectively. Virtually all of the input disturbance power is within the band 0 to 256 Hz. The average attenuation of the RMS LOS is therefore ~52.6:1. The HAC system required further development because, during the test, the diagnostic system indicated

from time to time that a PMA was saturated. Saturation occurs when a command generated by the controller exceeds the capacity of the PMA. It can be a source of reduced performance and even, in extreme cases, instability. More information on test results using 5A11 is contained in References 31 and 32.

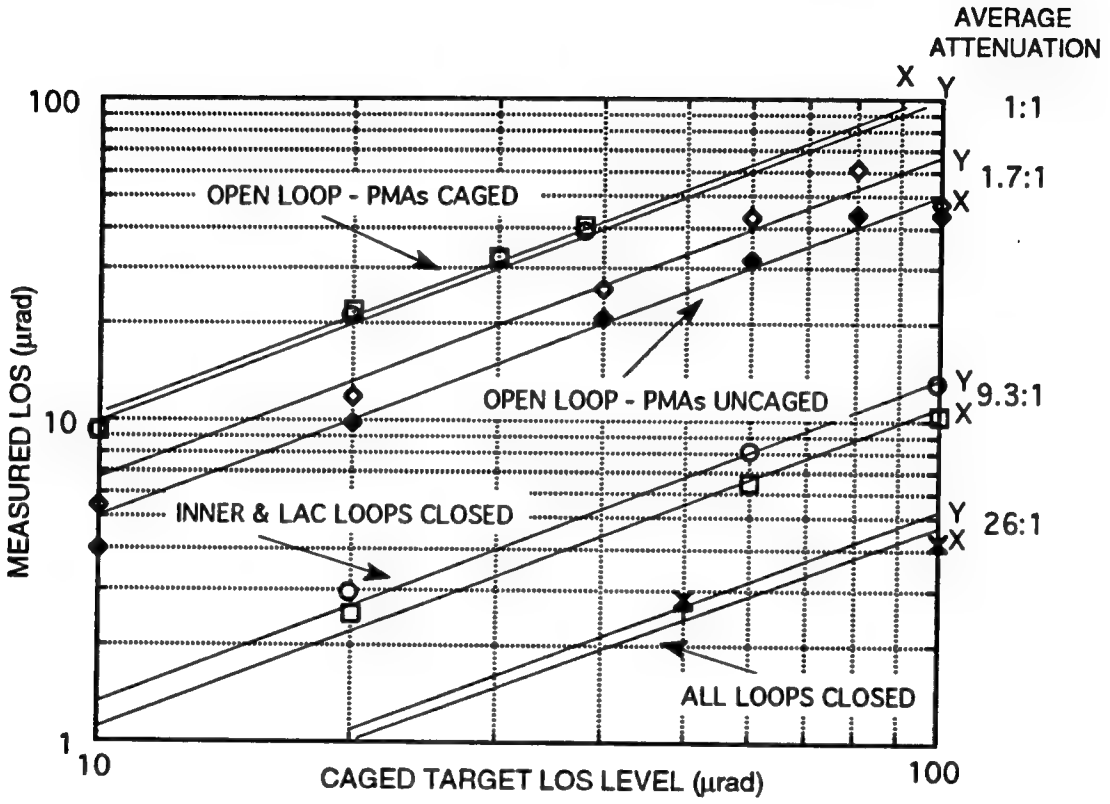

Figure 11. Summary of predicted attenuation data including the 20:1 HAC.

3.2.3 Sine Wave Attenuation Tests with Final HAC Version

Sine wave attenuation tests were performed with HAC 5A19, the final HAC system for Phase 1 of the Precision Pointing Experiment. Although not part of the main test sequence, sine wave attenuation tests serve as direct and easily understood demonstrations of attenuation by the HAC system. In these 20-s tests, the LAC was on and the HAC was off for the first 10 s, then the HAC was activated for the last 10 s. One of these tests was performed at 7.8 Hz, the center frequency of the dominant structural mode pair. Figures 13 shows that, when the HAC was turned on, the sine wave was strongly attenuated and the output LOS signals were reduced to noise. A second sine wave test is described in Subsection 3.4.5.

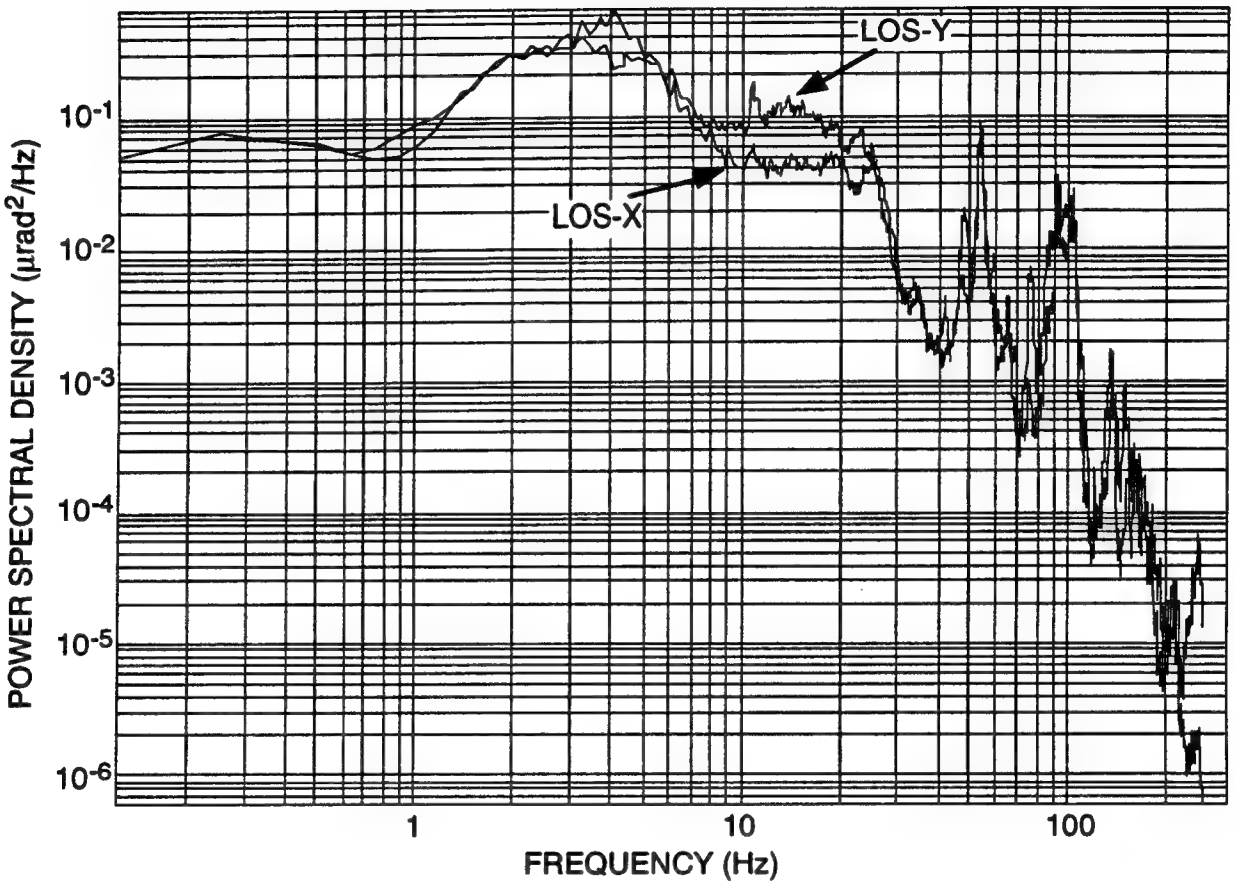

Figure 12. Residual PSDs after attenuation of 100-μrad disturbances by 5A11 HAC.

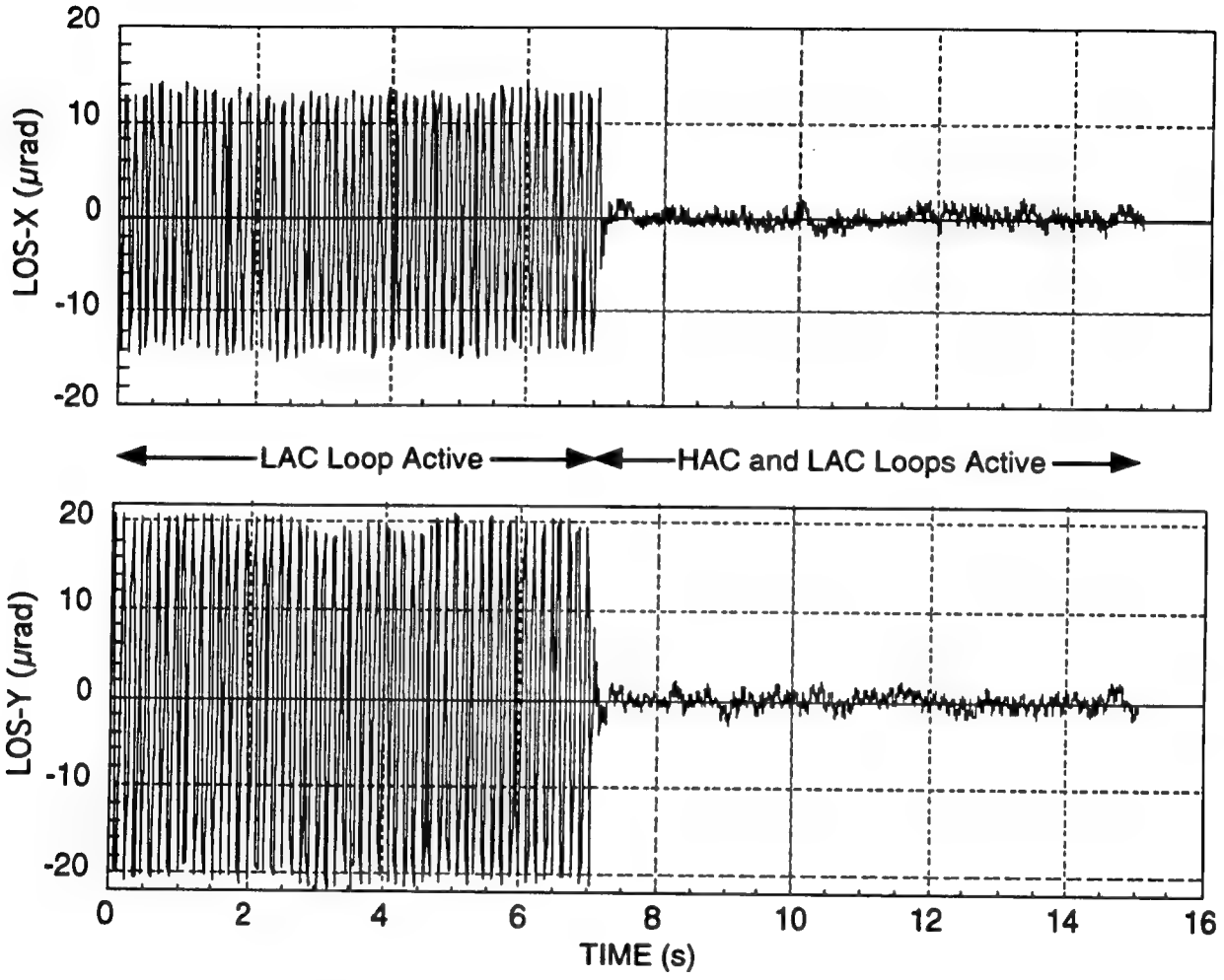

Figure 13. Attenuation of a 7.8-Hz sine wave disturbance by the final HAC (5A19).

3.3 THE FINAL HAC

3.3.1 The HAC Design Concept

A control system should be stable for small perturbations of the system under control. A control system that is overly sensitive to small perturbations is not properly designed. This is true for multiple input-multiple output as well as single input-single output systems. This was the fundamental concept adopted throughout the HAC design process.

The following are the key features of the HAC design, as applied to the SPICE structure and the Precision Pointing Experiment:

- A standard linear quadratic Gaussian (LQG) regulator was used to regulate the states of the structure. The cost function was constructed to minimize those parameters of interest. For SPICE, LOS, as defined by the LOS equation, is to be minimized. The regulator cost function is constructed to balance LOS, as a linear combination of states, against control authority. In addition, it is necessary to regulate torsion of the secondary mirror about the optical axis. The first flexible mode of the structure (other than PMA proof mass modes) is mainly torsion about the optical axis which results in very little LOS disturbance yet is very easy to excite with PMA forces. That is, in terms of the LOS cost function and control devices, torsion is nearly unobservable, yet very controllable. Significant spillover into the torsion mode due to small model errors could be eliminated only by including torsion in the cost function. All highly controllable degrees of freedom must be included in the cost function. The HAC system had encountered a problem because, although torsion is nearly orthogonal to LOS, it is highly controllable. It could have been eliminated if the structural model had been nearly perfect, but requiring such accuracy would violate the fundamental concept of HAC design. The cost function was modified to include the torsion mode. That fixed the problem with no degradation to RMS LOS performance.
- The structure was augmented with digital low-pass filters to force the regulator to roll off. There are 18 first-order low-pass filters, one per PMA, implemented digitally, with a break-frequency of 10.0 Hz. Control energy thereby becomes less efficient at higher frequencies. The regulator, in its quest to balance control energy with the parameters to be minimized, weighs LOS less at higher frequencies, thereby forcing roll-off. To effect roll-off, the filters must be part of the physical plant, rather than part of the cost function outside the physical plant.

- The states of the structure were estimated using a standard steady-state Kalman filter. The estimated states include the structure, SAVI rigid-body controller, PMAs, and the disturbances. Even though the disturbances were clearly not controllable by the PMAs, knowledge of the disturbances allowed the states of the controllable structure to be anticipated, resulting in improved performance.
- Measurements included displacements (provided by the OSS) and rates (provided by the integrated accelerometer signals). High frequency robustness (in the spillover region) can not be obtained if acceleration measurements are used instead of velocities. Acceleration, as a function of input force, does not inherently roll off with increased frequency whereas velocity does. Using velocity measurements in the estimator is similar to using low-pass filters in the regulator. Velocity measurements roll off into the measurement noise of the estimator. Although excellent performance was obtained in analysis using only velocity measurements, stability margin was very low. It is necessary for robustness to use both OSS and velocity measurements.
- Performance and stability margin were tuned by varying regulator and estimator weights. Proper tuning of the estimator, accomplished by increasing model measurement noise well beyond actual sensor noise, was essential to robustness. In the standard LQG approach to HAC used here, the designer must balance the regulator performance with that of the estimator. It is undesirable to have either the regulator or estimator greatly outperform the other component. For the SPICE HAC design, the design performance of the regulator alone is about one-half of the total design performance with both regulator and estimator.
- The DC gain of the HAC system was eliminated with a combination of 18 high-pass filters on the OSS measurements and 18 high-pass filters on the HAC PMA commands. An LQG regulator will have some DC gain but for the SPICE controller, that was undesirable since DC gain means proof-mass stroke, which must be conserved. The velocity measurements are already filtered with 0.2 Hz second-order high-pass analog filters with damping (ζ) of 0.5. There are no analog filters for the 18 OSS signals. Instead, 0.05-Hz first-order high-pass digital filters are applied in the array processor. To further reduce low-frequency response of the PMAs, it was necessary to add 18 digital 0.1-Hz high-pass filters on the HAC commands to the PMAs. These were also implemented in the Star array processor. None of the high-pass filters were included in the model used to design the HAC. They were appended to the controller after the regulator and estimator had been designed.
- The HAC system was designed using a discrete model of the plant. The regulator and estimator were computed using the MATRIXx commands DREGULATOR and

DESTIMATOR. DREGULATOR computes optimal constant-gain state-feedback matrices for discrete-time systems from the plant ("A"), input ("B"), and design-weighting matrices. DESTIMATOR calculates optimal state-estimator gain matrices for discrete-time systems from the plant ("A"), observation ("C"), and noise intensity matrices. Great effort was taken in the design of the real-time code to make the delay from sampling of all 36 input measurements to the output of all 18 PMA commands precisely one sample period, i.e., 1.0 ms. Consequently, the model of the digital processor was quite accurate.

- The entire control system was implemented in the array processor as a single 198 by 234 matrix multiplication at each sampling interval. All of the HAC functions were imbedded in the matrix (regulator, estimator, output limiting, digital low-pass filters for frequency shaping, and all digital low-frequency high-pass filters). The outputs of the matrix multiplication were fed back as inputs to the next cycle. The flexibility afforded the controls designer by having a processor capable of implementing large matrix multiplications with state feedback at high rates cannot be overstated.
- Even though the rigid-body modes of the structure and the SAVI rigid-body controller interact minimally with the flexible modes and the LOS, that interaction is sufficient to require their inclusion in the control model. The effect of excluding them from the model is not degradation in jitter reduction but increased PMA stroke and force at low frequencies.

3.3.2 Structural Modal Model Used in HAC

The final HAC design was based upon the SPICE5A structural modal model. The first 49 modes, i.e., all modes with frequency <50 Hz, were included in the design, up to 50 Hz. These include 6 rigid-body modes, 18 PMA modes, and 25 flexible modes. The frequencies and assumed modal dampings (ζ) are shown in Table 9.

The rigid-body frequencies were set to 0.18 Hz to approximate the effects of the gravity offload system. Damping of these modes was set, somewhat arbitrarily, to 2.0 per cent based upon SAVI rigid-body transfer functions. The frequencies of the PMA and flexible-body modes are those calculated by the finite element model and included in the SPICE5A model. Damping of the PMA modes was set to an arbitrarily low value. Damping within the PMA flexure was modeled discretely, as described next. Damping of the flexible modes was generally based upon modal damping measurements obtained during the last modal test. Damping values for modes 28 through 36 were taken directly from those modal damping measurements. Damping of modes

37 through 49 was set to 0.7 as an approximation of average damping in that frequency range (the modal damping estimates for those modes obtained during the modal test were not considered to be reliable).

Table 9. The HAC modal model summary.

Mode No.	Freq. (Hz)	Damping (ζ)	Comments		Mode No.	Freq. (Hz)	Damping (ζ)	Comments
1	0.18	2.00%	RIGID-BODY		26	7.82	0.10%	BENDING
2	0.18	2.00%	RIGID-BODY		27	7.88	0.10%	BENDING
3	0.18	2.00%	RIGID-BODY		28	15.52	0.32%	FLEXIBLE BODY
4	0.18	2.00%	RIGID-BODY		29	16.05	0.33%	FLEXIBLE BODY
5	0.18	2.00%	RIGID-BODY		30	16.92	0.44%	FLEXIBLE BODY
6	0.18	2.00%	RIGID-BODY		31	19.35	0.29%	FLEXIBLE BODY
7	4.63	0.02%	PMA		32	19.95	0.73%	FLEXIBLE BODY
8	4.84	0.02%	PMA		33	21.01	0.43%	FLEXIBLE BODY
9	4.85	0.02%	PMA		34	22.19	0.27%	FLEXIBLE BODY
10	4.95	0.02%	PMA		35	24.14	0.82%	FLEXIBLE BODY
11	4.95	0.02%	PMA		36	24.22	0.38%	FLEXIBLE BODY
12	4.96	0.02%	PMA		37	31.04	0.70%	FLEXIBLE BODY
13	4.98	0.02%	PMA		38	32.63	0.70%	FLEXIBLE BODY
14	4.98	0.02%	PMA		39	33.70	0.70%	FLEXIBLE BODY
15	4.98	0.02%	PMA		40	35.04	0.70%	FLEXIBLE BODY
16	4.98	0.02%	PMA		41	35.22	0.70%	FLEXIBLE BODY
17	4.98	0.02%	PMA		42	36.33	0.70%	FLEXIBLE BODY
18	4.99	0.02%	PMA		43	39.38	0.70%	FLEXIBLE BODY
19	4.99	0.02%	PMA		44	41.59	0.70%	FLEXIBLE BODY
20	4.99	0.02%	PMA		45	42.11	0.70%	FLEXIBLE BODY
21	4.99	0.02%	PMA		46	44.45	0.70%	FLEXIBLE BODY
22	5.03	0.02%	PMA		47	46.40	0.70%	FLEXIBLE BODY
23	5.04	0.02%	PMA		48	46.79	0.70%	FLEXIBLE BODY
24	5.04	0.02%	PMA		49	49.71	0.70%	FLEXIBLE BODY
25	6.80	0.10%	TORSION					

The modal damping used for the first three flexible modes was less than that obtained during the modal test. Modal test values were 0.51 per cent for torsion mode, 0.22 per cent for first bending mode, and 0.24 per cent for second bending mode. However, during the modal test, the PMAs were on the structure in their uncaged configuration. Much of the damping observed for the first three flexible modes during the modal test was due to the discrete damping provided by the PMA flexures. That level of damping is best modeled discretely rather than globally. To approximate the discrete effect, the following analysis was done:

- During bench testing of a PMA, about 32 dB of peaking was observed at 5 Hz. This corresponds to Q = 40. For high Q, damping (ζ) = 1/2Q = 0.0125.
- The damping gain (K_d) of the flexure that yields this ζ level is calculated by:

  $$K_d = 2\,\zeta\,(2\pi\,f_0)\,M_{pm} = (2)\,(0.0125)\,(2)\,(3.14)\,(5)\,(7.18) = 5.64 \text{ N-s/m}$$

  where M_{pm} is the mass of the moving proof mass (7.18 kg) and f_0 is the PMA resonant frequency (5 Hz).
- The PMA damping was modeled as 18 discrete dampers with gains of 5.64 N-s/m. The damping gain was applied to the relative rate between proof mass and the PMA housing.
- The nominal force levels, when applied at the six disturbance locations, resulted in about 108 μrad of LOS jitter per axis with the proof masses caged. Uncaging the proof masses resulted in an attenuation factor of ~1.7. Assuming that the attenuation was due entirely to damping, the change in modal damping of the first two bending modes (which accounted for the vast majority of LOS jitter) due to proof mass discrete damping was $\sim 1.7^2$, or ~3.0. This is because RMS levels go as the square of damping for lightly damped systems. Working backwards, the modal damping of the first three dominant modes, without the effect of PMA discrete damping, was roughly one-third that measured in the modal test. That is, from this analysis, the damping of the first three flexible modes was 0.51%/3 = 0.17 per cent for torsion, and 0.24%/3 = 0.08 per cent for the two bending modes. The levels were rounded to 0.1 per cent for all three modes, as shown in Table 9. The discrete damping of the PMAs will then bring the total level near that observed in the modal test.

The shapes of the 49 modes were described at degrees of freedom of interest for HAC design and analysis. These included PMA input forces (relative between proof mass and housing), disturbance inputs (three shaker locations on secondary mirror, and three SAVI z-axis), the individual SAVI actuators, the cross-axis degrees-of-freedom of the secondary mirror shaker stingers, PMA stroke, proof mass rates, PMA housing rates, OSS measurements, and LOS x and y. These modal degrees of freedom are listed in Tables 10 and 11.

The first 18 input forces are the PMA forces. These are relative forces between the proof masses and PMA housings. The next six input forces are the disturbance forces. As will be described later, these were applied by shakers at three locations on the secondary and by SAVI actuators at three locations around the bulkhead. The forces at the secondary were transmitted through the axis of stingers into the structure. However, the stingers have some cross-axis stiffness (they are very stiff in-axis), resulting in additional forces being applied to the structure when the secondary

is moved. These cross-axis forces were modeled using inputs 31 through 36. The three SAVI disturbance forces were applied one per SAVI vertex. They were obtained by applying equal forces to each of the two actuators in the SAVI vertex, resulting in a resultant force along the local SAVI z-axis. Because the SAVI rigid-body controller was modeled, the 6 individual forces applied by the SAVI controller were included in the nodal set as inputs 25 through 30.

Table 10. The HAC design degrees of freedom - input forces (N).

No.	Location	Description	No.	Location	Description
1	PMA 1	Housing - Proof Mass	19	SM Shaker Vertex 1 X-Axis	X-Axis at SM Vertex 1 Shaker
2	PMA 2	Housing - Proof Mass	20	SM Shaker Vertex 2 Y-Axis	Y-Axis at SM Vertex 2 Shaker
3	PMA 3	Housing - Proof Mass	21	SM Shaker Vertex 3 Z-Axis	Z-Axis at SM Vertex 3 Shaker
4	PMA 4	Housing - Proof Mass	22	SAVI Resultant Vertex 1	Resultant of Actuators 1 &2
5	PMA 5	Housing - Proof Mass	23	SAVI Resultant Vertex 2	Resultant of Actuators 3 &4
6	PMA 6	Housing - Proof Mass	24	SAVI Resultant Vertex 3	Resultant of Actuators 5 &6
7	PMA 7	Housing - Proof Mass	25	SAVI Actuator 1	Local SAVI Z-Axis Vertex 1
8	PMA 8	Housing - Proof Mass	26	SAVI Actuator 2	Local SAVI Z-Axis Vertex 1
9	PMA 9	Housing - Proof Mass	27	SAVI Actuator 3	Local SAVI Z-Axis Vertex 2
10	PMA 10	Housing - Proof Mass	28	SAVI Actuator 4	Local SAVI Z-Axis Vertex 2
11	PMA 11	Housing - Proof Mass	29	SAVI Actuator 5	Local SAVI Z-Axis Vertex 3
12	PMA 12	Housing - Proof Mass	30	SAVI Actuator 6	Local SAVI Z-Axis Vertex 3
13	PMA 13	Housing - Proof Mass	31	SM Vertex 1 Y-Axis	Cross Axis for X-Axis Shaker
14	PMA 14	Housing - Proof Mass	32	SM Vertex 1 Z-Axis	Cross Axis for X-Axis Shaker
15	PMA 15	Housing - Proof Mass	33	SM Vertex 2 X-Axis	Cross Axis for Y-Axis Shaker
16	PMA 16	Housing - Proof Mass	34	SM Vertex 2 Z-Axis	Cross Axis for Y-Axis Shaker
17	PMA 17	Housing - Proof Mass	35	SM Vertex 3 X-Axis	Cross Axis for Z-Axis Shaker
18	PMA 18	Housing - Proof Mass	36	SM Vertex 3 Y-Axis	Cross Axis for Z-Axis Shaker

The first 36 outputs represent the measurements that are the inputs to the HAC system. The next two outputs are LOS cost functions to be minimized by the controller. The PMA stroke was modeled for evaluation purposes as well as for possible use in the regulator cost function. Housing and proof-mass rates were used for modeling local-loop and LAC damping. The six SAVI displacements at the SAVI gaps were used in modeling the SAVI controller. The stinger cross-axis displacements were used in modeling stinger cross-axis forces.

3.3.3 Disturbance Models

Six band-limited random disturbances were input to the structure to induce about 100 μrad of open-loop LOS jitter. The three secondary mirror disturbance locations and force levels are

- 40 N RMS at secondary mirror vertex 1, along x-axis

Table 11. The HAC design degrees of freedom - outputs.

No	Location	Description	No	Location	Description
1	PMA Housing Rate 1	HAC Measurement (m/s)	53	PMA 15 Stroke	Housing–Proof Mass (m)
2	PMA Housing Rate 2	HAC Measurement (m/s)	54	PMA 16 Stroke	Housing–Proof Mass (m)
3	PMA Housing Rate 3	HAC Measurement (m/s)	55	PMA 17 Stroke	Housing–Proof Mass (m)
4	PMA Housing Rate 4	HAC Measurement (m/s)	56	PMA 18 Stroke	Housing–Proof Mass (m)
5	PMA Housing Rate 5	HAC Measurement (m/s)	57	PMA 1 Housing Vel.	m/s
6	PMA Housing Rate 6	HAC Measurement (m/s)	58	PMA 2 Housing Vel.	m/s
7	PMA Housing Rate 7	HAC Measurement (m/s)	59	PMA 3 Housing Vel.	m/s
8	PMA Housing Rate 8	HAC Measurement (m/s)	60	PMA 4 Housing Vel.	m/s
9	PMA Housing Rate 9	HAC Measurement (m/s)	61	PMA 5 Housing Vel.	m/s
10	PMA Housing Rate 10	HAC Measurement (m/s)	62	PMA 6 Housing Vel.	m/s
11	PMA Housing Rate 11	HAC Measurement (m/s)	63	PMA 7 Housing Vel.	m/s
12	PMA Housing Rate 12	HAC Measurement (m/s)	64	PMA 8 Housing Vel.	m/s
13	PMA Housing Rate 13	HAC Measurement (m/s)	65	PMA 9 Housing Vel.	m/s
14	PMA Housing Rate 14	HAC Measurement (m/s)	66	PMA 10 Housing Vel.	m/s
15	PMA Housing Rate 15	HAC Measurement (m/s)	67	PMA 11 Housing Vel.	m/s
16	PMA Housing Rate 16	HAC Measurement (m/s)	68	PMA 12 Housing Vel.	m/s
17	PMA Housing Rate 17	HAC Measurement (m/s)	69	PMA 13 Housing Vel.	m/s
18	PMA Housing Rate 18	HAC Measurement (m/s)	70	PMA 14 Housing Vel.	m/s
19	PMRS 1X	HAC Measurement (rad)	71	PMA 15 Housing Vel.	m/s
20	PMRS 1Y	HAC Measurement (rad)	72	PMA 16 Housing Vel.	m/s
21	PMRS 2X	HAC Measurement (rad)	73	PMA 17 Housing Vel.	m/s
22	PMRS 2Y	HAC Measurement (rad)	74	PMA 18 Housing Vel.	m/s
23	PMRS 3X	HAC Measurement (rad)	75	PMA 1 Proof Mass Vel.	m/s
24	PMRS 3Y	HAC Measurement (rad)	76	PMA 2 Proof Mass Vel.	m/s
25	PMRS 4X	HAC Measurement (rad)	77	PMA 3 Proof Mass Vel.	m/s
26	PMRS 4Y	HAC Measurement (rad)	78	PMA 4 Proof Mass Vel.	m/s
27	PMRS 5X	HAC Measurement (rad)	79	PMA 5 Proof Mass Vel.	m/s
28	PMRS 5Y	HAC Measurement (rad)	80	PMA 6 Proof Mass Vel.	m/s
29	PMRS 6X	HAC Measurement (rad)	81	PMA 7 Proof Mass Vel.	m/s
30	PMRS 6Y	HAC Measurement (rad)	82	PMA 8 Proof Mass Vel.	m/s
31	SMRS 7X	HAC Measurement (rad)	83	PMA 9 Proof Mass Vel.	m/s
32	SMRS 7Y	HAC Measurement (rad)	84	PMA 10 Proof Mass Vel.	m/s
33	SMTS 8X	HAC Measurement (m)	85	PMA 11 Proof Mass Vel.	m/s
34	SMTS 8Y	HAC Measurement (m)	86	PMA 12 Proof Mass Vel.	m/s
35	SMTS 9X	HAC Measurement (m)	87	PMA 13 Proof Mass Vel.	m/s
36	SMTS 9Y	HAC Measurement (m)	88	PMA 14 Proof Mass Vel.	m/s
37	LOS X	Cost Function (rad)	89	PMA 15 Proof Mass Vel.	m/s
38	LOS Y	Cost Function (rad)	90	PMA 16 Proof Mass Vel.	m/s
39	PMA 1 Stroke	Housing–Proof Mass (m)	91	PMA 17 Proof Mass Vel.	m/s
40	PMA 2 Stroke	Housing–Proof Mass (m)	92	PMA 18 Proof Mass Vel.	m/s
41	PMA 3 Stroke	Housing–Proof Mass (m)	93	SAVI Act. 1 Displ.	m
42	PMA 4 Stroke	Housing–Proof Mass (m)	94	SAVI Act. 2 Displ.	m
43	PMA 5 Stroke	Housing–Proof Mass (m)	95	SAVI Act. 3 Displ.	m
44	PMA 6 Stroke	Housing–Proof Mass (m)	96	SAVI Act. 4 Displ.	m
45	PMA 7 Stroke	Housing–Proof Mass (m)	97	SAVI Act. 5 Displ.	m
46	PMA 8 Stroke	Housing–Proof Mass (m)	98	SAVI Act. 6 Displ.	m
47	PMA 9 Stroke	Housing–Proof Mass (m)	99	SM Vertex 1 Y-Displ.	m
48	PMA 10 Stroke	Housing–Proof Mass (m)	100	SM Vertex 1 Z-Displ.	m
49	PMA 11 Stroke	Housing–Proof Mass (m)	101	SM Vertex 2 X-Displ.	m
50	PMA 12 Stroke	Housing–Proof Mass (m)	102	SM Vertex 2 Z-Displ.	m
51	PMA 13 Stroke	Housing–Proof Mass (m)	103	SM Vertex 3 X-Displ.	m
52	PMA 14 Stroke	Housing–Proof Mass (m)	104	SM Vertex 3 Y-Displ.	m

- 20 N RMS at secondary mirror vertex 2, along y-axis
- 20 N RMS at secondary mirror vertex 3, along z-axis

Three disturbances were applied using SAVI as a disturbance generator. One resultant force was applied at each SAVI vertex. There are two SAVI actuators at each vertex. At each vertex, the two actuators were commanded equally. The half-angle separating the two actuators is 12.2 deg. Letting f equal the force commanded to each actuator in a pair, the resultant force was

$$f_r = 2 \cos(12.2°)\, f = 1.95\, f$$

The resultant force was applied along the local SAVI z-axis, which is approximately coincident with the SPICE global z-axis, with some inclination toward the secondary mirror. The resultant forces applied at each SAVI vertex were

- 49.0 N RMS at vertex 1
- 75.6 N RMS at vertex 2
- 91.0 N RMS at vertex 3

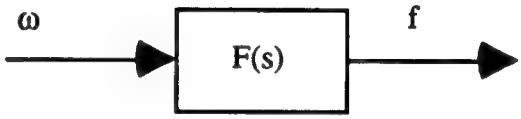

Figure 14. Model of disturbances.

The six disturbances were statistically independent. Each was shaped with a 5- to 10- Hz bandpass filter. They were modeled as shown in Figure 14, with:

ω = random noise input (N)
f = force applied to structure(N)
F(s) = analog shaping filter

The forces, f, were applied to the structure at inputs 19 through 24 in Table 10, with the above RMS levels. The shaping filter was

$$F(s) = \frac{K\, s^2}{\left(s^2 + 1.41\, \omega_1\, s + \omega_1^2\right)\left(s^2 + 1.41\, \omega_2\, s + \omega_2^2\right)}$$

where

$\omega_1 = 2\, \pi\, 5$ rad/s
$\omega_2 = 2\, \pi\, 10$ rad/s
K = 1146.7 (the gain required to yield unit variance force output for unit variance white noise input)

With the filter constructed in this manner, the standard deviation of the output force equaled the standard deviation of the input white noise. Each filter required 4 analog states, for a total of 24 states.

3.3.4 Sensor Noise Models

The OSS sensor noise was measured during open-loop testing and was reported in Reference 6. All sources of OSS noise, including atmospheric, generally resulted in an equivalent RMS LOS error measurement <200 nrad. Even in the worst atmospheric conditions, LOS jitter due to OSS noise was <500 nrad. Noise in the housing accelerometers similarly resulted in little error in measured rate (<2 μm/s, RMS).

The measurement noise model was selected such that its RMS was larger than measured sensor noise. It was chosen, however, not to reflect actual sensor noise but rather to tune the estimator for stability of the closed-loop system in the presence of model errors. For a discrete estimator, the PSD of measurement noise was flat from DC to the Nyquist frequency. For HAC, with a sample rate of 1000 Hz, the Nyquist frequency was 500 Hz. Specification of measurement noise for a digital controller means that the measurement error is independent from sample to sample as well as from sensor to sensor.

Although selection of a measurement noise model was not a straightforward process, a systematic method was developed. The DC to Nyquist sensor noise PSDs were treated as flat and a PSD level that was less than the closed-loop signal at low frequencies and greater than the signal at high frequencies was chosen. Consequently, the estimator had high gain at low frequencies and low gain in the spillover region. Iteration was required to get the final desired performance and stability. The final selected noise values are in Table 12.

Table 12. Selected estimator measurement noise.

Sensor	Root PSD Level	RMS Digital Noise
Rate	10.0 μm/s/Hz$^{1/2}$	316.0 μm/s
PMRS	0.15 μrad/Hz$^{1/2}$	4.74 μrad
SMRS	1.8 μrad/Hz$^{1/2}$	56.9 μrad
SMTS	5.1 μrad/Hz$^{1/2}$	161.3 μm

The PSD was assumed double sided. To get the RMS noise, the square root of the average PSD level was multiplied by $\sqrt{2}$ (to go from double sided to single sided), and then by $\sqrt{500}$ (to integrate from DC to Nyquist). The total multiplier was 31.623.

The RMS LOS resulting from this choice of OSS sensor noise was about 19 μrad. The vast majority of this was at frequencies well above the 5- to 10-Hz band where most of the energy was put into the structure and where high estimator gain was required.

3.3.5 Model of Local-Loop Rate Damping and LAC Used in HAC

Local-loop rate damping stabilizes the proof masses with respect to the PMA housings. Local-loop gain was set to 307 N-s/m. The relative rates are degrees of freedom available in the SPICE5A model (see Table 11). The 18 relative rates were multiplied by the local-loop gain, resulting in forces applied at the actuators (also relative forces). The local-loop gain provided about 70 per cent damping of the proof mass relative to the housing. The local-loop damping was the only true collocated rate feedback in the entire SPICE control system. This is because the PMA forces are themselves relative (i.e., housing force minus proof mass force) and, to get collocated rate feedback, the rates must also be relative.

The local-loop gain was augmented with the small damping inherent in the PMA flexures. This was computed to be 5.64 N-s/m. The total effective local-loop gain is 312.64 N-s/m.

The LAC damped the flexible modes of the structure. It was implemented with PMA forces proportional to housing rates. The LAC gain was 800 N-s/m. The structural rates at the PMA housings were multiplied by this gain, resulting in a force applied to the PMAs. Because the PMA forces are relative, while the housing rates are inertial, LAC is not inherently stable. In fact, the main purpose of local-loop damping was to stabilize the LAC loops. The LAC, in turn, by damping the flexible modes of the structure, helped to stabilize HAC.

The local-loop controller and the LAC system were modeled in the HAC design with no extra states. The housing and proof mass rates were modeled as the velocities of the 49 modes mapped into the 18 housing rates and 18 proof mass rates. The dynamics of the sensors themselves were not modeled. These analog loops were incorporated into the structural model before the continuous differential equation version of the structural model was converted to difference equation form to account for the finite sampling interval.

3.3.6 Stinger Cross-Axis Stiffness Model

The secondary mirror shaker stingers exhibited sufficient cross-axis stiffness to affect the SAVI rigid-body controller. Stinger cross-axis stiffness was never directly measured. However, the

effect of that stiffness was observed in measured SAVI rigid-body transfer functions. These transfer functions were measured with the stingers connected and disconnected. Based upon the change in the transfer functions, stinger cross-axis stiffness was approximated as 900 N/m per cross-axis degree of freedom. The SPICE5A structural model includes the six relevant cross-axis displacements. These displacements were scaled by the cross-axis stiffness, giving forces applied to the structure (with a negative sign) at the six relevant input force degrees of freedom. Modeling of the stinger cross-axis forces required no extra states.

3.3.7 The SAVI Controller Model

The SAVI controller was modeled and appended to the structural model (Fig. 15) before any of the other modeling features described were appended to the structural model. That is, the interaction of the SAVI controller with the SPICE5A structural model was modeled first, before inclusion of the stinger stiffness model, disturbance shaping filters, local-loop damping, or LAC. This simplified the process of modal truncation which is described later.

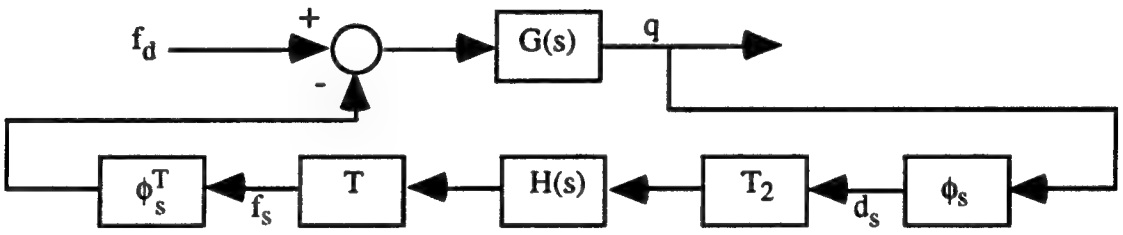

Legend:

G(s)	=	dynamic model of structure
f_d	=	6 input disturbances
q	=	49 modes of structure
ϕ_s	=	mode shapes at SAVI gaps
d_s	=	gap displacements
T_2	=	6 by 6 transform from SAVI gaps into 6 rigid-body degrees of freedom
H(s)	=	SAVI servo transfer function (identical for each degree of freedom)
T	=	6 by 6 transform from 6 rigid-body degrees of freedom into SAVI actuators (colocated at gaps)
f_s	=	SAVI actuator forces

Figure 15. Model of interaction of SAVI with the SPICE structure.

The coordinate transforms were computed as

$$T = \left(\phi^{T}_{s_{RB}}\right)^{-1}$$

and

$$T_2 = \left(\phi_{s_{RB}}\right)^{-1}$$

where the subscript RB means that the mode shape was extracted only for the six rigid-body modes.

The 6 by 6 transform T_2 maps gap displacements into the six rigid-body degrees of freedom under control. Similarly, the transform T maps the SAVI rigid-body control commands into SAVI actuator forces.

The SAVI servo, H(s), was the same for all six control degrees of freedom. The analog model of the servo included a 25-Hz digital servo, a digital delay of ~35 ms, and two analog low-pass filters. The analog representation of the digital servo is:

$$H_1(s) = \frac{K_0\left[\frac{s^2}{\omega_1^2} + \frac{(2)(0.4)s}{\omega_1} + 1\right]}{s\left(\frac{s}{\omega_2} + 1\right)\left(\frac{s^2}{\omega_3^2} + \frac{(2)(0.707)s}{\omega_3} + 1\right)}$$

where

$K_0 = 0.054665$ rad
$\omega_1 = 2\pi \times 0.25$ rad/s
$\omega_2 = 2\pi \times 8$ rad/s
$\omega_3 = 2\pi \times 9$ rad/s

The digital effects include the 25-Hz sampler and the 35-ms delay. These were approximated at low frequency with low-pass filters. The digital effects resulted in a phase loss at 1 Hz of about 19.8 deg. A set of filters that yield this much phase loss at 1 Hz is

$$H_2(s) = \frac{\omega_f^4}{\left(s^2 + 1.4\,\omega_f s + \omega_f^2\right)^2}$$

where

$$\omega_f = 2\pi \times 8.02 \text{ rad/s}$$

The transfer function of the additional two low-pass filters in the SAVI controller is

$$H_3(s) = \frac{K}{\left(s^2 + (2)(0.46)\omega_1 s + \omega_1^2\right)\left(s^2 + (2)(0.713)\omega_2 s + \omega_2^2\right)}$$

where

$$\omega_1 = 2\pi \times 28.6 \text{ rad/s}$$
$$\omega_2 = 2\pi \times 25.0 \text{ rad/s}$$
$$K = \omega_1^2 \omega_2^2 \quad (\text{rad/s})^4$$

The total servo model is

$$H(s) = H_1(s)\, H_2(s)\, H_3(s)$$

There are 12 states per SAVI degree of freedom, for a total of 72 states. These states were coupled with the structural model as shown in Figure 15. It was neither desirable nor necessary to model all 72 SAVI states once the SAVI loops were closed with the structural model. The 72 states were carried into the interaction to obtain the full effect of SAVI on the modes of the structure. However, many of the 72 states were not relevant to the HAC problem once their effect on the structure was taken into account. Modal reduction was used to reduce the number of states carried into the HAC design. In the modal reduction process:

(1) First, the SAVI controller was modeled and its interaction with the structure was modeled.

(2) Cross-axis stinger stiffness was modeled (this greatly affects the SAVI controller).

(3) The new structural model was put into state-space form.

(4) The system was transformed into modal form (Ref. 33).

(5) Unnecessary modes were truncated from the model by inspection of the modal frequencies and damping values. The structural modes were all retained; SAVI modes below a few hertz were retained. The SAVI modes corresponding to the low-pass filters and digital effects filters were eliminated. Table 13 is a listing of the modes retained and eliminated.

(6) The truncated model was saved for the HAC design.

Table 13. Modes retained from combined SAVI/structural model.

No.	Freq. (Hz)	ζ (%)	Description	States Retained	No.	Freq. (Hz)	ζ (%)	Description	States Retained
1	0.00157	100.00	SAVI	Deleted	47	7.97	71.61	SAVI Digital Effects	Deleted
2	0.00158	100.00	SAVI	Deleted	48	7.97	71.27	SAVI Digital Effects	Deleted
3	0.00434	100.00	SAVI	Deleted	49	7.97	71.30	SAVI Digital Effects	Deleted
4	0.00615	100.00	SAVI	Deleted	50	7.97	71.31	SAVI Digital Effects	Deleted
5	0.00618	100.00	SAVI	Deleted	51	7.97	71.32	SAVI Digital Effects	Deleted
6	0.00621	100.00	SAVI	Deleted	52	8.07	70.12	SAVI Digital Effects	Deleted
7	0.23	36.08	Rigid-Body/SAVI	2	53	8.07	70.13	SAVI Digital Effects	Deleted
8	0.23	35.96	Rigid-Body/SAVI	2	54	8.07	70.14	SAVI Digital Effects	Deleted
9	0.23	35.87	Rigid-Body/SAVI	2	55	8.07	70.17	SAVI Digital Effects	Deleted
10	0.28	27.94	Rigid-Body/SAVI	2	56	8.08	69.86	SAVI Digital Effects	Deleted
11	0.44	10.52	Rigid-Body/SAVI	2	57	8.08	69.86	SAVI Digital Effects	Deleted
12	0.44	10.40	Rigid-Body/SAVI	2	58	15.52	0.32	Flexible Body	2
13	0.70	100.00	SAVI	1	59	16.06	0.33	Flexible Body	2
14	0.70	100.00	SAVI	1	60	16.92	0.44	Flexible Body	2
15	0.70	100.00	SAVI	1	61	19.35	0.29	Flexible Body	2
16	0.72	100.00	SAVI	1	62	19.95	0.73	Flexible Body	2
17	0.78	100.00	SAVI	1	63	21.01	0.43	Flexible Body	2
18	0.78	100.00	SAVI	1	64	22.19	0.27	Flexible Body	2
19	1.56	77.91	SAVI	2	65	24.14	0.82	Flexible Body	2
20	1.56	77.90	SAVI	2	66	24.22	0.38	Flexible Body	2
21	1.56	77.89	SAVI	2	67	25.15	71.30	SAVI Low-Pass Filter	Deleted
22	1.56	77.89	SAVI	2	68	25.15	71.30	SAVI Low-Pass Filter	Deleted
23	1.57	77.25	SAVI	2	69	25.15	71.30	SAVI Low-Pass Filter	Deleted
24	1.57	77.25	SAVI	2	70	25.15	71.30	SAVI Low-Pass Filter	Deleted
25	4.63	0.02	PMA	2	71	25.15	71.30	SAVI Low-Pass Filter	Deleted
26	4.84	0.02	PMA	2	72	25.15	71.30	SAVI Low-Pass Filter	Deleted
27	4.85	0.02	PMA	2	73	28.65	46.00	SAVI Low-Pass Filter	Deleted
28	4.95	0.00	PMA	2	74	28.65	46.00	SAVI Low-Pass Filter	Deleted
29	4.95	0.02	PMA	2	75	28.65	46.00	SAVI Low-Pass Filter	Deleted
30	4.96	0.02	PMA	2	76	28.65	46.00	SAVI Low-Pass Filter	Deleted
31	4.98	0.02	PMA	2	77	28.65	46.00	SAVI Low-Pass Filter	Deleted
32	4.98	0.02	PMA	2	78	28.65	46.00	SAVI Low-Pass Filter	Deleted
33	4.98	0.02	PMA	2	79	31.04	0.70	Flexible Body	2
34	4.98	0.02	PMA	2	80	32.63	0.70	Flexible Body	2
35	4.98	0.02	PMA	2	81	33.70	0.70	Flexible Body	2
36	4.99	0.02	PMA	2	82	35.04	0.70	Flexible Body	2
37	4.99	0.02	PMA	2	83	35.22	0.70	Flexible Body	2
38	4.99	0.02	PMA	2	84	36.33	0.70	Flexible Body	2
39	4.99	0.02	PMA	2	85	39.38	0.70	Flexible Body	2
40	5.03	0.02	PMA	2	86	41.59	0.70	Flexible Body	2
41	5.04	0.02	PMA	2	87	42.11	0.70	Flexible Body	2
42	5.04	0.02	PMA	2	88	44.45	0.70	Flexible Body	2
43	6.80	0.10	Torsion	2	89	46.40	0.70	Flexible Body	2
44	7.83	0.10	Bending	2	90	46.79	0.70	Flexible Body	2
45	7.88	0.10	Bending	2	91	49.71	0.70	Flexible Body	2
46	7.97	71.60	SAVI Digital Effects	Deleted		**TOTAL STATES RETAINED = 116**			

The deleted modes included very low-frequency SAVI states, modes associated with modeling the digital effects, and the low-pass filters of the SAVI system. The total number of states retained was 116. (Modes with unity damping are single state modes; modes with damping less than unity were described with two states, as is standard.)

3.3.8 Regulator Design Process

The regulator is a matrix that maps the states of the system into force commands to the PMAs. If the states of the system were known exactly, the HAC controller would simply consist of a matrix that multiplies those states at each time step, yielding 18 PMA force commands. Because direct knowledge of the system states is not available, estimates are computed using an estimator. However, in the LQG approach used for the HAC, the regulator problem is decoupled from the estimation problem and they are computed separately. The regulator and estimator are tuned so that they are balanced with respect to each other.

The necessary ingredients for the regulator are a state-space model of the plant to be controlled, weighting matrices for control effort and cost functions, and a Riccati solver that computes the final regulator gain matrix.

The steps to building a SPICE state-space model to be regulated are:

(1) Begin with the 116-state model that includes the 49 structural modes coupled with the SAVI rigid-body controller. This model also includes the effects of stinger cross-axis stiffness.

(2) Include the effects of PMA local-loop damping and LAC, as described. There are no additional states.

(3) Append the 24-state disturbance shaping filter model to the main model. The inputs to the six shaping filters are white noise; the outputs are forces applied at the six input disturbance degrees of freedom, as described earlier. The number of states in the model is now 140.

(4) Discretize the model to the sample interval of 0.001 s. This is done using the MATRIXx command, DISCRETIZE, with the default option of zero-order hold.

(5) Construct the 18 digital low-pass filters. Each filter is first order, with a break frequency at 10 Hz, and unity DC gain. The filter is constructed so that there is no time delay. This results in a nonzero "D" matrix. The difference equation of this filter is

$$c_{i+1} = a\, c_i + b\, u_{i+1}$$

in which

$$a = 1 - b = e^{-\omega T}$$
$$\omega = 2\pi \times 10 \text{ rad/s}$$
$$T = 0.001 \text{ s}$$

(6) Append the 18 digital filters to the main digital model. The inputs to the filters are HAC commands; the outputs are shaped HAC commands to the 18 PMAs. These filters shape the overall transfer function of the plant, forcing regulator roll-off, and gain-stabilizing the regulator at high frequency. The number of states in the model is now 158.

The 158-state model is the final system to be regulated. The only inputs that need to be retained are the 18 PMA force inputs and the 6 disturbance inputs. The other inputs have already served their purpose in SAVI and stinger cross-axis modeling. The only outputs that need to be retained for HAC design purposes are the 36 measurements, 2 LOS, and 18 PMA strokes. The other outputs have already served their purpose in modeling SAVI, stinger cross-axis stiffness, local-loop damping, and LAC.

The next major step is the construction of the cost functions. Two weighting matrices are used in LQG regulator design, the control weighting matrix and the state weighting matrix. The control weighting matrix places a relative constraint on the amount of control force to be applied to each PMA; the greater the weight, the less force will be used. The state weighting matrix places constraints on the states of the system; the greater the weight, the more control force will be used to reduce those states.

Weighting matrices are in terms of inverse covariance matrices. Weighting is proportional to the inverse of the desired control force or state covariance matrices. The selection of the control force weighting matrix was somewhat arbitrary. Let

$\sigma_f = 85.0$ N desired control force standard deviation, per PMA

Then

$\sigma_f^2 = 7225.0$ N^2 desired control force variance, per PMA

Then

$w_f = 1/\sigma_f^2$ control force weighting, per PMA

And

$W_f = w_f I_{18}$ control force weighting matrix for all 18 PMAs

where I_{18} is an 18 by 18 identity matrix. The control weighting matrix is diagonal with equal values along the diagonal, so that the PMAs share equally in the control effort.

The state weighting matrix is more involved. The first step is to build the matrix mapping structural states into parameters to be minimized. For the HAC design, the parameters included in this cost function are LOS x and y, torsion about the optical axis as measured by the SMTSs, and PMA strokes. All of these are convenient outputs of the 158-state model (Table 11). Outputs 37 and 38 are LOS x and y. Strokes are outputs 39 through 56. Torsion is computed as a linear combination of the secondary mirror translation sensors.

The SPICE5A model outputs OSS measurements in local coordinates. Figure 16 shows the relationship between global and local coordinates for the SMTSs. For the purpose of the cost function, torsion is computed as the sum of SMTS8Y and SMTS9Y, in the local SMTS frames.

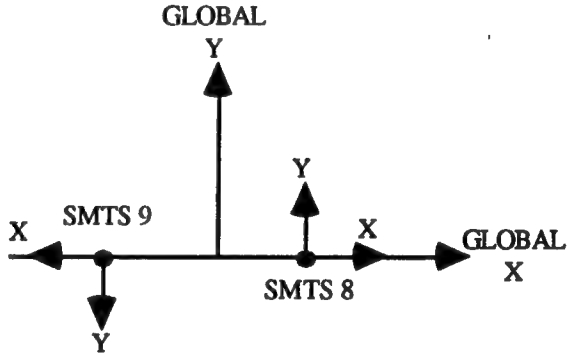

Figure 16. Global and SMTS local coordinates.

Let C be the matrix that maps states into model outputs. Then the components of the cost function are computed as

- LOS:

  $H_{los} = C(37:38, :)$ (radian/modal displacement unit); rows 37 and 38 of the C matrix

- Torsion:

  $H_{tors} = C(34,:) + C(36, :)$ (radian/modal displacement unit); sum of rows 34 (SMTS 8Y) and 36 (SMTS 9Y)

- Stroke:

  $H_{str} = C(39:56, :)$ (meter/modal displacement unit); rows 39 through 56 of C

The total cost function is the concatenation of the three components:

$$H_{cost} = \begin{bmatrix} H_{los} \\ H_{tors} \\ H_{str} \end{bmatrix}$$

The 21 by 158 matrix, H_{cost}, maps states into parameters to be regulated. The primary parameters to be regulated are the two LOS components. Torsion is regulated because it is nearly orthogonal to the LOS, yet very controllable. Stroke is regulated to a very small degree. Hardware tests were run to determine the benefit of including stroke in the cost function. A very light stroke constraint seemed to reduce low-frequency PMA response, with no adverse effect upon LOS performance.

After some iteration, the following cost function weights were selected:

$$\begin{aligned} \sigma_{losx} &= 5.6 \times 10^{-6} \text{ rad} \\ \sigma_{losy} &= 5.6 \times 10^{-6} \text{ rad} \\ \sigma_{tors} &= 0.12 \times 10^{-3} \text{ m} \\ \sigma_{str} &= 50. \times 10^{-3} \text{ m} \end{aligned}$$

Then, the individual weighting values are

$$\begin{aligned} w_{losx} &= 1/\sigma_{losx}^2 \\ w_{losy} &= 1/\sigma_{losy}^2 \\ w_{tors} &= 1/\sigma_{tors}^2 \\ w_{str} &= 1/\sigma_{str}^2 \end{aligned}$$

and the complete cost function weighting matrix is

$$W_{cf} = \begin{bmatrix} w_{losx} & 0 & 0 & 0 \\ 0 & w_{losy} & 0 & 0 \\ 0 & 0 & w_{tors} & 0 \\ 0 & 0 & 0 & w_{str} I_{18} \end{bmatrix}$$

The final state weighting matrix is

$$W_x = H_{cost}^T W_{cf} H_{cost}$$

All of the states of the plant are in the regulator model. These include the basic structure, the SAVI controller, the disturbance shaping filters, and the digital low-pass filters. The portions of the model required for computing the regulator are the state transition matrix, known as the "A" matrix, and the part of the input, or "B", matrix that maps PMA force commands into states. The regulated system is then represented in state-space form as:

$$x_{i+1} = A\, x_i + B_{pma}\, u_i$$

where

x = 158 states

u = regulator commands

B_{pma} = first 18 columns (corresponding to PMA inputs) of the system input matrix

The standard Riccati approach is used. In MATRIXx, the command

$$K_r = \text{DREGULATOR}(A, B_{pma}, W_x, W_f)$$

is executed to calculate the regulator gain matrix from the matrices A, B_{pma}, W_f, and W_x. The resulting regulator commands to be applied to the input of the digital low-pass filters are

$$u_i = -\, K_r\, x_i$$

The closed-loop response of the regulated system, for the six disturbances, is

$$x_{i+1} = (A - B_{pma}\, K_r)\, x_i + B_{dis}\, d_i$$

where

d = vector of six white noise inputs to the disturbance shaping filters

B_{dis} = system input matrix for the six disturbances (columns 19 - 24 of B)

The analog noise that drives the six analog shaping filters must be discretized along with the shaping filters. The equivalent digital noise (random DC to 500 Hz) that drives the discrete shaping filters has a standard deviation of

$$\sigma_{digital} = \sigma_{analog} \sqrt{1000}$$

The values are

σ_{smx} = 31.62 x 40. = 1264.8 N ; SM X shaker
σ_{smy} = 31.62 x 20. = 632.4 N ; SM Y shaker
σ_{smz} = 31.62 x 20. = 632.4 N ; SM Z shaker
σ_{vea1} = 31.62 x 49. = 1549.38 N ; SAVI vertex 1 resultant
σ_{vea2} = 31.62 x 75.6 = 2390.5 N ; SAVI vertex 2 resultant
σ_{vea3} = 31.62 x 91. = 2877.42 N ; SAVI vertex 3 resultant

The outputs of the six 5- to 10-Hz digital shaping filters have force RMS levels of 40.0, 20.0, 20.0, 49.0, 75.6, and 91.0 N, respectively, as desired.

The predicted components of the residual LOS jitter, for the 100-μrad open-loop input disturbance level, are given by

LOS_x = 0.54 μrad RMS
LOS_y = 0.84 μrad RMS

As will be seen later, this is roughly one-half the final performance level of the HAC system. This represents a good balance between the regulator and the estimator.

3.3.9 Estimator Design Process

The regulator presumes knowledge of the system states. Only 18 of the states are known exactly, the 18 digital low-pass filter states. These are known because they are updated within the control processor. The remaining 140 states are estimated using the 36 available measurements (18 PMA housing rates plus 18 OSS displacements). A standard steady-state Kalman filter is used. The required matrices for constructing the Kalman gain matrix are

- A 140 by 140 subset of the state transition matrix, denoted A_e, corresponding to the 140 unknown states to be estimated (these include the structure, the SAVI, and the disturbance filter states),
- A 36 by 140 subset of the system output matrix, denoted C_e, which maps the 140 unknown states into the 36 measurements,

- A 140 by 6 subset of the system input matrix, denoted B_d, which maps the 6 digital white noise disturbance inputs into the unknown states,
- The 6 by 6 covariance matrix of the input white noise, denoted Q, and
- The 36 by 36 covariance matrix of measurement noise, denoted R.

The matrices A_e, C_e, and B_d are obtained by extracting the appropriate partitions from the already existing system A, C, and B matrices.

The measurement noise covariance matrix is a diagonal matrix of variances computed using the noise values specified in Subsection 3.3.4. These values are repeated:

$$\sigma_{vel} = 316. \times 10^{-6} \text{ m/s}$$
$$\sigma_{pmrs} = 4.74 \times 10^{-6} \text{ rad}$$
$$\sigma_{smrs} = 56.9 \times 10^{-6} \text{ rad}$$
$$\sigma_{smts} = 161.3 \times 10^{-6} \text{ m}$$

The measurement noise covariance matrix, R, is computed as

$$R = \begin{bmatrix} \sigma_{vel}^2 I_{18} & 0 & 0 & 0 \\ 0 & \sigma_{pmrs}^2 I_{12} & 0 & 0 \\ 0 & 0 & \sigma_{smrs}^2 I_2 & 0 \\ 0 & 0 & 0 & \sigma_{smts}^2 I_4 \end{bmatrix}$$

In estimator design, process noise is expressed in terms of state noise. This is obtained by mapping the input white noise disturbances into system states via the input matrix. For the HAC estimator, this is

$$Q_x = B_d \, Q \, B_d^T$$

where Q is the covariance of the white noise disturbance. Using the previously defined variables, Q is

$$Q = \text{diag} \{ [\sigma_{smx}^2 \;\; \sigma_{smy}^2 \;\; \sigma_{smz}^2 \;\; \sigma_{vea1}^2 \;\; \sigma_{vea2}^2 \;\; \sigma_{vea3}^2] \}$$

where diag { [ ] } is a diagonal matrix whose elements are contained in the enclosed vector.

The Kalman gain matrix is computed using the MATRIXx command, DESTIMATOR:

$$K_e = \text{DESTIMATOR}(A_e , C_e , Q_x , R)$$

Propagation of the estimator alone is

$$x_{i+1} = (A_e - K_e C_e) x_i + K_e y_i$$

where

$$y = 36 \text{ measurements}$$

3.3.10 The HAC Implementation as Single Matrix Multiplication

The HAC was implemented so that the PMA force commands can be limited to preset values or completely nulled. Upon startup of the HAC, the output PMA commands are nulled for the first 10 s. This allows the estimator to reach steady state and gives the OSS high-pass filters time to remove OSS biases (Subsection 3.3.11). After 10 s, the output forces are sent to the digital-to-analog converters. The forces are limited to 30 N to reduce the likelihood of PMA saturation. Force-limiting requires radical modification to the normal way of implementing an LQG regulator/estimator. This section summarizes the implementation of the regulator and estimator for the HAC.

The states to be propagated with the controller include the estimated states, denoted x, and the digital low-pass filter states, denoted z. The estimated states are propagated using measurements, y, and commanded forces, f. The propagation of the estimated states is

$$x_{i+1} = (A_e - K_e C_e) x_i + K_e y_i + B_{plt} f_i$$

where A_e, K_e, and C_e are as previously defined and B_{plt} is the input matrix that maps the 18 PMA force commands into the 140 estimated states.

Note that B_{plt} is not readily available as a partition of the full system B matrix. Instead, the B matrix must be used just before concatenation of the 18 digital low-pass filters. The matrix B_{plt}

maps the outputs of the digital low-pass filters into the 140 estimated states (which include the structure, the SAVI, and the disturbance shaping filters).

The digital low-pass filter states are put into state-space form as

$$z_{i+1} = A_f z_i + B_f u_i$$
$$f_i = c_f z_i + D_f u_i$$

where u is the vector of regulator commands.

But the regulator commands are

$$u_i = - K_f z_i - K_s x_i$$

where K_f and K_s are partitions of the regulator gain matrix, K_r, mapping low-pass filter states and estimated states, respectively, into control commands. Assuming, for descriptive purposes, that the low-pass filter states precede the estimated structural states, the regulator gain matrix is partitioned as

$$K_r = [K_f \mid K_s]$$

The command forces to the PMAs may now be expressed as

$$f_i = (C_f - D_f K_f) z_i - D_f K_s x_i$$

The forces at interval i + 1 are

$$f_{i+1} = (C_f - D_f K_f) z_{i+1} - D_f K_s x_{i+1}$$

For the digital filters with the difference equation defined in Subsection 3.3.8:

$$f_{i+1} = a c_i + b u_{i+1}$$

the filter states are related to output forces as

$$z_{i+1} = C_f^{-1} A_f f_i$$

Then, propagation of the output forces can be written as

$$f_{i+1} = (I - D_f K_f C_f^{-1}) A_f f_i - D_f K_s x_{i+1}$$

Substituting for x_{i+1} gives

$$f_{i+1} = (A_f - D_f K_f C_f^{-1} A_f - D_f K_s B_{plt}) f_i - D_f K_s (A_e - K_e C_e) x_i - D_f K_s K_e y_i$$

With the inputs to state propagation defined as

$$v = \begin{bmatrix} y \\ f \\ x \end{bmatrix}$$

and the outputs of propagation defined as

$$w = \begin{bmatrix} f \\ x \end{bmatrix}$$

the output vector is propagated as

$$w_{i+1} = A_{hac} v_i$$

where A_{hac} is the single matrix implementing the HAC and allowing for limiting of the output command forces, f. Then A_{hac} is constructed as

$$A_{hac} = \begin{bmatrix} A_{11} A_{12} A_{13} \\ A_{21} A_{22} A_{23} \end{bmatrix}$$

where

$$A_{11} = - D_f K_s K_e$$
$$A_{12} = A_f - D_f K_f C_f^{-1} A_f - D_f K_s B_{plt}$$
$$A_{13} = - D_f K_s (A_e - K_e C_e)$$
$$A_{21} = K_e$$
$$A_{22} = B_{plt}$$
$$A_{23} = A_e - K_e C_e$$

The matrix, A_{hac}, is dimensioned 158 by 194. This matrix is computed as described and stored for final assembly into the matrix in the Star array processor.

3.3.11 Addition of Low-Frequency High-Pass Filters

The OSS biases are removed using digital high-pass filters implemented in the array processor. High-pass filter is accomplished by subtracting a low-pass filter from the input measurements.

$$\frac{s}{s+a} = 1 - \frac{a}{s+a}$$

The procedure for OSS filtering is

(1) Eighteen identical first-order low-pass filters with unity DC gain and break frequency at 0.05 Hz are constructed. The OSS low-pass filter states are denoted as c. The difference equation of these filters is:

$$c_{i+1} = a\, c_i + b\, y_i$$

where

y = 18 input OSS measurements
c = filter states
$a = 1 - b = e^{-\omega T}$
$\omega = 2\,\pi\, 0.05$ rad/s
$T = 0.001$ s

(2) Propagation of HAC commanded forces is augmented as

$$f_{i+1} = \ldots \; - T_{fo}\, c_i$$

where T_{fo} is the 18 by 18 partition of $(- D_f K_s K_e)$ that maps OSS measurements into force outputs.

(3) Similarly, estimated states are augmented by

$$x_{i+1} = \ldots - T_{xo}\, c_i$$

where T_{xo} is the 140 by 18 partition of K_e that maps OSS measurements into estimated states

High-pass filters are also applied to the output force commands. These are 0.1 Hz filters with unity DC gain. These 18 filters are implemented using integral feedback on the output forces (Fig. 17) in which

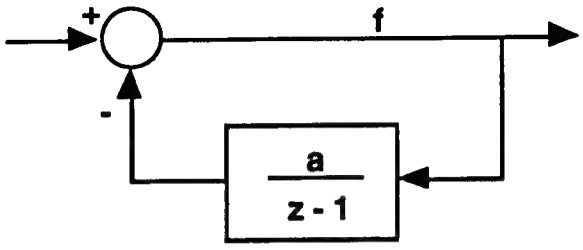

Figure 17. Integral feedback on output forces.

$$a = \omega T$$
$$\omega = 2 \pi 0.1 \text{ rad/s}$$
$$T = 0.001 \text{ s}$$

There are 18 states for integration of the output forces. The difference equation for each filter is

$$g_{i+1} = g_i + a f_i$$

Propagation of the output force commands is then augmented as follows:

$$f_{i+1} = \ldots - g_i$$

3.3.12 Packaging for Implementation in Star Array Processor

The implementation of the HAC system in the Star array processor is summarized in Figure 18. The first 18 outputs are the PMA force commands. The next two outputs are the LOS as computed using the 18 OSS measurements and the LOS equation. Outputs 21 and 22 are the LOS as estimated by the Kalman filter. These 22 outputs are limited and sent to the digital-to-analog converters. The next 140 outputs are the estimated states. The following 18 outputs are the PMA integrator states used for implementing high-pass filtering of the PMA force commands. The last 18 outputs are the OSS low-pass filter states, used for high-pass filtering the OSS measurements. The 198 outputs are fed back as the first 198 inputs to the matrix multiplication in the Star VP-3. The 18 OSS measurements and the 18 PMA housing rates are appended to these, bringing the total number of inputs to 234.

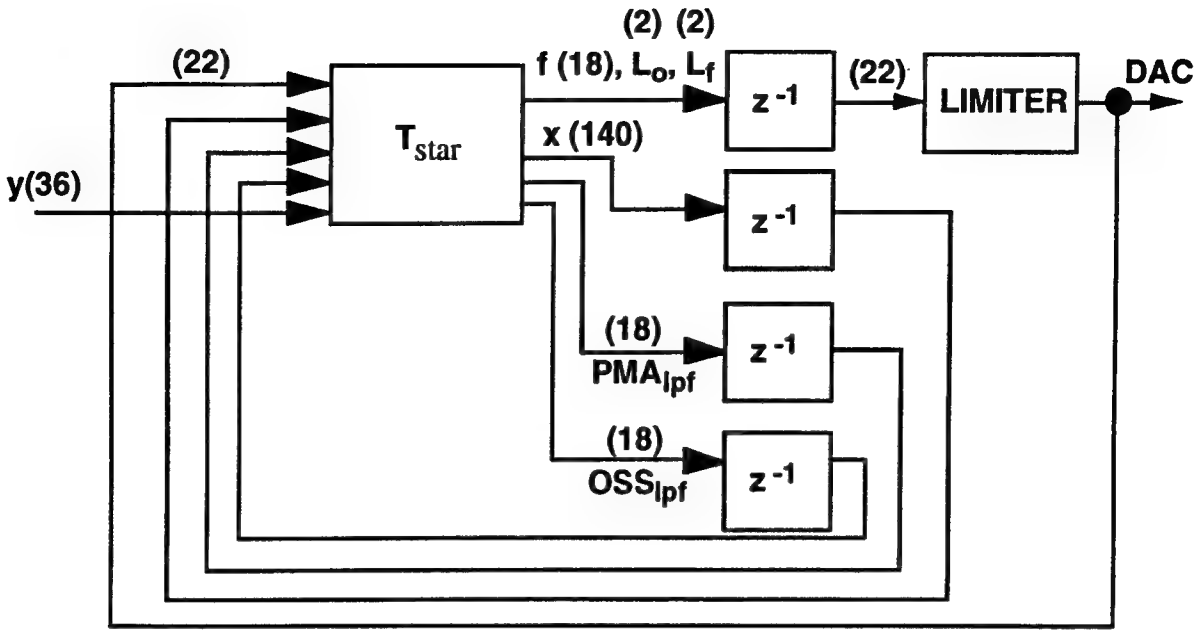

Figure 18. Implementation of HAC system in the Star VP-3 array processor.

The VP-3 does a 198 by 234 matrix multiplication at a 1-kHz rate. The output signals are limited. In practice, limiting only affects the 18 PMA commands. The limited commands are fed back into the Star VP-3 so that the Kalman filter has knowledge of the limiting. The total delay from analog-to-digital sampling to digital-to-analog sampling is precisely one sample interval, or 0.001 s.

The A_{hac} matrix derived earlier must be prepared before it can be loaded into the Star VP-3. The preparation functions include

- Reordering inputs and outputs to match those used in the VP-3,
- Converting 36 inputs and 22 outputs from engineering units into fixed point integer,
- Adding partitions for OSS LOS and estimated LOS, and
- Adding PMA command and OSS filters.

The first function, reordering, is accomplished by appropriate partitioning of A_{hac} and reassembling the partitions into T_{star}, the matrix in the array processor. The second function is accomplished with proper scaling of the 36 inputs and 22 outputs. The third function involves adding 2 partitions to T_{star}, one that maps the 18 OSS measurements into LOS x and y and one that uses the output matrix for the estimated states, C_e, to map the 140 estimated states into the LOS. Rows 37 and 38 of C_e, which correspond to the LOS, are used for this. The PMA and

OSS filters are added by appending appropriate partitions to T_{star} and modifying the force command outputs and state propagation using the equations derived in Subsection 3.3.11.

All of these functions are carried out in the MATRIXx command file BLDHACMAT4F.MX. An edited version of this file with added comments is shown in Figure 19. The output of this procedure is the final 198 by 234 matrix, T_{star}, saved into GSTAR.DAT. This file is loaded into the array processor with no additional processing.

3.3.13 Summary Of Closed-Loop System Design

Figure 20 summarizes the entire closed-loop system model. Each of the blocks contained within the figure have been discussed in detail in previous sections.

3.4 MAIN HAC TESTS

The HAC testing consisted of three main phases:

(1) Preliminary checkout tests using a 25:1 design,

(2) A series of development tests using the 50:1 design. During these tests, final weighting and cost function parameters were selected, and the OSS and PMA commands high-pass filters were added.

(3) A series of final HAC tests using the final design. The final design in no way represents the maximum performance attainable with this system. The final design was settled upon because it satisfied two objectives:

- The goal of 50:1 attenuation from 5 to 500 Hz was exceeded, and
- The system can be used for demonstration any time of day or night, without concern for environmental conditions. A higher performing system would have been more susceptible to atmospheric and wind disturbances, and thereby unable to consistently repeat high performance levels.

The tests of the final HAC test series were divided into three main subdivisions:

(1) Performance tests. During these tests, the final performance of the HAC system, as compared to LAC and the open-loop structure, was measured.

(2) Gain margin tests. This was a short series of tests to measure the stability margin of the system by applying gain errors to the HAC system.

(3) Transfer function tests. Various open- and closed-loop transfer functions of the HAC system were measured and compared with predictions.

```
// BLDHACMAT4F.MX
//
resize('sstack',1500000)
//
// This version includes 18 PMA command and OSS high-pass filters
//
// set dimensions
//
npma=18;                // number of PMAs
nmeas=36;               // number of HAC measurements
noss=18;                // number of OSS measurements
nvel=18;                // number of velocity measurements
nrow=198;               // number of rows of STAR matrix
ncol=234;               // number of columns in STAR matrix
//
// load TSTAR matrix and Kalman filter LOS output matrix
// (TSTAR as output from program DISSP5A2F.MX)     (This is Ahac)
// (Note: HFLOS maps HAC filter states into LOS)    (Subset of Ce)
//
load 'tstar.dat' tstar hflos
[nr nc]=size(tstar);                    // rows in TSTAR ; columns in TSTAR
ns=nr-npma;                             // number of HAC states  (this will be 140)
nsf=18;                                 // number of augmented filter states (for each filter)
//
// order of TSTAR as built by DISSP5A.MX      (this is the Ahac matrix)
//
// outputs:
//        PMA cmds                 18
//        states                   ns
// inputs:
//        vel meas                 18
//        OSS meas                 18
//        limited cmds             18
//        states                   ns
//
// desired order for implementation in STAR
//
// outputs:
//        PMA cmds                 18
//        OSS LOS                   2
//        filtered LOS              2
//        states                   ns
//        PMA LPF states           18
//        OSS LPF states           18
// inputs:
//        limited cmds             18
//        OSS LOS                   2
//        filt LOS                  2
//        states                   ns
//        LPF states               36
//        OSS meas                 18
//        vel meas                 18
//
// note:  states are ordered in TSTAR as follows:  (This is order of estimated states in Ahac)
//        structural states
//        disturbance states
```

Figure 19. MATRIXx command file with added comments.

```
// load OSS LOS matrix (assumes HAC design order, local coord)
//
load 'kal:hoss.dat' hoss
//
// Extract partition of HFLOS corresponding to estimated states only
// (HFLOS as input is in state order of DISSP5A.MX)
//
hflos=hflos(:,[19:ns+npma]);
//
// partition input TSTAR:
//
tpv=tstar(1:npma,1:nvel);                          // vel meas to PMA cmds
tpo=tstar(1:npma,[nvel+1:nvel+noss]);              // OSS meas to PMA cmds
tpu=tstar(1:npma,[nmeas+1:nmeas+npma]);            // cmds (last cycle) to cmds
tpx=tstar(1:npma,[nmeas+npma+1:nc]);               // HAC states to cmds
txv=tstar([npma+1:nr],1:nvel);                     // vel meas to HAC states
txo=tstar([npma+1:nr],[nvel+1:nvel+noss]);         // OSS meas to HAC states
txu=tstar([npma+1:nr],[nmeas+1:nmeas+npma]);       // last cycle cmds to states
txx=tstar([npma+1:nr],[nmeas+npma+1:nc]);          // last cycle states to states
//
// build PMA integrators, for use in high-pass filtering PMA cmds
//
wnlpf=2*pi*.1;
num=wnlpf;
den=[1 0];
[slpf nslpf]=sform(num,den);
tsamp=1./1000.;
slpf=discretize(slpf,nslpf,tsamp);
stemp=slpf;
nstemp=nslpf;
for k=2:18;[stemp nstemp]=append(stemp,nstemp,slpf,nslpf);end;
slpf=stemp;
nslpf=nstemp;
[alpf blpf clpf dlpf]=split(slpf,nslpf);
clear dlpf
//
// build OSS low-pass filters, for use in high-pass filtering OSS
//
wnlpf=2*pi*.05;
num=wnlpf;
den=[1 wnlpf];
[slpf nslpf]=sform(num,den);
tsamp=1./1000.;
slpf=discretize(slpf,nslpf,tsamp);
stemp=slpf;
nstemp=nslpf;
for k=2:18;[stemp nstemp]=append(stemp,nstemp,slpf,nslpf);end;
slpf=stemp;
nslpf=nstemp;
[alpf2 blpf2 clpf2 dlpf2]=split(slpf,nslpf);
clear dlpf dlpf2
//
tff=alpf;                  // state transition matrix for PMA integrators
tgg=alpf2;                 // state transition matrix for OSS low-pass filters
clear alpf alpf2
tfu=blpf;                  // input matrix for PMA integrators
```

Figure 19. Continued.

```
tgo=blpf2;              // input matrix for OSS low-pass filters
clear blpf blpf2
tpf=-clpf;              // maps PMA integrator states into change to force commands
tpg=-tpo*clpf2;         // maps OSS filter states into change to force commands
txg=-txo*clpf2;         // maps OSS filter states into change to estimated states
clear clpf clpf2
//
// rebuild TSTAR for STAR implementation
//
n18x2=0.*ones(18,2);
n2x2=0.*ones(2,2);
n2xns=0.*ones(2,ns);
n2xnsf=0.*ones(2,nsf);
//
// This reassembles STAR matrix using proper STAR ordering of inputs and outputs
// It also includes OSS and Kalman filter LOS outputs,
// It also includes PMA and OSS high-pass filtering
//
tstar=[tpu n18x2 n18x2 tpx tpf tpg tpo tpv; ..
  n18x2' n2x2 n2x2 n2xns n2xnsf n2xnsf hoss n18x2'; ..
  n18x2' n2x2 n2x2 hflos n2xnsf n2xnsf n18x2' n18x2'; ..
  txu n2xns' n2xns' txx 0.*ones(ns,nsf) txg txo txv; ..
  tfu 0.*ones(nsf,4+ns) tff 0.*ones(nsf,nsf+nvel+noss); ..
  0.*ones(nsf,18+4+ns+nsf) tgg tgo 0.*ones(nsf,nvel)];
//
// This next section scales inputs and outputs
// Define 0-peak measurements in engineering units
// (mechanical motions)
//
pkvel=.3*ones(1,18);                        // vel meas
pkpmtlt=ones(1,12)*240.e-6;                 // PMRS
pksmtlt=[1406. 1365.]*1e-6;                 // SMRS
pksmtrn=[4.161 4.202 4.218 4.225]*1e-3;     // SMTS
py=[pkpmtlt pksmtlt pksmtrn pkvel];         // all
//
// define 0-peak of outputs in engineering units
//
pkpma=40.*ones(1,npma);             // PMA cmds
pklososs=[1 1]*500.e-6;             // LOS from OSS
pklosflt=[1 1]*500.e-6;             // LOS from Kalman filter
//
pu=[pkpma pklososs pklosflt];       // all
//
// scale TSTAR
// (15 bit ADCs and 16 bit DACs)
//
sy=2*py/2**15;                      // meas. eng. units per LSB
su=(2**16)*ones(pu)./(2*pu);        // output LSBs per eng. unit
su=[su ones(1,ns+nsf+nsf)];         // 1s for states
sy=[ones(su)./su sy];               // 1s for states
tstar=diag(su)*tstar*diag(sy);      // final scaling of TSTAR
//
// output closed-loop HAC matrix to GSTAR.DAT
//
save 'gstar.dat' tstar
return
```

Figure 19. Concluded.

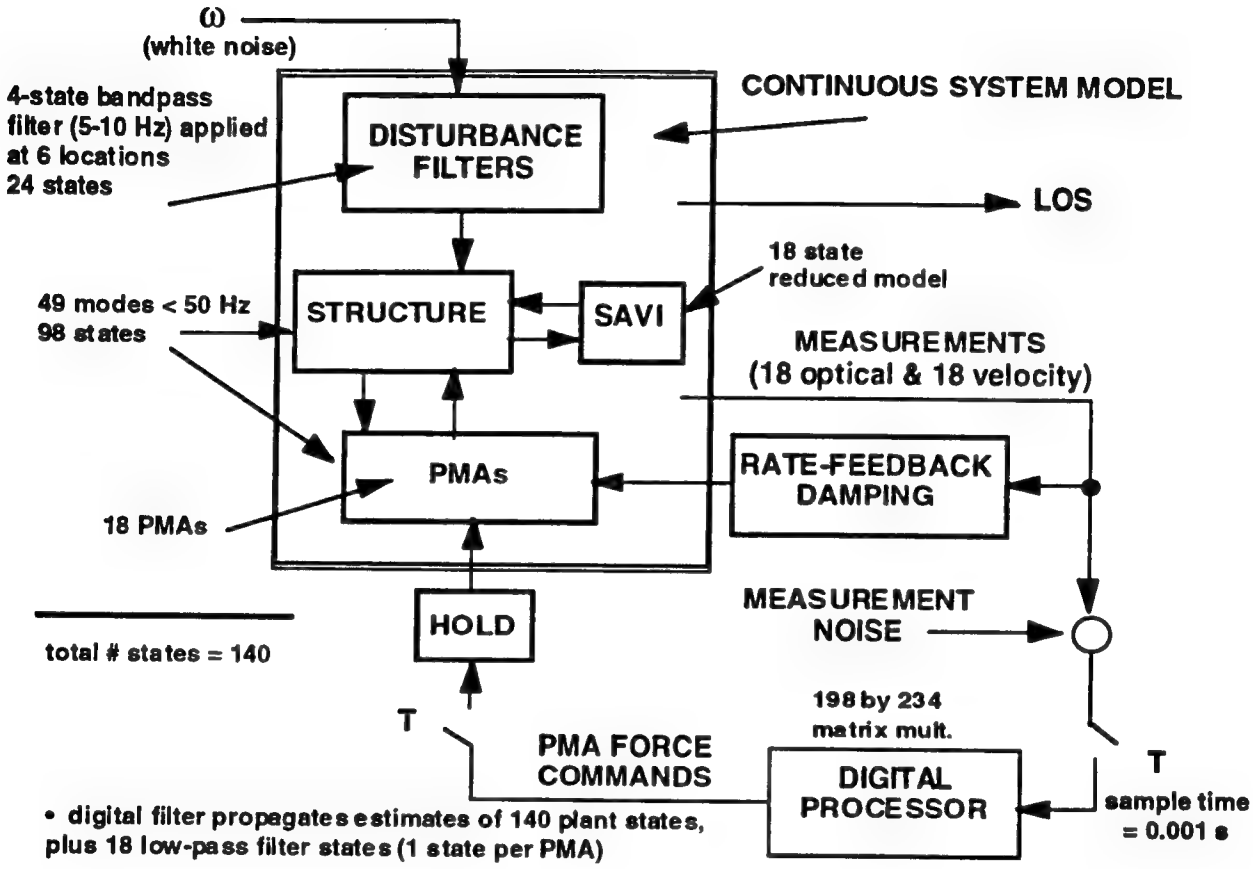

Figure 20. The HAC closed-loop system model.

3.4.1 Chronology of Final HAC Tests

The final HAC tests were accomplished over the course of 2 weeks. For all of the performance tests, PSDs of the outputs were computed by the modal system in near real time. A subset of the output PSDs was then analyzed and summarized for presentation here. The outputs analyzed include 36 HAC measurements, 2 OSS LOS components, and, for many but not all tests, 18 PMA strokes (as measured by the LVDTs). All PSDs cover the frequency range 0 to 128 Hz. For the LAC and HAC tests, frequency resolution was 0.03125 Hz over all frequencies. For the open-loop tests (both caged and uncaged) resolution was 0.0156 Hz from 0 to 64 Hz, and 0.03125 Hz from 64 to 128 Hz. The extra resolution was required for open-loop tests to properly sample the lightly damped dominant modes. As described next, an open-loop caged test from the open-loop test sequence was used to augment these tests. In that run, the PSD was taken from 0 to 32 Hz, with resolution of 0.0156 Hz.

The order of major tests and events is as follows (Subsection 3.2.1 defines caged-target LOS level):

(1) **HAC100**: Test of the HAC with 100-μrad caged-target LOS level disturbances on. The PSDs were acquired with the six shakers on at the 100-μrad open-loop disturbance level. All control loops were active (local-loop, LAC, and HAC).

(2) **HAC000**: Test of the HAC with quiescent conditions. All control loops were active, with disturbance shakers commanded to zero. This test was used to determine response of the HAC to sensor noise, atmospheric noise, and seismic disturbances.

(3) **LAC100**: Test of the LAC with 100-μrad caged-target LOS level disturbances. The local-loop and LAC loops were active, the HAC was off. The six disturbances were at the 100-μrad level.

(4) **LAC000**: Test of the LAC with quiescent conditions. Local loop and LAC loops were active, with disturbances commanded to zero.

(5) **OLU060**: Open-loop uncaged with 60-μrad caged-target LOS level disturbances on. The HAC, LAC, and local-loop rate feedback loops were off, and the PMAs were left uncaged. The disturbance level was limited to 60 μrad so that the SAVI rigid-body controller would not exceed its stroke limit in the SAVI actuator gaps.

(6) **OLU000**: Open-loop uncaged quiescent. All control loops were off, PMAs were uncaged, and the shakers were commanded to zero.

(7) In transitioning to the caged configuration of the PMAs, it was discovered that the secondary mirror z-axis stinger at vertex three was loose and slightly damaged. Tightening the stinger resulted in a change to the stinger stiffness that adversely

affected the SAVI rigid-body controller and resulted in unacceptable rigid-body oscillation. Various adjustments to the stinger failed to eliminate the oscillation. With limited available test time remaining, it was decided to replace the relatively stiff metal stinger threads with nylon threads with much less cross-axis stiffness. To maximize symmetry, the replacement was done at all three stinger locations. After the replacement, the SAVI control system worked without unacceptable rigid-body oscillation, and testing resumed.

(8) **OLC000**: Open-loop caged quiescent test. All control loops were off, the PMAs were caged, and the shakers were commanded to zero.

(9) **OLC030**: Open-loop caged with 30-μrad caged-target LOS level disturbance level. All control loops were off and the PMAs were caged.

(10) An earlier open-loop caged test using the 30-μrad caged-target LOS level disturbances (test P128 from the open-loop test sequence) had resulted in about 30 μrad of LOS jitter per axis. In OLC030, however, LOS jitter was about 24 μrad per axis, 80 per cent of the previous results. The change could only be attributed to increased damping in the stingers. It is believed that the nylon threads are much more damped in cross axis than the original metal threads. As will be shown later, the LOS PSDs from P128 and OLC030 are very similar, differing mainly in the amplitude of the resonance peak at 7.8 Hz. Since the damping introduced by the nylon stingers is overwhelmed by local-loop and LAC damping, the change in threads does not affect final HAC performance. In the final presentation of open-loop caged results, the results from test P128 are used below 30 Hz.

(11) Gain margin tests. In these tests, the disturbances were off (quiescent). The final HAC controller was on, except it had been modified to include a gain error on all 36 input measurements. A series of tests was run to determine the gain error at which the closed-loop system became unstable. The LOS PSDs were hard copied from the HP two-channel analyzer.

(12) An intermittent low-frequency oscillation was uncovered in the housing accelerometer in PMA 16. Due to a lack of time and funding, this sensor problem had not been fixed by the time of this report. A detailed analysis of data taken to date indicates that the problem existed in all of the HAC tests, to a greater or lesser degree. It does not appear to have existed during the open-loop test sequence at the beginning of subtask 02-09. A work-around procedure involving reseating electronics boards associated with that sensor successfully eliminated the sensor error for the duration of the open-loop and closed-loop FRF tests. However, shortly after completion of those tests, the noise reappeared. As a consequence of its

reappearance, it was decided not to repeat the above tests until the problem was completely fixed.

(13) Open-loop transfer function tests. In many control systems the open-loop transfer function is measured by taking FRFs at the proper test points in the closed-loop system. The result is a measure of the authority of the controller. A similar test was attempted for the HAC system.

(14) Closed-loop FRFs. Transfer functions from the 18 PMAs and 6 disturbances to the 38 measurements and the 2 LOS components were measured with the HAC loops closed.

3.4.2 Performance Test Results

This section summarizes the performance of the SPICE system. The four controls configurations tested were open loop with PMAs caged, open loop with PMAs uncaged, LAC loops closed, and HAC loops closed. The baseline open-loop configuration used to define the open-loop LOS level is with the PMAs caged. Uncaging the PMAs introduces a significant amount of flexure damping.

For each controls configuration, results are presented for two disturbance levels, quiescent and 100-μrad caged-target LOS level. In the quiescent level, the six disturbance sources are commanded to zero input force. Only sensor noise and ambient laboratory disturbance drive the control system and the structure. At the 100-μrad level, the shakers were commanded to the force levels that were determined to yield 100 μrad of LOS jitter per axis in the open-loop caged configuration. No open-loop tests were actually done at the full 100-μrad level due to stroke limits in SAVI. The 100-μrad level results presented here for those two tests (caged and uncaged) were extrapolated from reduced disturbance levels.

For the caged test, the 30-μrad disturbance force level was used. The 100-μrad response PSDs were computed from the quiescent and 30-μrad response PSDs as follows:

$$P_{100} = P_Q + (100/30)^2 (P_{30} - P_Q)$$

where

P_Q = quiescent PSD

P_{30} = PSD response for 30-μrad force level

For the uncaged test, the 60-μrad disturbance caged-target LOS level was used. The 100-μrad response PSDs were computed as

$$P_{100} = P_Q + (100/60)^2 (P_{60} - P_Q)$$

where

P_Q = quiescent PSD
P_{60} = PSD response for 60-μrad force level

As mentioned earlier, the open-loop caged test with the nylon stinger threads resulted in less LOS than was observed in the previous test with metal threads. This algorithm was used to extrapolate LOS PSDs from tests P128 and OLC030 to 100 μrad. The extrapolated OLC030 is denoted OLC100 on Figures 21 and 22 which compare LOS x and LOS y, respectively. There is very little visible difference above 5 Hz. The difference below 5 Hz is most likely due to atmospheric turbulence. In the P128 test, the high bay fans were off. It was decided after test P128 to run all HAC tests with air conditioning and fans on so that all tests would have the same conditions (with the fans off, thermal conditions change rapidly). Despite the difference below 5 Hz, most of the LOS is at the first pair of bending modes. The difference in stinger cross-axis damping is sufficient to cause a 20 per cent change in LOS response at the peak resonance.

All open-loop caged results presented in Subsection 3.4.2 are based upon data from test P128 and are referred to as OLC100 data.

3.4.2.1 Quiescent Test PSDs. Table 14 lists the PSDs obtained for the quiescent test condition. The graphs of those PSDs are in the appendix. Only a representative sample of output PSDs is presented. For the quiescent tests, each plot compares open-loop caged with LAC and HAC. The table lists the test condition, output degree of freedom, and the line style associated with the tests. The units of the PSDs are

- PMA housing rates: $(mm/s)^2/Hz$
- PMRS & SMRS angles: $\mu rad^2/Hz$
- SMTS translations: mm^2/Hz
- LOS: $\mu rad^2/Hz$
- LVDT stroke: mm^2/Hz

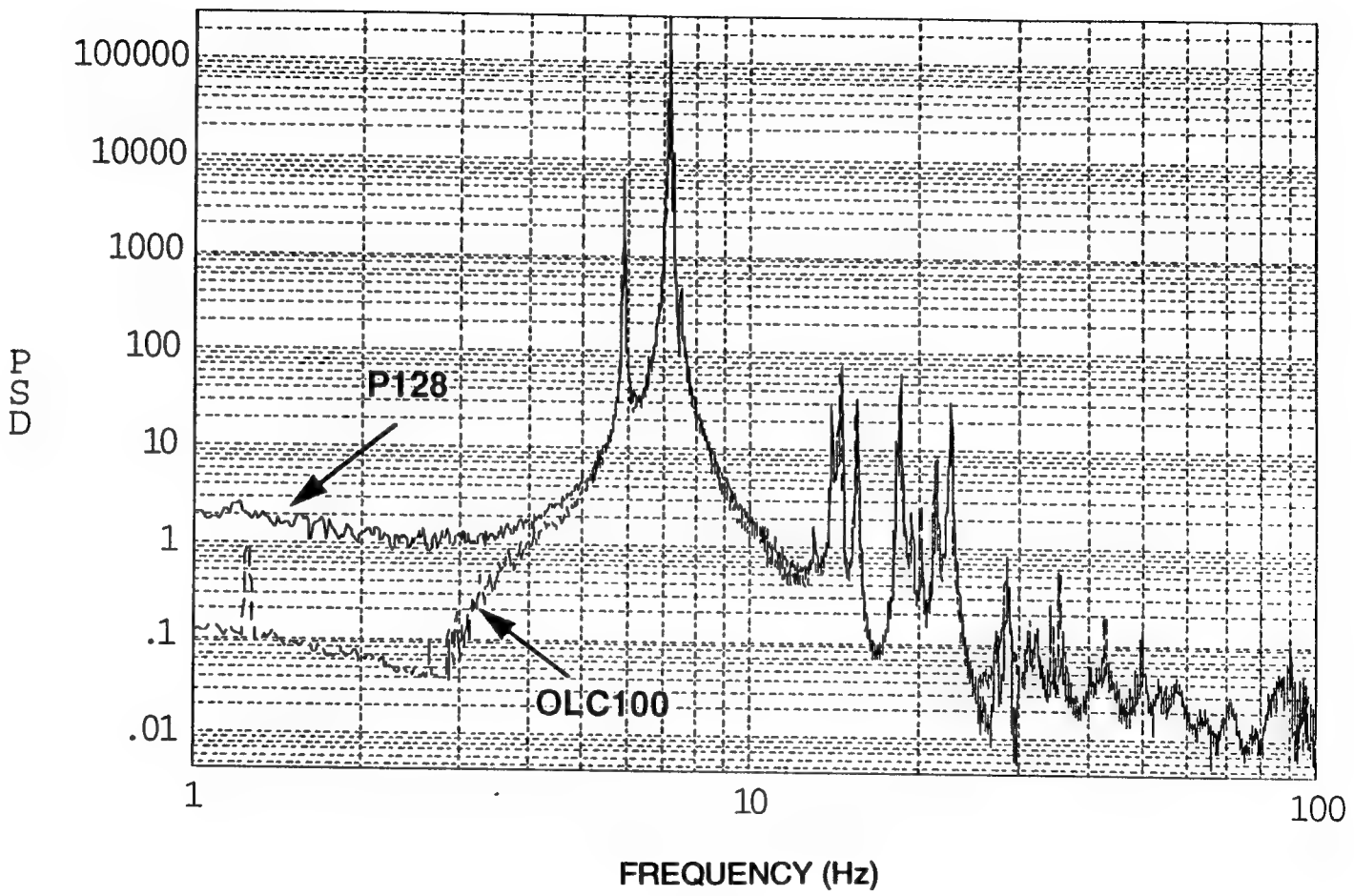

Figure 21. Effect of change in shaker stinger threads on LOS-x.

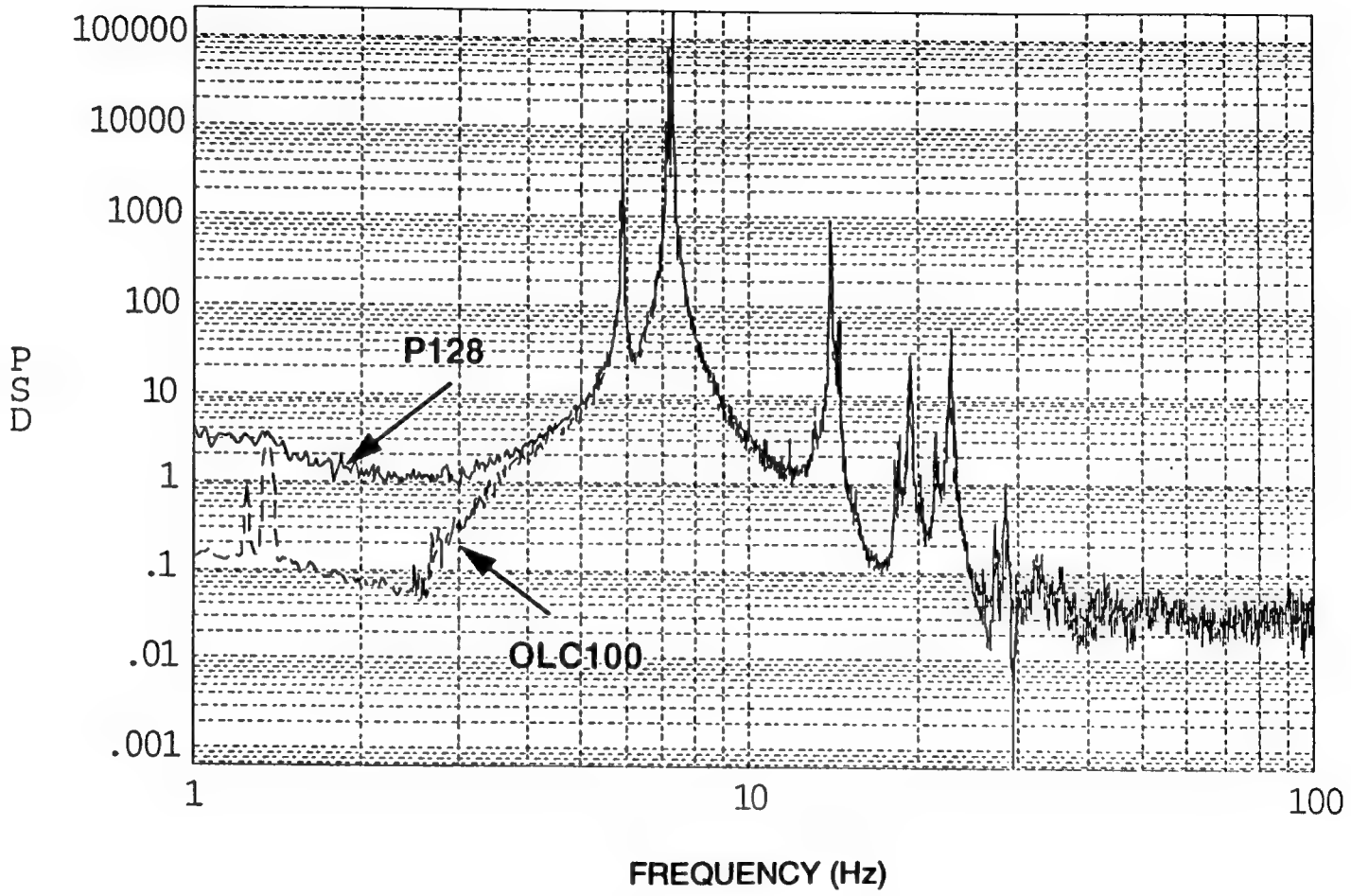

Figure 22. Effect of change in shaker stinger threads on LOS-y.

Table 14. Quiescent test PSDs.

Figure	Condition	Output	Solid Line	Dash-Dash	Dash-Dot
A-1	Quiescent	PMA 1 RATE	OLC000	LAC000	HAC000
A-2	Quiescent	PMA 2 RATE	OLC000	LAC000	HAC000
A-3	Quiescent	PMA 3 RATE	OLC000	LAC000	HAC000
A-4	Quiescent	PMA 4 RATE	OLC000	LAC000	HAC000
A-5	Quiescent	PMA 9 RATE	OLC000	LAC000	HAC000
A-6	Quiescent	PMA 10 RATE	OLC000	LAC000	HAC000
A-7	Quiescent	PMA 11 RATE	OLC000	LAC000	HAC000
A-8	Quiescent	PMA 12 RATE	OLC000	LAC000	HAC000
A-9	Quiescent	PMA 13 RATE	OLC000	LAC000	HAC000
A-10	Quiescent	PMA 14 RATE	OLC000	LAC000	HAC000
A-11	Quiescent	PMA 16 RATE	OLC000	LAC000	HAC000
A-12	Quiescent	PMRS 1X	OLC000	LAC000	HAC000
A-13	Quiescent	PMRS 1Y	OLC000	LAC000	HAC000
A-14	Quiescent	PMRS 2X	OLC000	LAC000	HAC000
A-15	Quiescent	PMRS 2Y	OLC000	LAC000	HAC000
A-16	Quiescent	PMRS 6X	OLC000	LAC000	HAC000
A-17	Quiescent	PMRS 6Y	OLC000	LAC000	HAC000
A-18	Quiescent	SMRS 7X	OLC000	LAC000	HAC000
A-19	Quiescent	SMRS 7Y	OLC000	LAC000	HAC000
A-20	Quiescent	SMTS 8X	OLC000	LAC000	HAC000
A-21	Quiescent	SMTS 8Y	OLC000	LAC000	HAC000
A-22	Quiescent	SMTS 9X	OLC000	LAC000	HAC000
A-23	Quiescent	SMTS 9Y	OLC000	LAC000	HAC000
A-24	Quiescent	LOS X	OLC000	LAC000	HAC000
A-25	Quiescent	LOS Y	OLC000	LAC000	HAC000

Several observations made with respect to these PSDs are

- The open-loop response of the quiescent structure is dominated by structural excitation. Even with the shakers off, most of the measurements and LOS is from the main bending mode of the structure. This is consistent with the earlier open-loop test sequence.
- The LAC by itself greatly attenuates the quiescent structural motion. The effect of rate feedback damping is evident for all outputs.
- The HAC significantly attenuates LAC residual motion at the main bending modes, with little evident spillover at higher frequencies.
- The PMA 16 rate stands out compared with PMAs 13 and 14. This is due to the housing accelerometer problem mentioned earlier.
- The PMRS 6X PSD stands out at high frequency. This is not a surprise. Reference 34 discusses a local mode identified during the open-loop test sequence.

It is evident from these plots that the HAC system does not significantly amplify quiescent noise. The exception to this is below 5 Hz, where atmospheric noise is amplified. However, it is unknown to what extent the amplification below 5 Hz is due to the PMA 16 sensor problem.

3.4.2.2 The PSDs for 100-μrad Input Force Level Tests. Table 15 lists the PSD plots for the tests with 100-μrad caged-target LOS force levels. The plots are in the Appendix. Most of these plots compare LAC100 with HAC100 and with the HAC100 prediction. The HAC prediction is referred to as the 5A19 model in the plots. Additionally, there are LOS comparisons among OLC100, LAC100, and HAC100.

Table 15. Shaker-driven test PSDs.

Figure	Condition	Output	Solid Line	Dash-Dash	Dash-Dot
A-26	100 μrad	LOS X	HAC100	LAC100	HAC Model
A-27	100 μrad	LOS Y	HAC100	LAC100	HAC Model
A-28	100 μrad	PMA 2 RATE	HAC100	LAC100	HAC Model
A-29	100 μrad	PMA 3 RATE	HAC100	LAC100	HAC Model
A-30	100 μrad	PMA 4 RATE	HAC100	LAC100	HAC Model
A-31	100 μrad	PMA 9 RATE	HAC100	LAC100	HAC Model
A-32	100 μrad	PMA 10 RATE	HAC100	LAC100	HAC Model
A-33	100 μrad	PMA 11 RATE	HAC100	LAC100	HAC Model
A-34	100 μrad	PMA 12 RATE	HAC100	LAC100	HAC Model
A-35	100 μrad	PMA 13 RATE	HAC100	LAC100	HAC Model
A-36	100 μrad	PMA 14 RATE	HAC100	LAC100	HAC Model
A-37	100 μrad	PMRS 1X	HAC100	LAC100	HAC Model
A-38	100 μrad	PMRS 1Y	HAC100	LAC100	HAC Model
A-39	100 μrad	PMRS 2X	HAC100	LAC100	HAC Model
A-40	100 μrad	PMRS 2Y	HAC100	LAC100	HAC Model
A-41	100 μrad	SMRS 7X	HAC100	LAC100	HAC Model
A-42	100 μrad	SMRS 7Y	HAC100	LAC100	HAC Model
A-43	100 μrad	SMTS 8X	HAC100	LAC100	HAC Model
A-44	100 μrad	SMTS 8Y	HAC100	LAC100	HAC Model
A-45	100 μrad	LVDT 1	HAC100	LAC100	HAC Model
A-46	100 μrad	LVDT 2	HAC100	LAC100	HAC Model
A-47	100 μrad	LVDT 3	HAC100	LAC100	HAC Model
A-48	100 μrad	LVDT 4	HAC100	LAC100	HAC Model
A-49	100 μrad	LVDT 13	HAC100	LAC100	HAC Model
A-50	100 μrad	LVDT 14	HAC100	LAC100	HAC Model
A-51	100 μrad	LOS X	OLC100	LAC100	HAC100
A-52	100 μrad	LOS Y	OLC100	LAC100	HAC100

From Figures A-26 through A-52 it can be observed that the HAC greatly attenuates LAC residual error within the HAC bandwidth (5-50 Hz). Outside the HAC bandwidth there is some amplification, or spillover. Generally, however, tremendous attenuation is achieved with little

spillover penalty. The predictions of HAC responses, although often quite good, are not exact and sometimes are quite poor. Like any well-behaved null-seeking servo, the HAC is able to perform well even though the level of that performance cannot be exactly predicted.

3.4.2.3 Data Summary Tables and Graphs The list of RMS values, by frequency band, for all of the final HAC test results (with extrapolation to 100-μrad caged-target LOS level where appropriate) is extensive (Table 16). Outputs include the 36 measurements, 2 LOS components, and 18 LVDT measurements of stroke for some of the tests. The frequency bands presented are: 0 to 5, 0 to 50, 0 to 128, 5 to 50, 5 to 128, and 50 to 128 Hz.

The LOS results are summarized in Table 17. Composite LOS represents the "average" per axis LOS. It is assumed that LOS x and LOS y are independent random processes. Consequently, the composite LOS is the square root of the average variance:

$$\sigma_{composite} = \sqrt{\frac{\sigma^2_{los\ x} + \sigma^2_{los\ y}}{2}}$$

The LOS jitter due to the shakers is computed as the LOS with the shakers on minus the LOS with the shakers off (quiescent). Because the shaker disturbances are independent of the quiescent environmental noise, the differencing is done on the variances.

$$\sigma_{due\ to\ shaker} = \sqrt{\sigma^2_{shaker\ on} - \sigma^2_{shaker\ off}}$$

The data in Tables 16 and 17 are summarized in a series of graphs. Table 18 lists the figures that summarize the RMS results in Table 16 for the frequency band from 0 to 128 Hz. Each figure graphs a particular output type. From these figures, it can be seen that LAC and HAC attenuate open-loop outputs over the entire frequency range. The HAC predictions from the 5A19 model are included for the cases in which the shaker were on.

The following observations are made from these graphs:

- The HAC has reduced sensor values from the LAC values for almost every sensor when the disturbances are active. For example, in Figure 23, the LAC is expected to reduce housing rates from the open-loop condition. It is not obvious that the HAC would further reduce housing rates for every PMA. But the HAC did exactly that for the PMA rates. Even most of the PMRS signals have been significantly reduced. At worst, there are a few PMRS signals where results with the HAC are the about the

Table 16. Residual RMS performance test results.

Measurement	5A19 Model	HAC100 0-5 Hz	HAC100 0-50 Hz	HAC100 0-128 Hz	HAC100 5-50 Hz	HAC100 5-128 Hz	HAC100 50-128 Hz
PMA 1 Rate	3.31E+00	1.35E+00	2.97E+00	2.97E+00	2.64E+00	2.64E+00	9.74E-02
PMA 2 Rate	3.20E+00	1.23E+00	2.75E+00	2.75E+00	2.46E+00	2.46E+00	1.41E-01
PMA 3 Rate	2.38E+00	5.80E-01	2.44E+00	2.44E+00	2.37E+00	2.37E+00	7.32E-02
PMA 4 Rate	2.39E+00	5.39E-01	2.41E+00	2.42E+00	2.35E+00	2.35E+00	1.30E-01
PMA 5 Rate	2.73E+00	9.47E-01	2.42E+00	2.42E+00	2.23E+00	2.23E+00	8.52E-02
PMA 6 Rate	3.11E+00	1.40E+00	2.72E+00	2.73E+00	2.33E+00	2.34E+00	1.32E-01
PMA 7 Rate	2.08E+00	3.35E-01	2.01E+00	2.02E+00	1.99E+00	1.99E+00	9.20E-02
PMA 8 Rate	1.73E+00	5.43E-01	1.51E+00	1.51E+00	1.41E+00	1.41E+00	9.84E-02
PMA 9 Rate	2.84E+00	1.30E+00	2.40E+00	2.40E+00	2.02E+00	2.02E+00	1.03E-01
PMA10 Rate	2.67E+00	1.03E+00	2.51E+00	2.52E+00	2.29E+00	2.30E+00	1.27E-01
PMA11 Rate	1.51E+00	5.35E-01	1.50E+00	1.50E+00	1.40E+00	1.41E+00	9.50E-02
PMA12 Rate	2.09E+00	3.52E-01	2.08E+00	2.08E+00	2.05E+00	2.05E+00	1.27E-01
PMA13 Rate	1.68E+00	8.72E-01	1.66E+00	1.67E+00	1.41E+00	1.42E+00	1.57E-01
PMA14 Rate	1.33E+00	6.82E-01	1.33E+00	1.34E+00	1.15E+00	1.16E+00	1.50E-01
PMA15 Rate	1.28E+00	6.86E-01	1.27E+00	1.28E+00	1.07E+00	1.08E+00	1.13E-01
PMA16 Rate	1.55E+00	7.48E-01	1.37E+00	1.37E+00	1.14E+00	1.15E+00	1.17E-01
PMA17 Rate	1.51E+00	7.67E-01	1.50E+00	1.51E+00	1.29E+00	1.30E+00	1.54E-01
PMA18 Rate	1.59E+00	7.89E-01	1.53E+00	1.54E+00	1.31E+00	1.32E+00	1.49E-01
PMRS 1 X	2.10E+00	4.64E-01	1.52E+00	1.67E+00	1.45E+00	1.60E+00	6.86E-01
PMRS 1 Y	1.22E+00	4.09E-01	1.29E+00	1.37E+00	1.23E+00	1.30E+00	4.47E-01
PMRS 2 X	2.78E+00	1.10E+00	2.93E+00	3.02E+00	2.71E+00	2.82E+00	7.67E-01
PMRS 2 Y	2.38E+00	5.46E-01	2.79E+00	2.84E+00	2.73E+00	2.79E+00	5.50E-01
PMRS 3 X	1.78E+00	5.02E-01	1.45E+00	1.57E+00	1.36E+00	1.49E+00	6.08E-01
PMRS 3 Y	1.42E+00	4.33E-01	1.49E+00	1.57E+00	1.43E+00	1.51E+00	4.99E-01
PMRS 4 X	2.54E+00	9.21E-01	2.38E+00	2.52E+00	2.19E+00	2.35E+00	8.36E-01
PMRS 4 Y	3.16E+00	8.29E-01	3.39E+00	3.45E+00	3.29E+00	3.34E+00	6.09E-01
PMRS 5 X	2.29E+00	6.05E-01	1.72E+00	1.89E+00	1.61E+00	1.79E+00	7.79E-01
PMRS 5 Y	1.04E+00	3.61E-01	1.11E+00	1.19E+00	1.05E+00	1.13E+00	4.24E-01
PMRS 6 X	2.16E+00	8.67E-01	2.11E+00	2.70E+00	1.93E+00	2.55E+00	1.68E+00
PMRS 6 Y	3.60E+00	8.89E-01	3.51E+00	3.56E+00	3.39E+00	3.44E+00	5.92E-01
SMRS 7 X	1.08E+01	4.08E+00	9.60E+00	9.64E+00	8.69E+00	8.73E+00	9.11E-01
SMRS 7 Y	1.41E+01	5.80E+00	1.27E+01	1.28E+01	1.13E+01	1.14E+01	1.46E+00
SMTS 8 X Trans.	3.28E-02	1.43E-02	2.81E-02	2.82E-02	2.41E-02	2.43E-02	2.63E-03
SMTS 8 Y Trans.	2.74E-02	1.92E-02	2.83E-02	2.85E-02	2.08E-02	2.10E-02	3.03E-03
SMTS 9 X Trans.	3.28E-02	1.57E-02	3.01E-02	3.02E-02	2.57E-02	2.58E-02	2.88E-03
SMTS 9 Y Trans.	3.02E-02	1.45E-02	2.65E-02	2.66E-02	2.21E-02	2.23E-02	2.96E-03
Line of Sight X	9.96E-01	1.15E+00	1.51E+00	1.66E+00	9.86E-01	1.20E+00	6.91E-01
Line of Sight Y	1.45E+00	1.02E+00	1.80E+00	1.92E+00	1.48E+00	1.62E+00	6.58E-01
LVDT 1	9.77E-01	1.25E+00	1.34E+00	1.34E+00	4.92E-01	4.92E-01	0.00E+00
LVDT 2	9.83E-01	1.23E+00	1.31E+00	1.31E+00	4.43E-01	4.43E-01	0.00E+00
LVDT 3	4.98E-01	8.12E-01	8.47E-01	8.47E-01	2.41E-01	2.41E-01	0.00E+00
LVDT 4	5.79E-01	7.90E-01	8.28E-01	8.28E-01	2.47E-01	2.47E-01	0.00E+00
LVDT 5	9.23E-01	1.18E+00	1.25E+00	1.25E+00	4.26E-01	4.26E-01	0.00E+00

Table 16. Continued.

Measurement	5A19 Model	HAC100 0-5 Hz	HAC100 0-50 Hz	HAC100 0-128 Hz	HAC100 5-50 Hz	HAC100 5-128 Hz	HAC100 50-128 Hz
LVDT 6	8.03E-01	8.84E-01	1.01E+00	1.01E+00	4.83E-01	4.83E-01	0.00E+00
LVDT 7	7.02E-01	8.83E-01	9.38E-01	9.38E-01	3.18E-01	3.18E-01	0.00E+00
LVDT 8	4.45E-01	6.77E-01	7.18E-01	7.18E-01	2.39E-01	2.39E-01	0.00E+00
LVDT 9	7.72E-01	8.59E-01	9.89E-01	9.89E-01	4.90E-01	4.90E-01	0.00E+00
LVDT 10	9.63E-01	1.17E+00	1.26E+00	1.26E+00	4.70E-01	4.70E-01	0.00E+00
LVDT 11	5.01E-01	6.59E-01	7.06E-01	7.06E-01	2.52E-01	2.52E-01	0.00E+00
LVDT 12	6.82E-01	8.25E-01	8.88E-01	8.88E-01	3.29E-01	3.29E-01	0.00E+00
LVDT 13	9.02E-01	1.14E+00	1.20E+00	1.20E+00	3.77E-01	3.77E-01	0.00E+00
LVDT 14	7.86E-01	1.08E+00	1.14E+00	1.14E+00	3.58E-01	3.58E-01	0.00E+00
LVDT 15	8.69E-01	1.09E+00	1.15E+00	1.15E+00	3.82E-01	3.82E-01	0.00E+00
LVDT 16	9.00E-01	1.15E+00	1.20E+00	1.20E+00	3.44E-01	3.44E-01	0.00E+00
LVDT 17	6.76E-01	9.70E-01	1.02E+00	1.02E+00	3.23E-01	3.23E-01	0.00E+00
LVDT 18	7.42E-01	9.55E-01	1.01E+00	1.01E+00	3.39E-01	3.39E-01	0.00E+00
Measurement		**LAC100 0-5 Hz**	**LAC100 0-50 Hz**	**LAC100 0-128 Hz**	**LAC100 5-50 Hz**	**LAC100 5-128 Hz**	**LAC100 50-128 Hz**
PMA 1 Rate		3.31E+00	9.86E+00	9.86E+00	9.29E+00	9.29E+00	6.28E-02
PMA 2 Rate		3.02E+00	9.39E+00	9.39E+00	8.89E+00	8.89E+00	8.67E-02
PMA 3 Rate		9.75E-01	4.01E+00	4.01E+00	3.89E+00	3.89E+00	6.33E-02
PMA 4 Rate		9.02E-01	4.01E+00	4.01E+00	3.91E+00	3.91E+00	9.39E-02
PMA 5 Rate		2.83E+00	8.63E+00	8.63E+00	8.16E+00	8.16E+00	7.20E-02
PMA 6 Rate		3.16E+00	9.52E+00	9.52E+00	8.98E+00	8.98E+00	7.56E-02
PMA 7 Rate		8.41E-01	3.43E+00	3.44E+00	3.33E+00	3.33E+00	7.86E-02
PMA 8 Rate		9.46E-01	3.62E+00	3.62E+00	3.50E+00	3.50E+00	8.93E-02
PMA 9 Rate		2.94E+00	8.86E+00	8.86E+00	8.36E+00	8.36E+00	7.29E-02
PMA10 Rate		3.48E+00	9.58E+00	9.58E+00	8.93E+00	8.93E+00	8.75E-02
PMA11 Rate		9.72E-01	3.90E+00	3.90E+00	3.77E+00	3.78E+00	9.26E-02
PMA12 Rate		1.13E+00	3.99E+00	3.99E+00	3.83E+00	3.83E+00	1.06E-01
PMA13 Rate		9.47E-01	3.62E+00	3.62E+00	3.49E+00	3.49E+00	1.52E-01
PMA14 Rate		7.18E-01	2.93E+00	2.94E+00	2.84E+00	2.85E+00	1.37E-01
PMA15 Rate		7.20E-01	3.13E+00	3.13E+00	3.05E+00	3.05E+00	1.03E-01
PMA16 Rate		8.62E-01	3.12E+00	3.12E+00	3.00E+00	3.00E+00	1.09E-01
PMA17 Rate		7.32E-01	2.95E+00	2.96E+00	2.86E+00	2.87E+00	1.31E-01
PMA18 Rate		7.45E-01	3.15E+00	3.16E+00	3.07E+00	3.07E+00	1.42E-01
PMRS 1 X		3.78E-01	2.03E+00	2.09E+00	1.99E+00	2.05E+00	5.05E-01
PMRS 1 Y		2.23E-01	1.37E+00	1.43E+00	1.35E+00	1.41E+00	4.00E-01
PMRS 2 X		2.33E+00	6.58E+00	6.62E+00	6.16E+00	6.19E+00	6.51E-01
PMRS 2 Y		5.49E-01	3.45E+00	3.49E+00	3.41E+00	3.45E+00	5.17E-01
PMRS 3 X		4.02E-01	2.18E+00	2.24E+00	2.15E+00	2.21E+00	5.05E-01
PMRS 3 Y		2.45E-01	1.48E+00	1.55E+00	1.46E+00	1.53E+00	4.32E-01
PMRS 4 X		2.17E+00	6.42E+00	6.45E+00	6.04E+00	6.08E+00	6.94E-01
PMRS 4 Y		6.47E-01	4.63E+00	4.66E+00	4.58E+00	4.61E+00	5.68E-01
PMRS 5 X		7.70E-01	2.62E+00	2.69E+00	2.51E+00	2.58E+00	5.84E-01
PMRS 5 Y		2.73E-01	1.16E+00	1.22E+00	1.13E+00	1.19E+00	3.79E-01

Table 16. Continued.

Measurement	LAC100 0-5 Hz	LAC100 0-50 Hz	LAC100 0-128 Hz	LAC100 5-50 Hz	LAC100 5-128 Hz	LAC100 50-128 Hz
PMRS 6 X	2.29E+00	5.89E+00	6.12E+00	5.43E+00	5.67E+00	1.64E+00
PMRS 6 Y	8.24E-01	4.71E+00	4.74E+00	4.64E+00	4.67E+00	5.35E-01
SMRS 7 X	1.19E+01	5.32E+01	5.32E+01	5.18E+01	5.18E+01	1.30E+00
SMRS 7 Y	1.58E+01	6.51E+01	6.51E+01	6.31E+01	6.31E+01	1.49E+00
SMTS 8 X Trans.	4.86E-02	2.19E-01	2.19E-01	2.14E-01	2.14E-01	2.09E-03
SMTS 8 Y Trans.	5.31E-02	1.98E-01	1.98E-01	1.91E-01	1.91E-01	1.99E-03
SMTS 9 X Trans.	5.18E-02	2.33E-01	2.33E-01	2.27E-01	2.27E-01	2.16E-03
SMTS 9 Y Trans.	4.60E-02	1.90E-01	1.90E-01	1.84E-01	1.84E-01	2.75E-03
Line of Sight X	2.34E+00	1.12E+01	1.12E+01	1.09E+01	1.10E+01	6.86E-01
Line of Sight Y	3.10E+00	1.42E+01	1.42E+01	1.38E+01	1.38E+01	6.07E-01
LVDT 1	3.23E-01	7.86E-01	7.86E-01	7.17E-01	7.17E-01	0.00E+00
LVDT 2	2.80E-01	7.10E-01	7.10E-01	6.53E-01	6.53E-01	0.00E+00
LVDT 3	9.62E-02	2.64E-01	2.64E-01	2.46E-01	2.46E-01	0.00E+00
LVDT 4	8.86E-02	2.58E-01	2.58E-01	2.42E-01	2.42E-01	0.00E+00
LVDT 5	2.74E-01	6.83E-01	6.83E-01	6.26E-01	6.26E-01	0.00E+00
LVDT 6	3.00E-01	7.16E-01	7.16E-01	6.50E-01	6.50E-01	0.00E+00
LVDT 7	8.21E-02	2.19E-01	2.19E-01	2.03E-01	2.03E-01	0.00E+00
LVDT 8	9.11E-02	2.47E-01	2.47E-01	2.29E-01	2.29E-01	0.00E+00
LVDT 9	2.87E-01	6.90E-01	6.90E-01	6.28E-01	6.28E-01	0.00E+00
LVDT 10	3.30E-01	7.71E-01	7.71E-01	6.97E-01	6.97E-01	0.00E+00
LVDT 11	9.30E-02	2.57E-01	2.57E-01	2.39E-01	2.39E-01	0.00E+00
LVDT 12	1.05E-01	2.67E-01	2.67E-01	2.45E-01	2.45E-01	0.00E+00
LVDT 13	9.61E-02	2.22E-01	2.22E-01	2.00E-01	2.00E-01	0.00E+00
LVDT 14	7.34E-02	1.82E-01	1.82E-01	1.67E-01	1.67E-01	0.00E+00
LVDT 15	7.72E-02	2.01E-01	2.01E-01	1.85E-01	1.85E-01	0.00E+00
LVDT 16	8.97E-02	1.99E-01	1.99E-01	1.78E-01	1.78E-01	0.00E+00
LVDT 17	8.05E-02	1.91E-01	1.91E-01	1.73E-01	1.73E-01	0.00E+00
LVDT 18	8.08E-02	2.01E-01	2.01E-01	1.84E-01	1.84E-01	0.00E+00
Measurement	**HAC000 0-5 Hz**	**HAC000 0-50 Hz**	**HAC000 0-128 Hz**	**HAC000 5-50 Hz**	**HAC000 5-128 Hz**	**HAC000 50-128 Hz**
PMA 1 Rate	1.38E-01	1.45E-01	1.48E-01	4.52E-02	5.42E-02	2.98E-02
PMA 2 Rate	1.13E-01	1.22E-01	1.28E-01	4.63E-02	5.90E-02	3.67E-02
PMA 3 Rate	5.46E-02	6.64E-02	7.06E-02	3.77E-02	4.47E-02	2.41E-02
PMA 4 Rate	5.19E-02	6.79E-02	7.54E-02	4.38E-02	5.46E-02	3.27E-02
PMA 5 Rate	9.50E-02	1.04E-01	1.07E-01	4.21E-02	4.87E-02	2.46E-02
PMA 6 Rate	1.49E-01	1.57E-01	1.60E-01	4.75E-02	5.91E-02	3.53E-02
PMA 7 Rate	3.82E-02	5.16E-02	5.72E-02	3.48E-02	4.26E-02	2.46E-02
PMA 8 Rate	5.75E-02	7.00E-02	7.59E-02	3.99E-02	4.94E-02	2.93E-02
PMA 9 Rate	1.36E-01	1.42E-01	1.44E-01	4.04E-02	4.89E-02	2.76E-02
PMA10 Rate	1.14E-01	1.23E-01	1.29E-01	4.51E-02	5.90E-02	3.81E-02
PMA11 Rate	5.92E-02	6.82E-02	7.24E-02	3.39E-02	4.17E-02	2.43E-02
PMA12 Rate	4.53E-02	5.90E-02	6.90E-02	3.78E-02	5.20E-02	3.57E-02
PMA13 Rate	8.55E-02	9.02E-02	1.09E-01	2.90E-02	6.74E-02	6.08E-02

Table 16. Continued.

Measurement	HAC000 0-5 Hz	HAC000 0-50 Hz	HAC000 0-128 Hz	HAC000 5-50 Hz	HAC000 5-128 Hz	HAC000 50-128 Hz
PMA14 Rate	6.89E-02	7.42E-02	9.52E-02	2.74E-02	6.57E-02	5.97E-02
PMA15 Rate	9.66E-02	1.00E-01	1.13E-01	2.70E-02	5.94E-02	5.29E-02
PMA16 Rate	2.21E-01	2.22E-01	2.29E-01	2.72E-02	5.95E-02	5.29E-02
PMA17 Rate	8.51E-02	8.95E-02	1.09E-01	2.77E-02	6.74E-02	6.15E-02
PMA18 Rate	9.14E-02	9.53E-02	1.10E-01	2.71E-02	6.05E-02	5.41E-02
PMRS 1 X	1.04E-01	1.15E-01	2.11E-01	4.85E-02	1.84E-01	1.78E-01
PMRS 1 Y	1.13E-01	1.25E-01	1.77E-01	5.36E-02	1.36E-01	1.25E-01
PMRS 2 X	1.09E-01	1.38E-01	2.88E-01	8.56E-02	2.67E-01	2.52E-01
PMRS 2 Y	7.75E-02	1.13E-01	2.29E-01	8.19E-02	2.16E-01	1.99E-01
PMRS 3 X	8.72E-02	1.06E-01	2.37E-01	5.95E-02	2.20E-01	2.12E-01
PMRS 3 Y	7.88E-02	9.66E-02	1.60E-01	5.58E-02	1.39E-01	1.28E-01
PMRS 4 X	1.24E-01	1.45E-01	2.97E-01	7.63E-02	2.70E-01	2.59E-01
PMRS 4 Y	1.32E-01	1.53E-01	2.41E-01	7.68E-02	2.01E-01	1.86E-01
PMRS 5 X	1.78E-01	1.86E-01	2.89E-01	5.58E-02	2.28E-01	2.21E-01
PMRS 5 Y	1.81E-01	1.91E-01	2.31E-01	6.11E-02	1.44E-01	1.30E-01
PMRS 6 X	1.68E-01	1.88E-01	7.90E-01	8.41E-02	7.72E-01	7.67E-01
PMRS 6 Y	1.63E-01	1.79E-01	2.42E-01	7.20E-02	1.78E-01	1.63E-01
SMRS 7 X	5.47E-01	6.00E-01	6.97E-01	2.46E-01	4.32E-01	3.56E-01
SMRS 7 Y	8.24E-01	8.89E-01	1.07E+00	3.33E-01	6.90E-01	6.04E-01
SMTS 8 X Trans.	3.88E-03	4.06E-03	4.11E-03	1.17E-03	1.34E-03	6.36E-04
SMTS 8 Y Trans.	3.68E-03	3.81E-03	3.92E-03	9.99E-04	1.36E-03	9.22E-04
SMTS 9 X Trans.	4.78E-03	4.91E-03	4.96E-03	1.12E-03	1.34E-03	7.34E-04
SMTS 9 Y Trans.	3.75E-03	3.86E-03	4.01E-03	9.20E-04	1.42E-03	1.09E-03
Line of Sight X	3.37E-01	3.48E-01	4.45E-01	8.55E-02	2.91E-01	2.78E-01
Line of Sight Y	3.68E-01	3.79E-01	4.61E-01	9.04E-02	2.78E-01	2.63E-01
LVDT 1	3.90E-01	3.90E-01	3.90E-01	1.28E-02	1.28E-02	0.00E+00
LVDT 2	3.17E-01	3.17E-01	3.17E-01	7.96E-03	7.96E-03	0.00E+00
LVDT 3	2.76E-01	2.76E-01	2.76E-01	7.79E-03	7.79E-03	0.00E+00
LVDT 4	3.07E-01	3.07E-01	3.07E-01	7.01E-03	7.01E-03	0.00E+00
LVDT 5	3.02E-01	3.02E-01	3.02E-01	7.37E-03	7.37E-03	0.00E+00
LVDT 6	2.61E-01	2.61E-01	2.61E-01	8.85E-03	8.85E-03	0.00E+00
LVDT 7	2.98E-01	2.98E-01	2.98E-01	8.80E-03	8.80E-03	0.00E+00
LVDT 8	1.71E-01	1.71E-01	1.71E-01	4.90E-03	4.90E-03	0.00E+00
LVDT 9	2.56E-01	2.57E-01	2.57E-01	9.06E-03	9.06E-03	0.00E+00
LVDT 10	3.31E-01	3.31E-01	3.31E-01	1.03E-02	1.03E-02	0.00E+00
LVDT 11	1.54E-01	1.54E-01	1.54E-01	6.81E-03	6.81E-03	0.00E+00
LVDT 12	2.59E-01	2.59E-01	2.59E-01	6.83E-03	6.83E-03	0.00E+00
LVDT 13	4.32E-01	4.32E-01	4.32E-01	1.06E-02	1.06E-02	0.00E+00
LVDT 14	3.41E-01	3.41E-01	3.41E-01	1.01E-02	1.01E-02	0.00E+00
LVDT 15	4.10E-01	4.10E-01	4.10E-01	1.15E-02	1.15E-02	0.00E+00
LVDT 16	4.84E-01	4.85E-01	4.85E-01	1.16E-02	1.16E-02	0.00E+00
LVDT 17	2.00E-01	2.01E-01	2.01E-01	7.75E-03	7.75E-03	0.00E+00
LVDT 18	2.39E-01	2.39E-01	2.39E-01	7.88E-03	7.88E-03	0.00E+00

Table 16. Continued.

Measurement	LAC000 0-5 Hz	LAC000 0-50 Hz	LAC000 0-128 Hz	LAC000 5-50 Hz	LAC000 5-128 Hz	LAC000 50-128 Hz
PMA 1 Rate	6.29E-02	8.71E-02	8.96E-02	6.02E-02	6.39E-02	2.13E-02
PMA 2 Rate	7.07E-02	9.82E-02	1.01E-01	6.82E-02	7.25E-02	2.45E-02
PMA 3 Rate	2.54E-02	4.51E-02	4.93E-02	3.73E-02	4.23E-02	2.00E-02
PMA 4 Rate	3.06E-02	5.32E-02	5.84E-02	4.35E-02	4.98E-02	2.41E-02
PMA 5 Rate	8.35E-02	1.09E-01	1.11E-01	7.00E-02	7.31E-02	2.12E-02
PMA 6 Rate	5.39E-02	8.76E-02	9.12E-02	6.90E-02	7.36E-02	2.56E-02
PMA 7 Rate	3.33E-02	4.97E-02	5.44E-02	3.69E-02	4.30E-02	2.21E-02
PMA 8 Rate	2.69E-02	5.12E-02	5.74E-02	4.35E-02	5.07E-02	2.60E-02
PMA 9 Rate	6.23E-02	9.10E-02	9.31E-02	6.64E-02	6.92E-02	1.94E-02
PMA10 Rate	8.47E-02	1.05E-01	1.08E-01	6.15E-02	6.72E-02	2.71E-02
PMA11 Rate	3.55E-02	5.40E-02	5.83E-02	4.07E-02	4.62E-02	2.19E-02
PMA12 Rate	3.86E-02	5.46E-02	6.09E-02	3.85E-02	4.71E-02	2.70E-02
PMA13 Rate	3.93E-02	5.39E-02	7.71E-02	3.68E-02	6.63E-02	5.52E-02
PMA14 Rate	5.74E-02	7.02E-02	8.83E-02	4.04E-02	6.72E-02	5.36E-02
PMA15 Rate	5.93E-02	7.00E-02	8.50E-02	3.71E-02	6.09E-02	4.83E-02
PMA16 Rate	1.88E-01	1.92E-01	1.98E-01	3.44E-02	6.13E-02	5.07E-02
PMA17 Rate	5.59E-02	6.86E-02	8.82E-02	3.99E-02	6.83E-02	5.54E-02
PMA18 Rate	4.70E-02	5.90E-02	7.79E-02	3.57E-02	6.22E-02	5.09E-02
PMRS 1 X	1.13E-01	1.22E-01	1.88E-01	4.67E-02	1.50E-01	1.43E-01
PMRS 1 Y	1.38E-01	1.50E-01	1.90E-01	5.86E-02	1.31E-01	1.17E-01
PMRS 2 X	1.15E-01	1.44E-01	2.79E-01	8.71E-02	2.55E-01	2.39E-01
PMRS 2 Y	9.16E-02	1.24E-01	2.36E-01	8.36E-02	2.18E-01	2.01E-01
PMRS 3 X	1.04E-01	1.19E-01	2.32E-01	5.81E-02	2.07E-01	1.99E-01
PMRS 3 Y	1.05E-01	1.22E-01	1.71E-01	6.22E-02	1.35E-01	1.20E-01
PMRS 4 X	1.58E-01	1.81E-01	3.01E-01	8.85E-02	2.56E-01	2.40E-01
PMRS 4 Y	1.81E-01	2.02E-01	2.76E-01	8.90E-02	2.08E-01	1.88E-01
PMRS 5 X	2.21E-01	2.28E-01	2.93E-01	5.65E-02	1.93E-01	1.85E-01
PMRS 5 Y	2.30E-01	2.38E-01	2.69E-01	6.09E-02	1.40E-01	1.26E-01
PMRS 6 X	2.25E-01	2.43E-01	8.33E-01	9.26E-02	8.02E-01	7.97E-01
PMRS 6 Y	2.18E-01	2.32E-01	2.79E-01	7.87E-02	1.75E-01	1.56E-01
SMRS 7 X	5.72E-01	8.16E-01	9.68E-01	5.82E-01	7.81E-01	5.21E-01
SMRS 7 Y	5.00E-01	7.01E-01	9.55E-01	4.91E-01	8.14E-01	6.49E-01
SMTS 8 X Trans.	4.14E-03	4.60E-03	4.62E-03	1.99E-03	2.06E-03	5.03E-04
SMTS 8 Y Trans.	3.78E-03	4.36E-03	4.45E-03	2.16E-03	2.34E-03	9.06E-04
SMTS 9 X Trans.	4.16E-03	4.58E-03	4.62E-03	1.93E-03	2.01E-03	5.45E-04
SMTS 9 Y Trans.	3.90E-03	4.40E-03	4.54E-03	2.04E-03	2.32E-03	1.09E-03
Line of Sight X	3.92E-01	4.20E-01	5.25E-01	1.52E-01	3.49E-01	3.14E-01
Line of Sight Y	4.21E-01	4.49E-01	5.24E-01	1.55E-01	3.11E-01	2.70E-01

Table 16. Continued.

Measurement	OLU000 0-5 Hz	OLU000 0-50 Hz	OLU000 0-128 Hz	OLU000 5-50 Hz	OLU000 5-128 Hz	OLU000 50-128 Hz
PMA 1 Rate	5.98E-02	2.05E-01	2.06E-01	1.96E-01	1.97E-01	2.60E-02
PMA 2 Rate	6.85E-02	2.23E-01	2.26E-01	2.13E-01	2.15E-01	3.26E-02
PMA 3 Rate	2.56E-02	1.29E-01	1.31E-01	1.26E-01	1.28E-01	2.36E-02
PMA 4 Rate	2.85E-02	1.40E-01	1.44E-01	1.38E-01	1.41E-01	3.20E-02
PMA 5 Rate	7.72E-02	2.32E-01	2.34E-01	2.19E-01	2.21E-01	2.65E-02
PMA 6 Rate	5.33E-02	2.15E-01	2.18E-01	2.08E-01	2.11E-01	3.36E-02
PMA 7 Rate	3.08E-02	1.19E-01	1.22E-01	1.15E-01	1.18E-01	2.70E-02
PMA 8 Rate	2.51E-02	1.38E-01	1.42E-01	1.36E-01	1.40E-01	3.29E-02
PMA 9 Rate	6.37E-02	2.23E-01	2.24E-01	2.13E-01	2.14E-01	2.22E-02
PMA10 Rate	7.79E-02	2.27E-01	2.30E-01	2.13E-01	2.16E-01	3.48E-02
PMA11 Rate	3.73E-02	1.54E-01	1.56E-01	1.49E-01	1.52E-01	2.65E-02
PMA12 Rate	3.51E-02	1.33E-01	1.37E-01	1.28E-01	1.33E-01	3.45E-02
PMA13 Rate	3.68E-02	9.16E-02	1.23E-01	8.39E-02	1.17E-01	8.21E-02
PMA14 Rate	5.19E-02	1.13E-01	1.38E-01	1.00E-01	1.28E-01	8.03E-02
PMA15 Rate	5.34E-02	1.06E-01	1.26E-01	9.15E-02	1.14E-01	6.77E-02
PMA16 Rate	1.77E-01	1.92E-01	2.04E-01	7.44E-02	1.01E-01	6.80E-02
PMA17 Rate	5.49E-02	1.14E-01	1.39E-01	9.94E-02	1.27E-01	7.95E-02
PMA18 Rate	4.50E-02	1.01E-01	1.25E-01	8.99E-02	1.16E-01	7.37E-02
PMRS 1 X	9.79E-02	1.50E-01	2.39E-01	1.14E-01	2.18E-01	1.86E-01
PMRS 1 Y	1.24E-01	1.58E-01	2.04E-01	9.74E-02	1.62E-01	1.29E-01
PMRS 2 X	9.65E-02	1.77E-01	3.22E-01	1.49E-01	3.07E-01	2.69E-01
PMRS 2 Y	8.44E-02	1.78E-01	2.76E-01	1.56E-01	2.63E-01	2.12E-01
PMRS 3 X	5.60E-02	1.43E-01	2.69E-01	1.31E-01	2.63E-01	2.28E-01
PMRS 3 Y	6.11E-02	1.25E-01	1.86E-01	1.09E-01	1.75E-01	1.37E-01
PMRS 4 X	6.21E-02	1.84E-01	3.32E-01	1.73E-01	3.27E-01	2.77E-01
PMRS 4 Y	9.59E-02	1.87E-01	2.73E-01	1.60E-01	2.55E-01	1.99E-01
PMRS 5 X	1.09E-01	1.59E-01	2.61E-01	1.16E-01	2.37E-01	2.07E-01
PMRS 5 Y	1.37E-01	1.74E-01	2.21E-01	1.08E-01	1.74E-01	1.36E-01
PMRS 6 X	9.74E-02	1.84E-01	8.91E-01	1.56E-01	8.86E-01	8.72E-01
PMRS 6 Y	1.26E-01	1.93E-01	2.64E-01	1.46E-01	2.32E-01	1.80E-01
SMRS 7 X	4.91E-01	1.59E+00	1.67E+00	1.51E+00	1.59E+00	5.06E-01
SMRS 7 Y	4.29E-01	1.31E+00	1.49E+00	1.24E+00	1.43E+00	7.07E-01
SMTS 8 X Trans.	3.82E-03	5.74E-03	5.77E-03	4.28E-03	4.32E-03	5.93E-04
SMTS 8 Y Trans.	3.67E-03	6.93E-03	7.00E-03	5.88E-03	5.96E-03	9.98E-04
SMTS 9 X Trans.	3.76E-03	5.89E-03	5.93E-03	4.54E-03	4.58E-03	6.41E-04
SMTS 9 Y Trans.	3.57E-03	6.73E-03	6.83E-03	5.71E-03	5.83E-03	1.19E-03
Line of Sight X	3.56E-01	5.40E-01	6.31E-01	4.06E-01	5.21E-01	3.26E-01
Line of Sight Y	3.65E-01	4.69E-01	5.54E-01	2.95E-01	4.17E-01	2.94E-01

Table 16. Continued.

Measurement	OLU100 0-5 Hz	OLU100 0-50 Hz	OLU100 0-128 Hz	OLU100 5-50 Hz	OLU100 5-128 Hz	OLU100 50-128 Hz
PMA 1 Rate	2.93E+00	3.47E+01	3.47E+01	3.45E+01	3.45E+01	0.00E+00
PMA 2 Rate	2.79E+00	3.43E+01	3.43E+01	3.42E+01	3.42E+01	0.00E+00
PMA 3 Rate	8.95E-01	1.58E+01	1.58E+01	1.57E+01	1.57E+01	0.00E+00
PMA 4 Rate	8.77E-01	1.54E+01	1.54E+01	1.54E+01	1.54E+01	1.76E-01
PMA 5 Rate	2.55E+00	3.29E+01	3.29E+01	3.28E+01	3.28E+01	0.00E+00
PMA 6 Rate	2.90E+00	3.98E+01	3.98E+01	3.97E+01	3.97E+01	2.82E-01
PMA 7 Rate	7.45E-01	1.41E+01	1.41E+01	1.41E+01	1.41E+01	1.68E-01
PMA 8 Rate	8.88E-01	1.62E+01	1.62E+01	1.62E+01	1.62E+01	0.00E+00
PMA 9 Rate	2.70E+00	3.79E+01	3.79E+01	3.78E+01	3.78E+01	2.75E-01
PMA10 Rate	2.96E+00	3.43E+01	3.43E+01	3.42E+01	3.42E+01	0.00E+00
PMA11 Rate	9.20E-01	1.75E+01	1.75E+01	1.74E+01	1.74E+01	1.87E-01
PMA12 Rate	9.41E-01	1.59E+01	1.59E+01	1.59E+01	1.59E+01	0.00E+00
PMA13 Rate	9.39E-01	1.34E+01	1.34E+01	1.34E+01	1.34E+01	1.64E-01
PMA14 Rate	7.47E-01	1.21E+01	1.21E+01	1.21E+01	1.21E+01	1.56E-01
PMA15 Rate	7.51E-01	1.19E+01	1.19E+01	1.19E+01	1.19E+01	0.00E+00
PMA16 Rate	2.27E+00	1.21E+01	1.21E+01	1.19E+01	1.19E+01	0.00E+00
PMA17 Rate	7.68E-01	1.17E+01	1.17E+01	1.17E+01	1.17E+01	1.53E-01
PMA18 Rate	7.72E-01	1.12E+01	1.12E+01	1.12E+01	1.12E+01	1.50E-01
PMRS 1 X	6.18E-01	5.64E+00	5.66E+00	5.61E+00	5.63E+00	5.19E-01
PMRS 1 Y	6.69E-01	2.93E+00	2.96E+00	2.86E+00	2.89E+00	4.05E-01
PMRS 2 X	2.37E+00	1.71E+01	1.71E+01	1.69E+01	1.70E+01	5.85E-01
PMRS 2 Y	7.18E-01	8.90E+00	8.91E+00	8.87E+00	8.88E+00	4.92E-01
PMRS 3 X	5.31E-01	6.33E+00	6.35E+00	6.31E+00	6.33E+00	4.91E-01
PMRS 3 Y	4.27E-01	2.83E+00	2.86E+00	2.80E+00	2.83E+00	4.13E-01
PMRS 4 X	2.19E+00	1.90E+01	1.90E+01	1.88E+01	1.88E+01	6.46E-01
PMRS 4 Y	8.54E-01	1.23E+01	1.23E+01	1.23E+01	1.23E+01	5.44E-01
PMRS 5 X	8.20E-01	7.73E+00	7.75E+00	7.68E+00	7.70E+00	5.62E-01
PMRS 5 Y	5.77E-01	2.13E+00	2.16E+00	2.05E+00	2.09E+00	3.64E-01
PMRS 6 X	2.24E+00	1.71E+01	1.71E+01	1.69E+01	1.70E+01	1.45E+00
PMRS 6 Y	1.01E+00	1.12E+01	1.12E+01	1.12E+01	1.12E+01	4.73E-01
SMRS 7 X	1.35E+01	2.14E+02	2.14E+02	2.14E+02	2.14E+02	2.93E+00
SMRS 7 Y	1.81E+01	2.49E+02	2.49E+02	2.48E+02	2.48E+02	2.23E+00
SMTS 8 X Trans.	5.73E-02	8.60E-01	8.60E-01	8.58E-01	8.58E-01	4.15E-03
SMTS 8 Y Trans.	5.47E-02	7.79E-01	7.79E-01	7.77E-01	7.77E-01	3.95E-03
SMTS 9 X Trans.	6.03E-02	9.09E-01	9.09E-01	9.07E-01	9.07E-01	4.26E-03
SMTS 9 Y Trans.	5.20E-02	7.66E-01	7.66E-01	7.64E-01	7.64E-01	0.00E+00
Line of Sight X	2.92E+00	4.83E+01	4.83E+01	4.82E+01	4.82E+01	7.61E-01
Line of Sight Y	3.81E+00	5.58E+01	5.58E+01	5.57E+01	5.57E+01	5.79E-01

Table 16. Continued.

Measurement	OLC000 0-5 Hz	OLC000 0-50 Hz	OLC000 0-128 Hz	OLC000 5-50 Hz	OLC000 5-128 Hz	OLC000 50-128 Hz
PMA 1 Rate	1.03E-01	2.57E-01	2.58E-01	2.36E-01	2.37E-01	1.73E-02
PMA 2 Rate	8.84E-02	3.67E-01	3.67E-01	3.56E-01	3.57E-01	1.53E-02
PMA 3 Rate	6.12E-02	1.50E-01	1.51E-01	1.37E-01	1.38E-01	1.59E-02
PMA 4 Rate	5.70E-02	1.88E-01	1.89E-01	1.79E-01	1.81E-01	2.00E-02
PMA 5 Rate	9.68E-02	3.73E-01	3.73E-01	3.60E-01	3.60E-01	1.34E-02
PMA 6 Rate	9.82E-02	3.19E-01	3.20E-01	3.04E-01	3.04E-01	2.08E-02
PMA 7 Rate	5.42E-02	1.77E-01	1.77E-01	1.68E-01	1.69E-01	1.49E-02
PMA 8 Rate	7.02E-02	1.85E-01	1.86E-01	1.71E-01	1.72E-01	1.95E-02
PMA 9 Rate	8.89E-02	3.42E-01	3.42E-01	3.30E-01	3.31E-01	1.33E-02
PMA10 Rate	1.06E-01	3.02E-01	3.03E-01	2.83E-01	2.84E-01	2.87E-02
PMA11 Rate	6.64E-02	1.95E-01	1.95E-01	1.83E-01	1.84E-01	1.23E-02
PMA12 Rate	6.35E-02	1.50E-01	1.52E-01	1.36E-01	1.38E-01	1.94E-02
PMA13 Rate	5.47E-02	1.42E-01	1.49E-01	1.31E-01	1.38E-01	4.47E-02
PMA14 Rate	5.90E-02	1.85E-01	1.93E-01	1.75E-01	1.83E-01	5.51E-02
PMA15 Rate	6.08E-02	1.37E-01	1.43E-01	1.23E-01	1.30E-01	4.26E-02
PMA16 Rate	1.60E+00	1.61E+00	1.61E+00	1.18E-01	1.25E-01	4.39E-02
PMA17 Rate	5.84E-02	1.81E-01	1.85E-01	1.71E-01	1.75E-01	3.90E-02
PMA18 Rate	5.86E-02	1.34E-01	1.44E-01	1.21E-01	1.32E-01	5.19E-02
PMRS 1 X	1.88E-01	2.25E-01	2.68E-01	1.23E-01	1.91E-01	1.45E-01
PMRS 1 Y	2.25E-01	2.51E-01	2.71E-01	1.11E-01	1.51E-01	1.02E-01
PMRS 2 X	1.43E-01	2.35E-01	3.24E-01	1.86E-01	2.91E-01	2.23E-01
PMRS 2 Y	1.32E-01	2.26E-01	2.97E-01	1.84E-01	2.66E-01	1.93E-01
PMRS 3 X	8.70E-02	1.75E-01	2.48E-01	1.52E-01	2.33E-01	1.76E-01
PMRS 3 Y	9.78E-02	1.47E-01	1.81E-01	1.09E-01	1.53E-01	1.07E-01
PMRS 4 X	1.01E-01	2.30E-01	3.28E-01	2.06E-01	3.12E-01	2.34E-01
PMRS 4 Y	1.51E-01	2.62E-01	3.15E-01	2.14E-01	2.77E-01	1.75E-01
PMRS 5 X	1.99E-01	2.46E-01	2.92E-01	1.44E-01	2.13E-01	1.57E-01
PMRS 5 Y	2.35E-01	2.57E-01	2.82E-01	1.06E-01	1.56E-01	1.15E-01
PMRS 6 X	2.30E-01	3.30E-01	8.62E-01	2.37E-01	8.30E-01	7.96E-01
PMRS 6 Y	2.65E-01	3.08E-01	3.45E-01	1.57E-01	2.20E-01	1.54E-01
SMRS 7 X	1.02E+00	3.81E+00	3.86E+00	3.68E+00	3.73E+00	6.22E-01
SMRS 7 Y	6.99E-01	2.56E+00	2.65E+00	2.46E+00	2.55E+00	6.81E-01
SMTS 8 X Trans.	6.24E-03	1.02E-02	1.02E-02	8.03E-03	8.04E-03	4.51E-04
SMTS 8 Y Trans.	5.60E-03	1.19E-02	1.20E-02	1.05E-02	1.06E-02	8.18E-04
SMTS 9 X Trans.	6.05E-03	1.06E-02	1.06E-02	8.65E-03	8.67E-03	4.82E-04
SMTS 9 Y Trans.	5.56E-03	1.14E-02	1.14E-02	9.94E-03	9.98E-03	9.55E-04
Line of Sight X	5.72E-01	7.83E-01	8.60E-01	5.35E-01	6.41E-01	3.54E-01
Line of Sight Y	6.09E-01	7.95E-01	8.41E-01	5.12E-01	5.80E-01	2.72E-01

Table 16. Continued.

Measurement	OLC100 0-5 Hz	OLC100 0-50 Hz	OLC100 0-128 Hz	OLC100 5-50 Hz	OLC100 5-128 Hz	OLC100 50-128 Hz
PMA 1 Rate	1.88E+00	6.54E+01	6.54E+01	6.54E+01	6.54E+01	0.00E+00
PMA 2 Rate	1.69E+00	6.47E+01	6.47E+01	6.47E+01	6.47E+01	0.00E+00
PMA 3 Rate	7.09E-01	2.57E+01	2.57E+01	2.57E+01	2.57E+01	0.00E+00
PMA 4 Rate	7.42E-01	2.56E+01	2.56E+01	2.56E+01	2.56E+01	2.26E-01
PMA 5 Rate	1.55E+00	6.12E+01	6.12E+01	6.12E+01	6.12E+01	0.00E+00
PMA 6 Rate	2.14E+00	6.20E+01	6.20E+01	6.19E+01	6.19E+01	0.00E+00
PMA 7 Rate	5.87E-01	2.30E+01	2.30E+01	2.30E+01	2.30E+01	0.00E+00
PMA 8 Rate	7.53E-01	2.33E+01	2.33E+01	2.33E+01	2.33E+01	0.00E+00
PMA 9 Rate	2.04E+00	5.86E+01	5.86E+01	5.86E+01	5.86E+01	0.00E+00
PMA10 Rate	1.89E+00	6.66E+01	6.66E+01	6.65E+01	6.65E+01	0.00E+00
PMA11 Rate	7.50E-01	2.48E+01	2.48E+01	2.48E+01	2.48E+01	0.00E+00
PMA12 Rate	6.71E-01	2.69E+01	2.69E+01	2.69E+01	2.69E+01	0.00E+00
PMA13 Rate	8.93E-01	1.89E+01	1.89E+01	1.89E+01	1.89E+01	1.94E-01
PMA14 Rate	6.76E-01	1.84E+01	1.84E+01	1.83E+01	1.83E+01	1.92E-01
PMA15 Rate	6.99E-01	1.80E+01	1.80E+01	1.80E+01	1.80E+01	0.00E+00
PMA16 Rate	1.95E+00	1.71E+01	1.71E+01	1.70E+01	1.70E+01	1.85E-01
PMA17 Rate	7.77E-01	1.75E+01	1.75E+01	1.74E+01	1.74E+01	0.00E+00
PMA18 Rate	7.49E-01	1.71E+01	1.71E+01	1.71E+01	1.71E+01	1.85E-01
PMRS 1 X	3.07E-01	9.30E+00	9.32E+00	9.30E+00	9.31E+00	4.75E-01
PMRS 1 Y	2.49E-01	3.41E+00	3.43E+00	3.40E+00	3.43E+00	3.81E-01
PMRS 2 X	1.11E+00	3.67E+01	3.67E+01	3.66E+01	3.66E+01	6.63E-01
PMRS 2 Y	4.79E-01	1.37E+01	1.37E+01	1.37E+01	1.37E+01	5.74E-01
PMRS 3 X	2.44E-01	1.09E+01	1.09E+01	1.09E+01	1.09E+01	4.67E-01
PMRS 3 Y	1.88E-01	4.32E+00	4.34E+00	4.32E+00	4.34E+00	3.99E-01
PMRS 4 X	1.14E+00	3.74E+01	3.74E+01	3.74E+01	3.74E+01	7.73E-01
PMRS 4 Y	6.83E-01	1.72E+01	1.72E+01	1.72E+01	1.72E+01	5.87E-01
PMRS 5 X	5.19E-01	1.23E+01	1.23E+01	1.23E+01	1.23E+01	5.20E-01
PMRS 5 Y	3.00E-01	2.91E+00	2.93E+00	2.89E+00	2.92E+00	3.93E-01
PMRS 6 X	1.11E+00	3.70E+01	3.71E+01	3.70E+01	3.70E+01	1.87E+00
PMRS 6 Y	7.00E-01	1.54E+01	1.54E+01	1.53E+01	1.54E+01	5.54E-01
SMRS 7 X	9.27E+00	3.61E+02	3.61E+02	3.61E+02	3.61E+02	4.66E+00
SMRS 7 Y	1.21E+01	3.72E+02	3.72E+02	3.72E+02	3.72E+02	2.73E+00
SMTS 8 X Trans.	3.61E-02	1.26E+00	1.26E+00	1.25E+00	1.25E+00	0.00E+00
SMTS 8 Y Trans.	3.18E-02	1.38E+00	1.38E+00	1.38E+00	1.38E+00	0.00E+00
SMTS 9 X Trans.	3.82E-02	1.34E+00	1.34E+00	1.34E+00	1.34E+00	0.00E+00
SMTS 9 Y Trans.	3.12E-02	1.32E+00	1.32E+00	1.32E+00	1.32E+00	0.00E+00
Line of Sight X	1.65E+00	7.99E+01	7.99E+01	7.99E+01	7.99E+01	1.13E+00
Line of Sight Y	2.32E+00	8.06E+01	8.06E+01	8.05E+01	8.06E+01	1.45E+00

Table 16. Concluded.

Measurement	OLC-P128 0-5 Hz	OLC-P128 0-50 Hz	OLC-P128 0-128 Hz	OLC-P128 5-50 Hz	OLC-P128 5-128 Hz	OLC-P128 50-128 Hz
PMA 1 Rate	1.94E+00	6.54E+01	6.54E+01	6.54E+01	6.54E+01	0.00E+00
PMA 2 Rate	1.70E+00	7.07E+01	7.07E+01	7.06E+01	7.06E+01	0.00E+00
PMA 3 Rate	6.56E-01	2.72E+01	2.72E+01	2.72E+01	2.72E+01	0.00E+00
PMA 4 Rate	6.16E-01	2.94E+01	2.94E+01	2.93E+01	2.93E+01	0.00E+00
PMA 5 Rate	1.59E+00	6.77E+01	6.77E+01	6.77E+01	6.77E+01	0.00E+00
PMA 6 Rate	2.17E+00	7.10E+01	7.10E+01	7.10E+01	7.10E+01	0.00E+00
PMA 7 Rate	5.00E-01	2.67E+01	2.67E+01	2.67E+01	2.67E+01	0.00E+00
PMA 8 Rate	6.95E-01	2.84E+01	2.84E+01	2.83E+01	2.83E+01	0.00E+00
PMA 9 Rate	2.07E+00	7.01E+01	7.01E+01	7.01E+01	7.01E+01	0.00E+00
PMA10 Rate	1.95E+00	6.73E+01	6.73E+01	6.72E+01	6.72E+01	0.00E+00
PMA11 Rate	7.28E-01	3.02E+01	3.02E+01	3.02E+01	3.02E+01	0.00E+00
PMA12 Rate	6.53E-01	2.79E+01	2.79E+01	2.79E+01	2.79E+01	0.00E+00
PMA13 Rate	9.13E-01	2.52E+01	2.52E+01	2.52E+01	2.52E+01	2.24E-01
PMA14 Rate	7.16E-01	2.65E+01	2.65E+01	2.65E+01	2.65E+01	0.00E+00
PMA15 Rate	6.82E-01	2.23E+01	2.23E+01	2.23E+01	2.23E+01	0.00E+00
PMA16 Rate	1.79E+00	2.58E+01	2.58E+01	2.57E+01	2.57E+01	0.00E+00
PMA17 Rate	8.11E-01	2.58E+01	2.58E+01	2.58E+01	2.58E+01	2.27E-01
PMA18 Rate	7.81E-01	2.13E+01	2.13E+01	2.13E+01	2.13E+01	2.06E-01
PMRS 1 X	2.92E-01	8.54E+00	8.55E+00	8.54E+00	8.55E+00	4.75E-01
PMRS 1 Y	2.52E-01	3.79E+00	3.81E+00	3.79E+00	3.80E+00	3.82E-01
PMRS 2 X	1.16E+00	3.53E+01	3.53E+01	3.52E+01	3.53E+01	6.51E-01
PMRS 2 Y	5.43E-01	1.57E+01	1.57E+01	1.57E+01	1.57E+01	5.61E-01
PMRS 3 X	6.41E-01	1.14E+01	1.14E+01	1.14E+01	1.14E+01	4.54E-01
PMRS 3 Y	6.41E-01	4.87E+00	4.89E+00	4.83E+00	4.85E+00	4.01E-01
PMRS 4 X	1.09E+00	3.72E+01	3.72E+01	3.72E+01	3.72E+01	8.18E-01
PMRS 4 Y	6.87E-01	2.28E+01	2.28E+01	2.28E+01	2.28E+01	5.65E-01
PMRS 5 X	4.77E-01	1.28E+01	1.28E+01	1.28E+01	1.28E+01	5.30E-01
PMRS 5 Y	2.45E-01	3.35E+00	3.38E+00	3.35E+00	3.37E+00	3.93E-01
PMRS 6 X	1.10E+00	3.98E+01	3.98E+01	3.97E+01	3.98E+01	1.87E+00
PMRS 6 Y	7.05E-01	1.68E+01	1.68E+01	1.68E+01	1.68E+01	5.50E-01
SMRS 7 X	9.85E+00	4.66E+02	4.66E+02	4.66E+02	4.66E+02	4.32E+00
SMRS 7 Y	1.28E+01	4.91E+02	4.91E+02	4.91E+02	4.91E+02	0.00E+00
SMTS 8 X Trans.	4.43E-02	1.68E+00	1.68E+00	1.68E+00	1.68E+00	0.00E+00
SMTS 8 Y Trans.	3.84E-02	1.74E+00	1.74E+00	1.74E+00	1.74E+00	0.00E+00
SMTS 9 X Trans.	5.27E-02	1.77E+00	1.77E+00	1.77E+00	1.77E+00	0.00E+00
SMTS 9 Y Trans.	4.47E-02	1.69E+00	1.69E+00	1.69E+00	1.69E+00	0.00E+00
Line of Sight X	2.89E+00	1.08E+02	1.08E+02	1.08E+02	1.08E+02	0.00E+00
Line of Sight Y	3.58E+00	1.08E+02	1.08E+02	1.08E+02	1.08E+02	1.47E+00

Table 17. Summary of residual LOS jitter performance results.

Disturbance Condition	LOS Component	Freq. Band (Hz)	Open-Loop Caged	Open-Loop Uncaged	LAC	HAC
100-µrad Caged-Target Level Active	X	0 - 5	2.89E+00	2.92E+00	2.34E+00	1.15E+00
	X	5 - 50	1.08E+02	4.82E+01	1.09E+01	9.86E-01
	X	50 - 128	5.00E-01	7.61E-01	6.86E-01	6.91E-01
	X	0 - 128	1.08E+02	4.83E+01	1.12E+01	1.66E+00
	X	5 - 128	1.08E+02	4.82E+01	1.10E+01	1.20E+00
	Y	0 - 5	3.58E+00	3.81E+00	3.10E+00	1.02E+00
	Y	5 - 50	1.08E+02	5.57E+01	1.38E+01	1.48E+00
	Y	50 - 128	1.47E+00	5.79E-01	6.07E-01	6.58E-01
	Y	0 - 128	1.08E+02	5.58E+01	1.42E+01	1.92E+00
	Y	5 - 128	1.08E+02	5.57E+01	1.38E+01	1.62E+00
	Composite	0 - 5	3.26E+00	3.40E+00	2.75E+00	1.09E+00
	Composite	5 - 50	1.08E+02	5.21E+01	1.25E+01	1.26E+00
	Composite	50 - 128	1.10E+00	6.76E-01	6.47E-01	6.75E-01
	Composite	0 - 128	1.08E+02	5.22E+01	1.28E+01	1.80E+00
	Composite	5 - 128	1.08E+02	5.21E+01	1.25E+01	1.43E+00
Noise Only - No Input Disturbance	X	0 - 5	5.72E-01	3.56E-01	3.92E-01	3.37E-01
	X	5 - 50	5.35E-01	4.06E-01	1.52E-01	8.55E-02
	X	50 - 128	3.54E-01	3.26E-01	3.14E-01	2.78E-01
	X	0 - 128	8.60E-01	6.31E-01	5.25E-01	4.45E-01
	X	5 - 128	6.41E-01	5.21E-01	3.49E-01	2.91E-01
	Y	0 - 5	6.09E-01	3.65E-01	4.21E-01	3.68E-01
	Y	5 - 50	5.12E-01	2.95E-01	1.55E-01	9.04E-02
	Y	50 - 128	2.72E-01	2.94E-01	2.70E-01	2.63E-01
	Y	0 - 128	8.41E-01	5.54E-01	5.24E-01	4.61E-01
	Y	5 - 128	5.80E-01	4.17E-01	3.11E-01	2.78E-01
	Composite	0 - 5	5.91E-01	3.61E-01	4.07E-01	3.53E-01
	Composite	5 - 50	5.23E-01	3.55E-01	1.53E-01	8.80E-02
	Composite	50 - 128	3.16E-01	3.11E-01	2.93E-01	2.71E-01
	Composite	0 - 128	8.50E-01	5.94E-01	5.24E-01	4.53E-01
	Composite	5 - 128	6.11E-01	4.72E-01	3.31E-01	2.85E-01
Shakers Only - Noise Subtracted from 100-µrad Result	X	0 - 5	2.84E+00	2.90E+00	2.30E+00	1.10E+00
	X	5 - 50	1.08E+02	4.82E+01	1.09E+01	9.82E-01
	X	50 - 128	3.53E-01	6.87E-01	6.09E-01	6.33E-01
	X	0 - 128	1.08E+02	4.83E+01	1.12E+01	1.60E+00
	X	5 - 128	1.08E+02	4.82E+01	1.10E+01	1.17E+00
	Y	0 - 5	3.53E+00	3.80E+00	3.07E+00	9.56E-01
	Y	5 - 50	1.08E+02	5.57E+01	1.38E+01	1.48E+00
	Y	50 - 128	1.44E+00	4.98E-01	5.44E-01	6.03E-01
	Y	0 - 128	1.08E+02	5.58E+01	1.42E+01	1.86E+00
	Y	5 - 128	1.08E+02	5.57E+01	1.38E+01	1.60E+00
	Composite	0 - 5	3.20E+00	3.38E+00	2.72E+00	1.03E+00
	Composite	5 - 50	1.08E+02	5.21E+01	1.25E+01	1.25E+00
	Composite	50 - 128	1.05E+00	6.00E-01	5.77E-01	6.18E-01
	Composite	0 - 128	1.08E+02	5.22E+01	1.28E+01	1.74E+00
	Composite	5 - 128	1.08E+02	5.21E+01	1.25E+01	1.40E+00

Table 18. List of summary performance graphs.

Figure #	Shakers	Outputs	Tests Compared
23	ON	PMA 1-18 RATES	5A19, HAC100, LAC100, OLC100
24	ON	PMRS 1-12	5A19, HAC100, LAC100, OLC100
25	ON	SMTS 8-9	5A19, HAC100, LAC100, OLC100
26	ON	SMRS 7 & LOS	5A19, HAC100, LAC100, OLC100
27	ON	LVDT 1-18	5A19, HAC100, LAC100
28	OFF	PMA 1-18 RATES	HAC000, LAC000, OLC000
29	OFF	PMRS 1-12	HAC000, LAC000, OLC000
30	OFF	SMTS 8-9	HAC000, LAC000, OLC000
31	OFF	SMRS 7 & LOS	HAC000, LAC000, OLC000

same as those obtained with only the LAC operating. For the SMTS, SMRS, and LOS signals, there are drastic reductions from open loop to LAC, and again from LAC to HAC. These data indicate that the control system is not minimizing the LOS cost function at the expense of other degrees of freedom. That is, the controller is not quieting LOS while exciting some other structural motion. In bringing about the minimization of LOS, it quiets the entire structure.

- The one exception to this is LVDT motion. The HAC requires more stroke from the PMAs than the LAC does. Even the prediction of stroke exceeds LAC stroke. But this is to be expected since stroke is proportional to force at lower frequencies and it is PMA force that implements the HAC. As can be seen from the PSDs presented earlier, the discrepancy between HAC stroke and predicted HAC stroke is predominantly below 5 Hz. This also is expected since the HAC model is most in error in this region due to PMA flexure nonlinearity and inaccurate modeling of rigid-body constraints. In addition, model predictions do not include the rapid increase in atmospheric turbulence below a few hertz.
- As can be seen from Figures 23 through 26, the predictions of output motion agree quite well with actual HAC responses. These are total responses from near DC to 128 Hz. The individual PSDs indicate that agreement is not as good for a frequency by frequency comparison. Nonetheless, average response of the system is exceedingly predictable.
- Figures 28 through 31 are for quiescent tests. It is evident that LAC greatly quiets the open-loop outputs. The PMA housing rates slightly improve with HAC. The PMRS motion tends to be neither improved nor degraded with HAC. The same is generally true for the SMTS, SMRS, and LOS outputs. The fact that HAC has not degraded LAC quiescent performance is very good news. Part of the reason for benign HAC quiescent performance is that much of the quiescent input to HAC is residual LAC

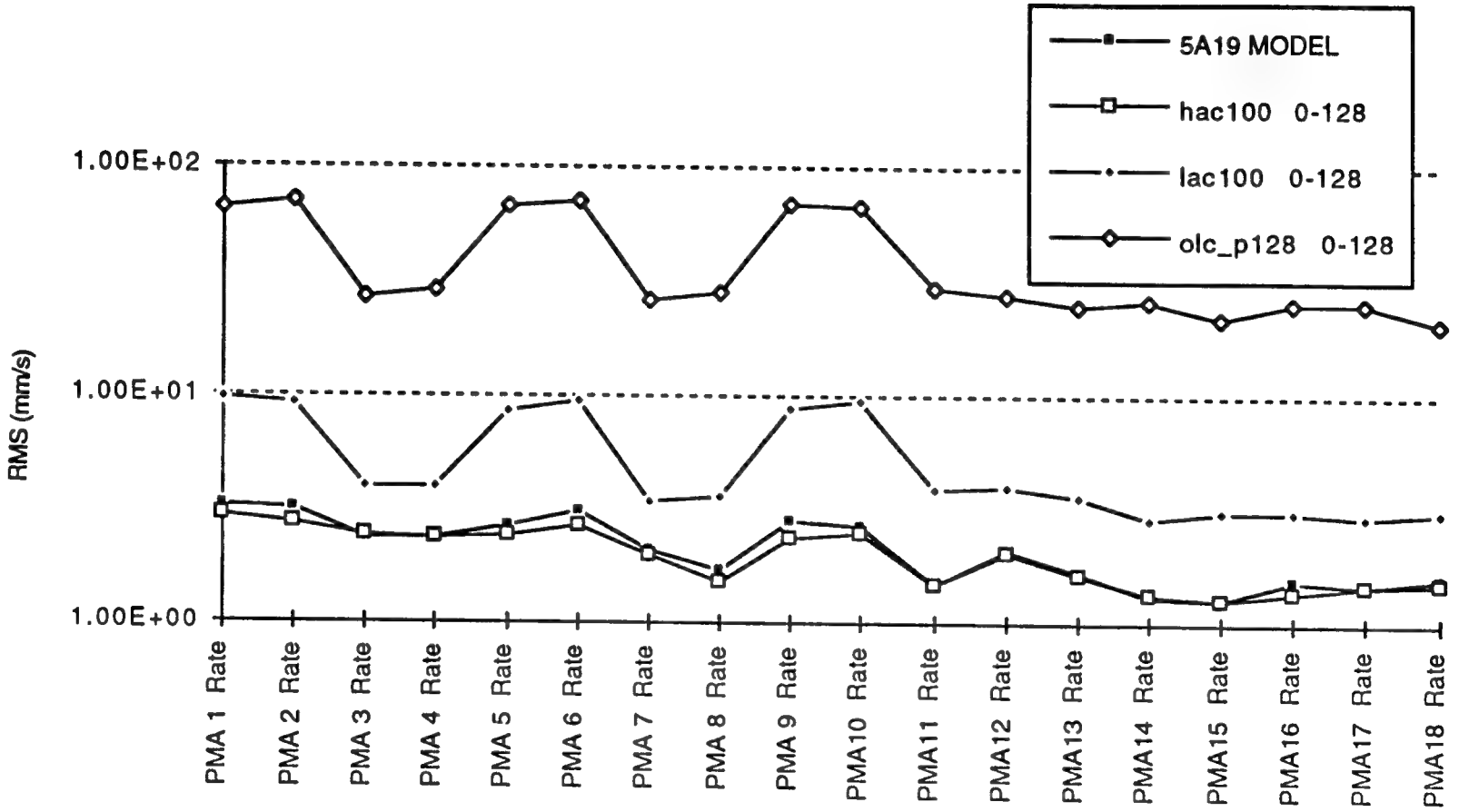

Figure 23. Calculated and measured RMS PMA rates - 100-μrad disturbances.

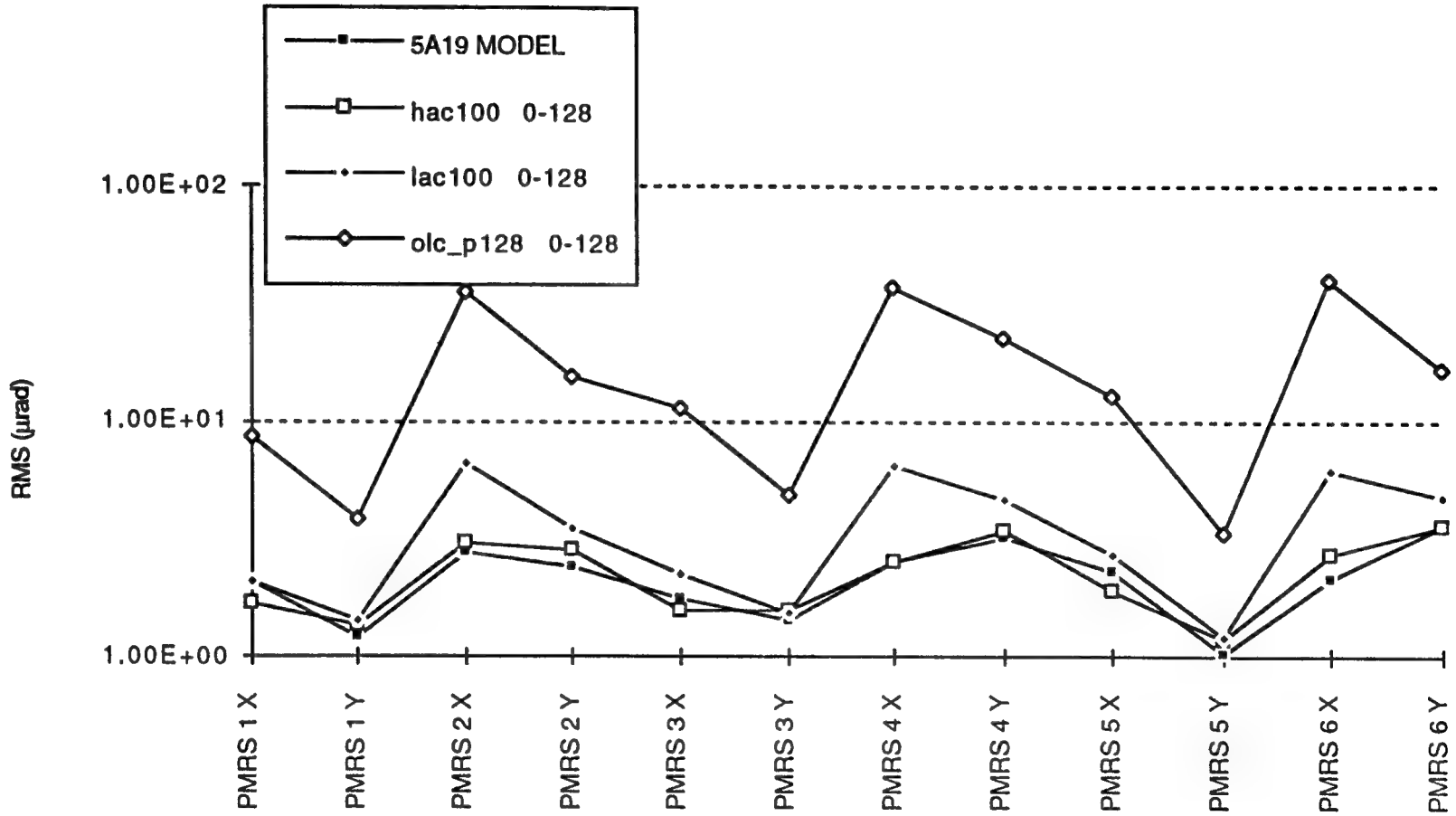

Figure 24. Calculated and measured RMS PMRS outputs - 100-µrad disturbances.

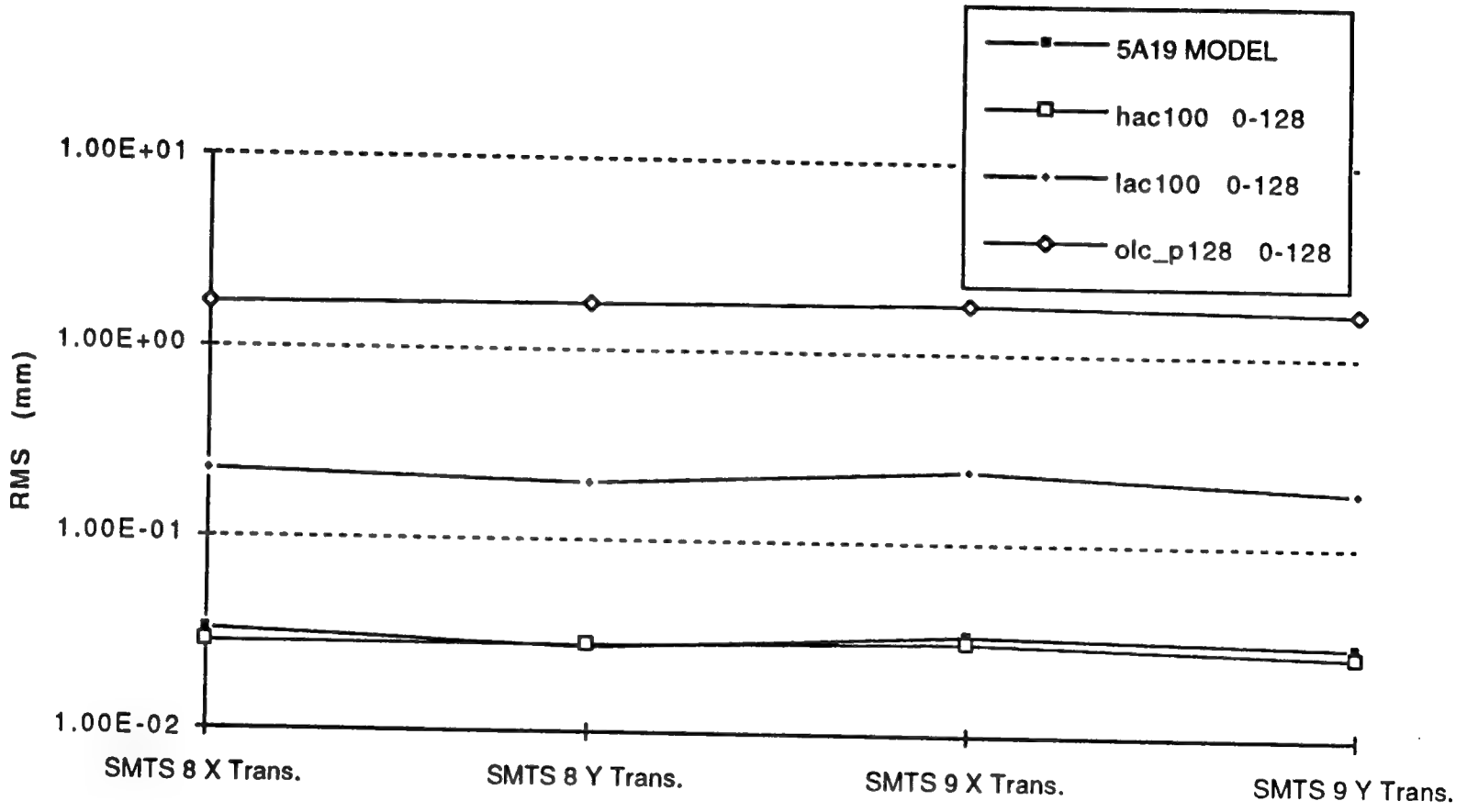

Figure 25. Calculated and measured RMS SMTS outputs - 100-μrad disturbances.

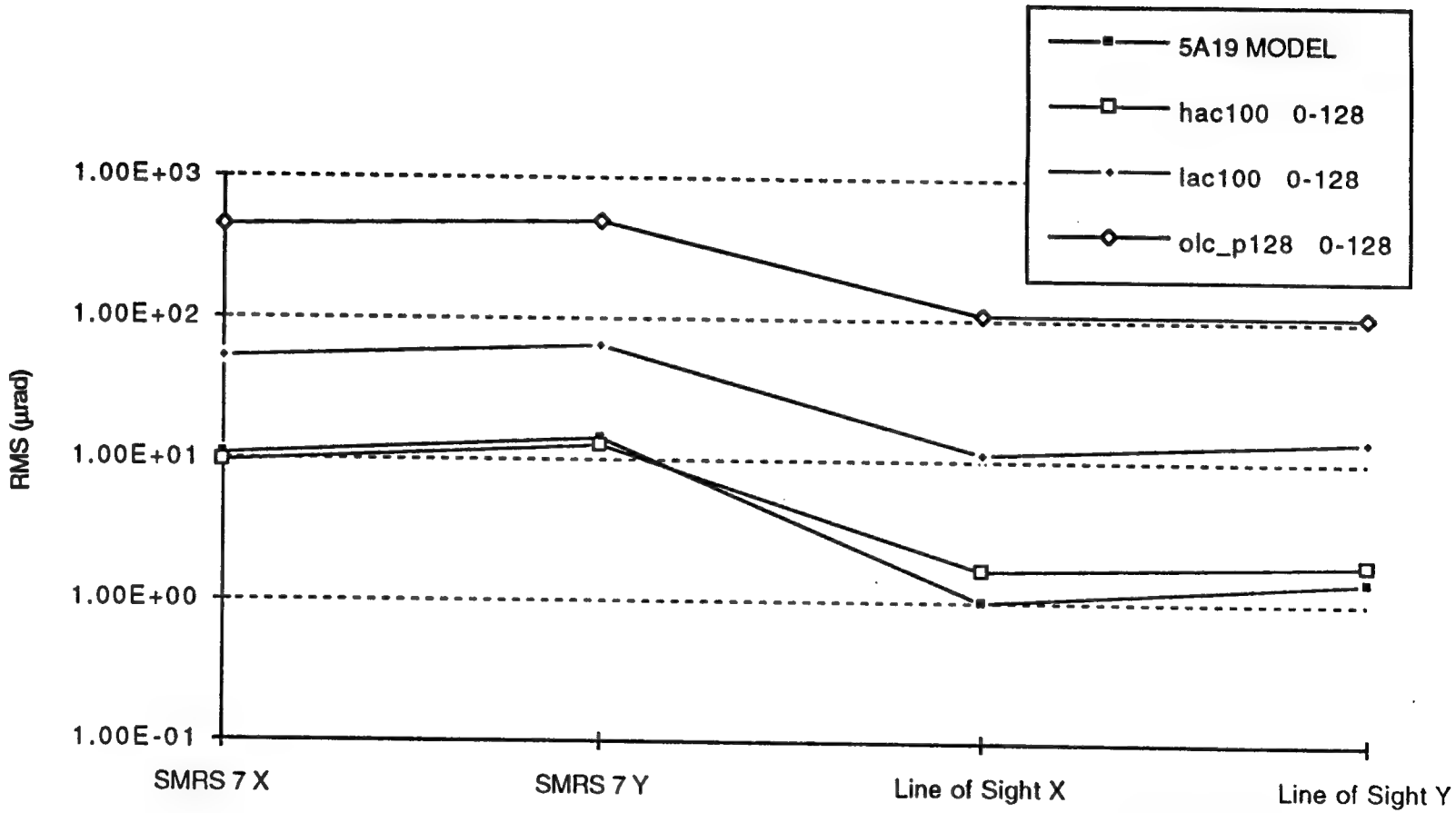

Figure 26. Calculated and measured RMS SMRS and LOS outputs - 100-µrad disturbances.

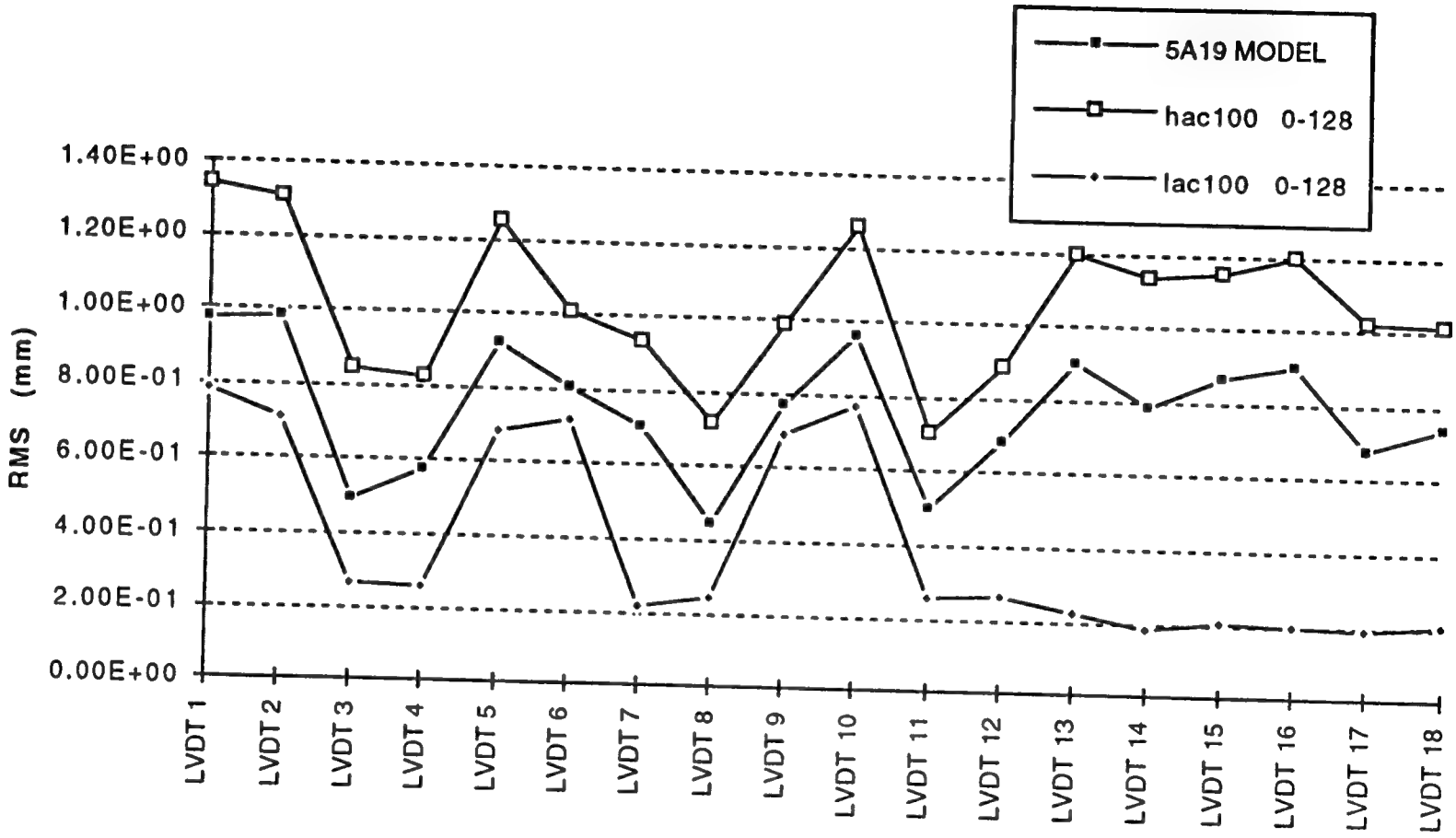

Figure 27. Calculated and measured LVDT outputs - 100-μrad disturbances.

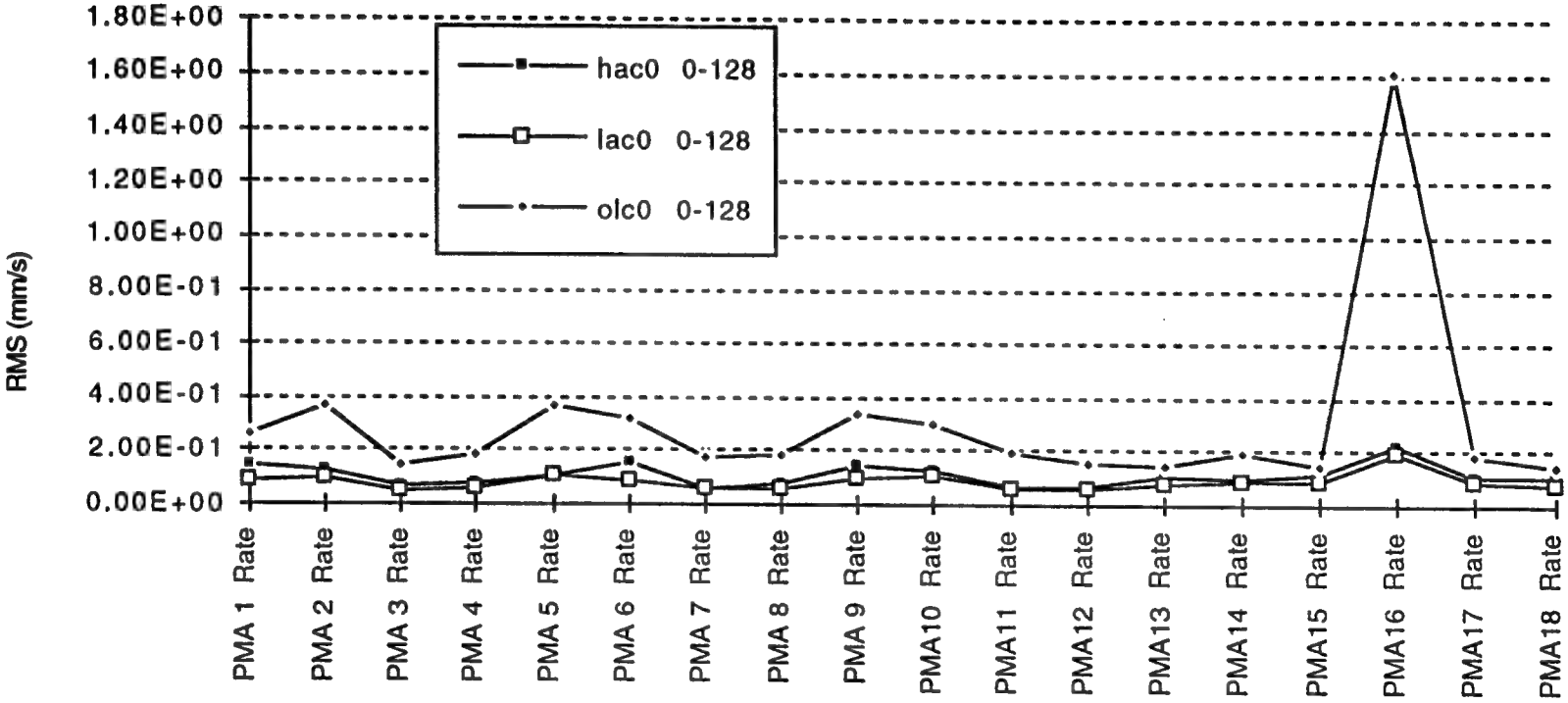

Figure 28. Calculated and measured RMS PMA rates - quiescent.

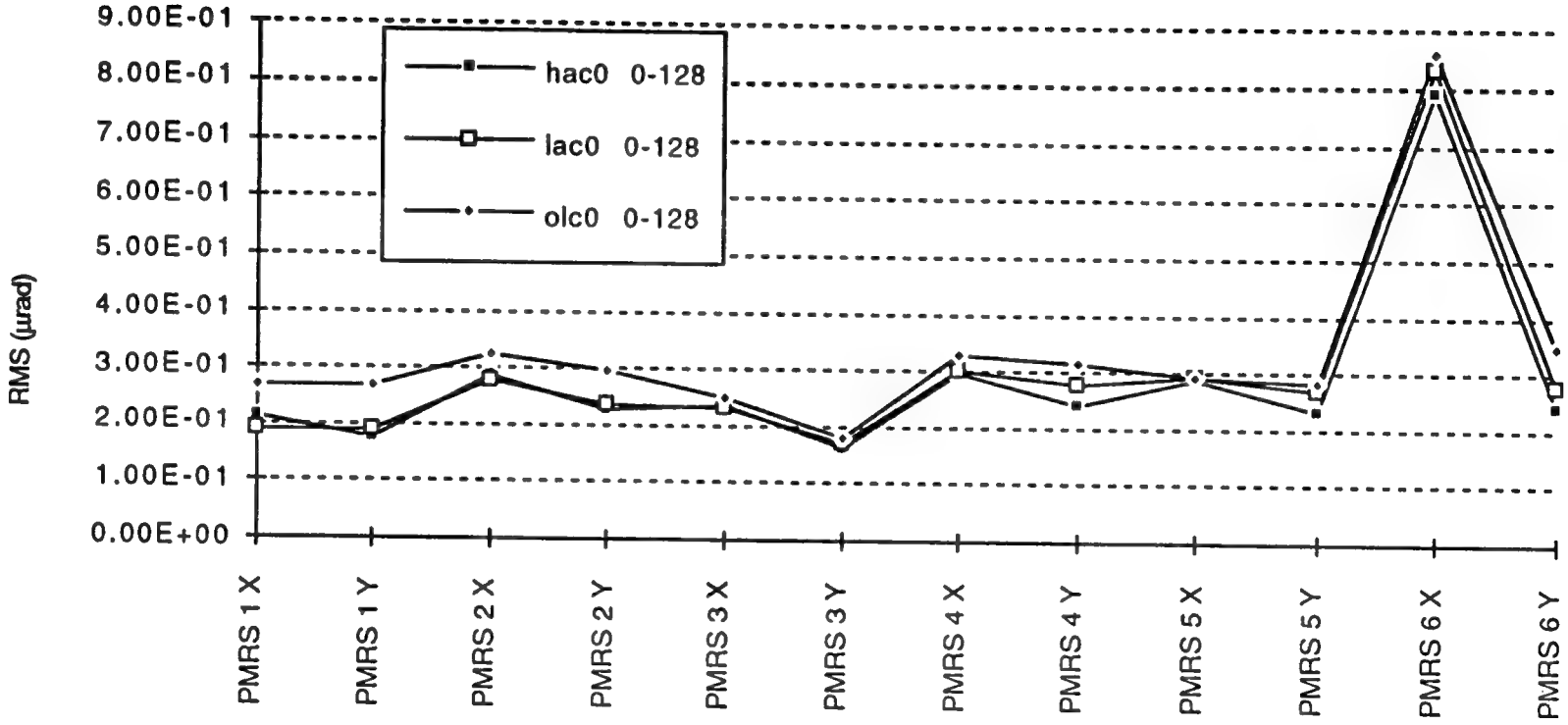

Figure 29. Calculated and measured RMS PMRS outputs - quiescent.

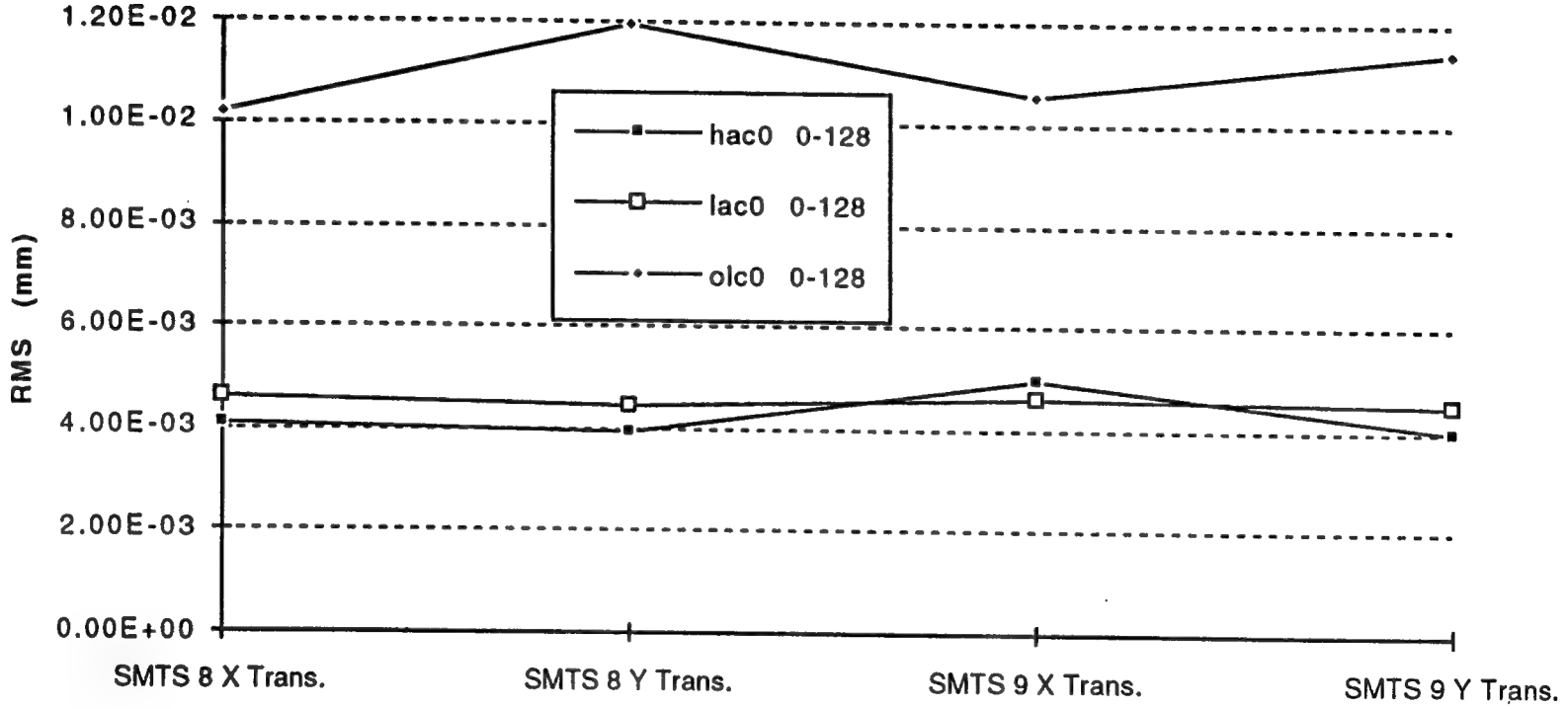

Figure 30. Calculated and measured RMS SMTS outputs - quiescent.

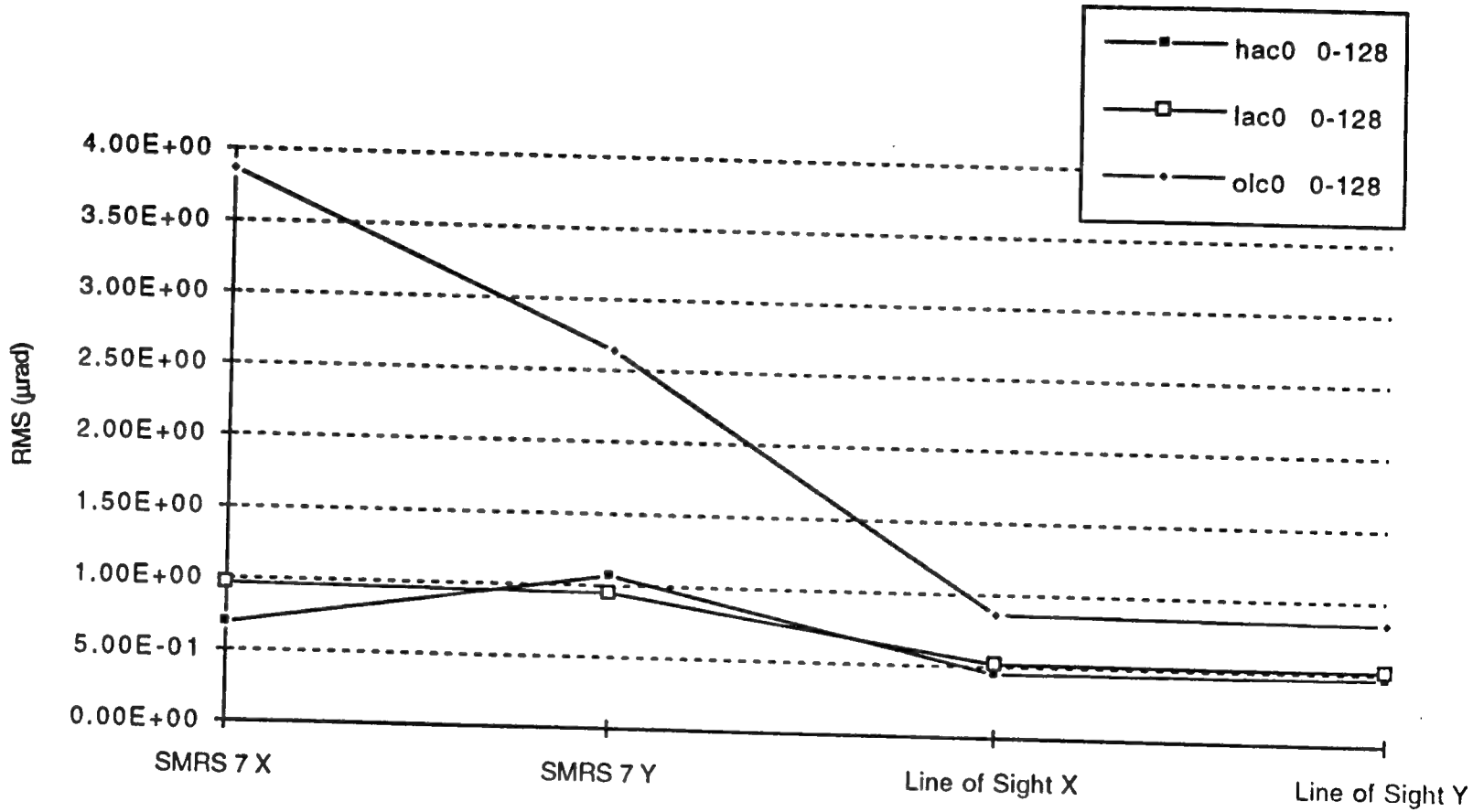

Figure 31. Calculated and measured RMS SMRS and LOS outputs - quiescent.

structural motion, as opposed to sensor noise. The HAC attenuates the structural motion beyond what LAC has done, thereby improving overall quiescent performance. Still, it is clear from these graphs and the individual PSDs that HAC is not significantly amplifying ambient noise. This is true in the spillover frequencies as well.

- The problem with the QA700 housing accelerometer at PMA 16 is very evident in Figure 28. The problem manifests itself most strongly in the open-loop configuration.
- The segment six local panel mode problem is evident in Figure 29 at PMRS 6X. This shows up strongly for all three configurations.

The LOS data in Table 17 are graphically displayed in Figures 32 - 40. These figures are listed in Table 19. The configurations compared are open-loop caged, open-loop uncaged, LAC, and HAC. There are five frequency bins in each figure. The 0- to 5-Hz bin contains frequencies below the PMA flexure frequencies. The main authority of the HAC is in the second bin of 5 to 50 Hz. The third bin lies in the spillover region, 50 to 128 Hz. The fourth bin spans all frequencies, 0 to 128 Hz.

Table 19. List of LOS performance figures.

Figure #	LOS Component	Disturbance Condition
32	X	Shakers On
33	Y	Shakers On
34	Composite	Shakers On
35	X	Quiescent
36	Y	Quiescent
37	Composite	Quiescent
38	X	Due to Shakers
39	Y	Due to Shakers
40	Composite	Due to Shakers

The fifth bin, 5 to 128 Hz, is equivalent to the scoreable range of frequencies, the frequency range for which the HAC is to attain 50:1 attenuation as a goal. The SPICE Statement of Work lists the frequency range for which attenuation is to be demonstrated as 5 to 500 Hz. However, the residual disturbance above 128 Hz was shown to be insignificant. In a test specifically designed to demonstrate this, the full 100-μrad caged-target LOS set of disturbances was input to the structure, the HAC/LAC system was activated, and residuals were observed in band 128 to 512 Hz. The results, 0.17 μrad for LOS-x and 0.11 μrad for LOS-y, are insignificant compared to the 5- to 128-Hz band residuals. When LOS residuals for the two bands are combined in an RMS sense, results differ from the 5 to 128 Hz numbers only in the third significant figure.

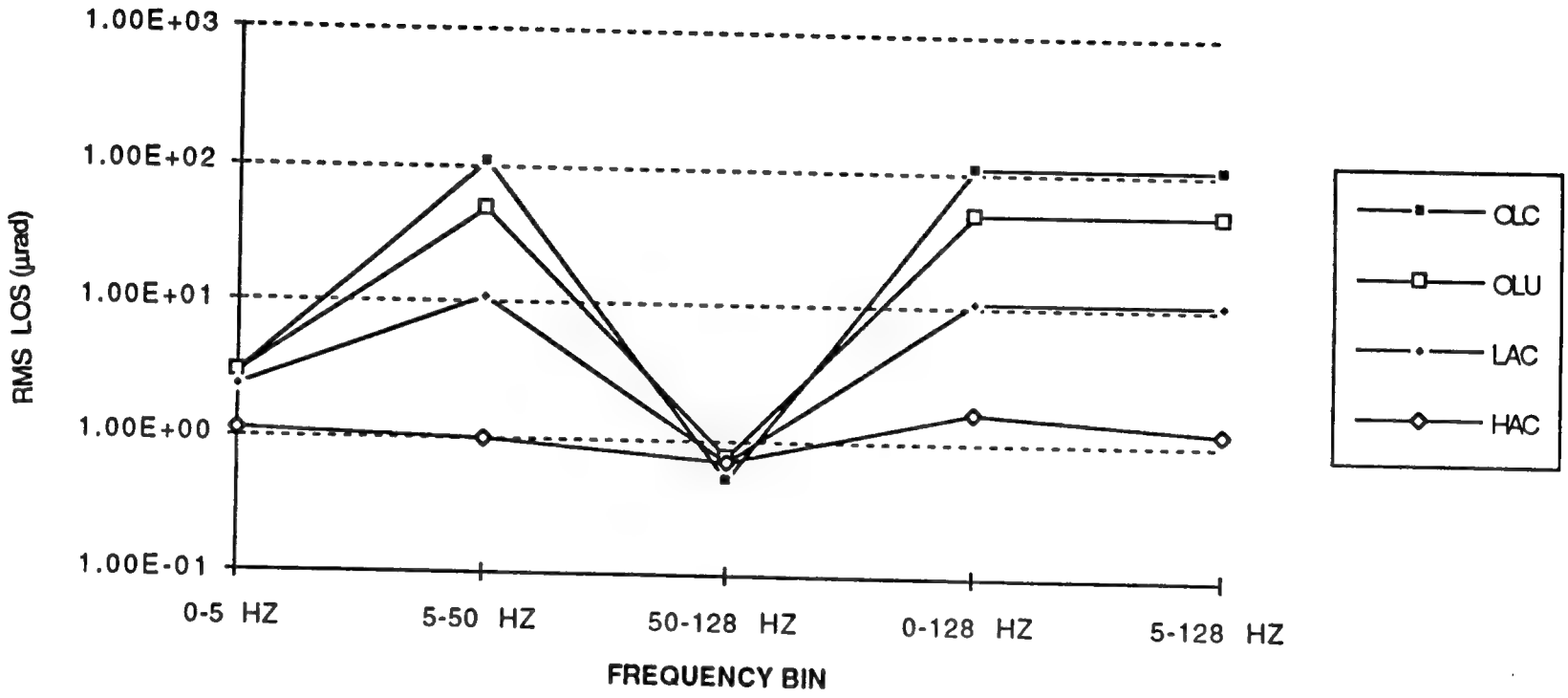

Figure 32. Frequency bin distribution of RMS LOS-x - 100-µrad disturbances.

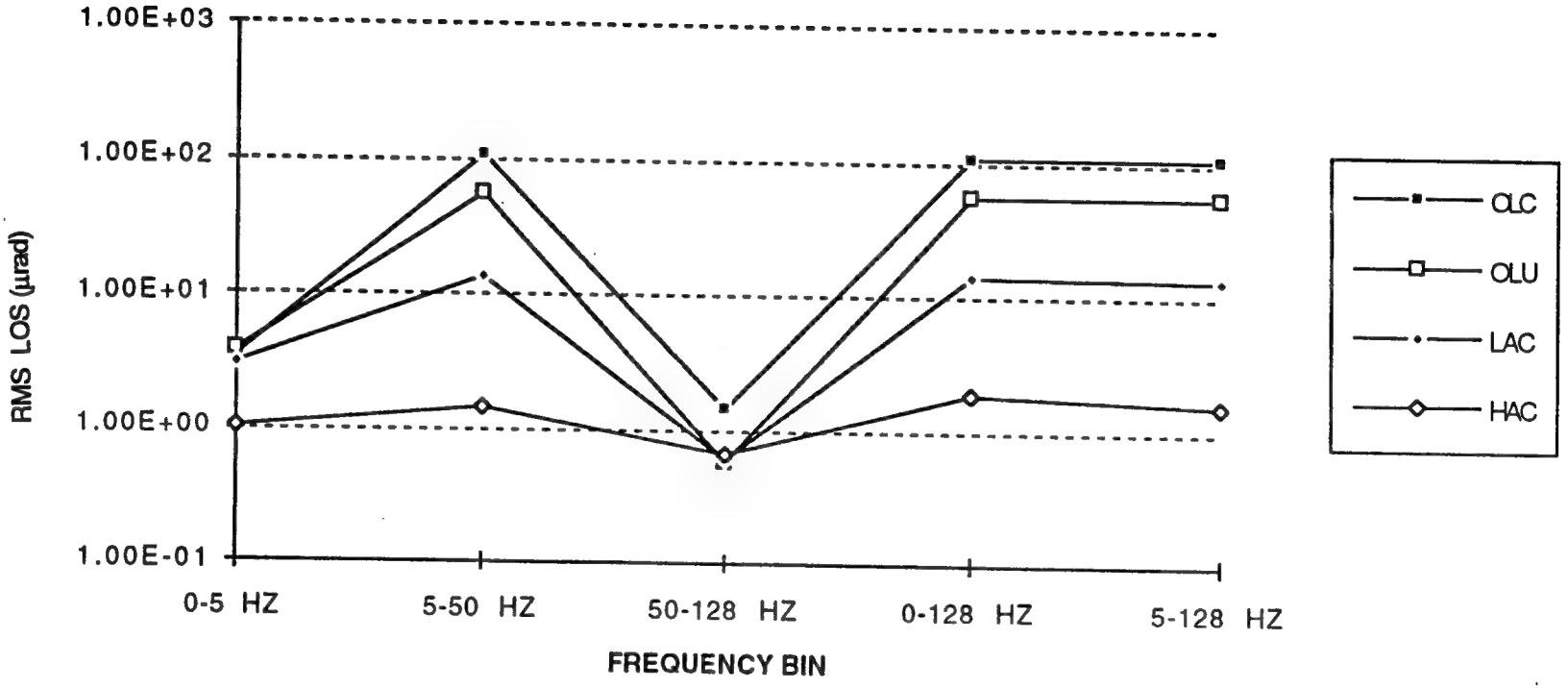

Figure 33. Frequency bin distribution of RMS LOS-y - 100-µrad disturbances.

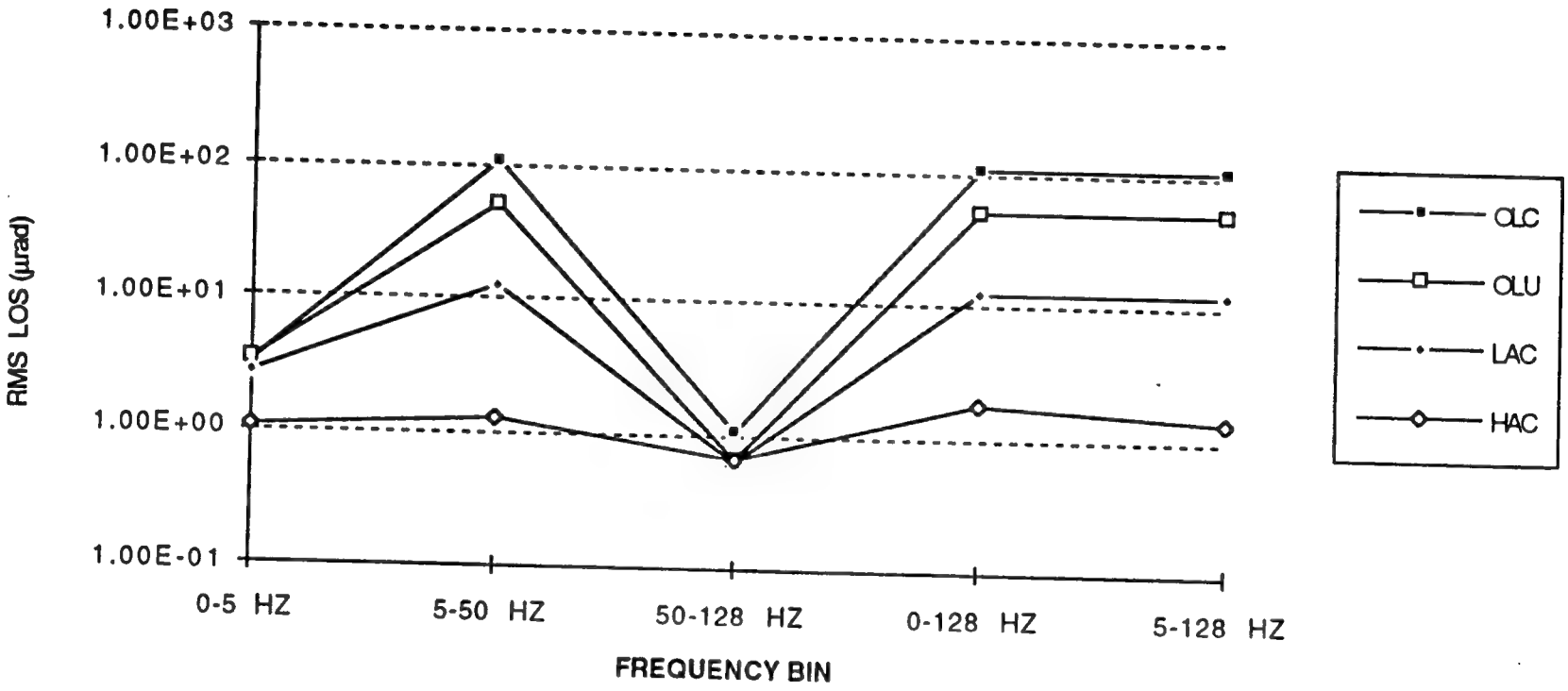

Figure 34. Frequency bin distribution of composite RMS LOS - 100-µrad disturbances.

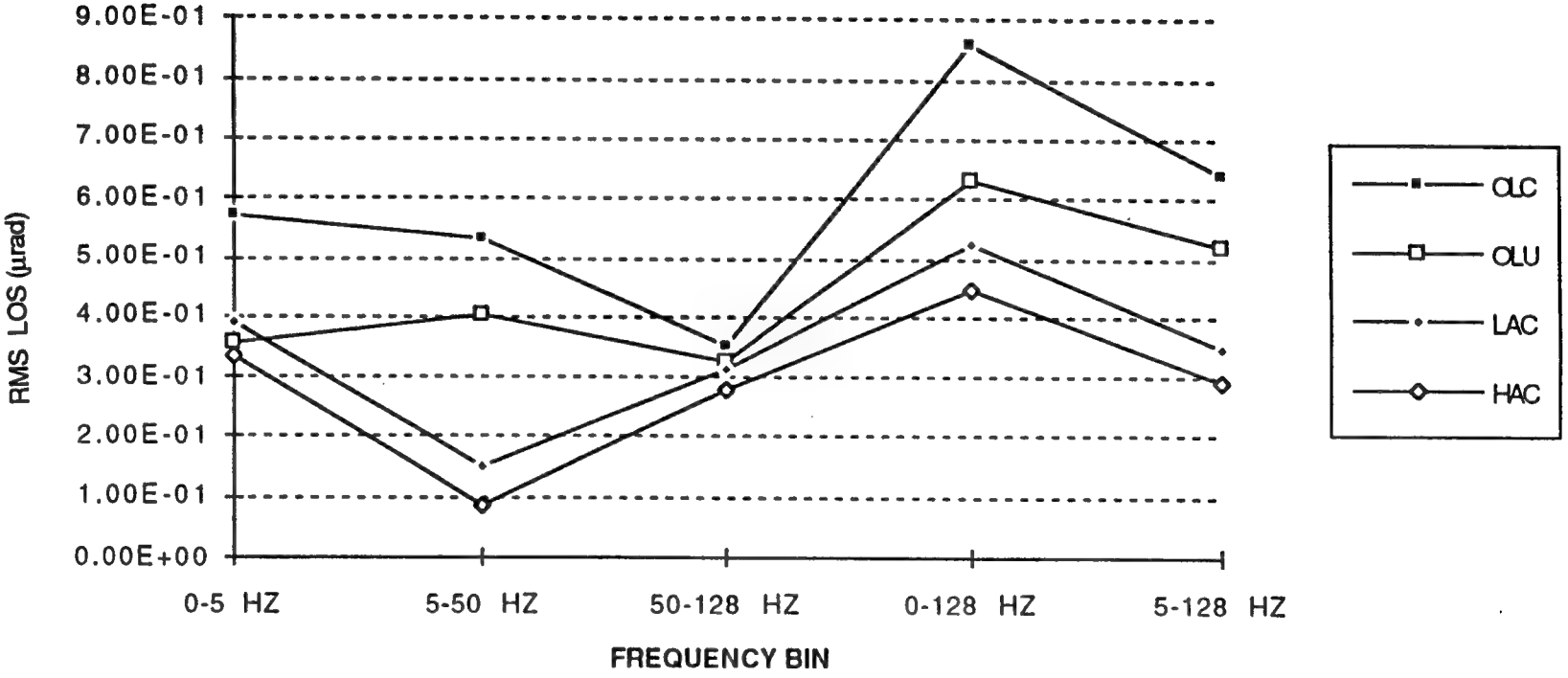

Figure 35. Frequency bin distribution of RMS LOS-x - quiescent.

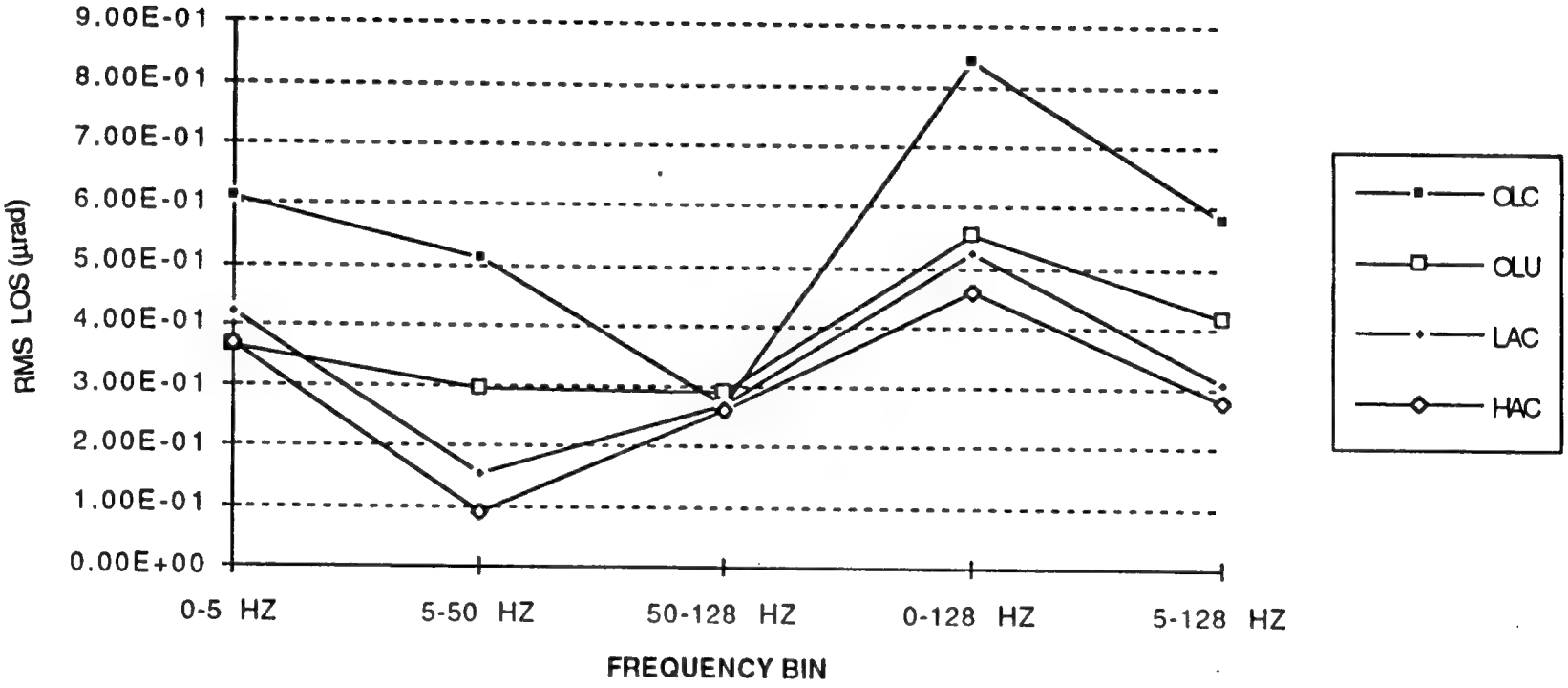

Figure 36. Frequency bin distribution of RMS LOS-y - quiescent.

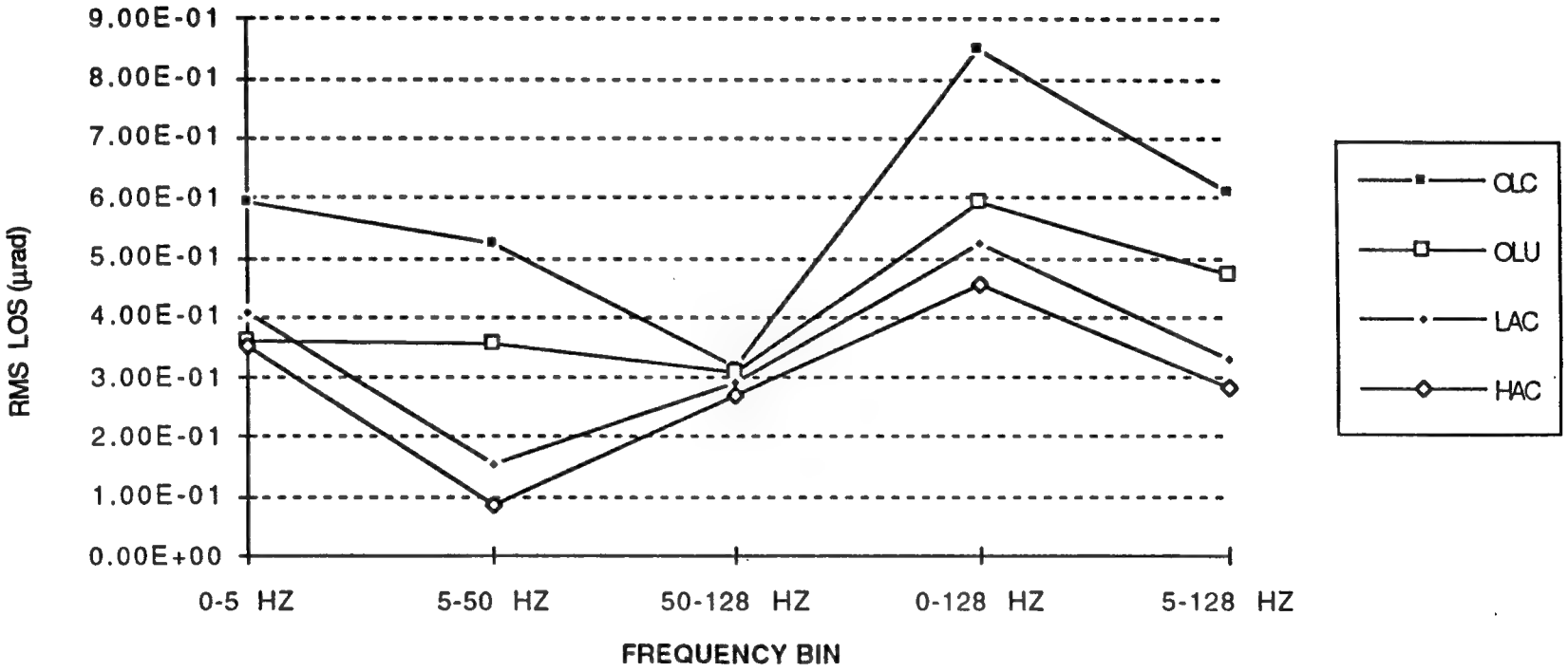

Figure 37. Frequency bin distribution of composite RMS LOS - quiescent.

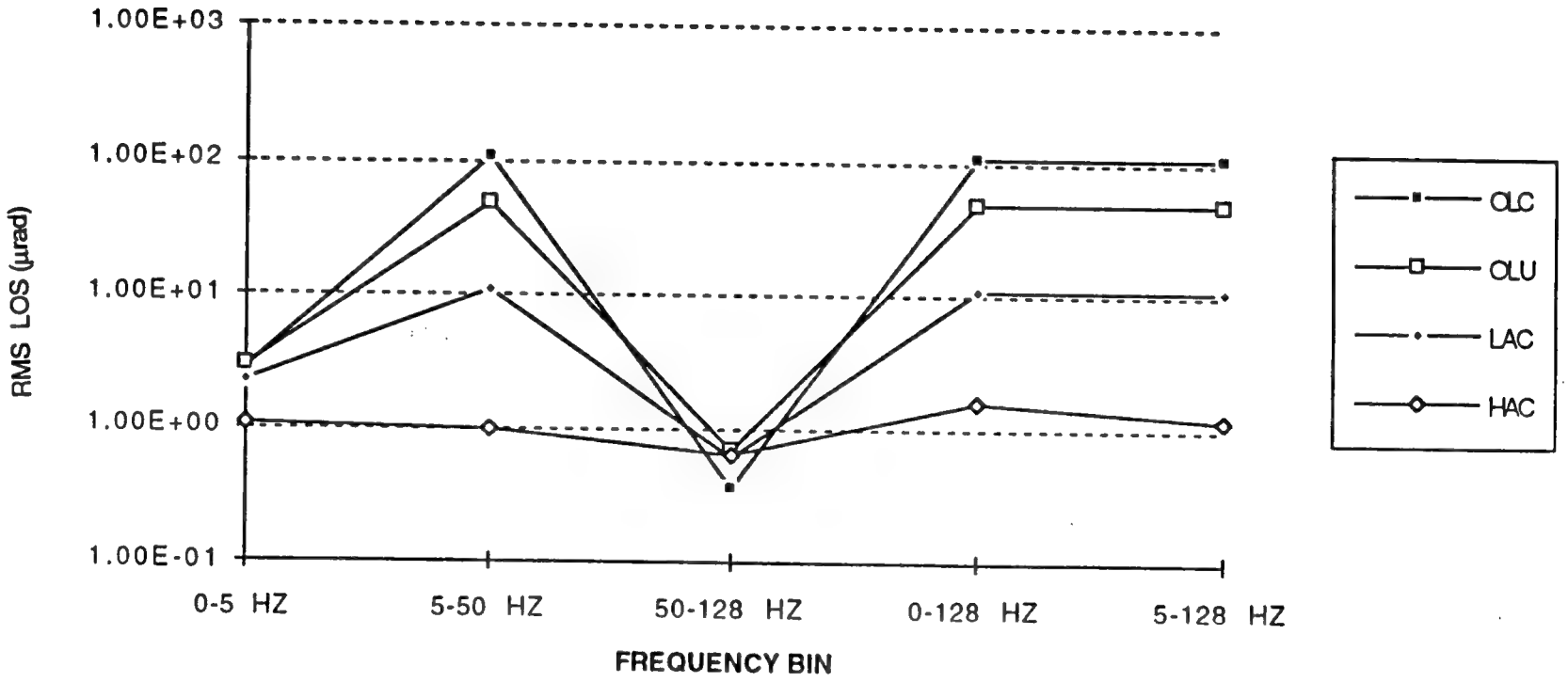

Figure 38. Frequency bin distribution of RMS LOS-x due to disturbances only.

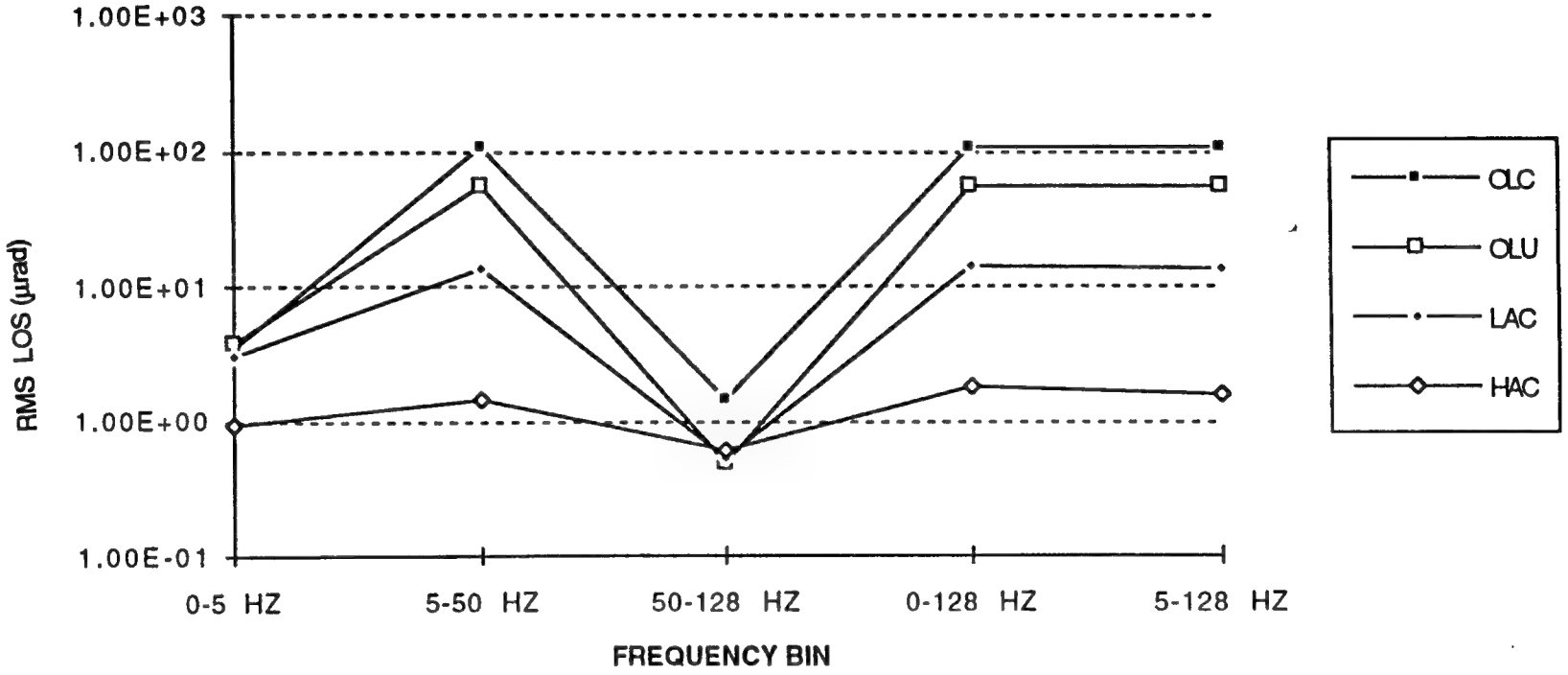

Figure 39. Frequency bin distribution of RMS LOS-y due to disturbances only.

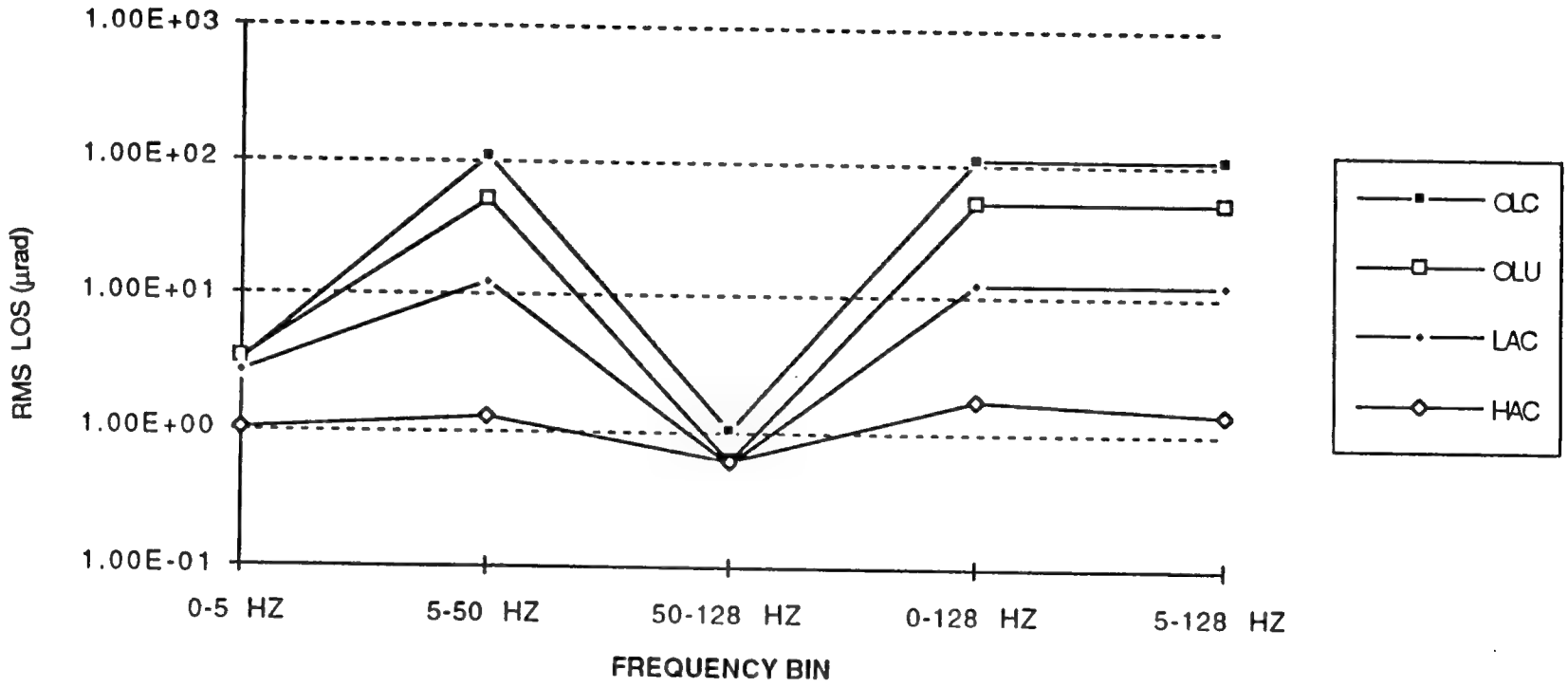

Figure 40. Frequency bin distribution of composite RMS LOS due to disturbances only.

Therefore the cost of retaining the higher frequency residuals in either extra effort or reduced frequency resolution was found to be unjustified. The 5- to 128-Hz bin contains virtually all of the residual in the 5- to 500-Hz range.

These figures offer several observations.

(1) The HAC outperforms LAC in the first bin of 0 to 5 Hz. This is mainly due to attenuation from 3 to 5 Hz that compensates for slight amplification below 3 Hz.

(2) In the bin of high HAC gain, 5 to 50 Hz, with the disturbances on, the HAC attenuates the LAC residual LOS by ~10:1. Total attenuation from open-loop caged to HAC in this frequency bin is 85:1. Even for the quiescent tests, HAC improves over LAC in this frequency range.

(3) In the spillover region, 50 to 128 Hz, there is little difference among the four test configurations. There is little amplification by HAC in this region. Consequently, 85:1 attenuation of LOS has been attained in the 5 to 50 bin with insignificant degradation above 50 Hz.

(4) As a result, attenuation from open-loop caged to HAC, for composite LOS in the 5 to 128 Hz frequency bin, is 75:1. Final composite LOS is 1.43 μrad RMS.

(5) With the disturbances off, the composite LOS from 5 to 128 Hz is 285 nrad.

(6) The residual composite LOS from 5 to 128 Hz due to the shakers is 1.40 μrad.

(7) Even if the 0- to 5-Hz bin is included, composite LOS attenuation is 60:1.

The significant result is that 85:1 attenuation was achieved over the frequency range of HAC authority, with no degradation in performance in the spillover region or below the PMA flexure frequencies. The goal of 50:1 attenuation from 5 to 128 Hz (equivalent to the full scoring frequency band previously discussed) was comfortably exceeded with no indication of HAC instability.

3.4.3 Gain Margin Test Results

A series of gain margin tests was run to determine one measure of system stability margin. The tests were run with the HAC system modified as shown in Figure 41. The structure and HAC controller are the baseline system. For the gain margin test, a scalar gain, K, was incorporated

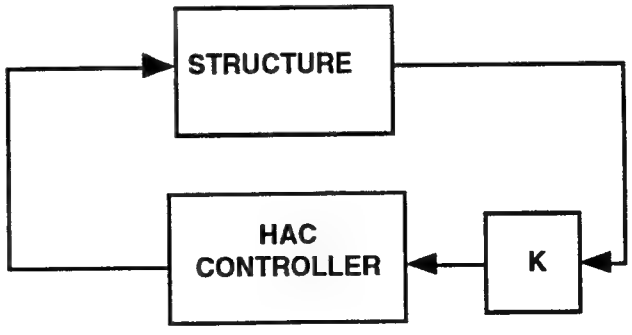

Figure 41. Modification of HAC for gain margin tests.

directly into the control matrix as a multiplier to the 36 measurement inputs to the HAC controller. No hardware modification was necessary. For the nominal system, K = 1.0. The tests were run with the disturbances off (quiescent mode). For each value of K tested, LOS PSDs were acquired using the HP two-channel analyzer. Final data consists of hard copies of those PSDs. The scalar gain was increased in increments of 0.25 until the system became unstable and then decreased in steps of 0.25 to determine the effect of lower gain upon stability.

The results are presented in Reference 35. The control system became unstable at K = 2.0. Thus, the gain margin is between 1.75 and 2.0. Gain was reduced to 0.25 with no sign of instability. It was evident that the modes causing instability at K = 2.0 are the 11-Hz suspension mode and the 90-Hz panel mode. These modes are not in the HAC design model. It is quite conceivable that the 11-Hz suspension mode instability could be eliminated by modeling that mode, or modes, in the HAC design. It is not reasonable to expect accurate modeling of the 90-Hz panel modes. Because these modes are in the HAC spillover region, HAC authority sufficient to obtain in excess of 100:1 attenuation can be used only if the panel modes are passively damped or the underlying structural conditions leading to the problem are fixed.

It is encouraging that a global controller with over 50:1 attenuation has a stability gain margin of nearly 2.0. Global structural controllers can be designed with more robustness than previously thought possible.

3.4.4 Transfer Function Test Results

Closed-loop transfer functions were acquired and compared with predicted transfer functions. These tests were done along the same lines as earlier open-loop and LAC transfer function tests. In the HAC tests, the transfer functions were measured with the HAC loops closed. The 24 inputs included 18 PMA force commands and 6 disturbance forces. The 38 outputs included 18 PMA housing rates, 18 OSS measurements, and 2 LOS components. The 5A19 HAC design model was used to predict these transfer functions. The test transfer functions were compared with the predicted transfer functions and the level of agreement was scored. The results are documented in Reference 36. As was the case in the open-loop and LAC transfer function tests, the scores range from very good to poor. The significant difference with the HAC tests is that the coherence of the measured FRFs is very poor below about 10 Hz. This is because there is very little signal below 10 Hz with the HAC loops closed. Between 5 and 10 Hz, the HAC gain is very high, resulting in little signal; below 5 Hz the PMA forces roll off rapidly, also resulting in little signal.

A subset of open-loop transfer functions with the HAC loops closed was acquired and compared with predicted open-loop transfer functions. The object was to obtain the open-loop transfer function of the regulator. For an optimal regulator and estimator, the transfer function of the regulator is computed with the estimator having full knowledge of the test force applied to the structure. This is represented in Figure 42.

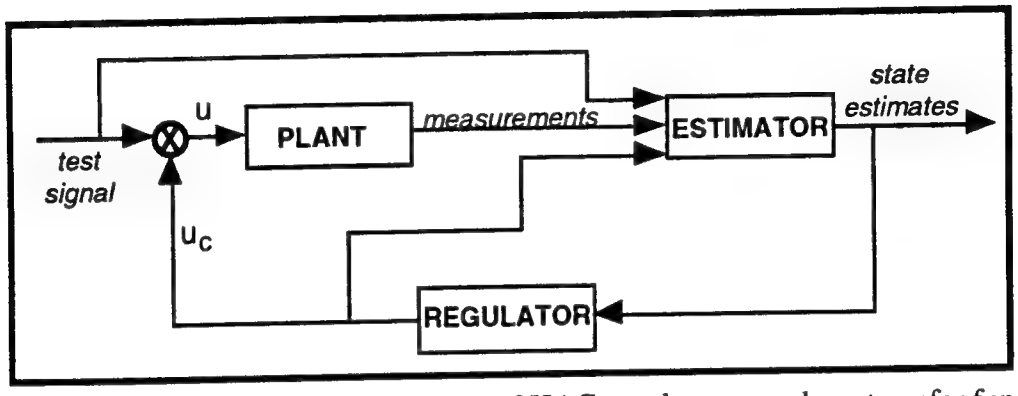

Figure 42. Configuration for measurement of HAC regulator open-loop transfer function.

In Figure 42, the regulator includes the regulator gain matrix, K_r, and the 18 digital low-pass filters. The output of these filters drives the plant. In the test configuration, it is most convenient to add a test signal to the PMA force commands from the HAC. Just as the regulator states are used to estimate the states of the structure in the estimator, so must these test signals be fed forward into the estimator. With the test signals fed forward into the estimator, the transfer function from u to u_c is the regulator open-loop transfer function, representing the open-loop gain of a control signal. If the test signal is not fed forward, the transfer function from u to u_c is the open-loop gain of PMA noise. For the purposes of evaluating stability margin, it is the control gain, not noise gain, that is relevant.

The open-loop transfer function of the regulator, from u to u_c, was predicted using the final or 5A19 HAC design model. The singular values of this 18 by 18 matrix are the gains of the open-loop regulator at each frequency. These singular values are plotted in Figure 43. Note the high gain at the main bending modes, the controller roll-off above 10 Hz, and unity gain crossover at about 26 Hz. The two dominant traces reflect the gain for the LOS cost functions. The third dominant trace in the vicinity of 5 Hz shows the influence of the torsion cost function. The regulator has DC gain; this is why high-pass filters were required on the OSS sensors to eliminate PMA biases. Note also the strong gain in the vicinity of 50 Hz. These modes were expected to be troublesome but actually the controller was stable at and above 50 Hz.

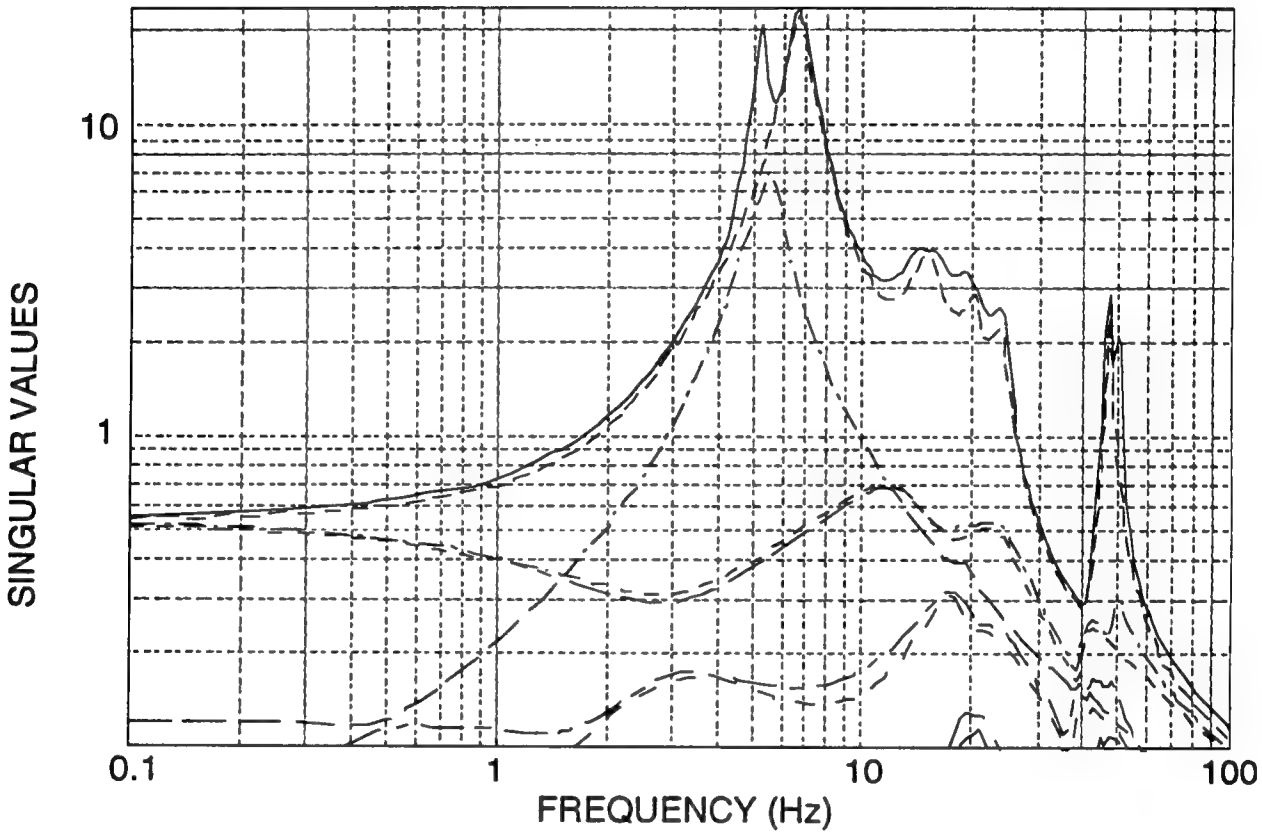

Figure 43. Predicted singular values of the regulator in the final (5A19) HAC design.

Open-loop transfer functions from PMAs 1 and 2 to all 18 PMAs were measured in two different ways. In the first way, the test signals were fed forward into the estimator. In the second way, the test signals were not fed forward. The transfer functions from the test signal at PMA 1 to the resulting HAC command to PMA 1 using the two methods are displayed in Figure 44 along with the predicted open-loop transfer function. Ideally, the transfer function with feed forward should match the prediction; it does not. There is significant difference between the feed-forward and nonfeed-forward cases. There is no precise explanation for why the agreement is so poor. It is likely, however, that there is sufficient model error to account for the difference, resulting in the control signal being estimated as a disturbance signal, and vice-versa. Despite the disagreement, it is encouraging that the control system performs well with ample gain margin. Once again, it appears that a good, but not perfect, model is required for high gain structural control.

3.4.5 Conclusion

In summary, the three main points to be made concerning the HAC performance tests are

- Attenuation of LOS jitter by 75:1 in the band 5 to 500 Hz was achieved with little spillover into unmodeled modes or unregulated degrees of freedom.
- The control system is robust, with gain margin ≥1.75.
- Although many input-output transfer functions are predicted very well, model predictions are not uniformly impressive and, in many cases, the sources of the discrepancies are not known. The good news from this is that near-perfect model accuracy is not, as was previously believed, a prerequisite for a high performance global controller. Very good, but not unattainable, model accuracy is required.

To demonstrate the error attenuation at its best, a test was run in which a 6.3-Hz sinusoid with amplitude of 100 N was injected at SAVI vertex 2. Twenty seconds of data were collected, 10 s with only the LAC loops on, and 10 s with the HAC loops closed. During the first 10 s, the HAC estimator and OSS high-pass filters were also active. At t = 10 s, the regulator was closed. The 6.3-Hz frequency was chosen because the error attenuation of HAC relative to LAC is maximum at this frequency. This test was specifically set up to demonstrate what high attenuation really means. A subset of the data was collected and plotted. Figure 45 shows the time traces of LOS x and y. When the regulator loop is closed, there is very little transient and the steady-state attenuation is remarkable. Figure 46 is an x-y plot of LOS for this same subset. The large oval is LAC response, the small circle is the locus of LOS with HAC loops closed. These figures show the difference between LAC and HAC. The LAC by itself attenuates the open-loop

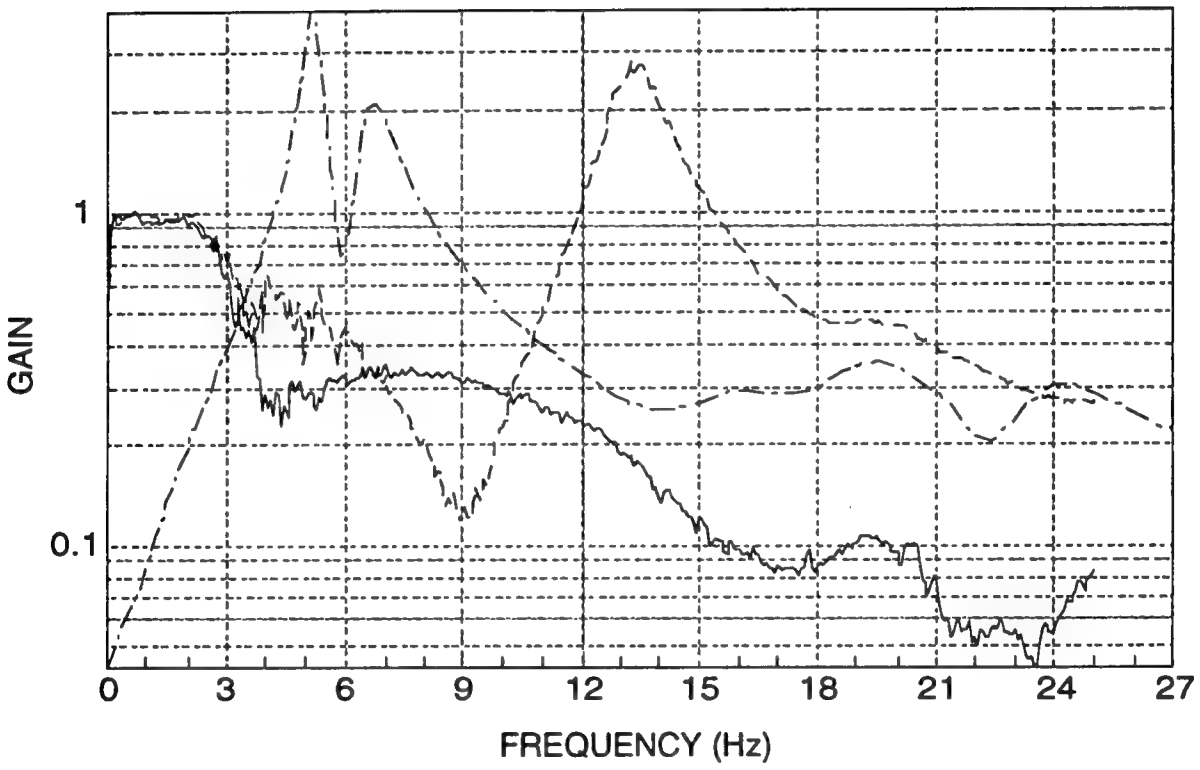

Figure 44. Open-loop transfer functions from PMA 1 to PMA 1.

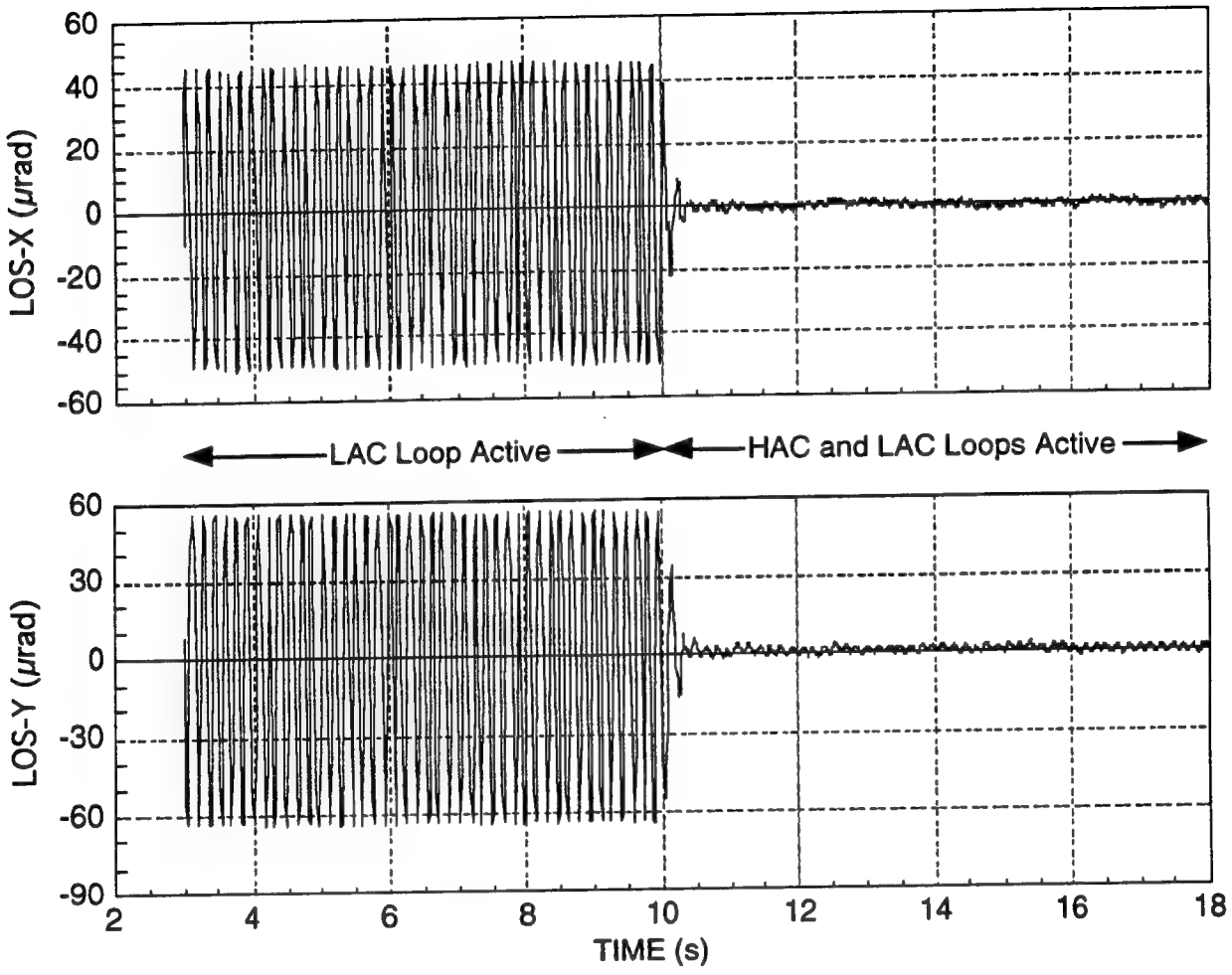

Figure 45. Attenuation of a 6.3-Hz sine wave disturbance by the final HAC (5A19).

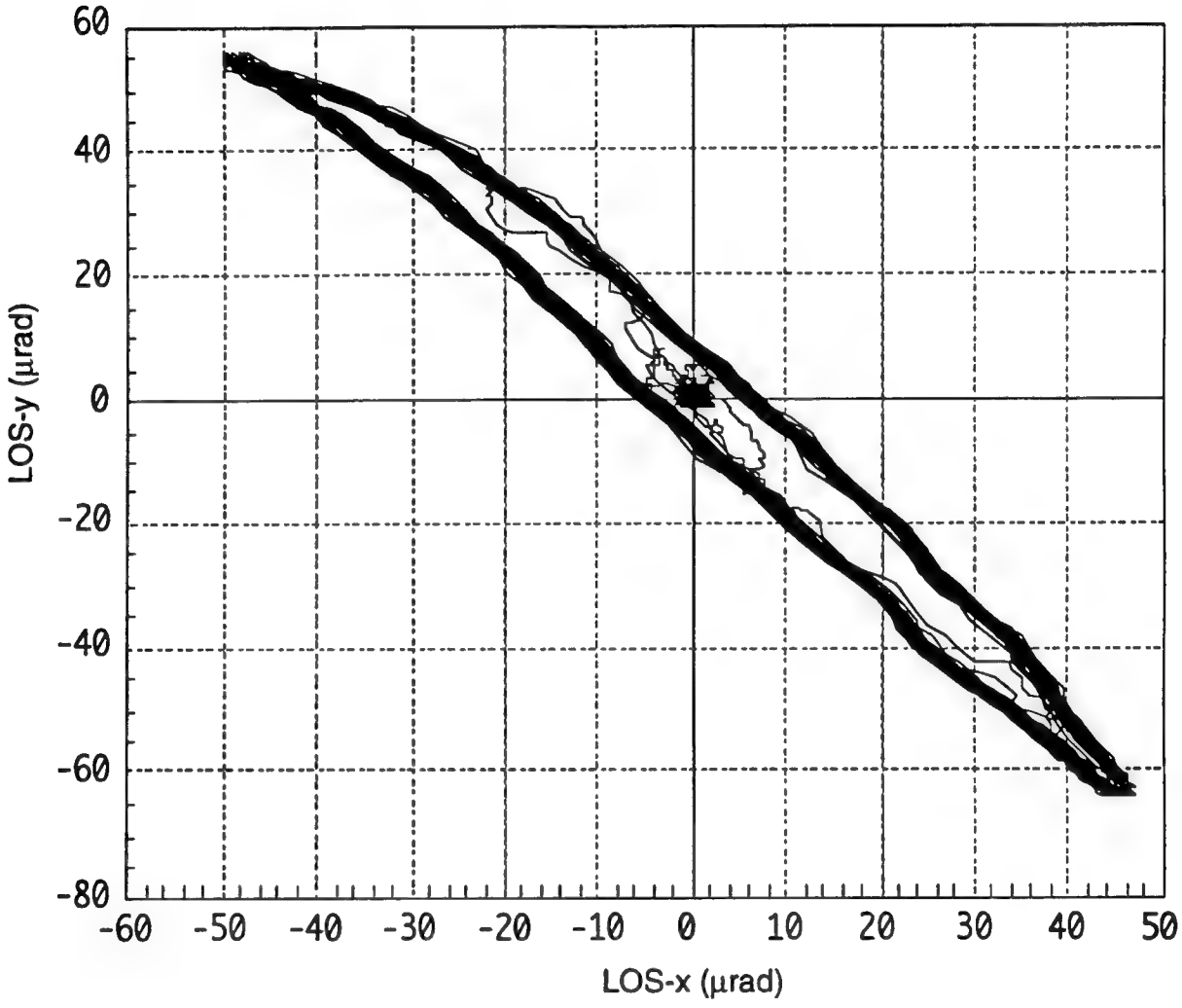

Figure 46. The LOS in the 6.3-Hz sine wave test: LAC- oval, HAC- spot inside oval.

disturbance by ≥8:1. This is what global control can achieve and, indeed, did achieve in Phase I of the SPICE Precision Pointing Experiment.

4.0 LESSONS LEARNED

4.1 TEAMWORK

The SPICE "Integration Week" meetings (held every 4-6 weeks) brought together people from different companies in different states often enough for team members to get to know each other's strengths and to become personally acquainted. This led to an understanding of the role of each individual, resulting in a team that worked well together despite the inconvenience of long distances. The value of these weeks in supporting this type of personal and professional interaction even outweighed the value the TIMs as mechanisms of formal reporting to the government.

4.2 ELECTRONICS

The following two observations are vital to maintaining data quality and schedule in a large, complex experiment:

- Do not try to cut corners in interface electronics! The methods used in SPICE required more expensive cables, connectors, and parts and labor to build interface circuitry, as well as other costs to correctly implement grounding, shielding, buffering, etc. The resulting clean data and freedom from the need to diagnose and repair ground loop problems every time a new scope was connected were ample compensation for the extra effort.
- Provide the line engineer with the authority to specify and purchase spares. He is best qualified to determine the type and quantity of spares to stock. Most spares do get used, are needed immediately when they do, and are least costly when included in the original order.

It was discovered during the Precision Pointing Experiment that certain types of accelerometers are completely unusable in the vicinity of pulse-driven actuators. This showed up in both structural accelerometers mounted near the SAVI actuators, and in the Wilcoxon accelerometers on the PMAs. In the latter case, it was necessary to replace pulse width modulation techniques with linear power amplifiers for driving the PMA because it was too late to change the accelerometer. It was determined that the problem was sensitivity to actual mechanical motion at the pulse width modulation frequency and not any form of electromagnetic coupling. Accelerometers that have high bandwidths apparently sometimes have huge internal resonances in the 20-kHz region and, even when the outputs were electrically filtered, the performance of the units was destroyed by the

presence of pulse width modulation background vibrations. Noise floors, even when measured only below 100 Hz, were observed to increase by a factor of 100 or more.

4.3 CONVENTIONS AND COORDINATES

The SPICE established a master block diagram that defined, on a single E-sized sheet, all hardware conventions including signal names and numbers, scaling and polarity, coordinate frames, etc. Having this material available early and distributed to all members of the team avoided many of the usual problems during integration of subsystems. For example, the PMAs and the OSS sensors have their local coordinate systems; their integration was facilitated by having standards already determined. Polarity problems were routinely identified and corrected. The effort required to maintain the SPICE "Big Drawing" was not insignificant but it was dwarfed by the benefits it provided in eliminating confusion.

4.4 CALIBRATION

A calibration issue that arose during the FRF/LAC tests points to the need to verify sensor calibrations *in situ*, especially if the sensor is a custom unit.

The OSS was calibrated on the optical bench in a special test setup. When it was later suspected that the gain in volts per radian or volts per meter might be incorrect (some system level data suggested this), a way was found to take calibration data in place on the structure. The data showed that all four axes of the SMTSs were in error by the same factor, and both axes of the SMRS also had identical errors. This indicated an error in the calibration reference, i.e., the bench test setup. After recalibration, several of the open-loop system-level tests had to be repeated. The ability to easily verify calibration *in-situ* should be designed *ab initio* into any custom sensor.

4.5 TEST PLANNING

Careful and well-documented test planning requires a lot of time and effort but pays dividends in many ways. For example, identification of vital capital procurements when there was still enough time to complete them without slowing up test schedules greatly enhanced the success of SPICE.

4.6 SUBTASK PLANNING

Most of the efforts on SPICE that ran over budget did so because the budget was cut from the original estimate during the planning process. It is easier to get someone to agree to do a task for less than it is to get him to actually do it for less, especially when hardware is involved. Trust plans and cost estimates; if sufficient resources are not available to complete a task, adjust the scope of the task accordingly.

4.7 NONPRECISION HARDWARE ON A PRECISION STRUCTURE

Attaching unmodeled, nonprecision hardware, i.e., the shaker stingers that input vibration to the secondary mirror mass simulator, to the SPICE precision structure caused difficulties that were unanticipated and that tended to be discovered through anomalies in test data. The shaker stingers were initially regarded merely as devices that input forces to the structure along their axes. The significance of their cross-axis stiffness and damping was not considered. Moreover, remedies for these oversights tended not to be permanent because of the nonprecision nature of the stingers. A better method of introducing vibration into the secondary should have been devised during planning for the Precision Pointing Experiment. The hardware cost savings from using equipment that happened to be available was unimportant compared to the lost time.

4.8 DATA MANAGEMENT PLANNING

In a data-intensive experiment like SPICE, it is extremely important to consider in advance the amount of data to be generated and what will be done with it. The impossibility of extracting and printing the results of some of the FRF tests in a reasonable time, much less evaluating them, led to realization of the necessity to automate the data review. The FRF scoring algorithm (Ref. 5) and other data evaluation tools were developed before the data became overwhelming.

4.9 SIMULATION

At the outset of the SPICE Precision Pointing Experiment, the SAVI was regarded only as the provider of a low frequency boundary condition for the SPICE beam expander. In the FRF/LAC tests, the unexpected nonlinear damping of major structural modes observed in the data could not be explained until the SAVI control system was viewed as an integral part of the whole and interactions were carefully modeled. Detailed models of SAVI were developed that made it possible to understand and eliminate the damping as discussed in Reference 5.

The SAVI system probably should have been incorporated in the nonlinear high-fidelity simulation sooner than it was. That it was not was because interest was concentrated on interaction of the controls with the structure - not with other controls. The simulation was 10 times slower with the full SAVI model added but it did predict the problem of the interaction of the SAVI control system with the SPICE structural control system when it was run after the problem had been identified. It might have given the program a heads-up and saved some time if the full model had been assembled and used earlier.

The "parallel simulation" approach used in SPICE uncovered a few important modeling errors over the years, thus keeping confidence in the integrity of the tools high enough to depend upon them for decision making. This practice is worth the money spent.

4.10 PROOF MASS ACTUATORS

The development of the PMAs was one of the most difficult aspects of the SPICE program. The specifications imposed on this device were extraordinary, and some failures along the way should have been expected. The development was planned in a very success-oriented manner, rendering every difficulty highly visible.

Certain aspects of the PMA design, such as the suspension flexure, were allowed to go far too long without careful modeling and analysis by the SPICE team. This was due in part to confidence in the subcontractor's ability to deliver based upon their extensive prior experience. The SPICE PMA specifications were, however, unprecedented in the subcontractor's experience and such confidence was not necessarily justified. The value of having two analytical models maintained within the SPICE team to check each other has been noted in Subsection 4.9. From experience with the PMAs, it is prudent to also do modeling in parallel with the subcontractor on a developmental effort such as this.

4.11 DIFFICULTY WITH ADSs

The ADSs were depended upon for measurements crucial to understanding atmospheric turbulence. In preparations for the tests, the ADS transfer functions were not found to be as advertised in the manufacturer's literature and almost one-half of the channels on the three triaxial cubes were found to be dead. It is unwise to plan an experimental procedure around a set of sensors that is old, for which recent data are not available, and which cannot be calibrated (Ref. 6).

The SPICE team was fortunate that its analyst was able to devise an alternative approach to measuring the effect of atmospheric turbulence on the LOS measurements.

5.0 CONCLUSION

Phase 1 of the SPICE Precision Pointing Experiment was successful. The goals of the HAC/LAC demonstration were achieved, even exceeded. The primary goal of understanding the results of each test was never compromised. The test plans for the open-loop tests (Ref. 19), the FRF/LAC tests (Ref. 20) and the HAC/LAC tests (Ref. 21), the final reports of the open-loop tests (Ref. 6) and the FRF/LAC tests (Ref. 5), and this document prove that test plans were backed up by analysis. When unforeseen obstacles were encountered, existing analytical tools were utilized and new ones were developed if needed for diagnosis and correction.

Specific performance goals were considered important but not as important as understanding test results. The goal of achieving 50:1 attenuation in the 5- to 500-Hz band of RMS LOS jitter due to input disturbances was exceeded. Attenuation of 75:1 was achieved in that band by the HAC/LAC system.

REFERENCES

1. Hamilton, B., Space Active Vibration Isolation (SAVI), PL-TN-93-1068, Phillips Laboratory, Kirtland AFB, NM, August 1993.

2. Control Design Drawings and Associated Lists, LMSC/F284266, Lockheed Missiles & Space Co., Sunnyvale, CA, 28 September 1990.

3. SPICE Quick Look Report 003: Frequency Response Function / Low Authority Control Tests - Open Loop Disturbance Tuning Tests Revisited, LMSC/P031670-2, Lockheed Missiles & Space Co., Sunnyvale, CA, 21 May 1993.

4. SPICE Quick Look Report 005: Frequency Response Function / Low Authority Control Tests - Open Loop Disturbance Tuning Tests Concluded, LMSC/P031670-4, Lockheed Missiles & Space Co., Sunnyvale, CA, 30 June 1993.

5. SPICE Frequency Response Function / Low Authority Control Tests Final Report, LMSC/P031678, Lockheed Missiles & Space Co., Sunnyvale, CA, 18 August 1993.

6. SPICE Open Loop Tests Final Report, LMSC/P031673, Lockheed Missiles & Space Co., Sunnyvale, CA, 25 June 1993.

7. Optical Sensing System Final Report, LMSC/P031669, Lockheed Missiles & Space Co., Sunnyvale, CA, 4 May 1993.

8. SPICE Proof Mass Actuator Specifications, LMSC/F284488-3, Lockheed Missiles & Space Co., Sunnyvale, CA, 15 December 1992.

9. Proof Mass Actuator Final Report, Honeywell #0329.16.3-10, LMSC/P031671, Lockheed Missiles & Space Co., Sunnyvale, CA, 10 May 1993.

10. SPICE Interface Control Document, Revision E, LMSC/P031677, Lockheed Missiles & Space Co., Sunnyvale, CA, 12 May 1993.

11. SPICE Configuration Control Plan, LMSC/F284481, Lockheed Missiles & Space Co., Sunnyvale, CA, 24 April 1992.

12. SPICE Electronics Report, Honeywell #0329.11.1-5, Lockheed Missiles & Space Co., Sunnyvale, CA, 9 September 1993.

13. SPICE Task Area 2 Technical Integration Meeting Proceedings, LMSC/F284528-17, Lockheed Missiles & Space Co., Sunnyvale, CA, 07 May, 1992.

14. SPICE Task Area 2 Technical Integration Meeting Proceedings, LMSC/F284528-18, Lockheed Missiles & Space Co., Sunnyvale, CA, 24 June, 1992.

15. SPICE Task Area 2 Technical Integration Meeting Proceedings, LMSC/F284528-19, Lockheed Missiles & Space Co., Sunnyvale, CA, 26 August, 1992.

16. SPICE Task Area 2 Technical Integration Meeting Proceedings, LMSC/F284528-20, Lockheed Missiles & Space Co., Sunnyvale, CA, 21 October, 1992.

REFERENCES (Continued)

17. SPICE Task Area 2 Technical Integration Meeting Proceedings, LMSC/F284528-21, Lockheed Missiles & Space Co., Sunnyvale, CA, 27 January, 1993.

18. SPICE Executive Test Plan, LMSC/F284484, Lockheed Missiles & Space Co., Sunnyvale, CA, 12 May 1992.

19. SPICE Open Loop Test Plan, LMSC/F284484-1, Lockheed Missiles & Space Co., Sunnyvale, CA, 28 August 1992.

20. SPICE Frequency Response Function / Low Authority Control Test Plan, LMSC/F284484-2, Lockheed Missiles & Space Co., Sunnyvale, CA, 2 February 1993.

21. SPICE High Authority Control / Low Authority Control Test Plan, LMSC/F284484-3, Lockheed Missiles & Space Co., Sunnyvale, CA, 4 June 1993.

22. Software User's Manual for the SPICE Real-Time Control System Software, LMSC/P031682, Lockheed Missiles & Space Co., Sunnyvale, CA, 30 September 1993.

23. Data Analysis Utilities User's Manual for the SPICE Real-Time Control System Software, LMSC/P031683, Lockheed Missiles & Space Co., Sunnyvale, CA, 30 September 1993.

24. Real-Time Control System Software Final Report for the Precision Pointing Experiment, LMSC/P031684, Lockheed Missiles & Space Co., Sunnyvale, CA, 30 September 1993.

25. Software Version Description Document for the SPICE Real-Time Control System Software, LMSC/P031685, Lockheed Missiles & Space Co., Sunnyvale, CA, 30 September 1993.

26. Structural Dynamics Finite Element Model for Active/Passive Development, Version SPICE2, LMSC/294363, Lockheed Missiles & Space Co., Sunnyvale, CA, 23 May 1990.

27. SPICE 3A Structural Model, LMSC/F284447, Lockheed Missiles & Space Co., Sunnyvale, CA, 23 August 1991.

28. SPICE 4A Structural Model, LMSC/F284482, Lockheed Missiles & Space Co., Sunnyvale, CA, 15 June 1992.

29. SPICE5 Structural Models, LMSC/P031687, Lockheed Missiles & Space Co., Sunnyvale, CA, 23 September 1993.

30. SPICE Quick Look Report 007: Frequency Response Function / Low Authority Control Tests - Preliminary High Authority Control / Low Authority Control Disturbance Attenuation Results, LMSC/P031670-6, Lockheed Missiles & Space Co., Sunnyvale, CA, 30 June 1993.

31. SPICE Quick Look Report 001: High Authority Control / Low Authority Control Tests - Test of Preliminary HAC Model 5A11, LMSC/P031679, Lockheed Missiles & Space Co., Sunnyvale, CA, 13 August 1993.

REFERENCES (Concluded)

32. SPICE Quick Look Report 002: High Authority Control / Low Authority Control Tests - Test of Preliminary HAC Model 5A11 with Extended Frequency Band, LMSC/P031679-1, Lockheed Missiles & Space Co., Sunnyvale, CA, 20 August 1993.

33. Blankinship, R., SPICE Engineering Memorandum: A Discussion of SAVI Interaction at 9 Hz and Subsequent Actions, LMSC/P031697, Lockheed Missiles & Space Co., Sunnyvale, CA, 27 May 1993.

34. SPICE Quick Look Report 005: Open Loop Tests - Local Resonance of SPICE Structure Found During Noise Tests, LMSC/P031664-4, Lockheed Missiles & Space Co., Sunnyvale, CA, 6 January 1992.

35. SPICE Quick Look Report 006: High Authority Control / Low Authority Control Tests - Gain Margin Tests of the Final HAC (Version 5A19), LMSC/P031679-5, Lockheed Missiles & Space Co., Sunnyvale, CA, 23 August 1993.

36. SPICE Quick Look Report 007: High Authority Control / Low Authority Control Tests - HAC/LAC Closed Loop FRF Tests, LMSC/P031679-6, Lockheed Missiles & Space Co., Sunnyvale, CA, 2 September 1993.

APPENDIX

GRAPHS

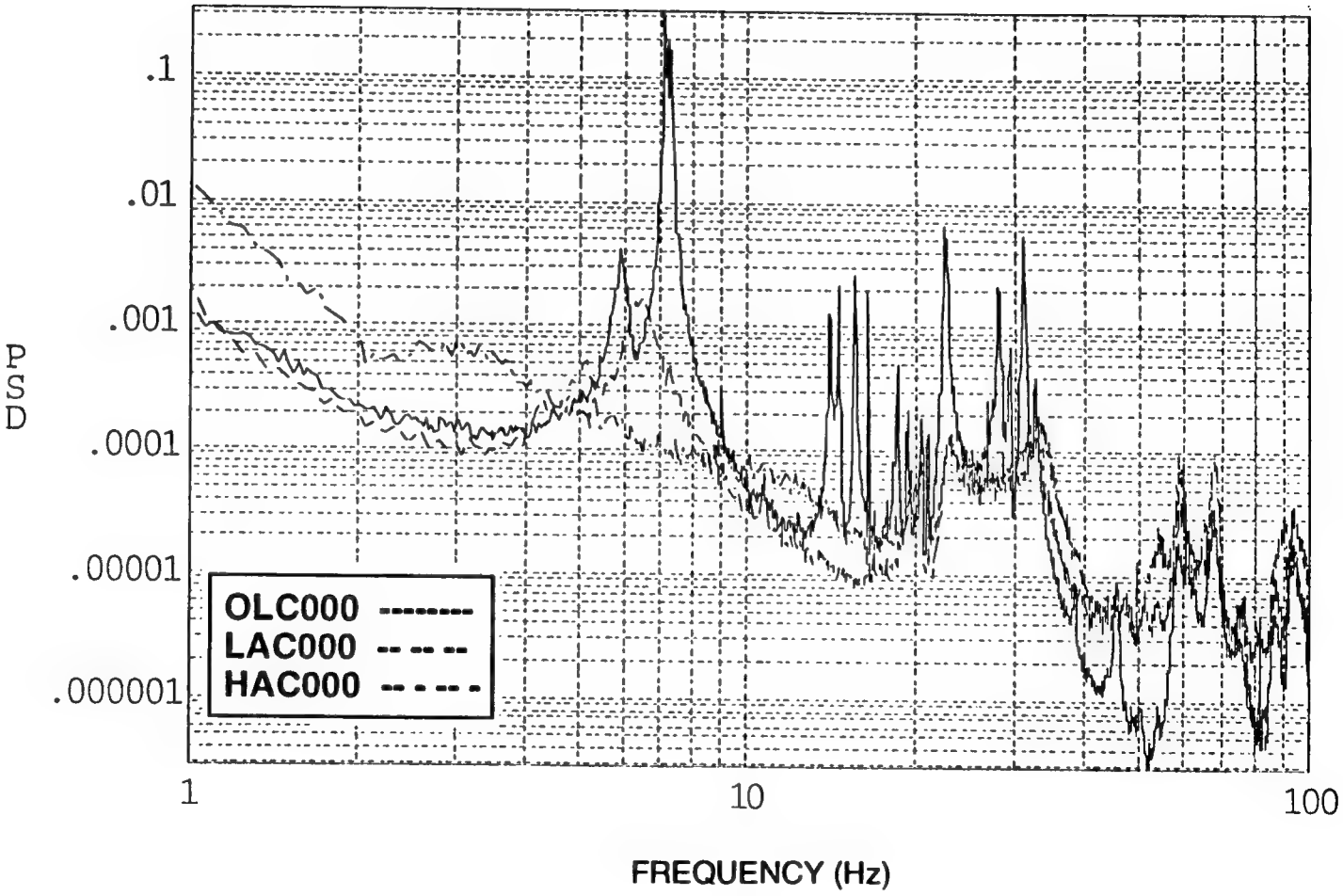

Figure A-1. Spectra of PMA 1 rate - quiescent conditions.

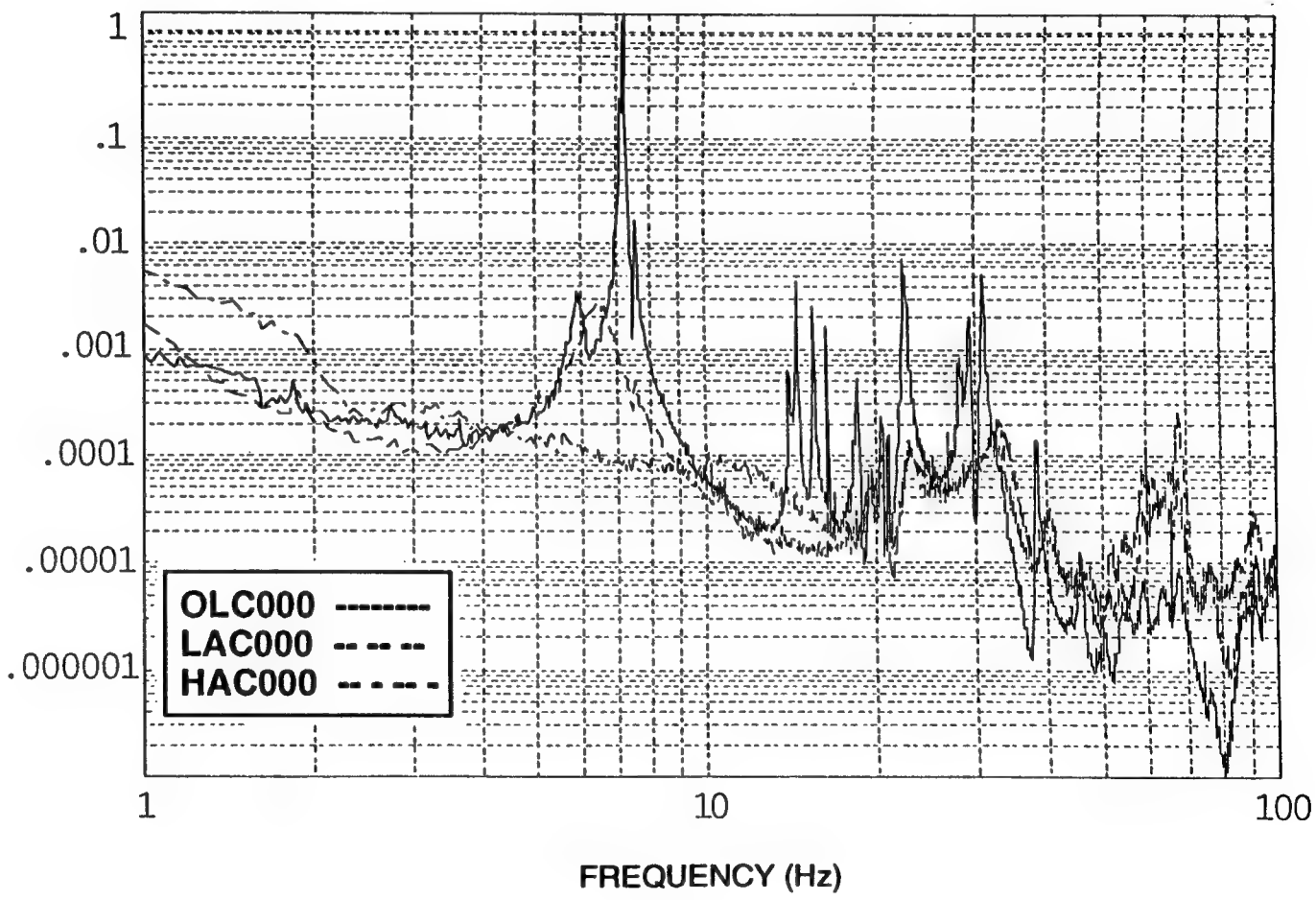

Figure A-2. Spectra of PMA 2 rate - quiescent conditions.

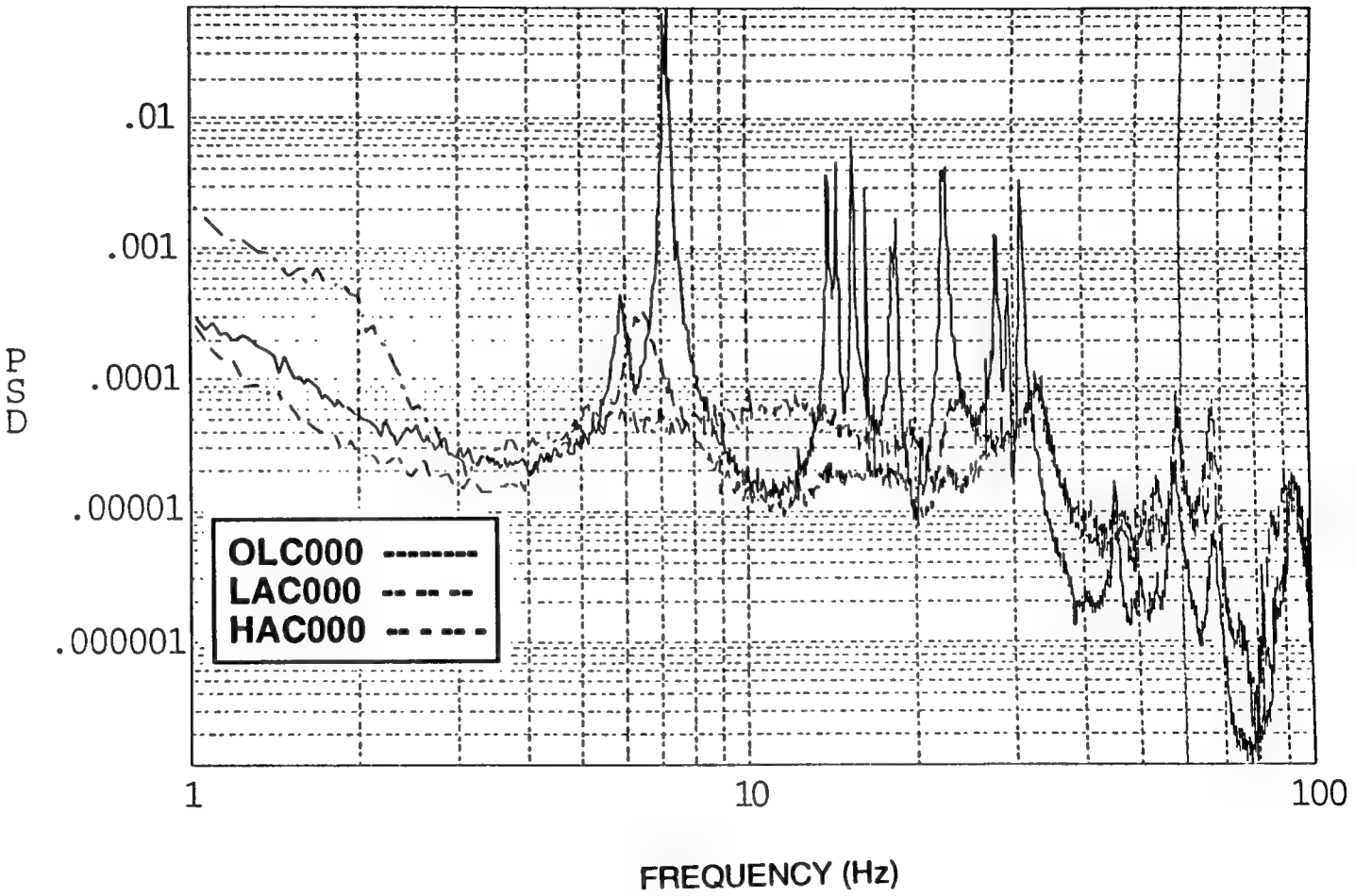

Figure A-3. Spectra of PMA 3 rate - quiescent conditions.

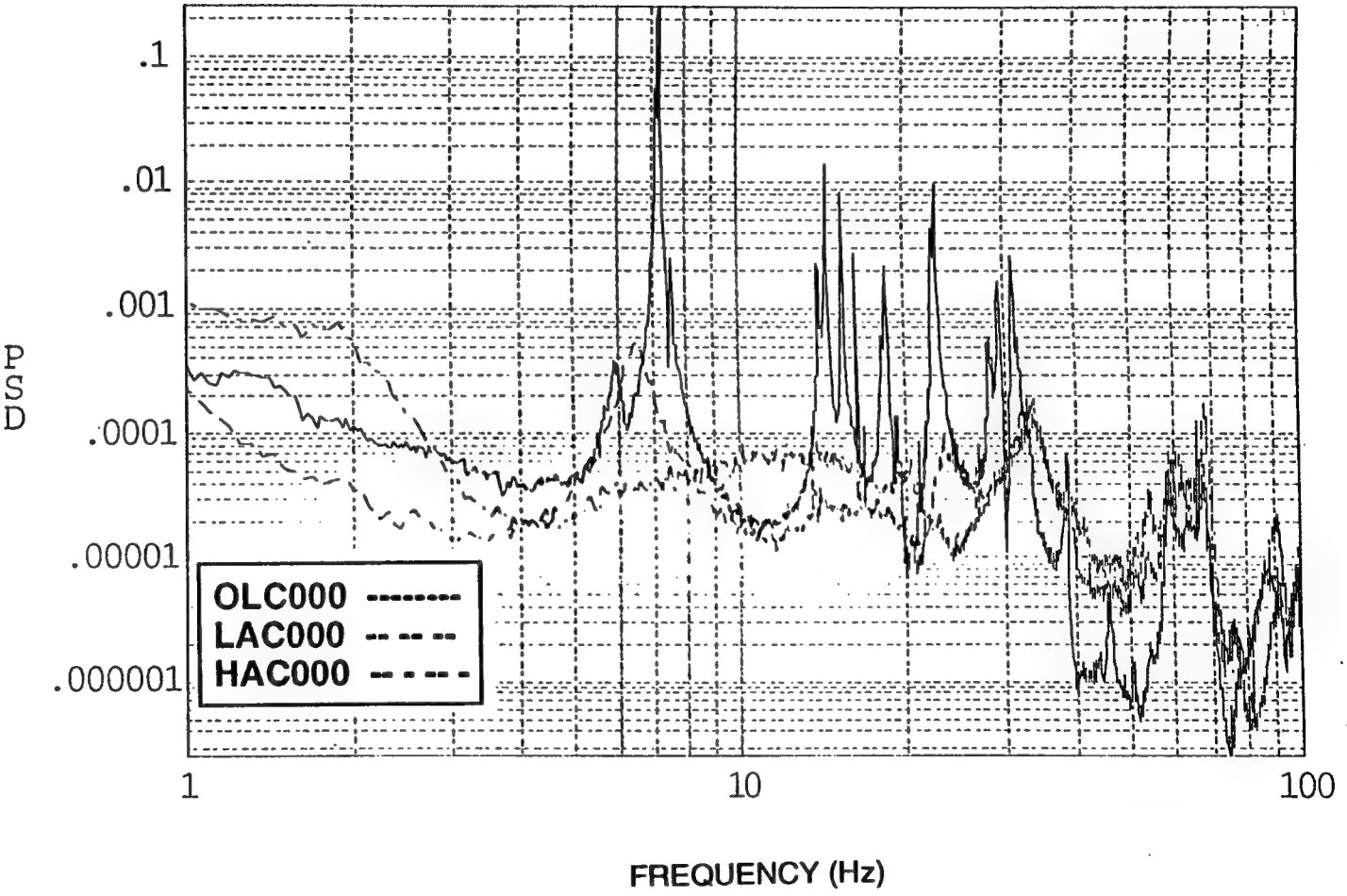

Figure A-4. Spectra of PMA 4 rate - quiescent conditions.

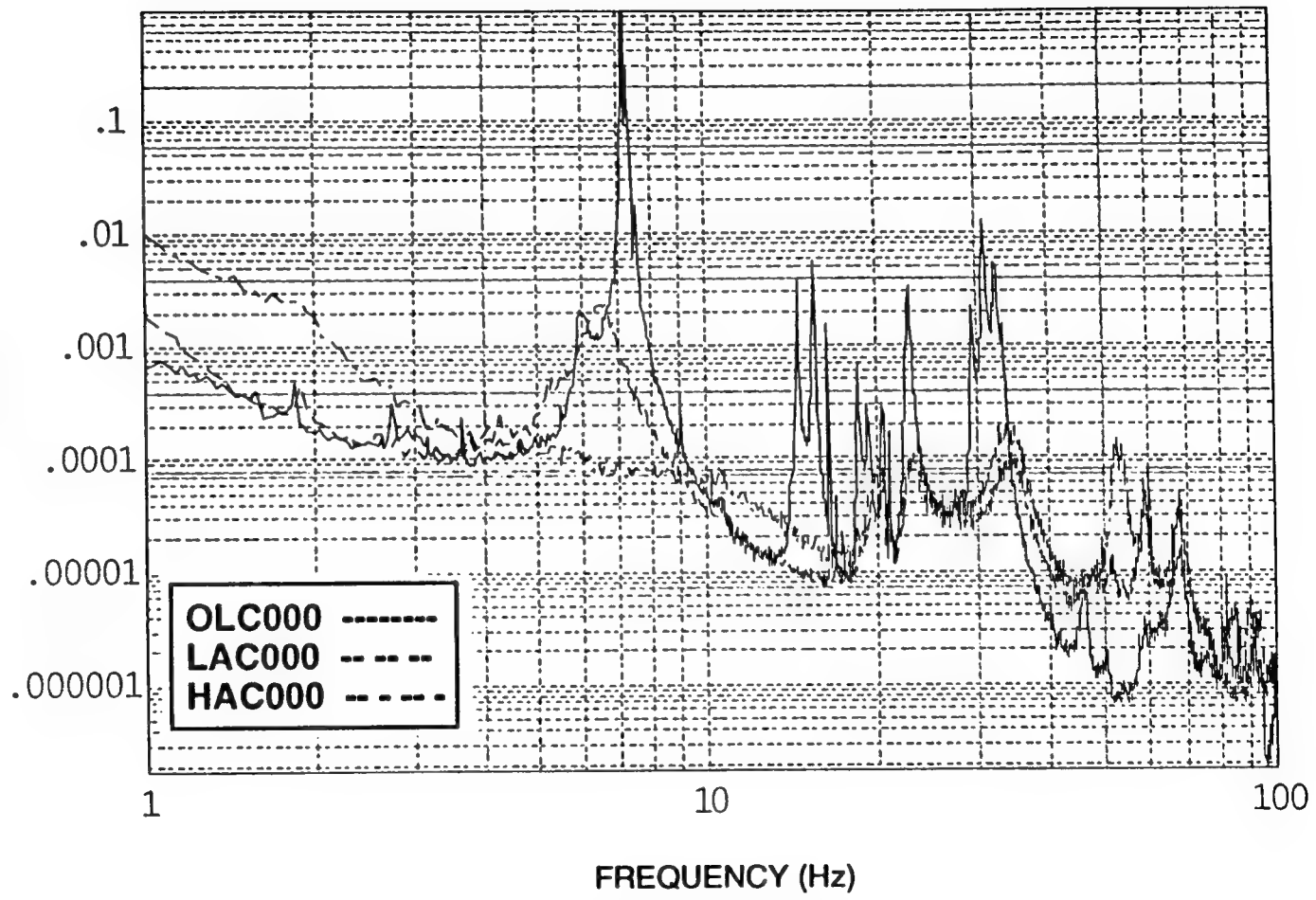

Figure A-5. Spectra of PMA 9 rate - quiescent conditions.

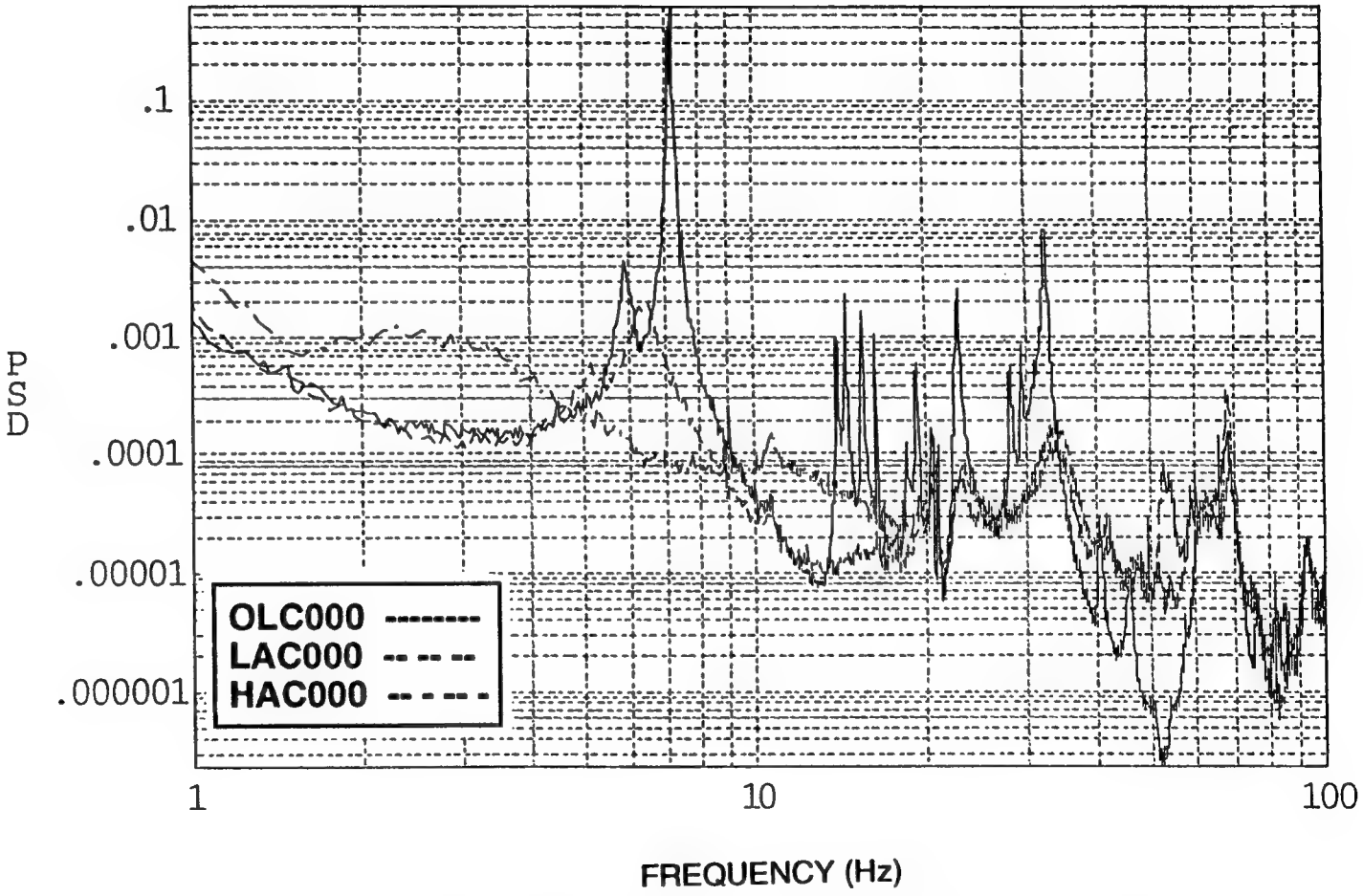

Figure A-6. Spectra of PMA 10 rate - quiescent conditions.

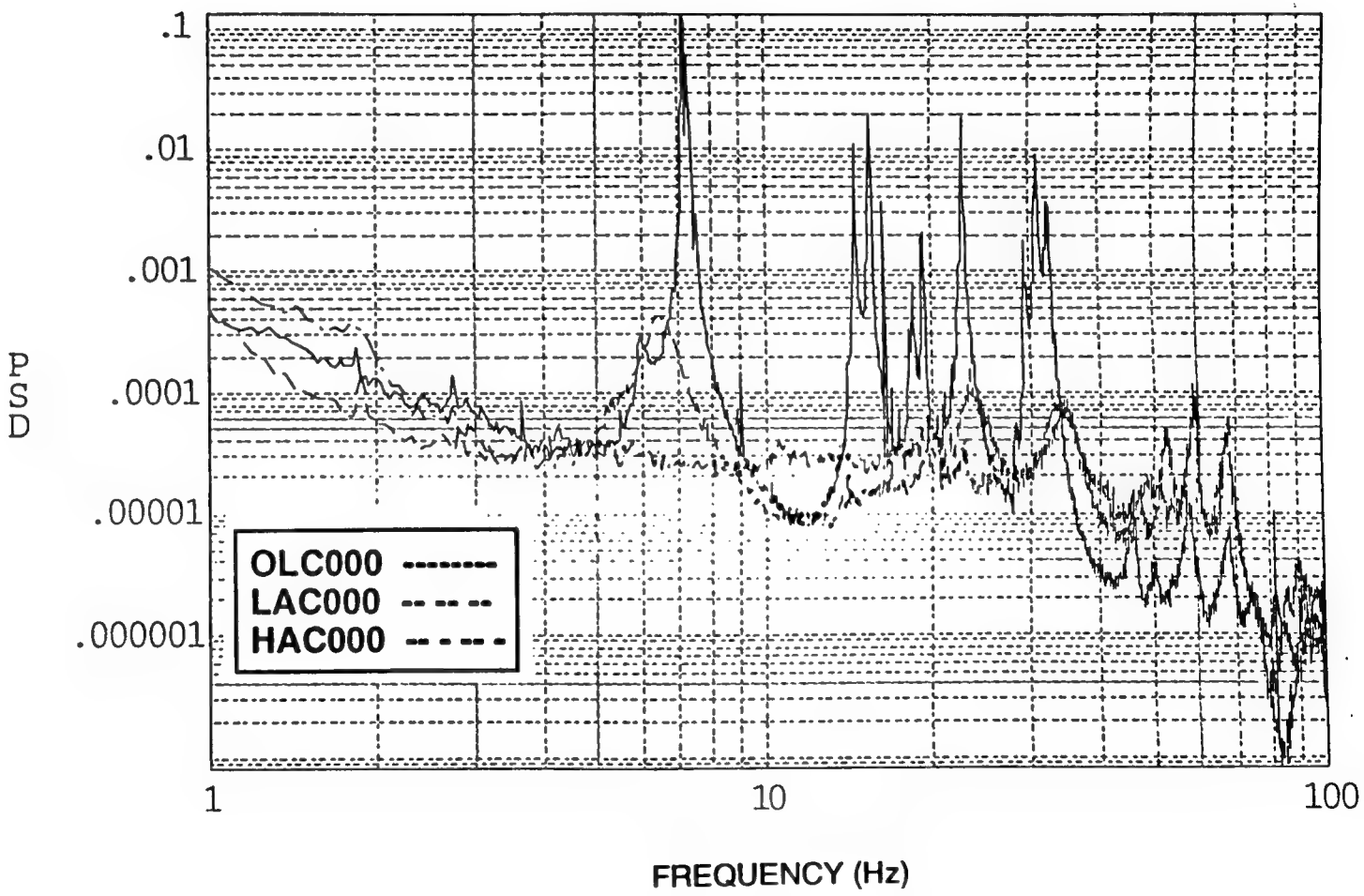

Figure A-7. Spectra of PMA 11 rate - quiescent conditions.

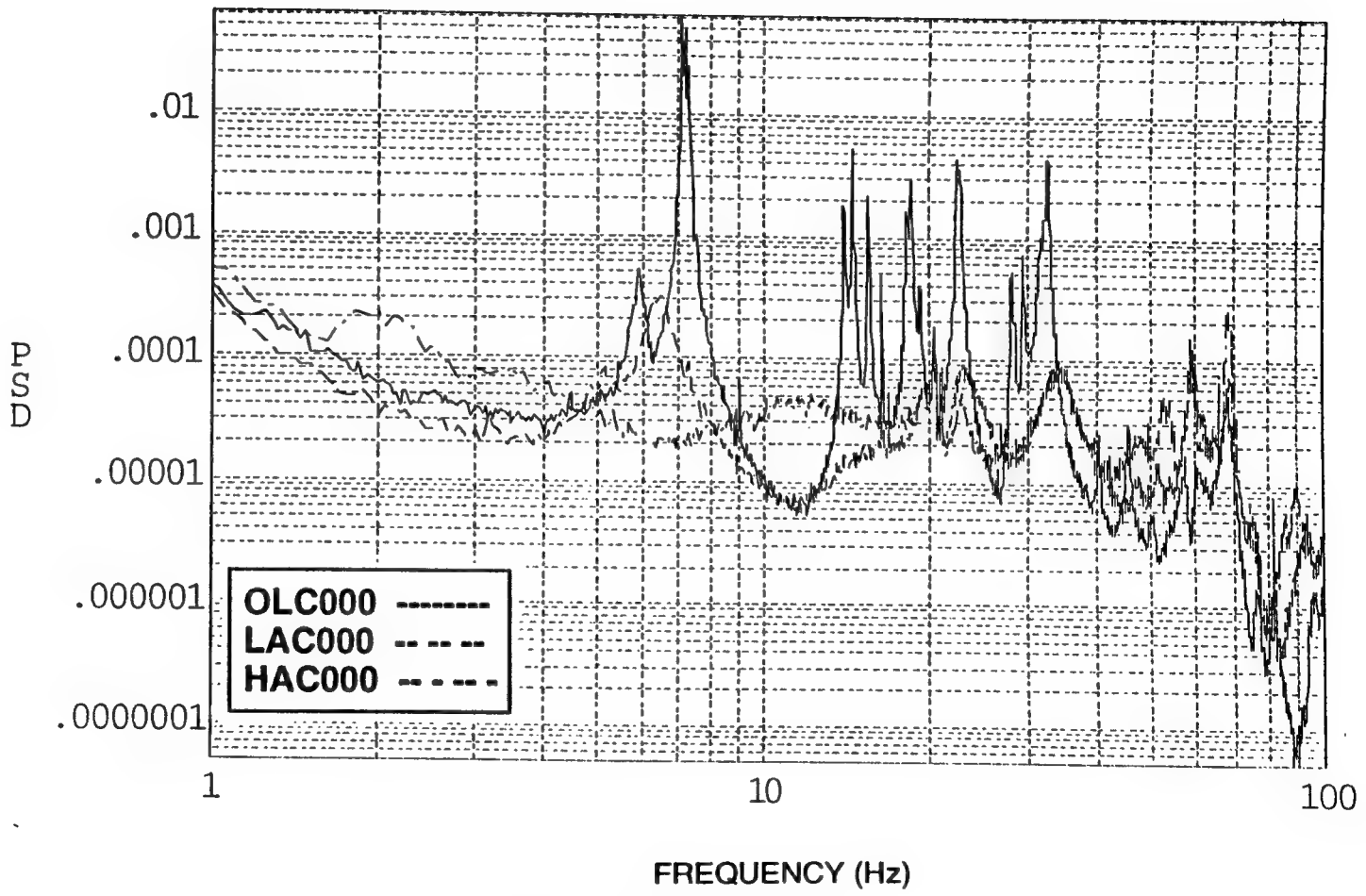

Figure A-8. Spectra of PMA 12 rate - quiescent conditions.

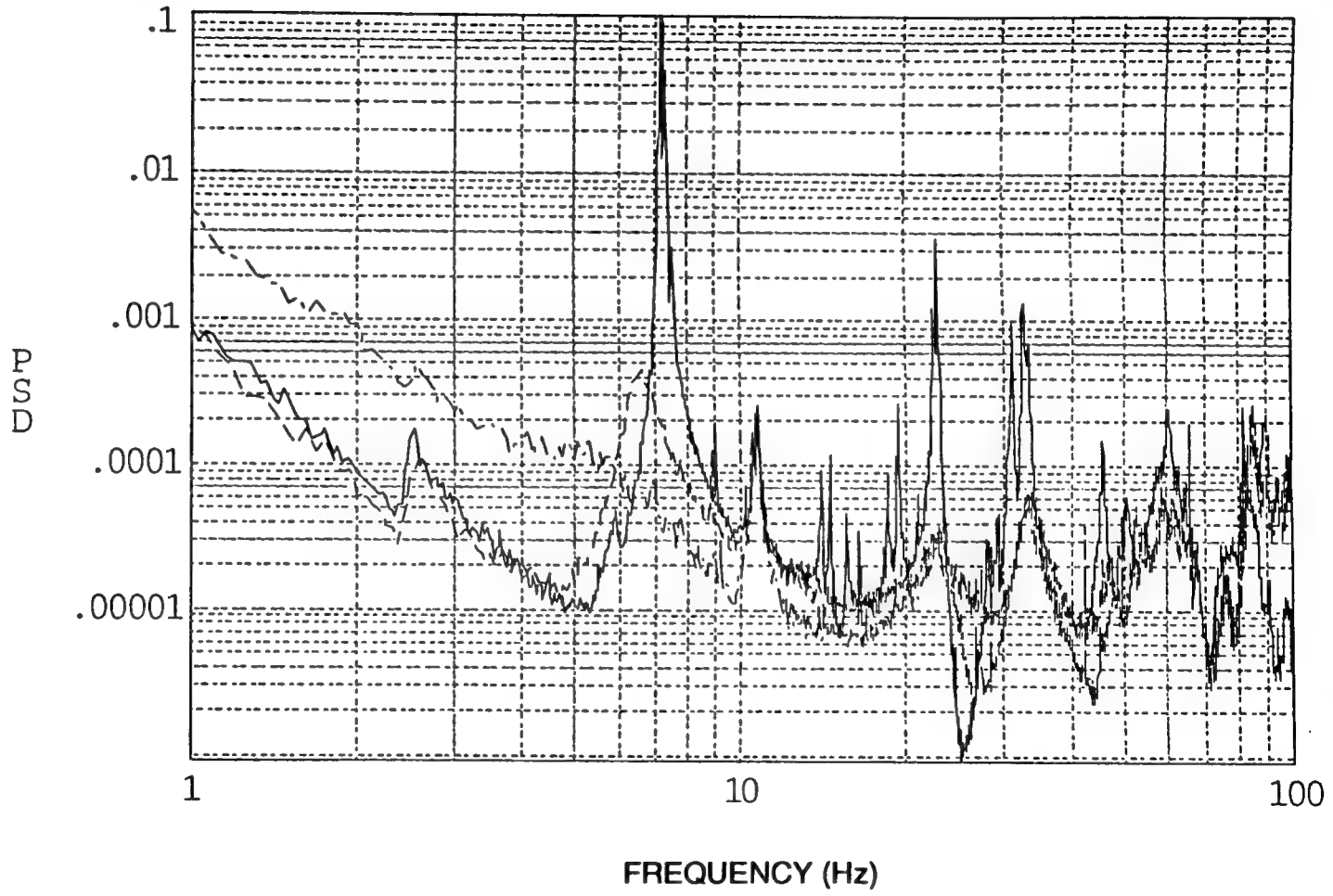

Figure A-9. Spectra of PMA 13 rate - quiescent conditions.

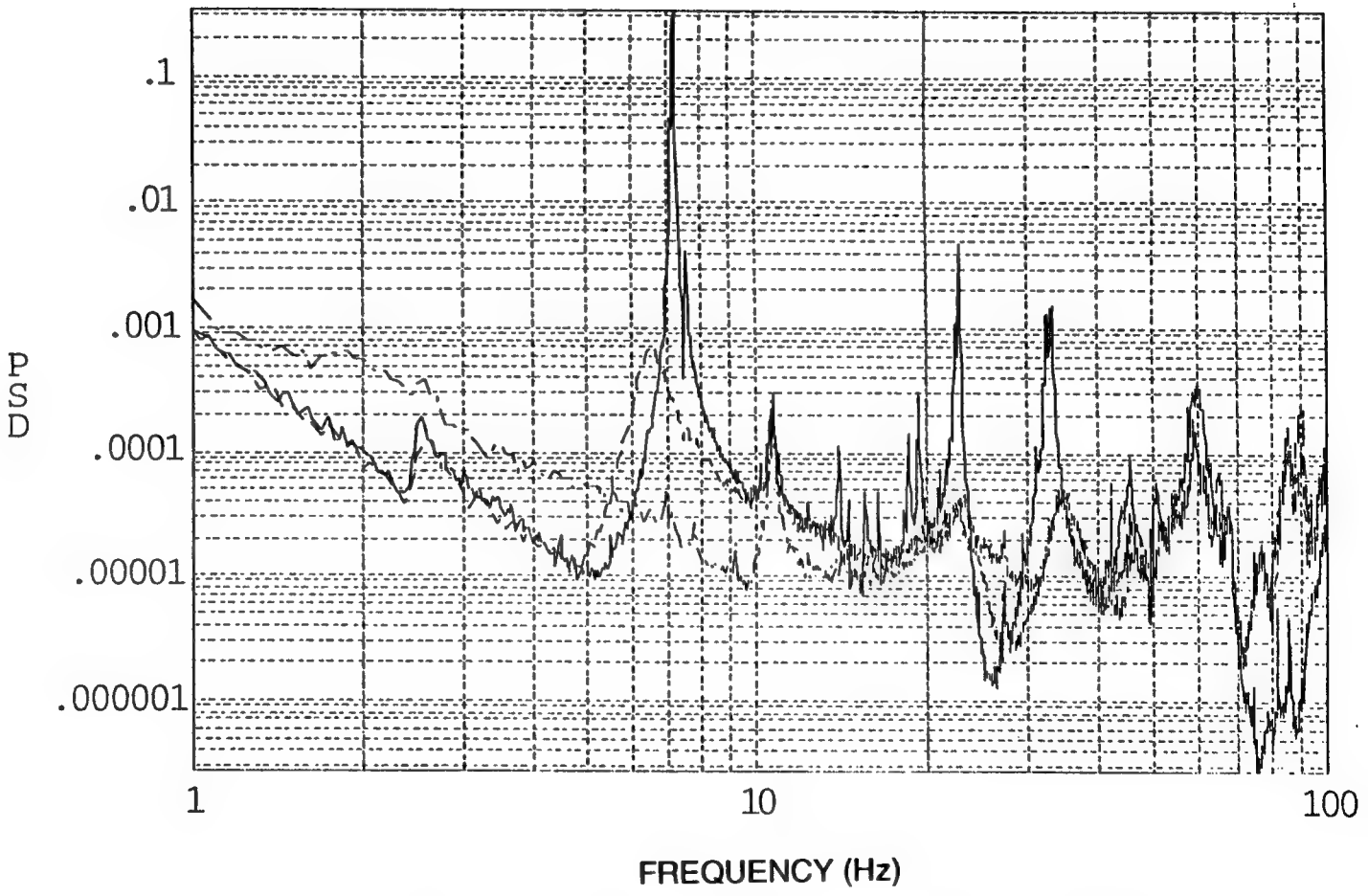

Figure A-10. Spectra of PMA 14 rate - quiescent conditions.

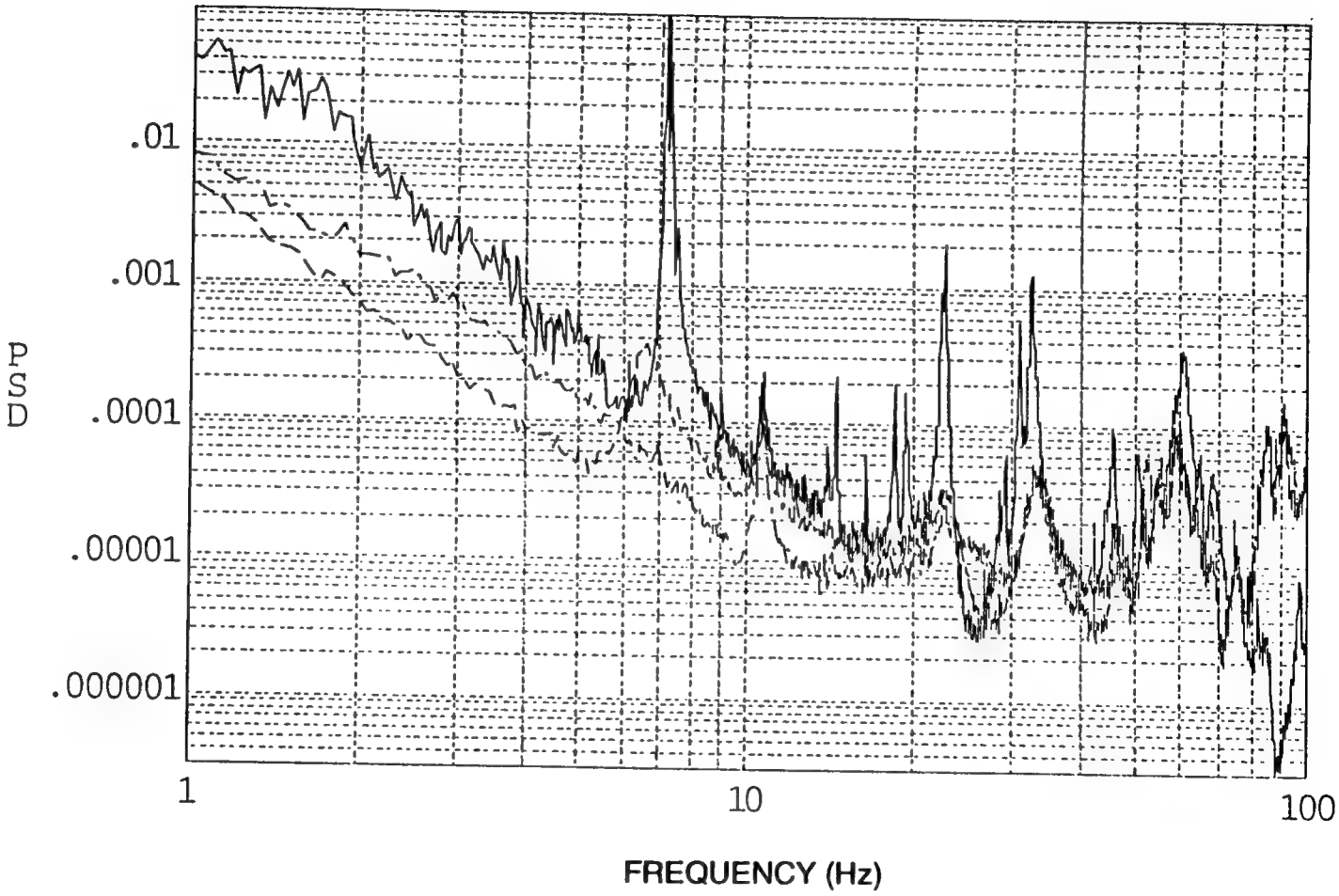

Figure A-11. Spectra of PMA 16 rate - quiescent conditions.

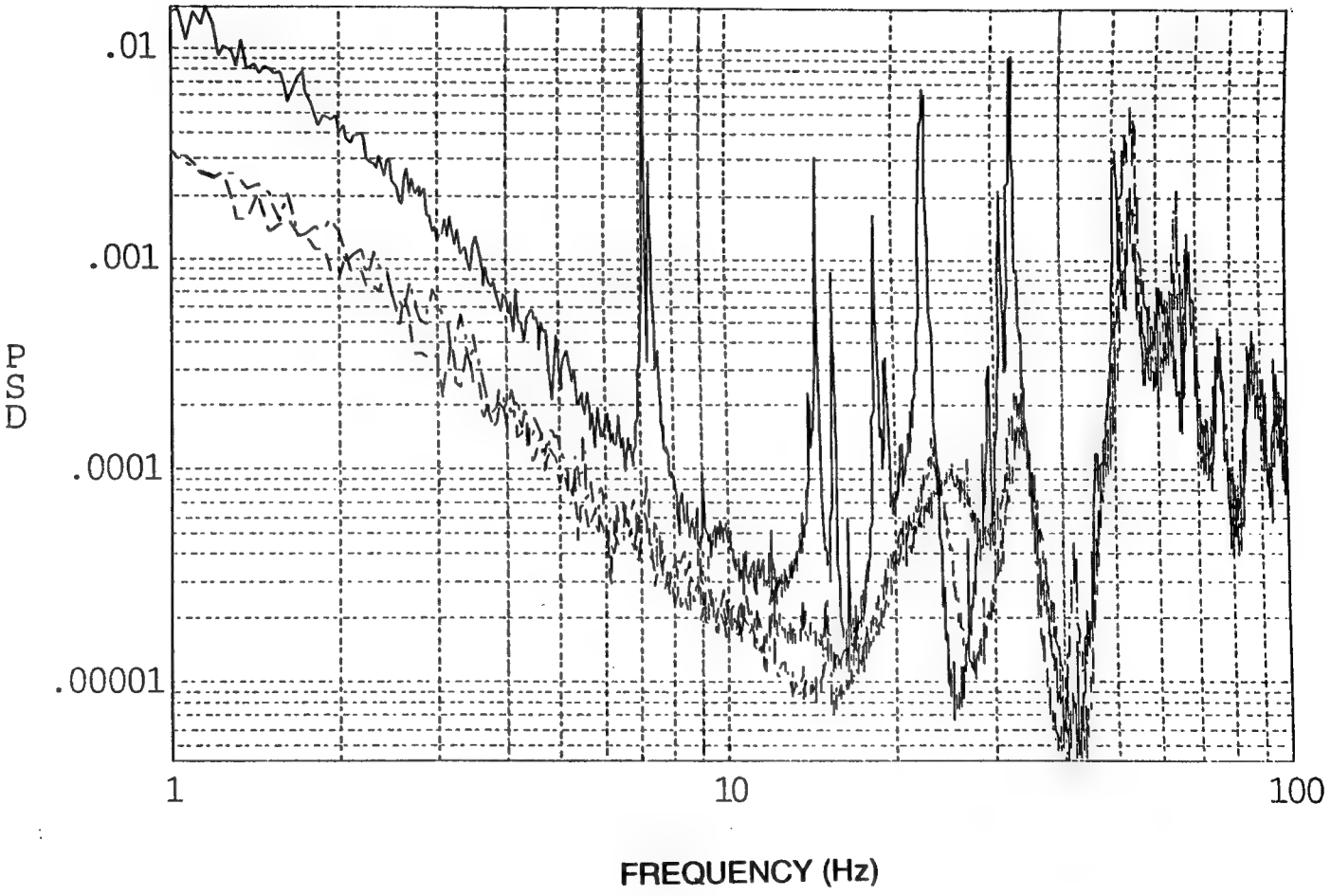

Figure A-12. Spectra of local x-axis signal for PMRS 1 - quiescent conditions.

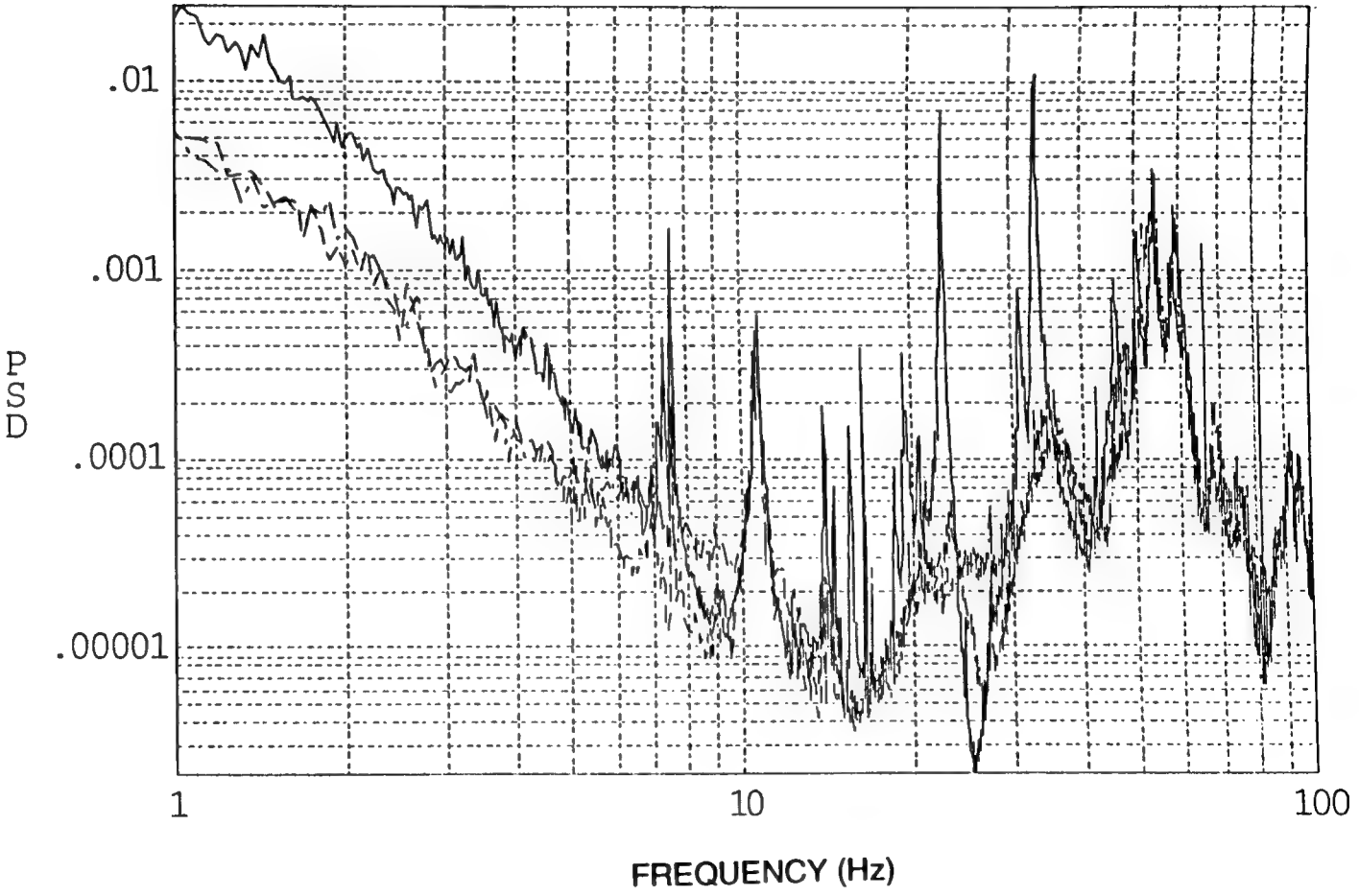

Figure A-13. Spectra of local y-axis signal for PMRS 1 - quiescent conditions.

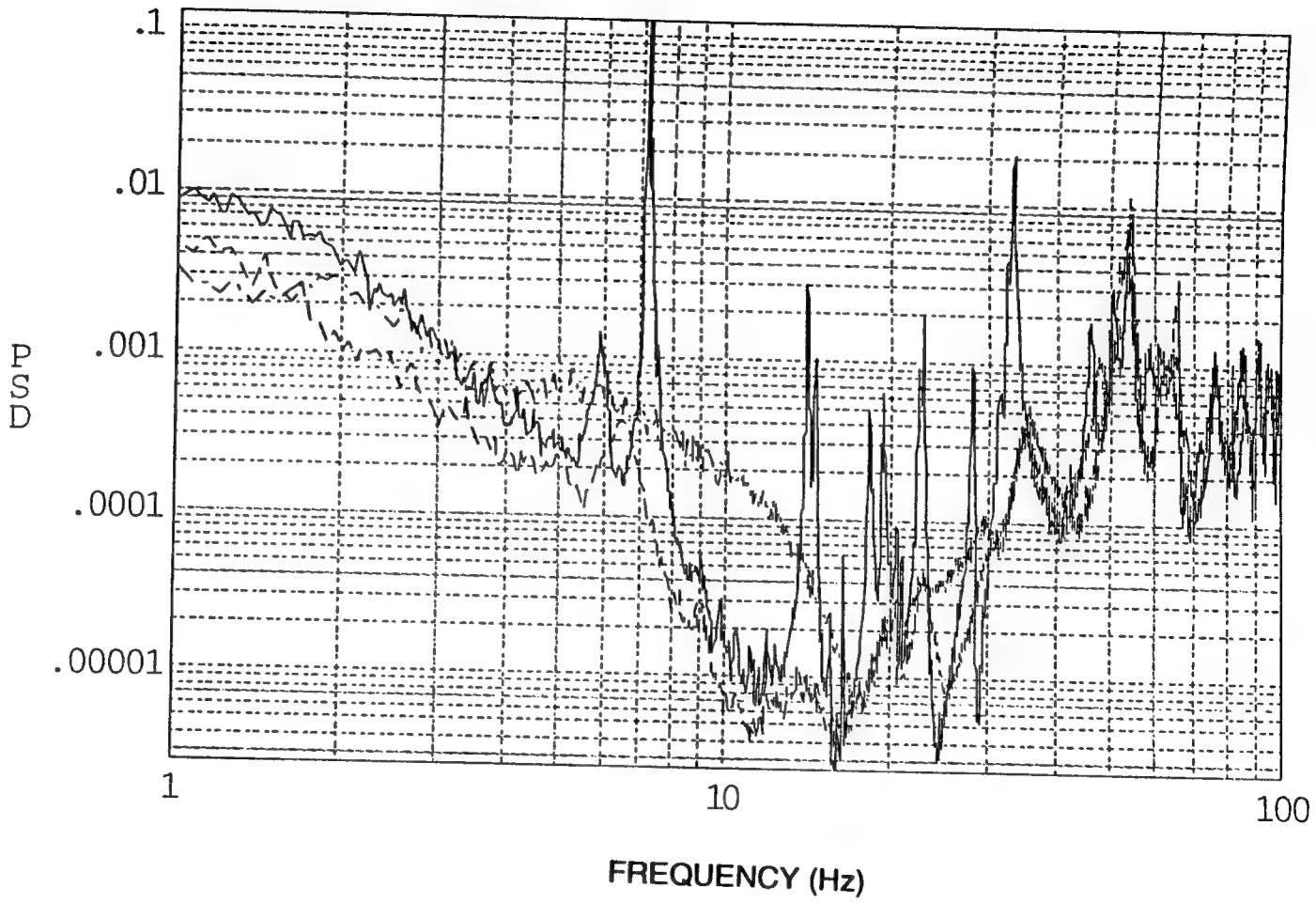

Figure A-14. Spectra of local x-axis signal for PMRS 2 - quiescent conditions.

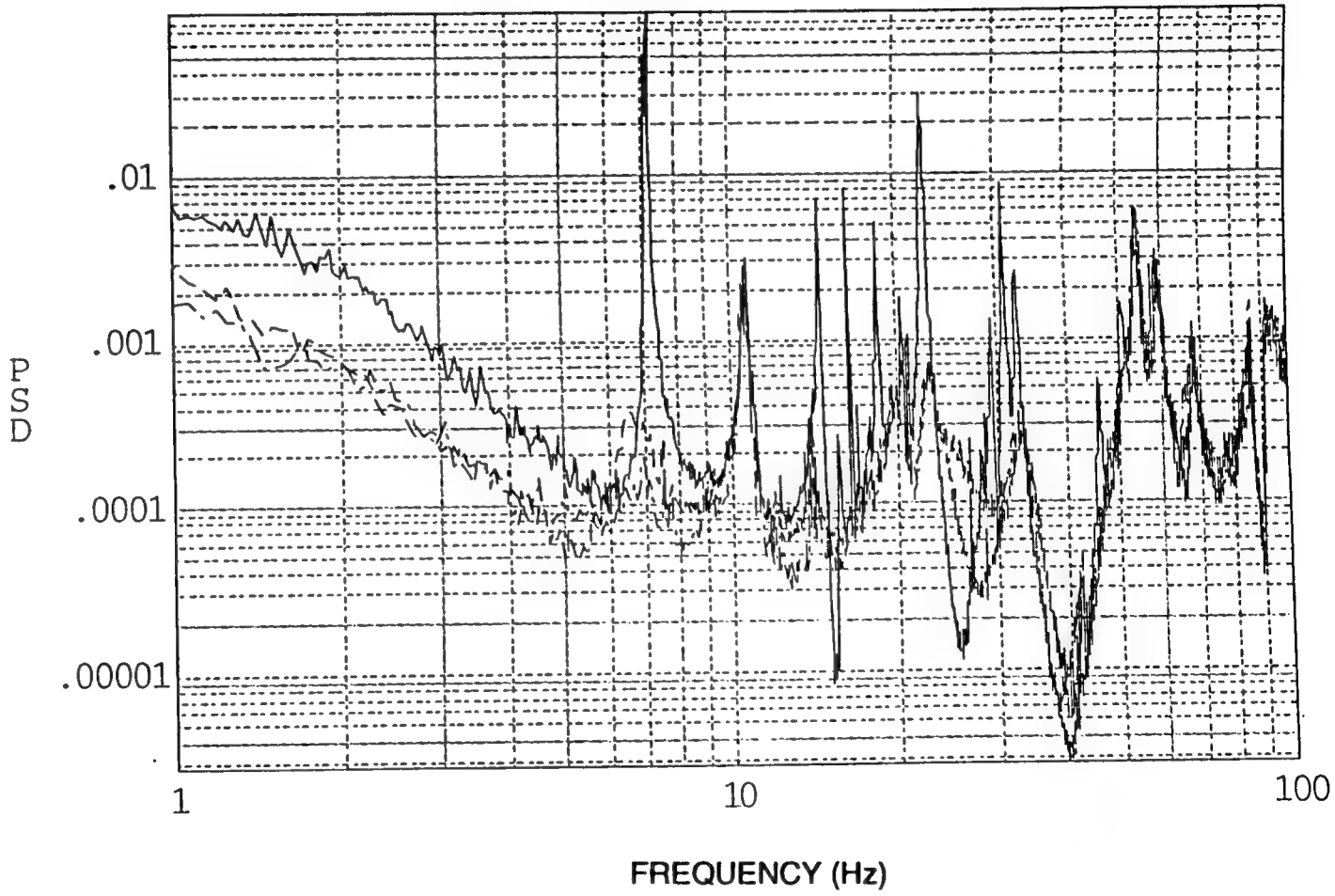

Figure A-15. Spectra of local y-axis signal for PMRS 2 - quiescent conditions.

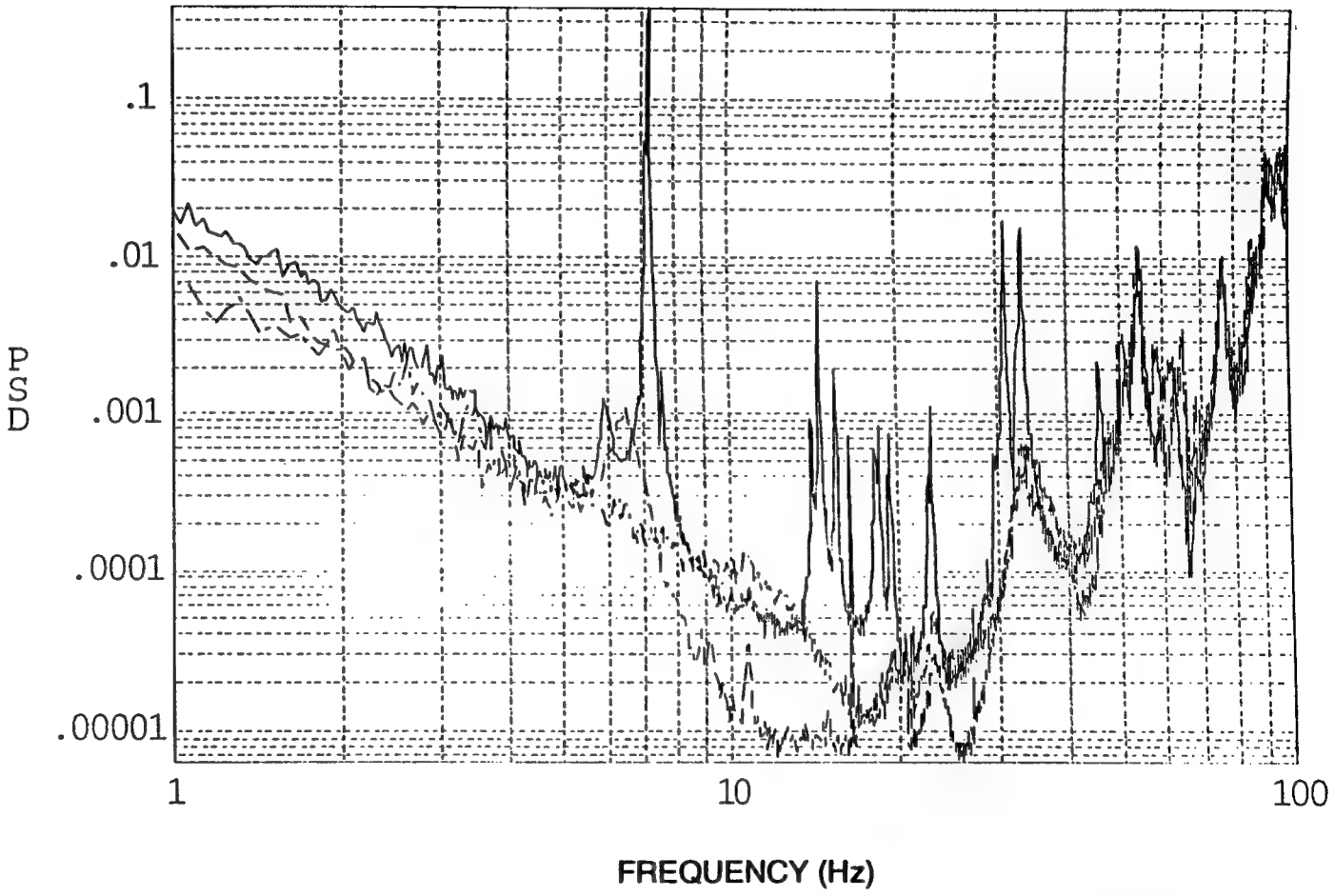

Figure A-16. Spectra of local x-axis signal for PMRS 6 - quiescent conditions.

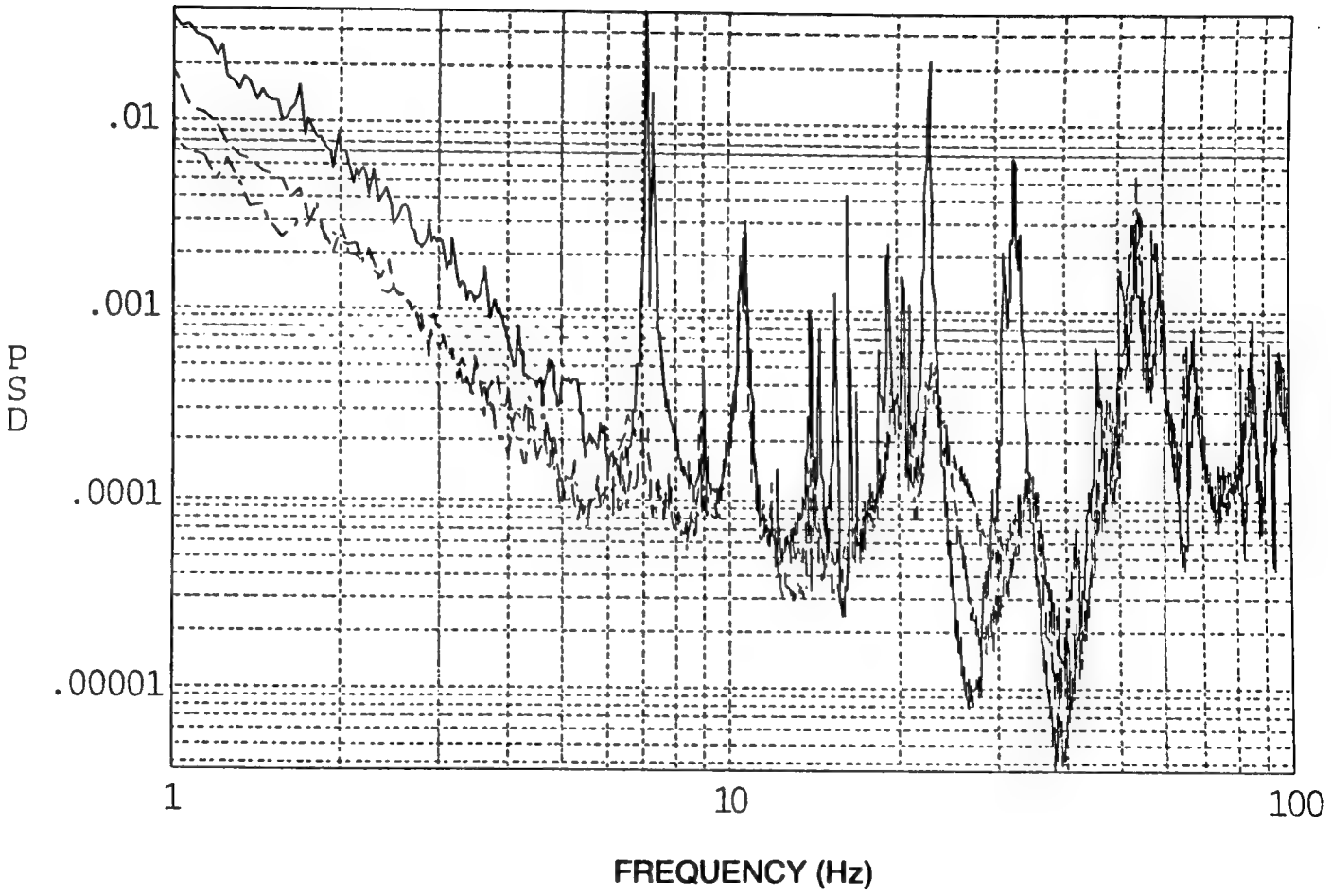

Figure A-17. Spectra of local y-axis signal for PMRS 6 - quiescent conditions.

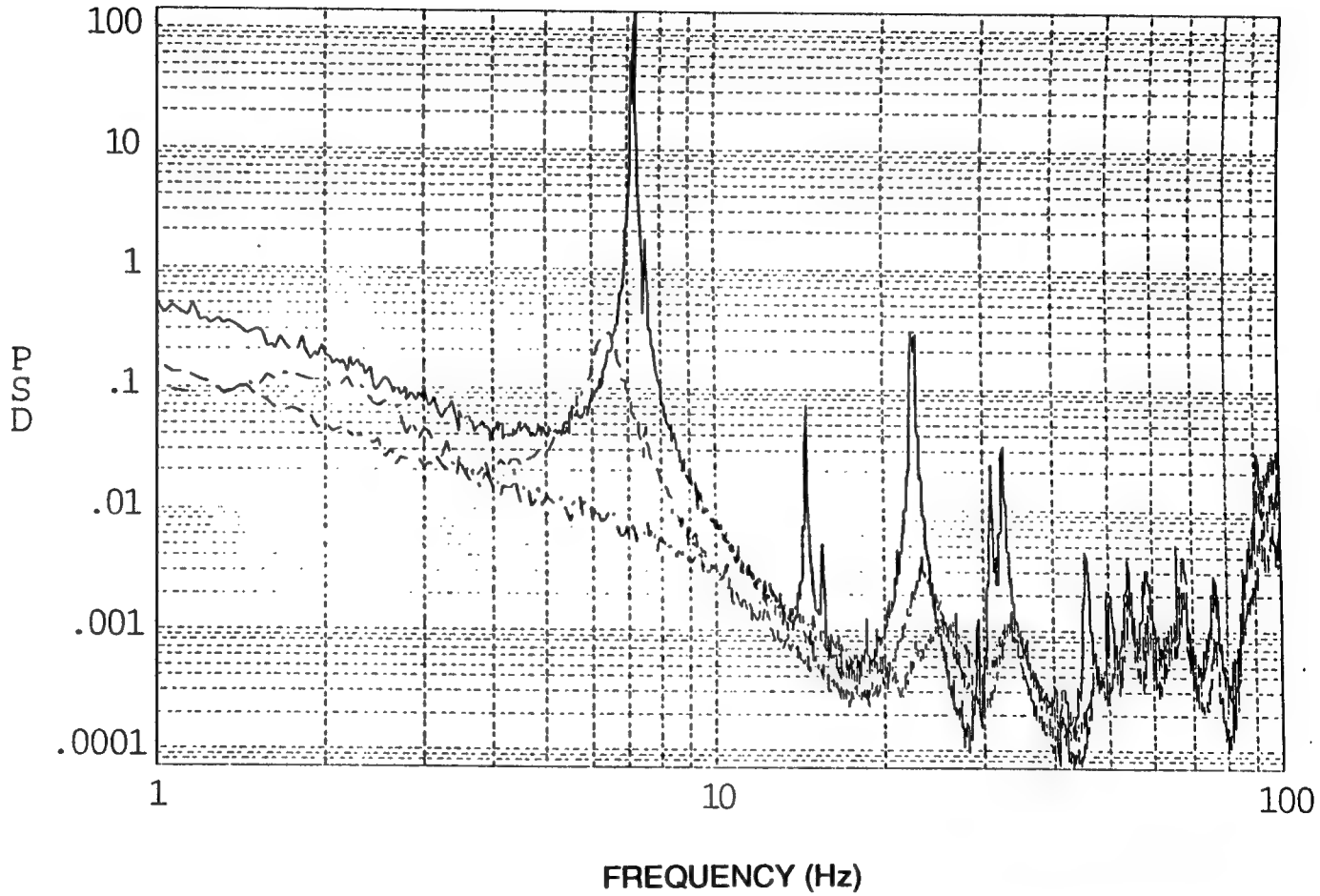

Figure A-18. Spectra of local x-axis signal for SMRS - quiescent conditions.

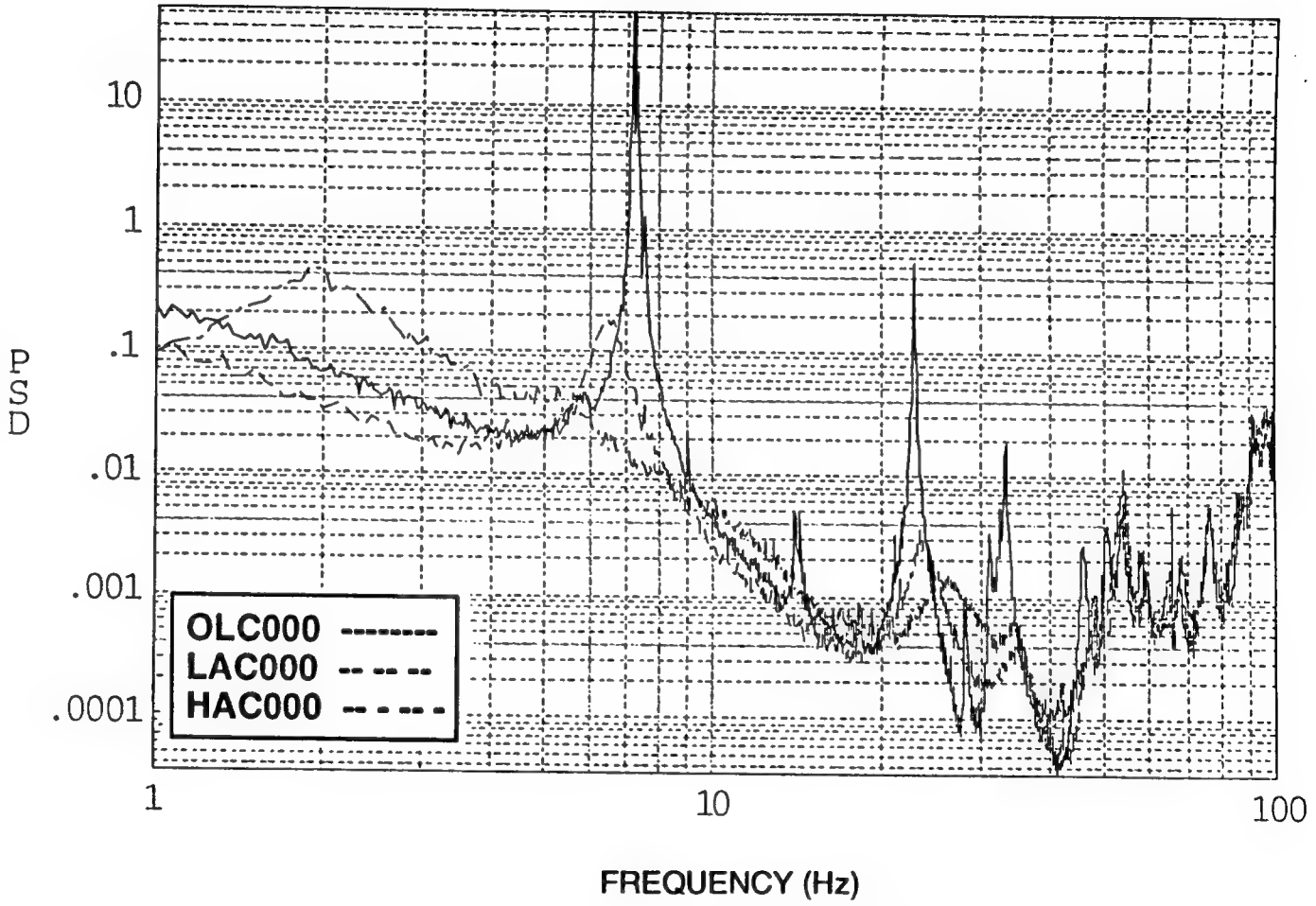

Figure A-19. Spectra of local y-axis signal for SMRS - quiescent conditions.

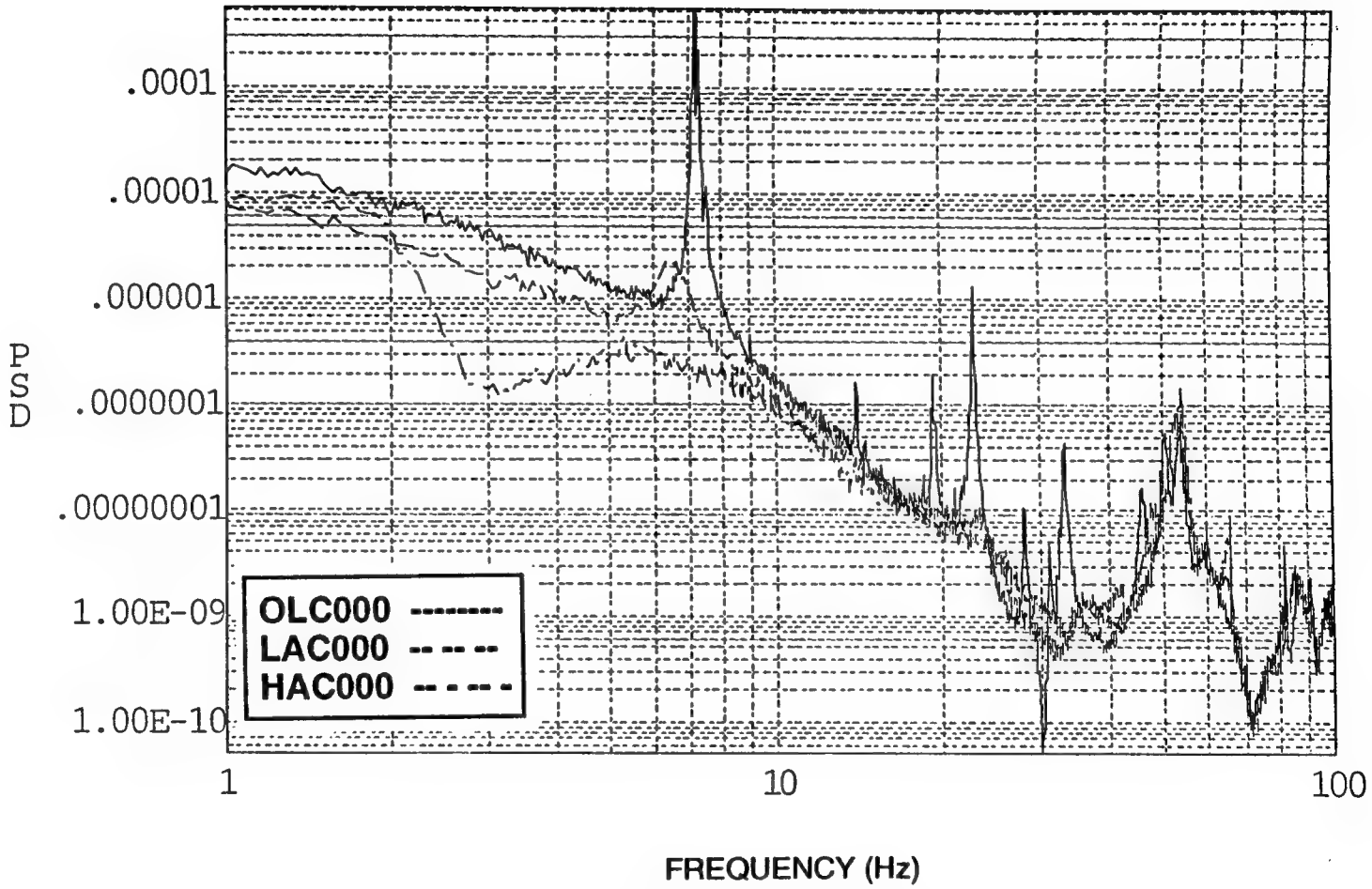

Figure A-20. Spectra of local x-axis signal for SMTS 8 - quiescent conditions.

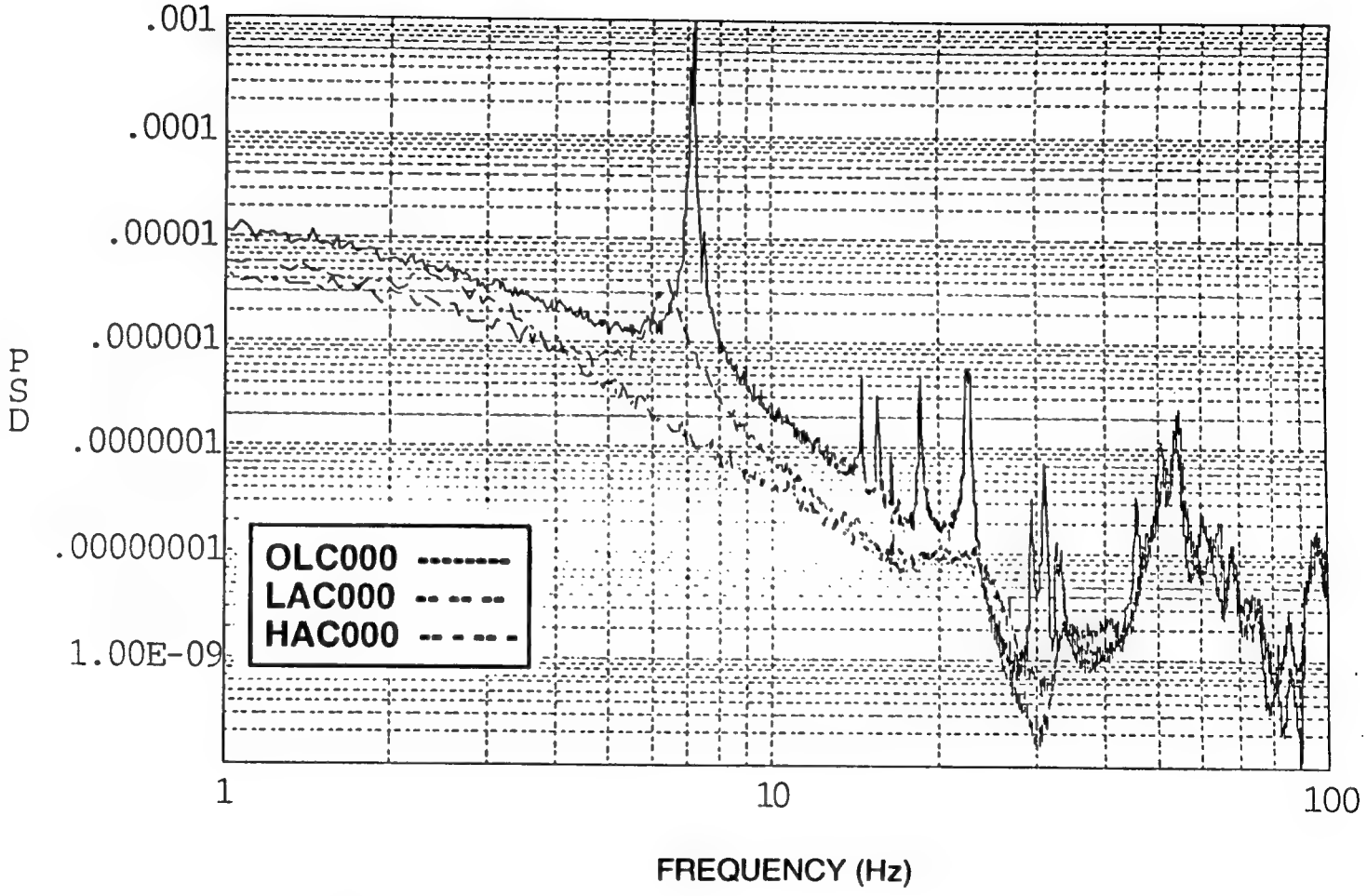

Figure A-21. Spectra of local y-axis signal for SMTS 8 - quiescent conditions.

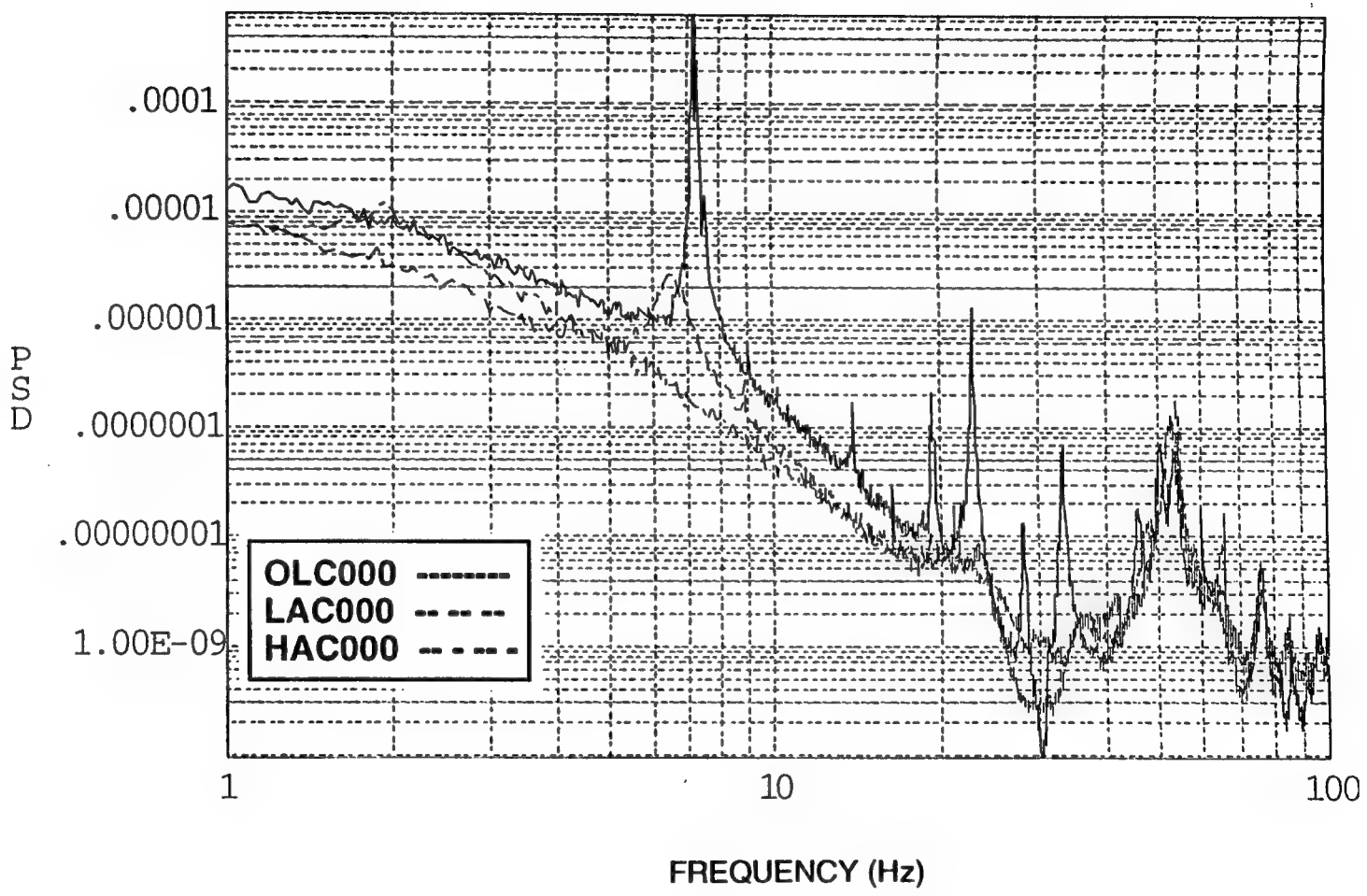

Figure A-22. Spectra of local x-axis signal for SMTS 9 - quiescent conditions.

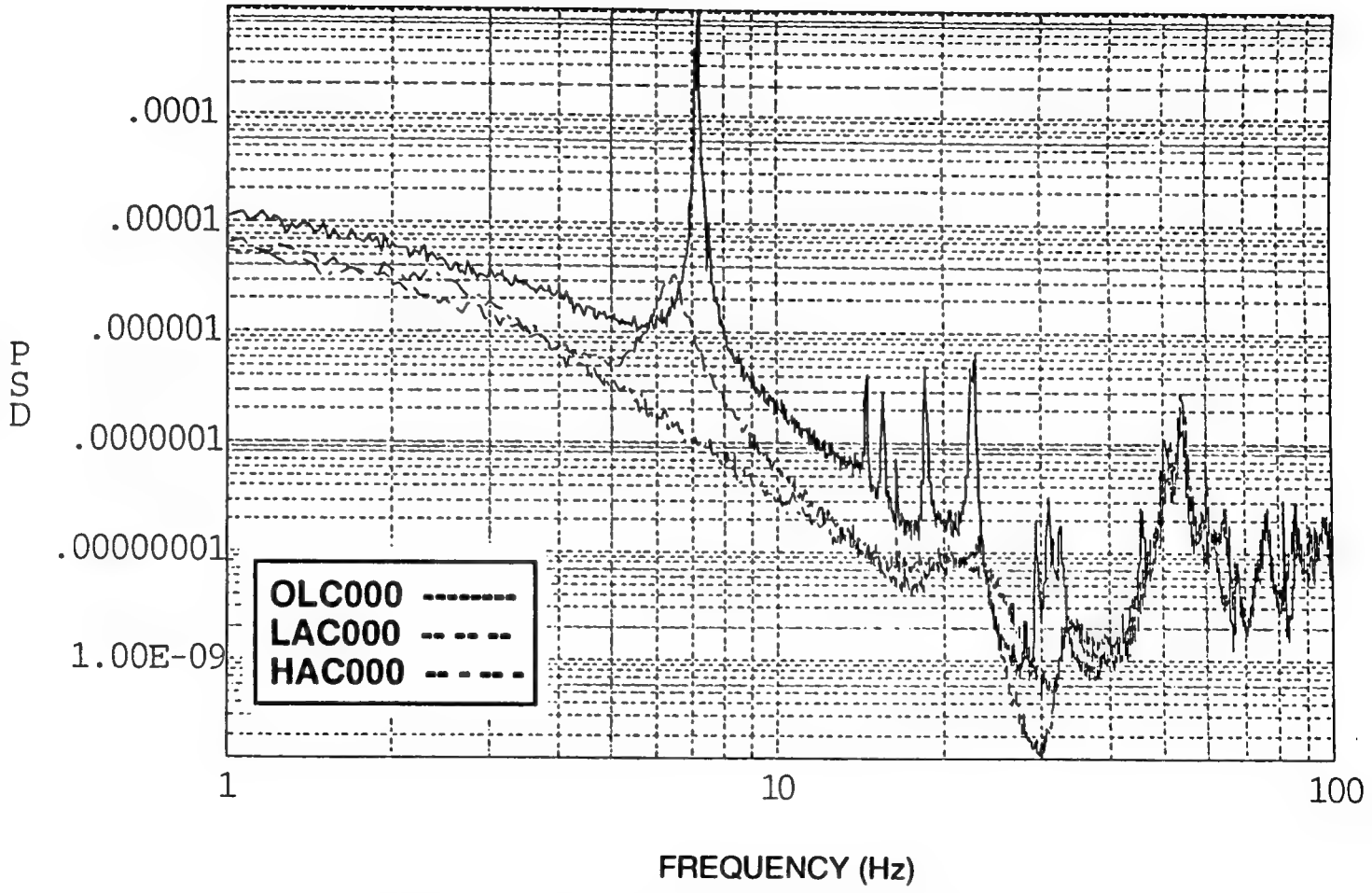

Figure A-23. Spectra of local y-axis signal for SMTS 9 - quiescent conditions.

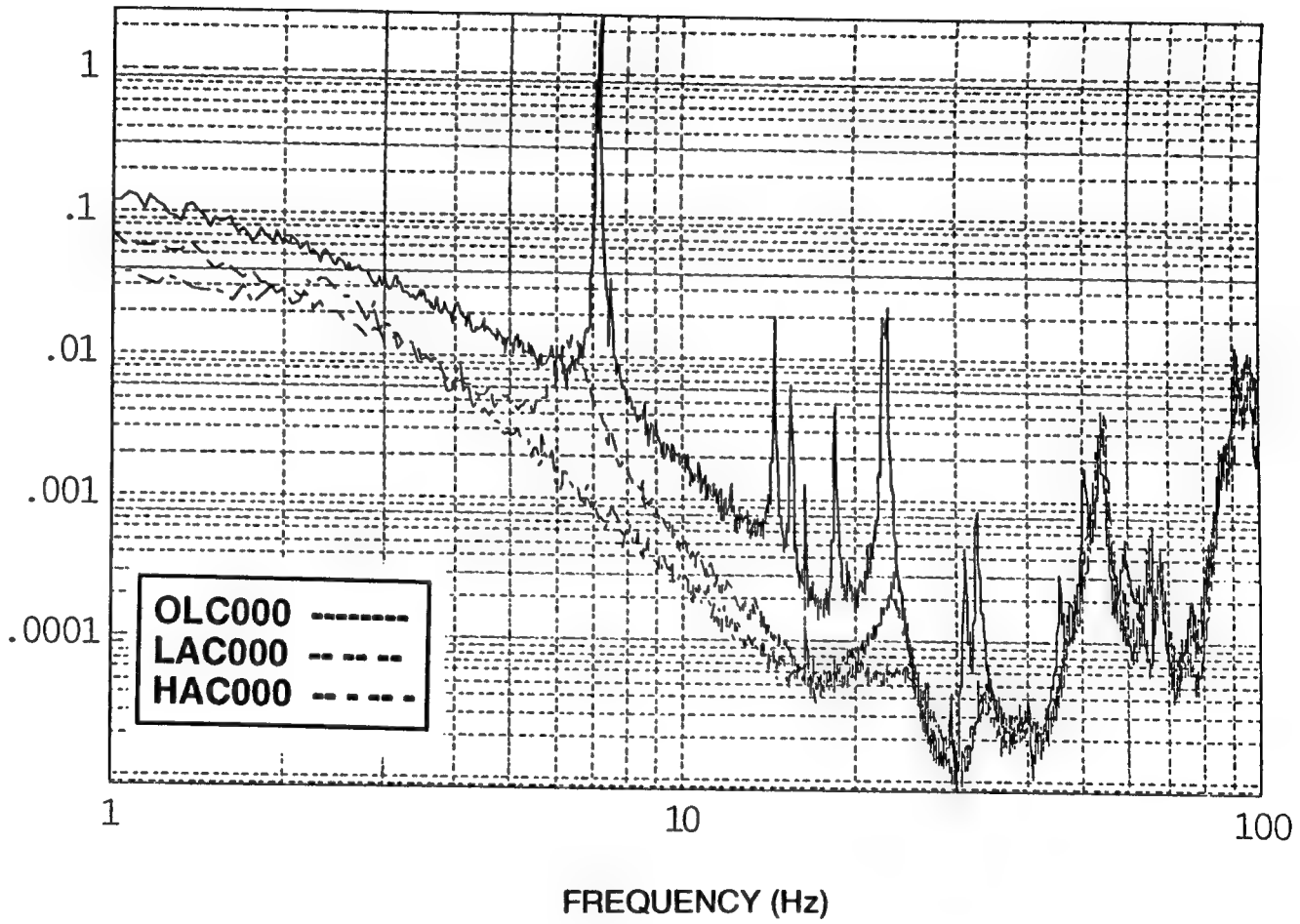

Figure A-24. Spectra of LOS-x signal - quiescent conditions.

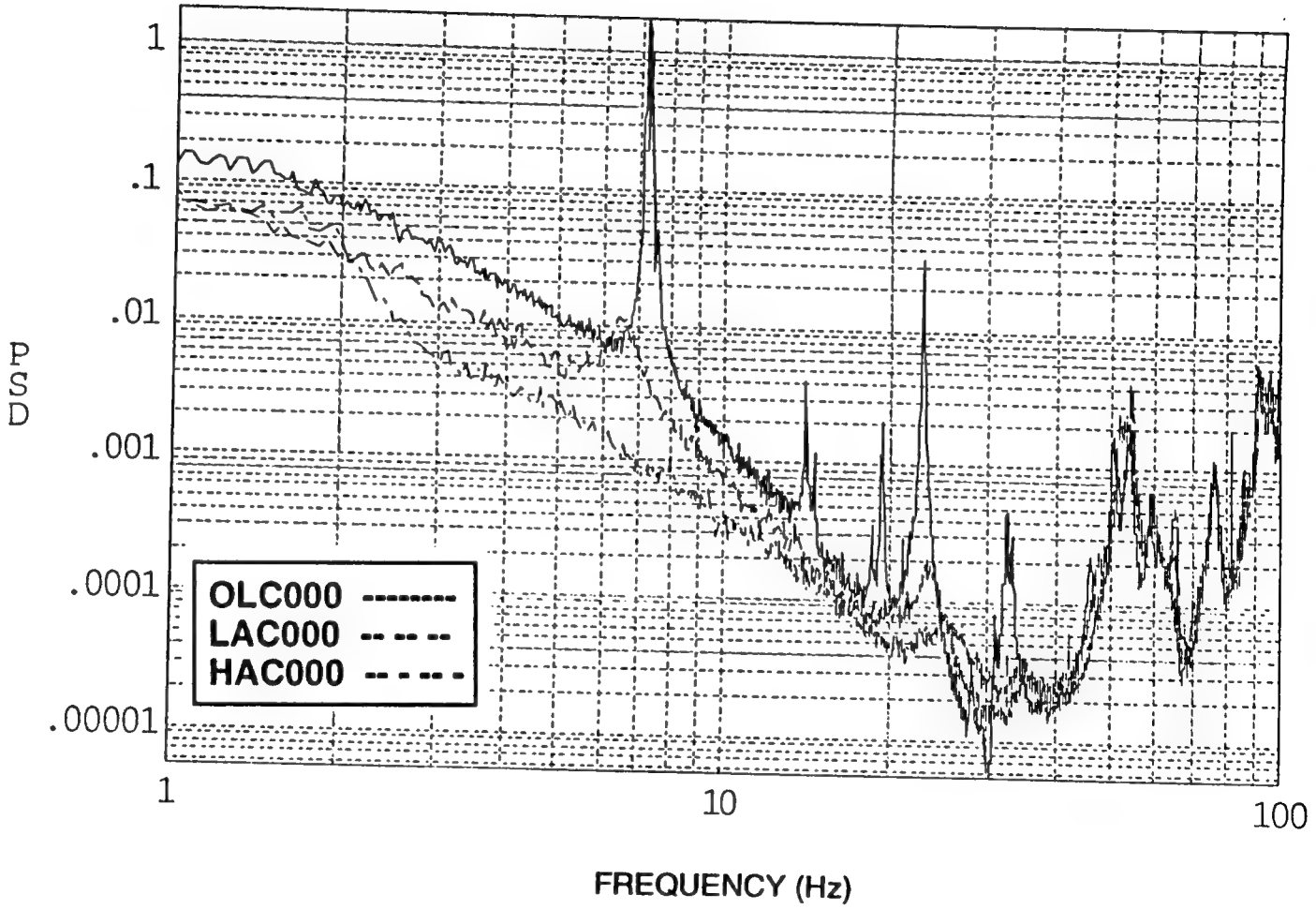

Figure A-25. Spectra of LOS-y signal - quiescent conditions.

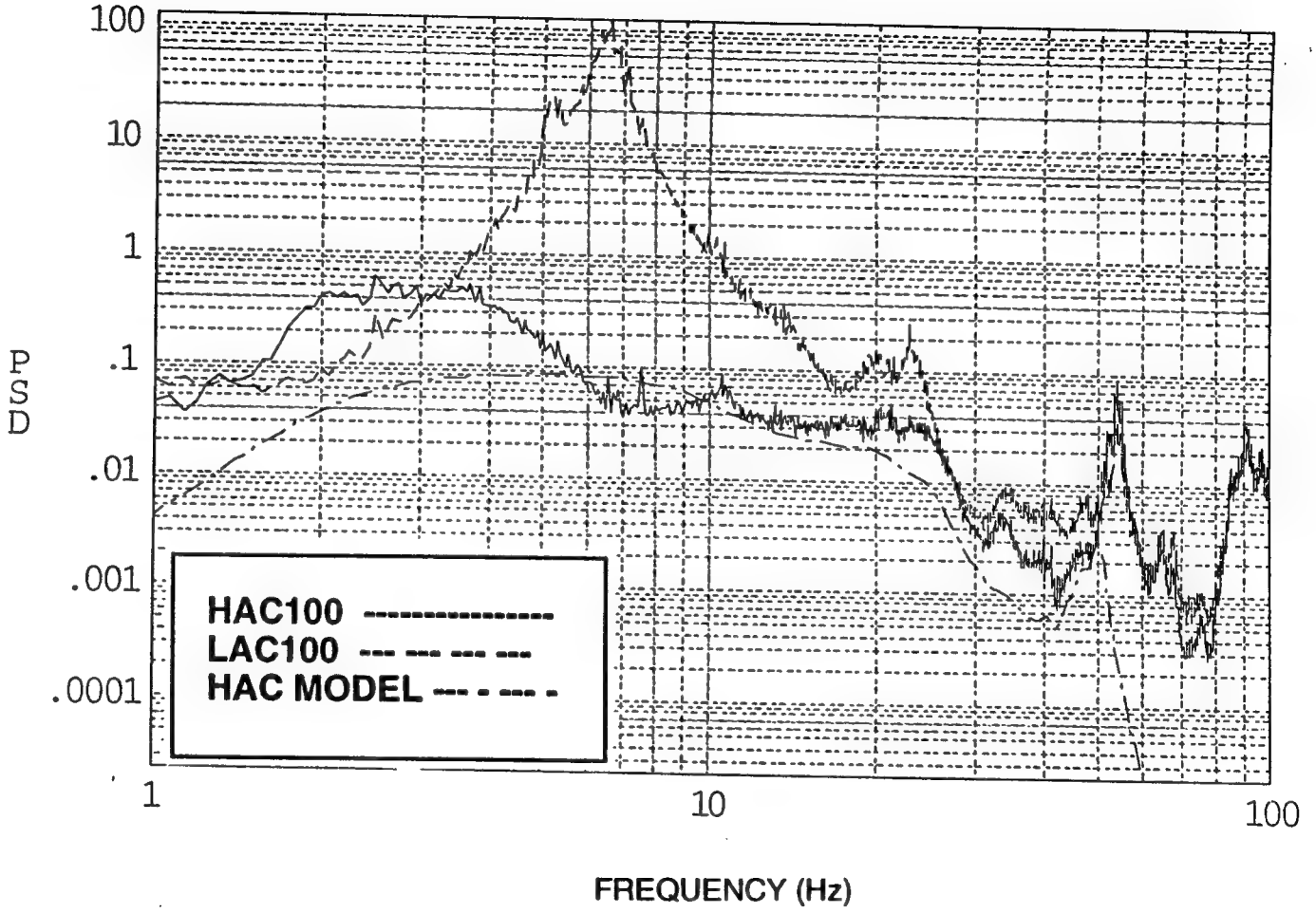

Figure A-26. Spectra of LOS-x - 100-μrad caged-target LOS disturbances.

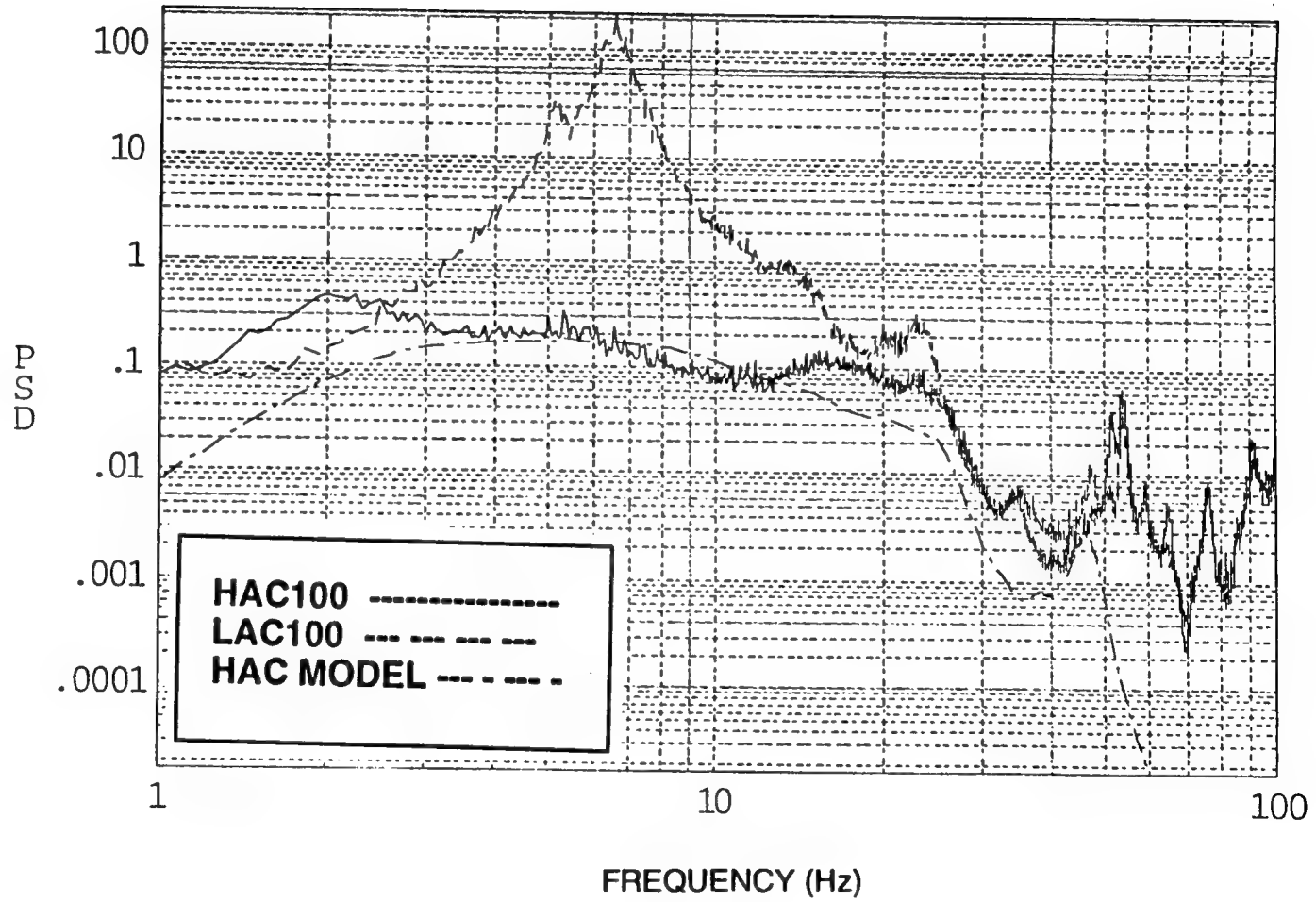

Figure A-27. Spectra of LOS-y - 100-μrad caged-target LOS disturbances.

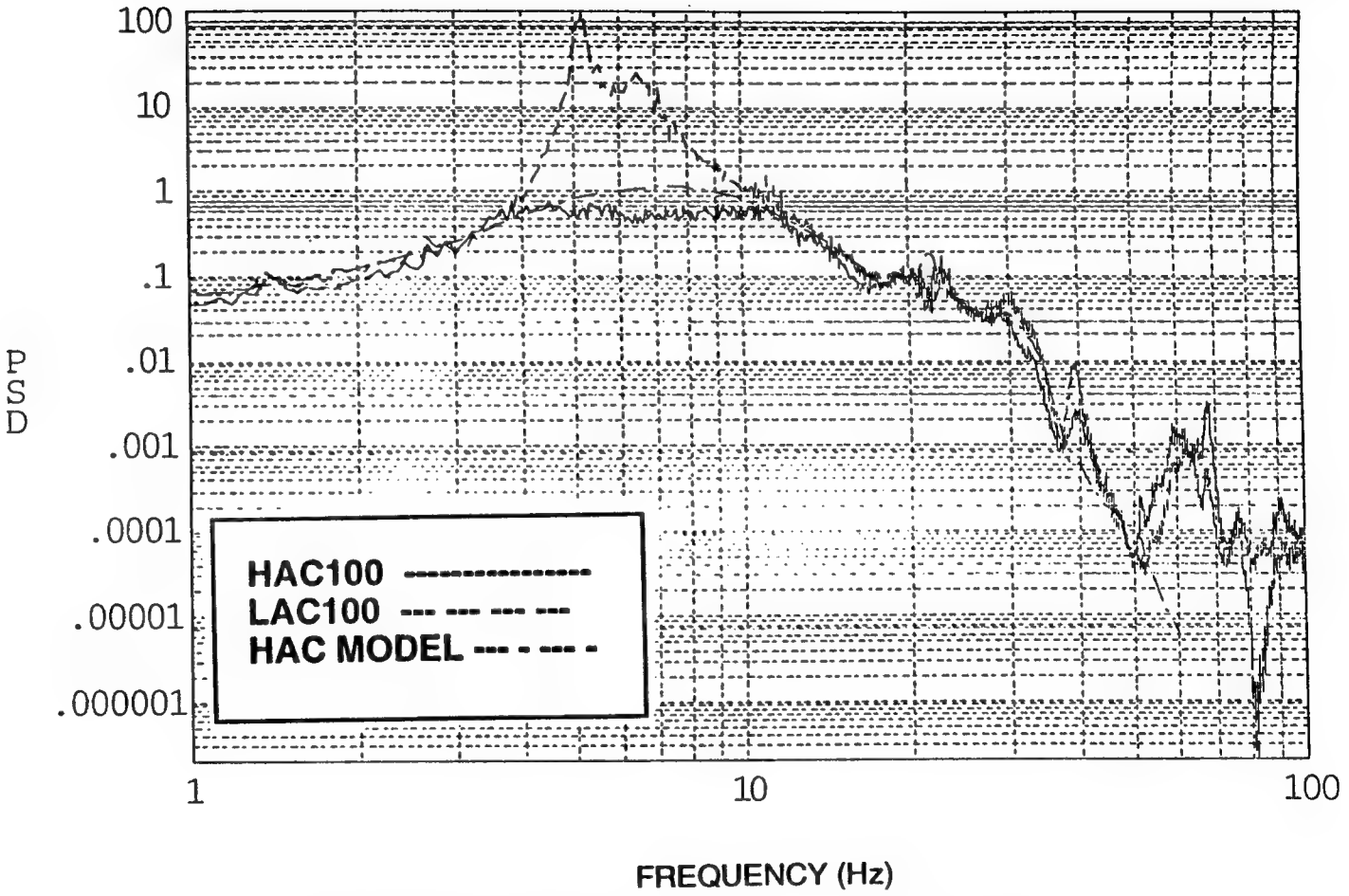

Figure A-28. Spectra of PMA 2 rate - 100-µrad caged-target LOS disturbances.

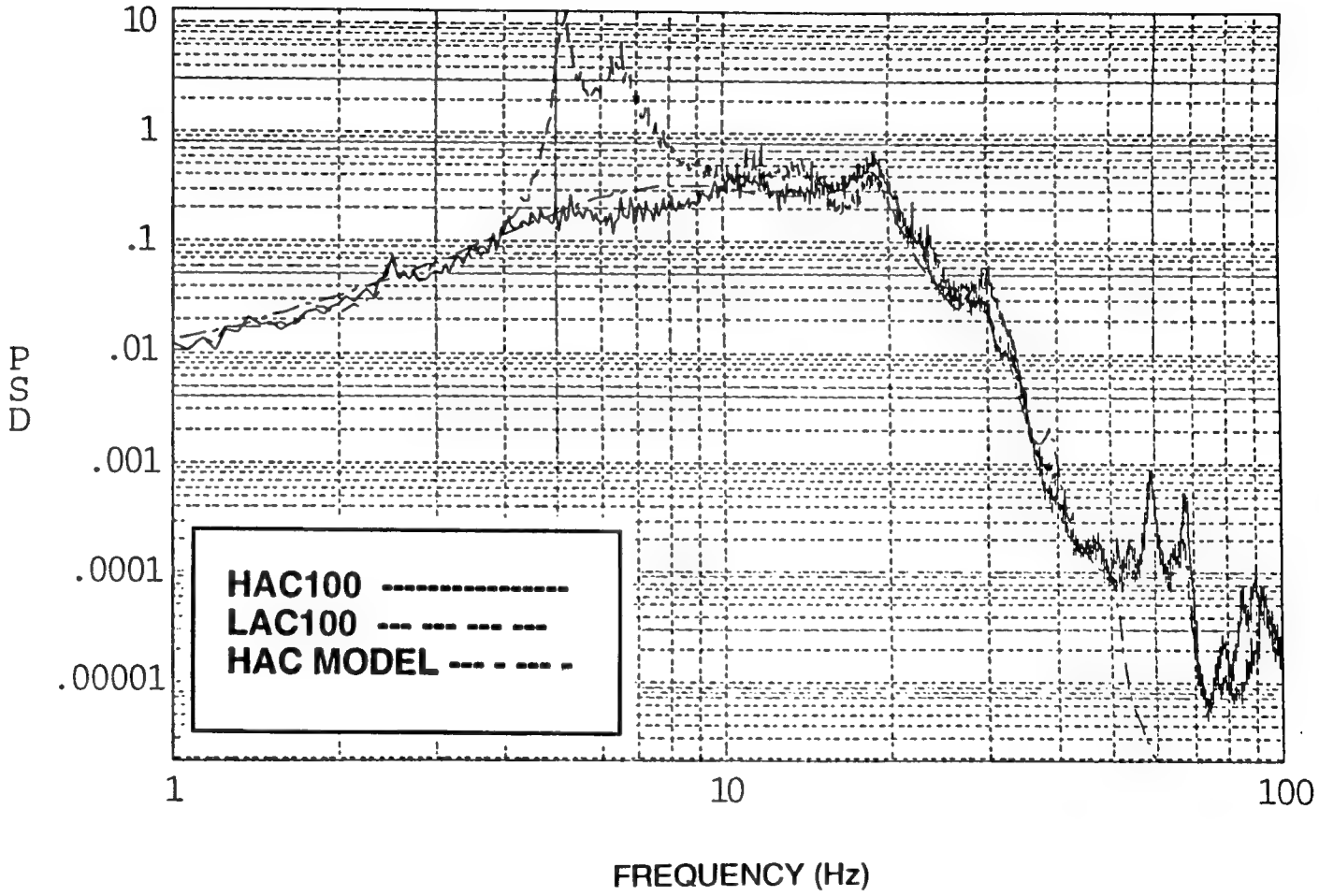

Figure A-29. Spectra of PMA 3 rate - 100-µrad caged-target LOS disturbances.

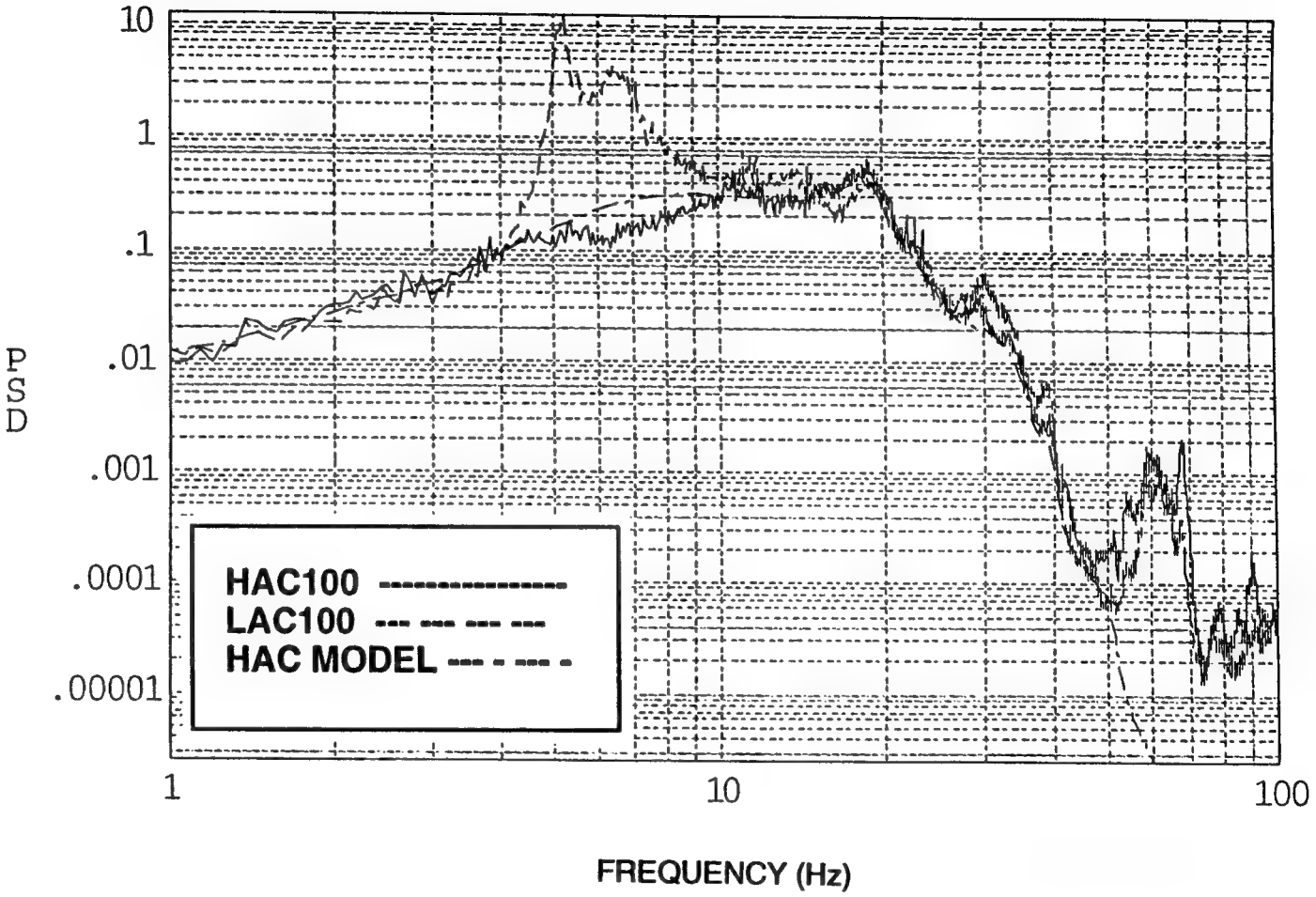

Figure A-30. Spectra of PMA 4 rate - 100-μrad caged-target LOS disturbances.

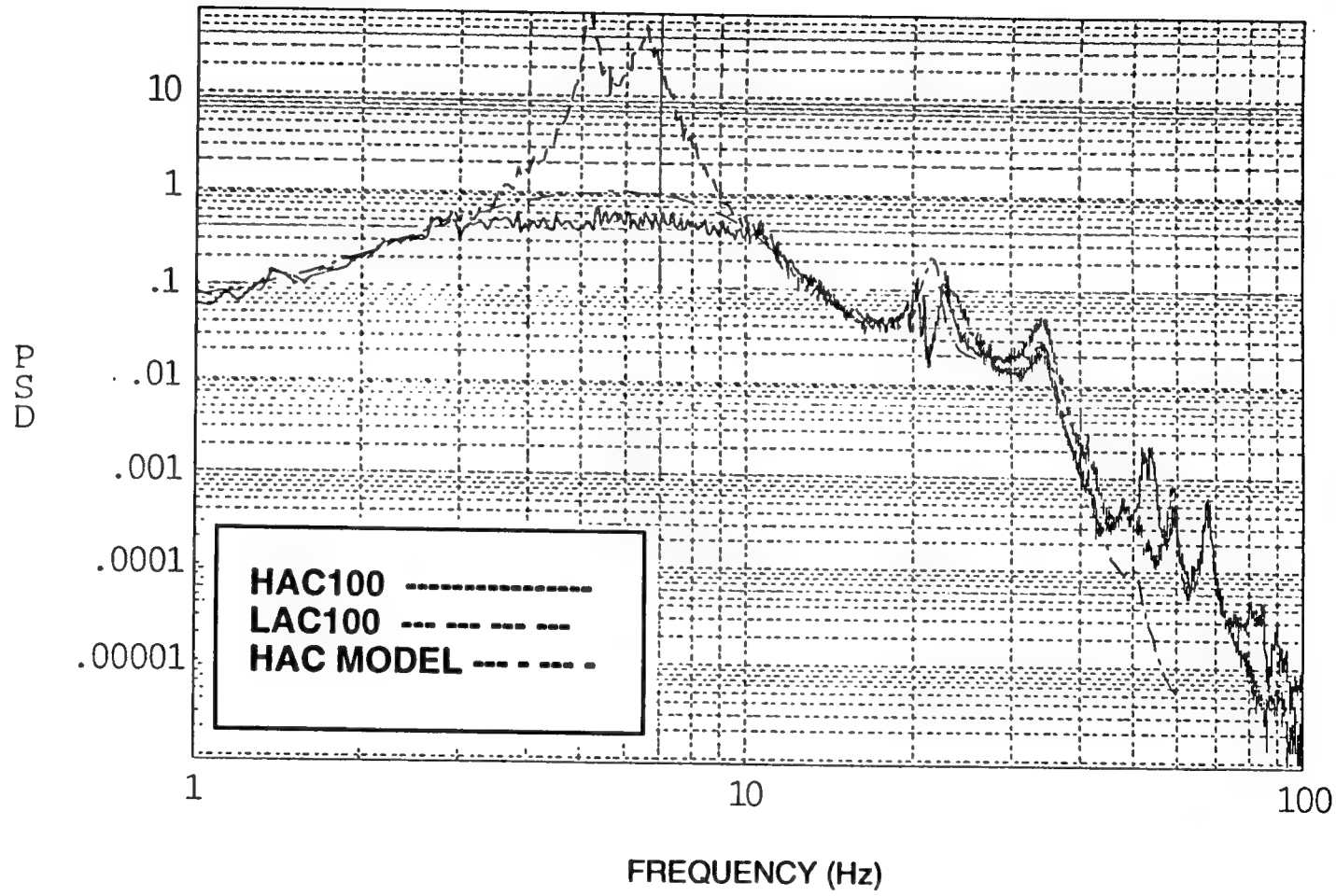

Figure A-31. Spectra of PMA 9 rate - 100-µrad caged-target LOS disturbances.

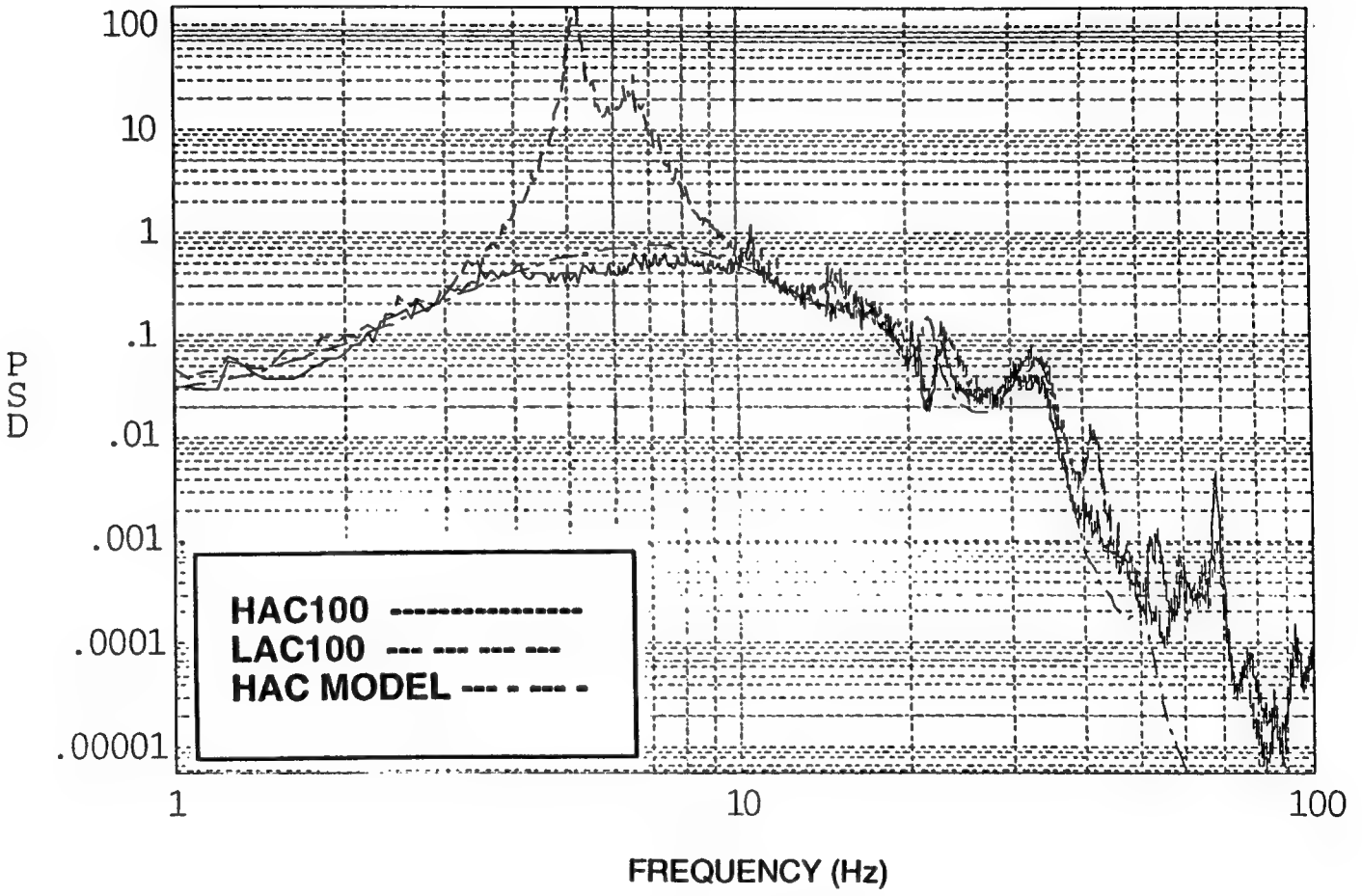

Figure A-32. Spectra of PMA 10 rate - 100-µrad caged-target LOS disturbances.

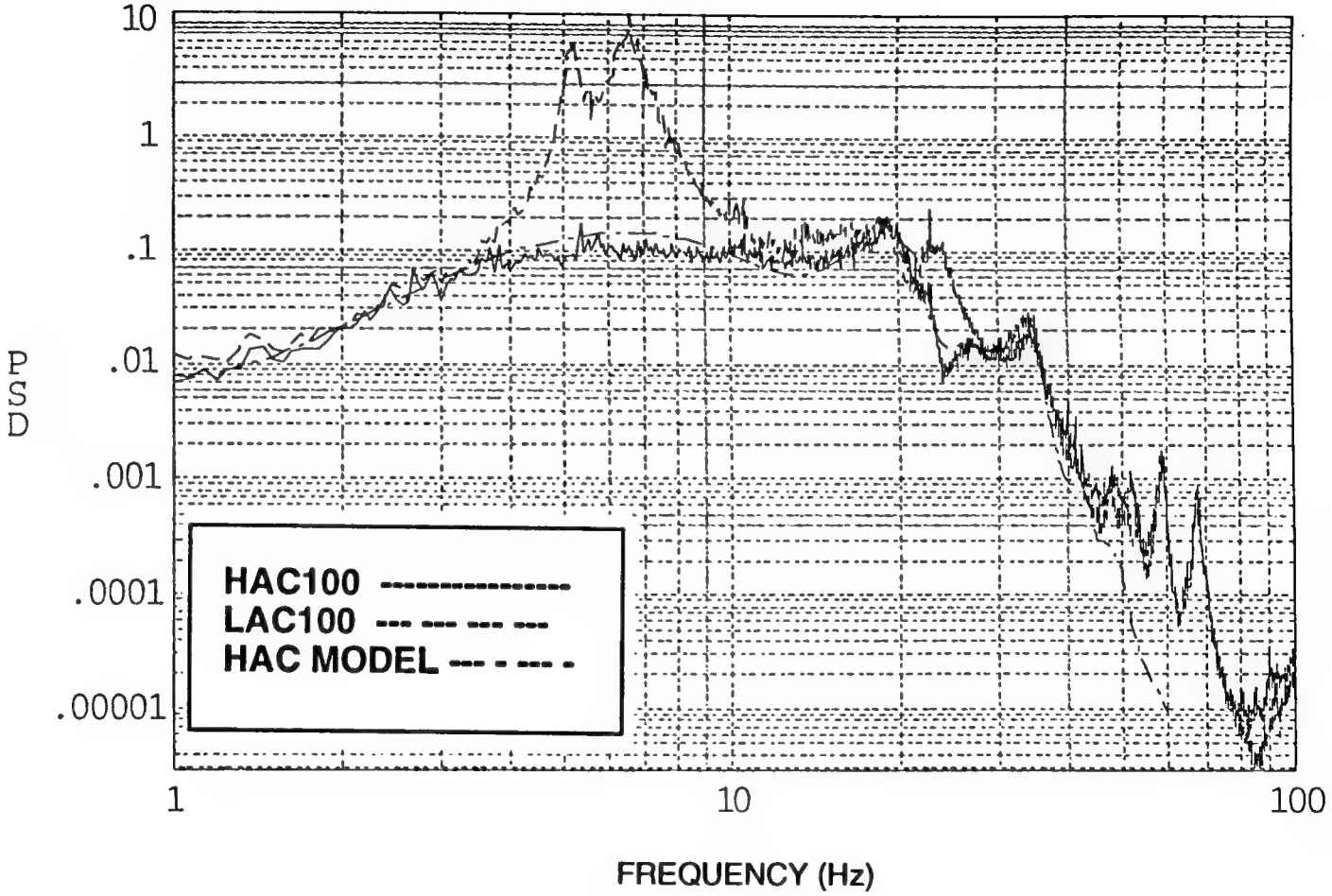

Figure A-33. Spectra of PMA 11 rate - 100-µrad caged-target LOS disturbances.

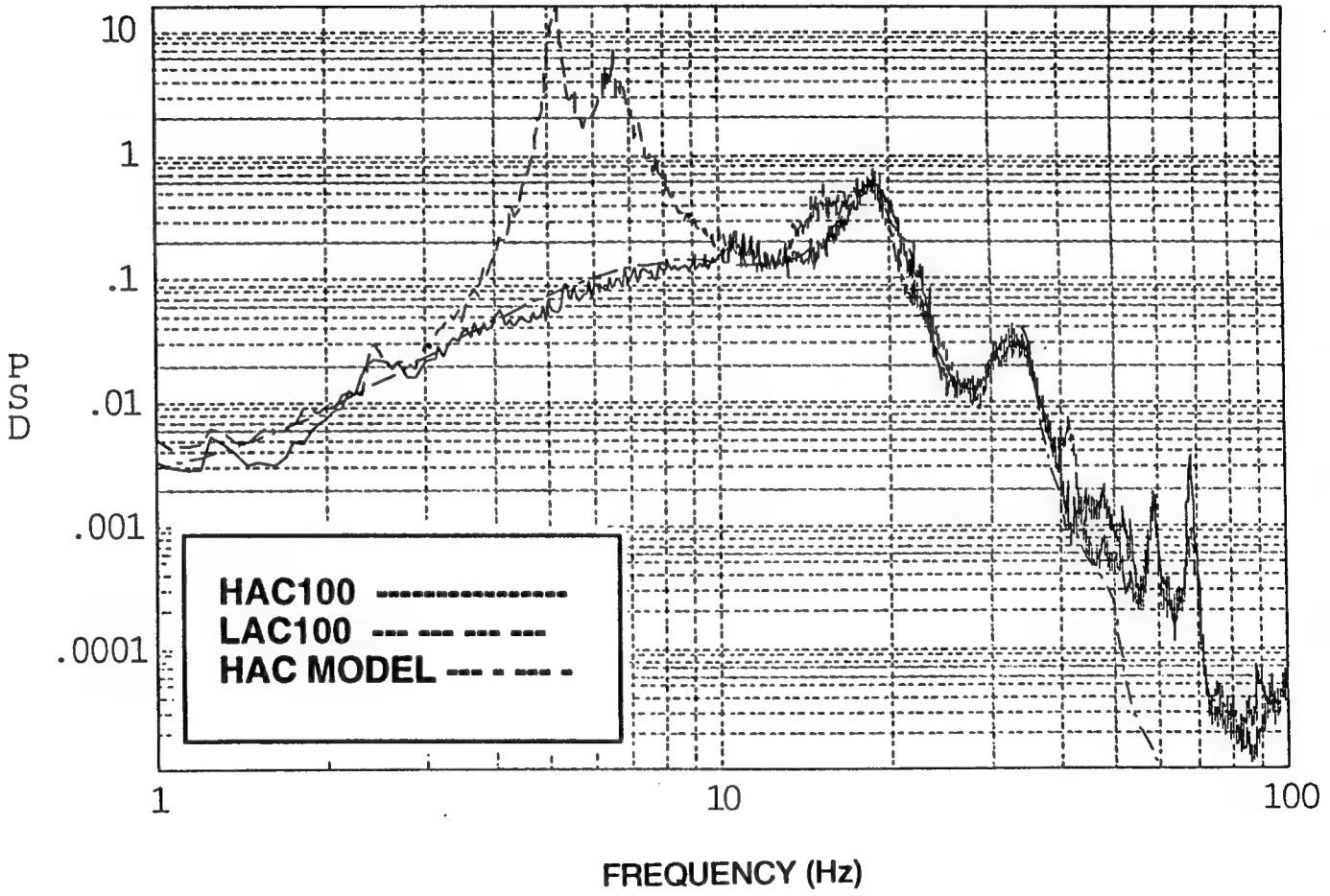

Figure A-34. Spectra of PMA 12 rate - 100-µrad caged-target LOS disturbances.

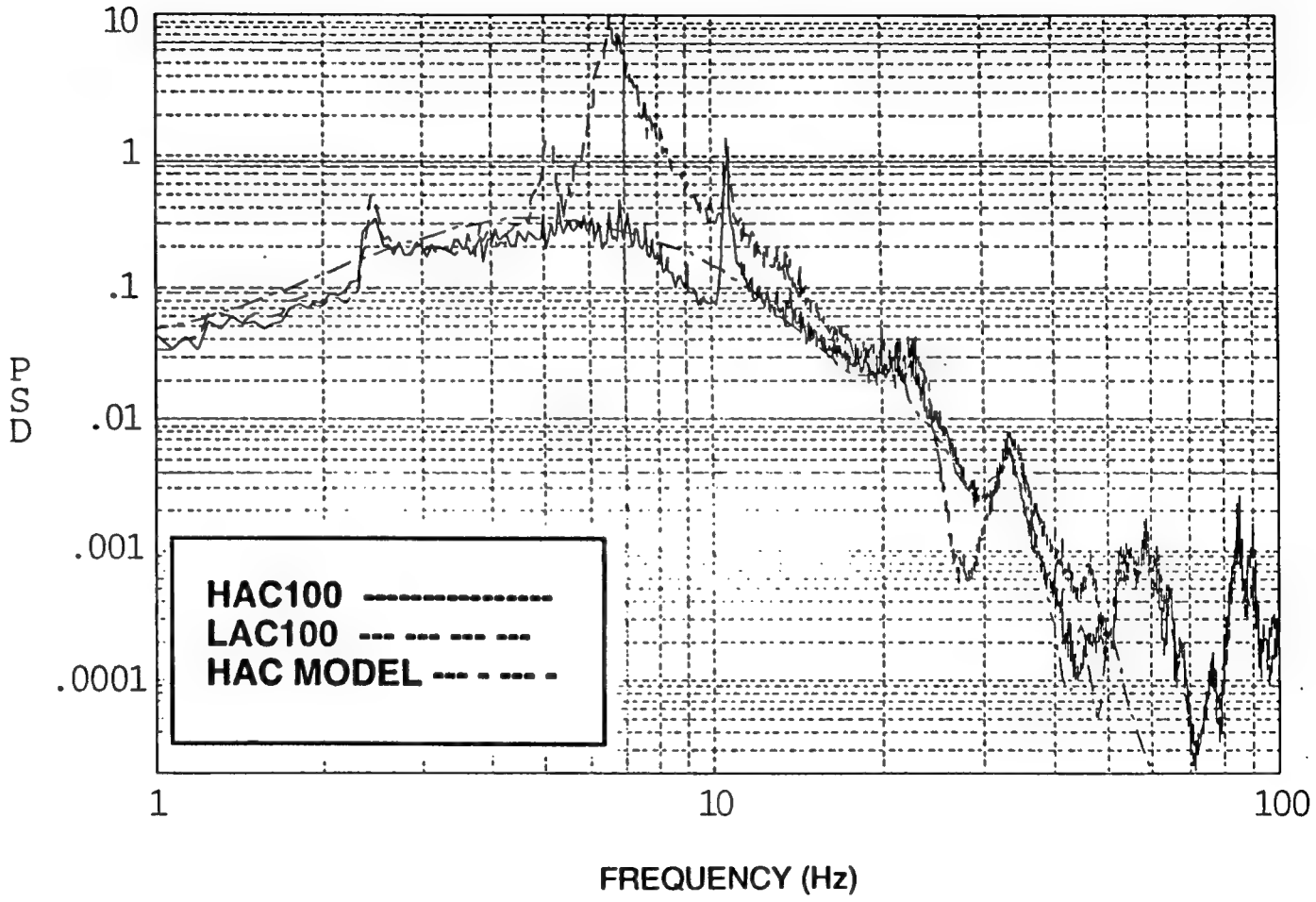

Figure A-35. Spectra of PMA 13 rate - 100-µrad caged-target LOS disturbances.

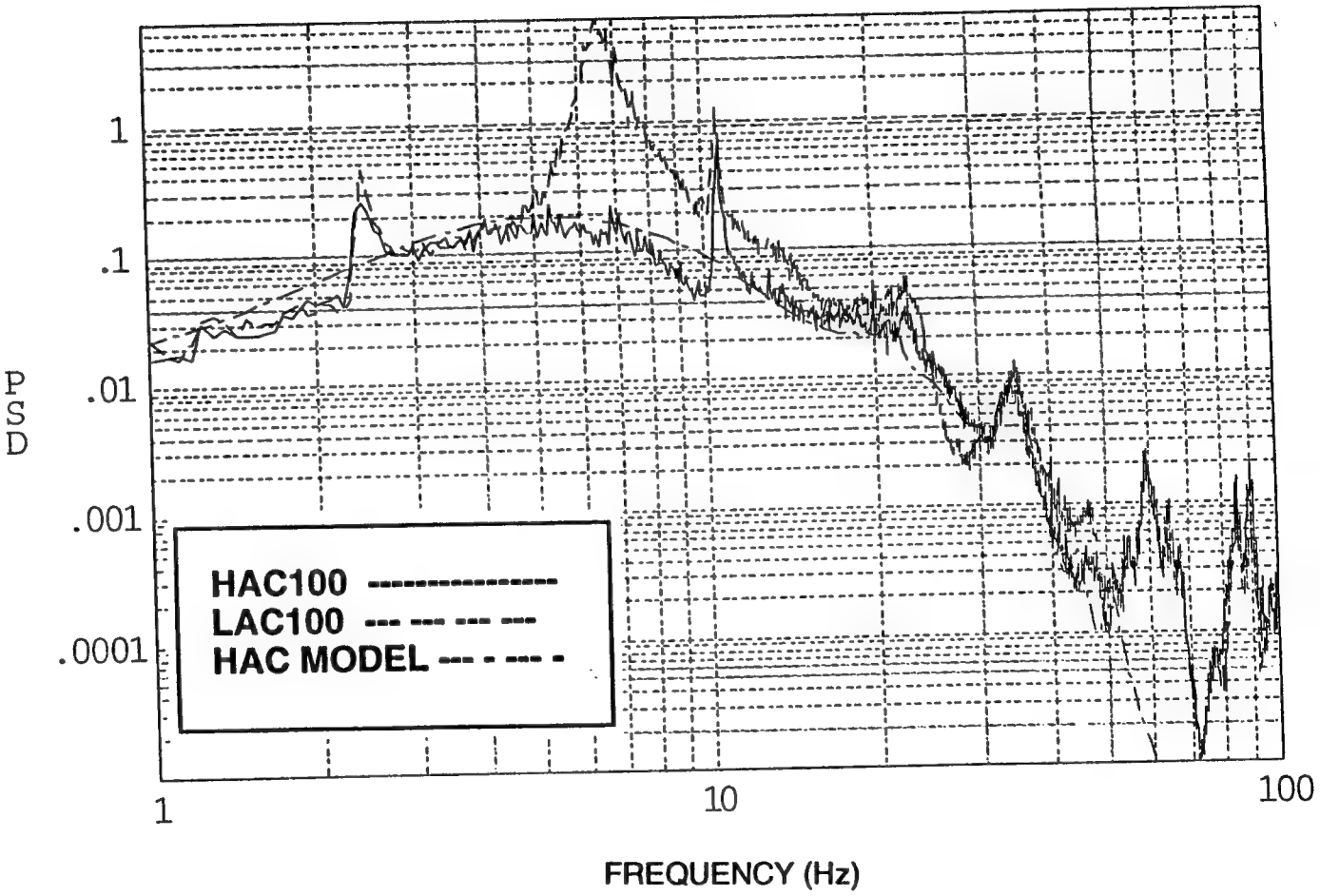

Figure A-36. Spectra of PMA 14 rate - 100-μrad caged-target LOS disturbances.

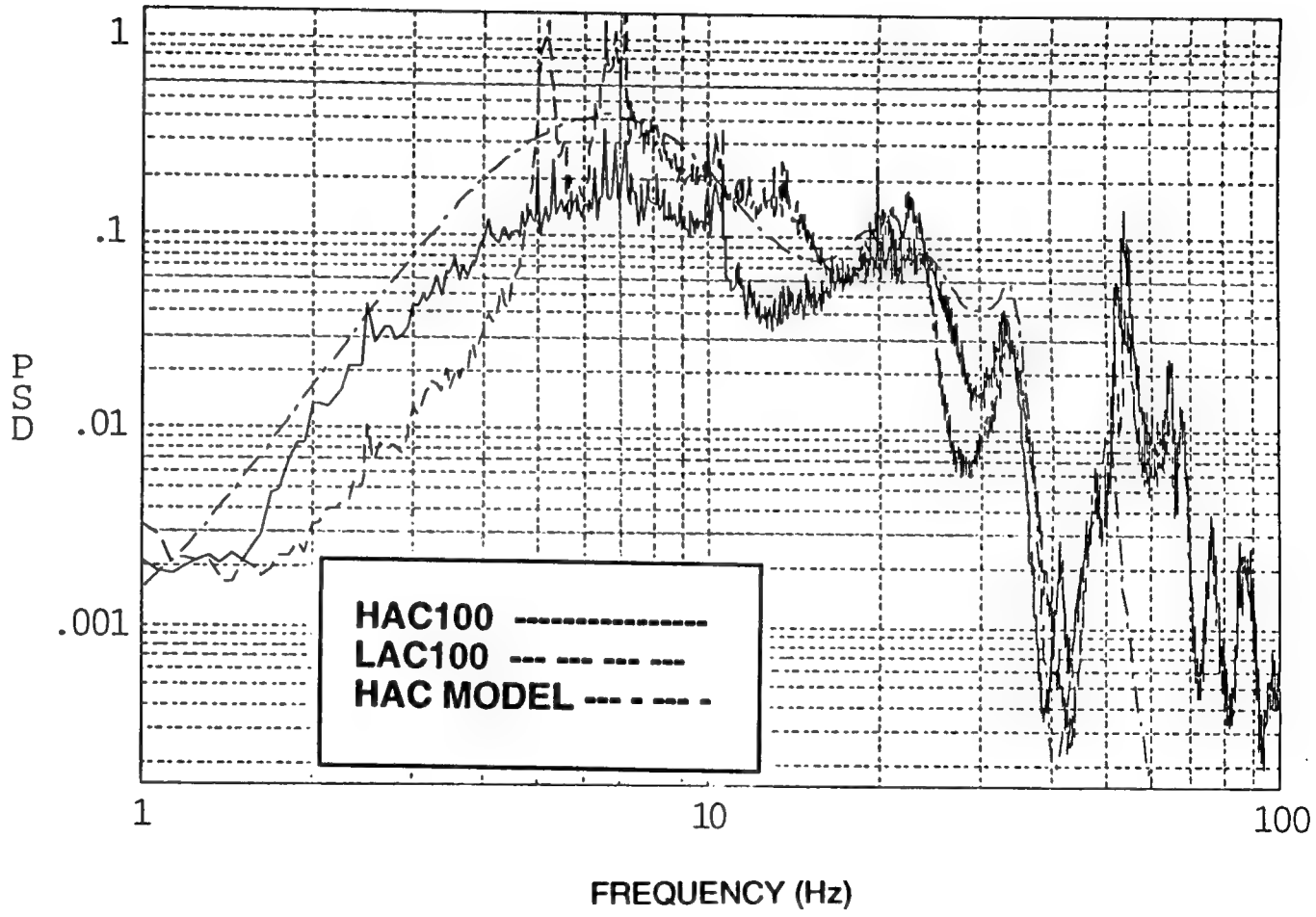

Figure A-37. Spectra of PMRS 1 x-axis signal - 100-μrad caged-target LOS disturbances.

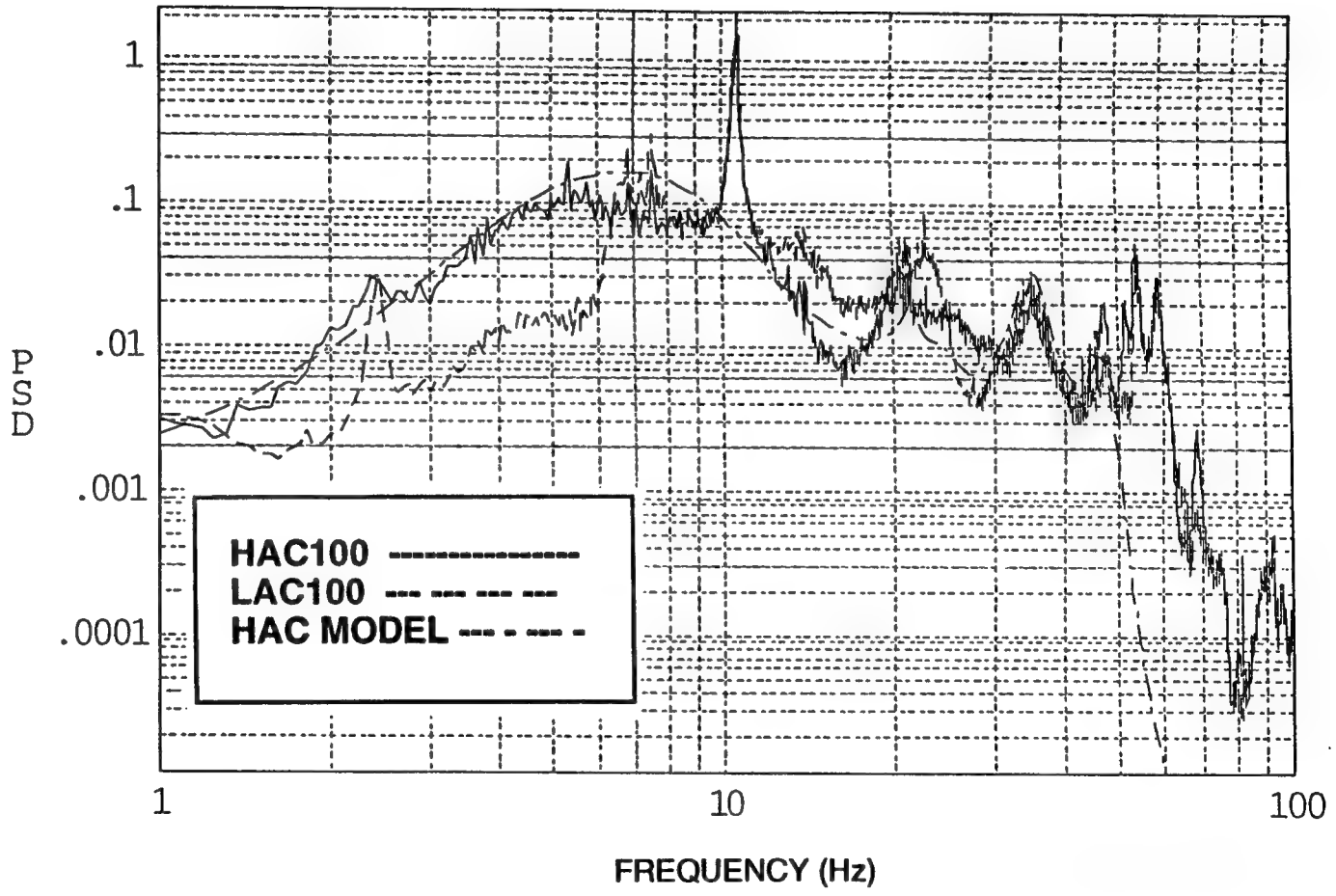

Figure A-38. Spectra of PMRS 1 y-axis signal - 100-µrad caged-target LOS disturbances.

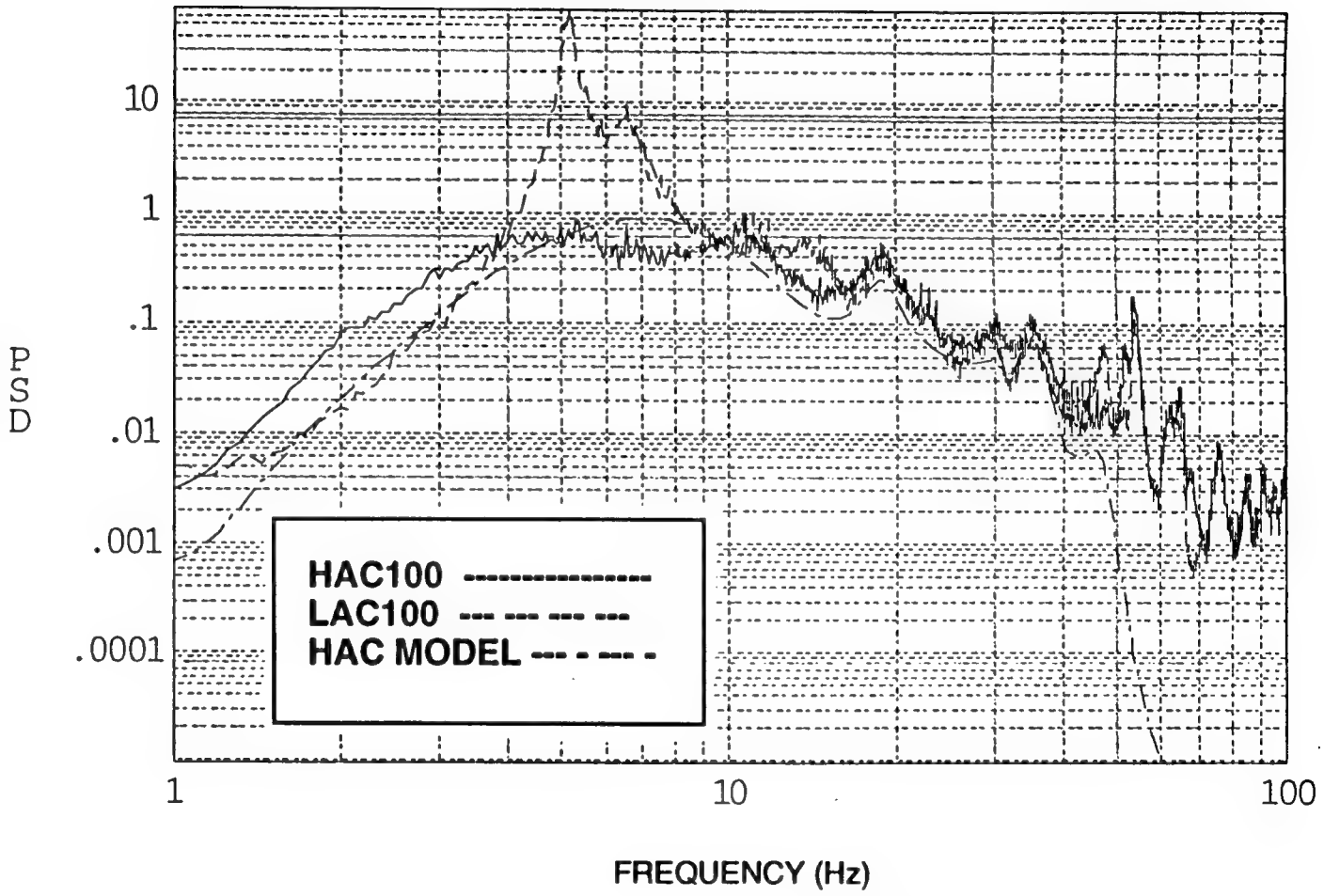

Figure A-39. Spectra of PMRS 2 x-axis signal - 100-µrad caged-target LOS disturbances.

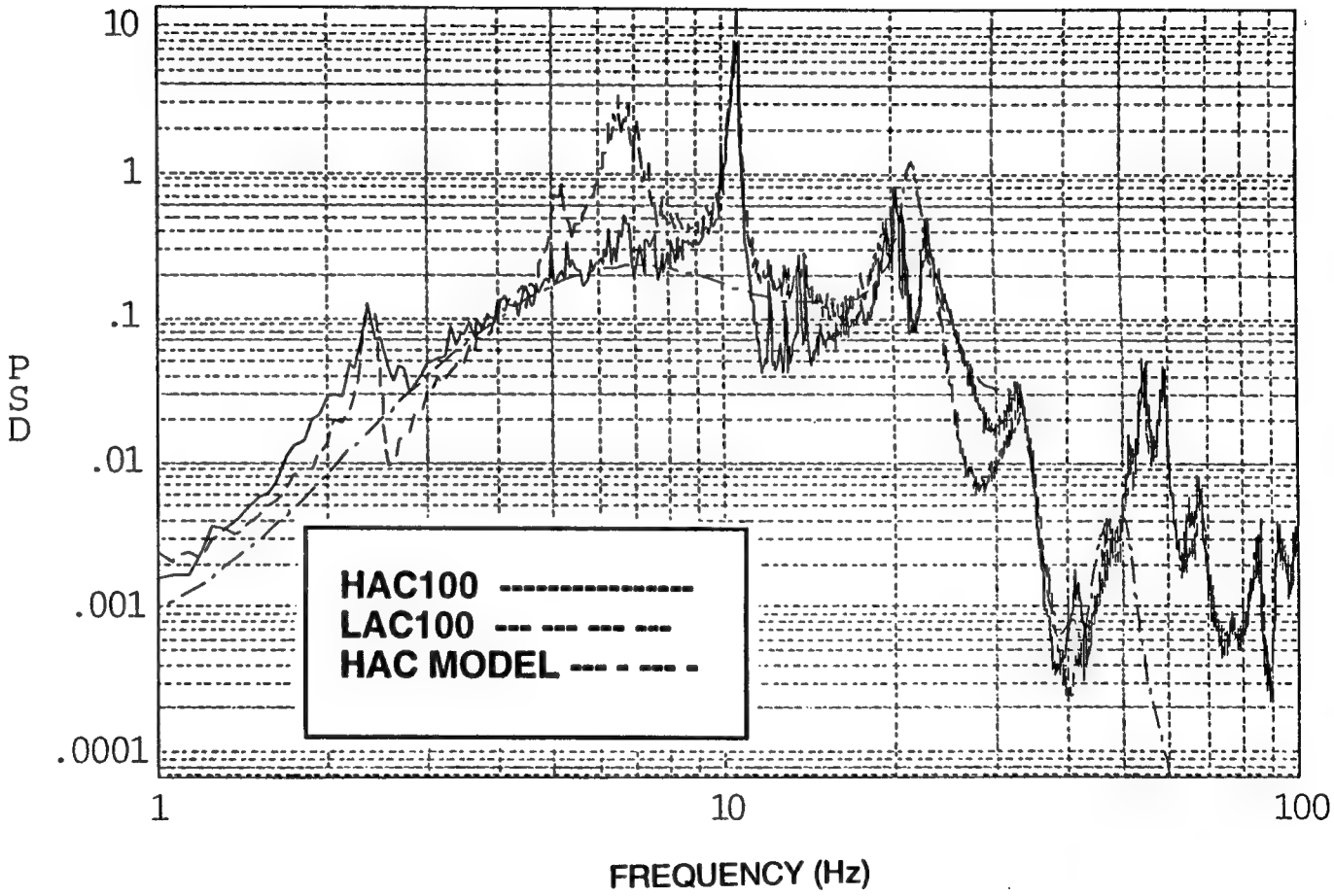

Figure A-40. Spectra of PMRS 2 y-axis signal - 100-µrad caged-target LOS disturbances.

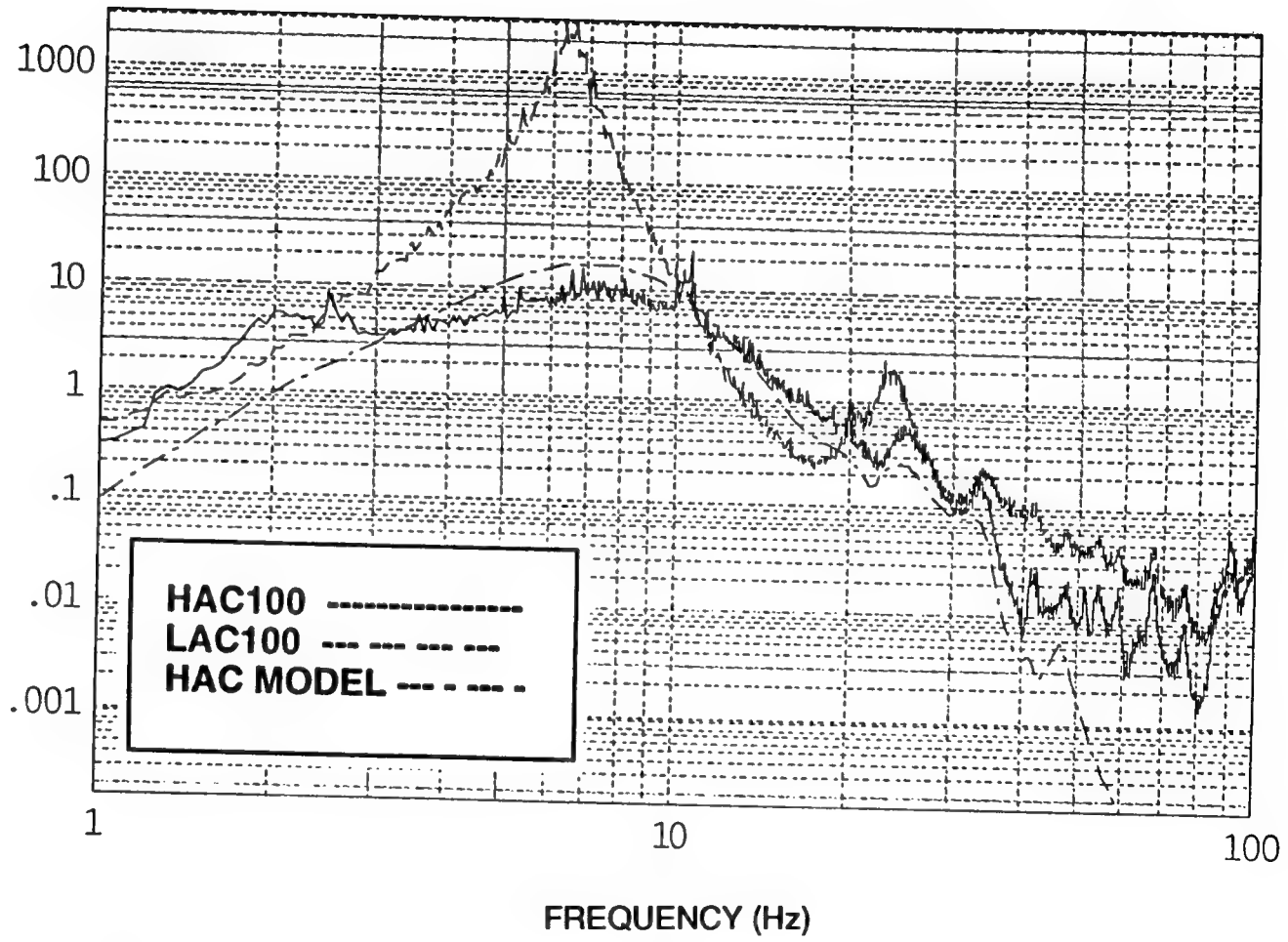

Figure A-41. Spectra of SMRS x-axis signal - 100-µrad caged-target LOS disturbances.

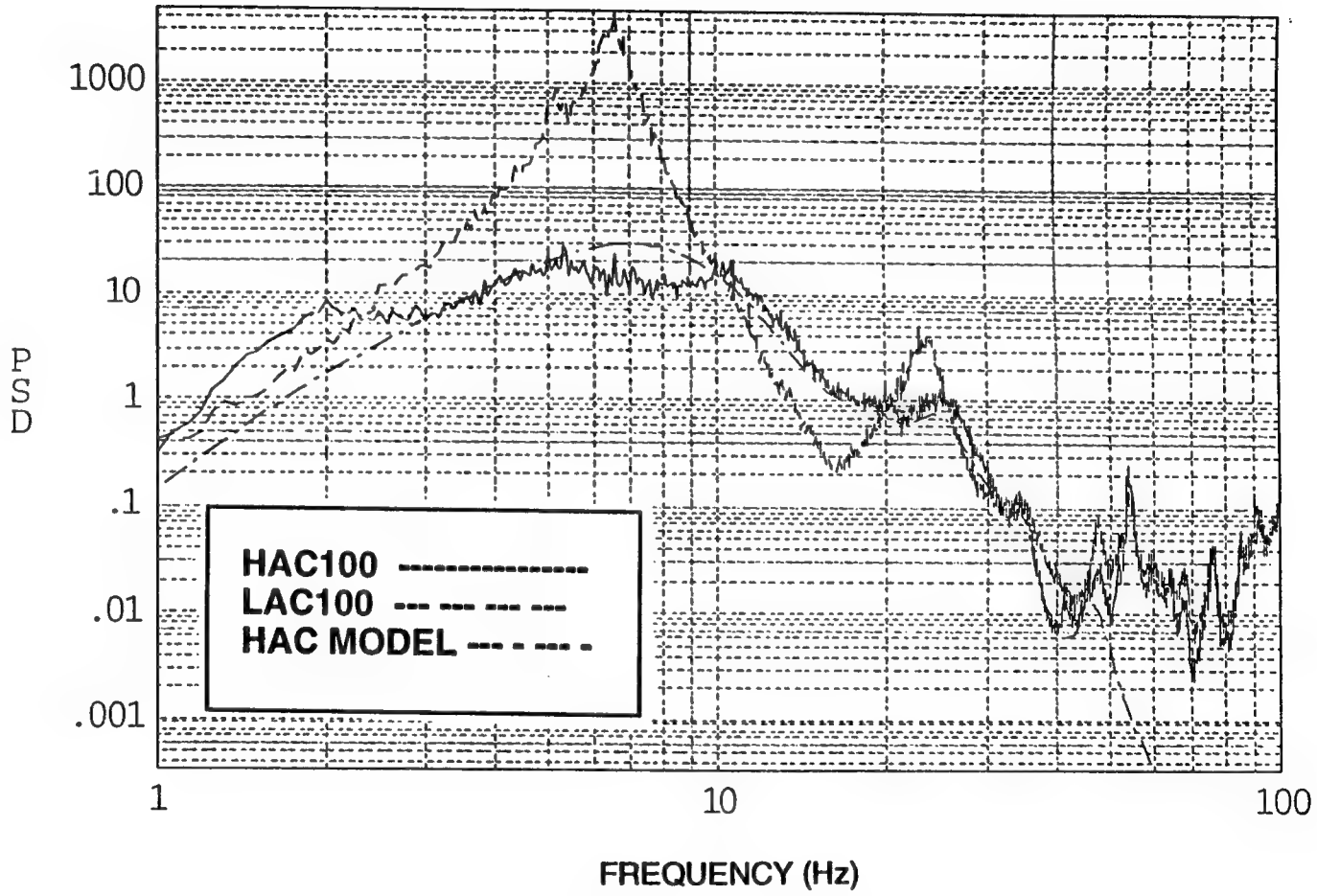

Figure A-42. Spectra of SMRS y-axis signal - 100-μrad caged-target LOS disturbances.

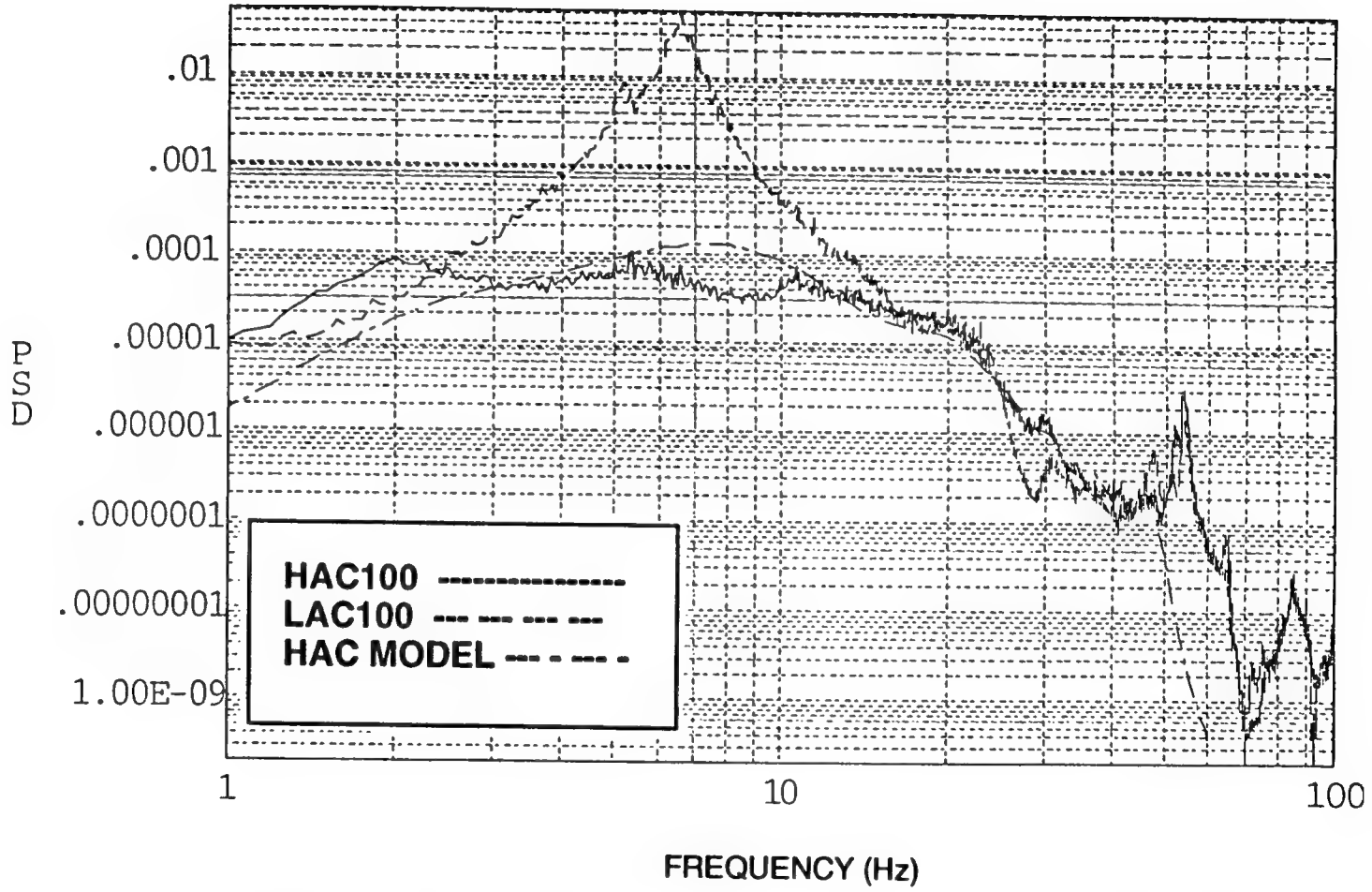

Figure A-43. Spectra of SMTS 8 x-axis signal - 100-µrad caged-target LOS disturbances.

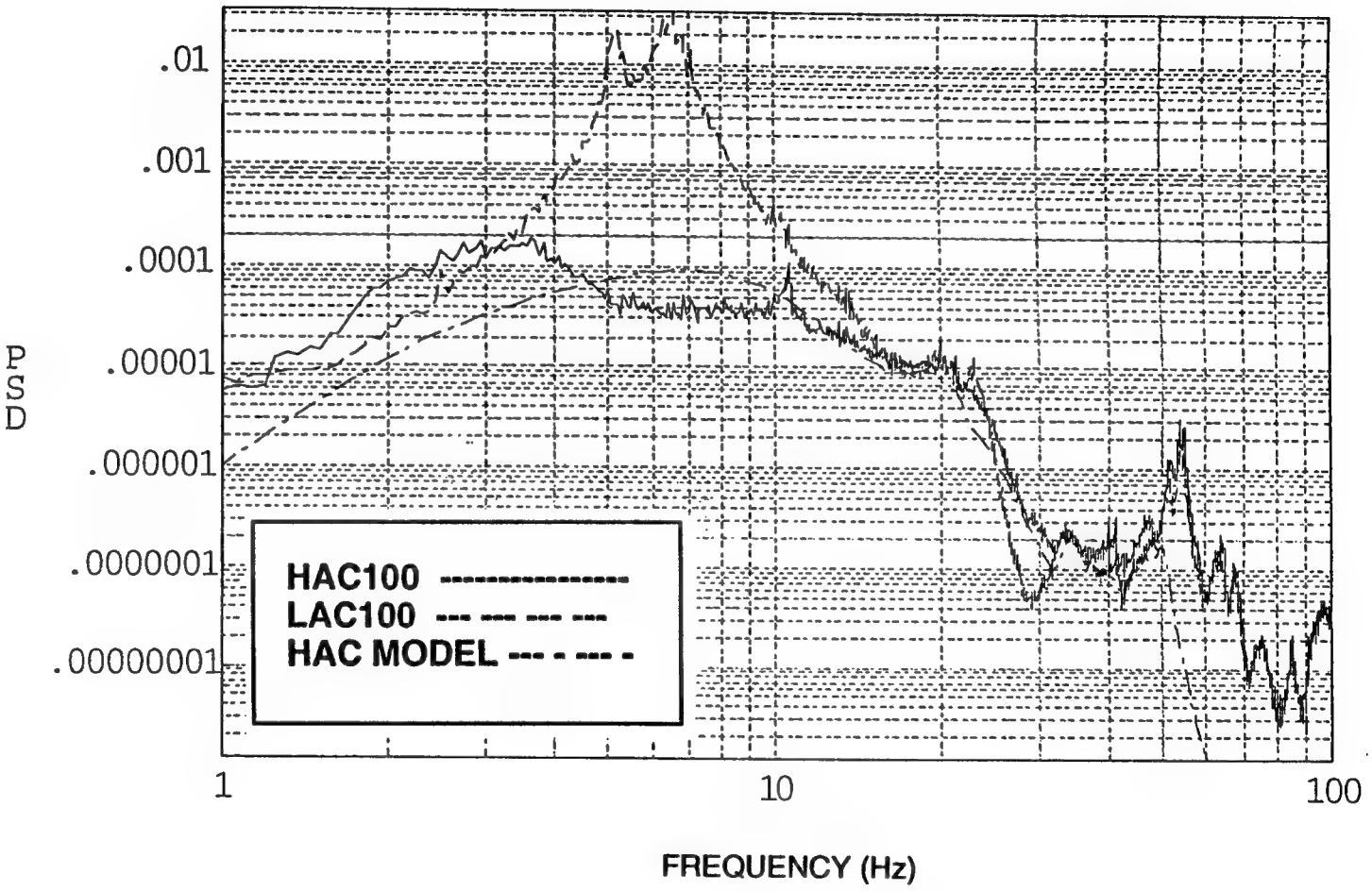

Figure A-44. Spectra of SMTS 8 y-axis signal - 100-μrad caged-target LOS disturbances.

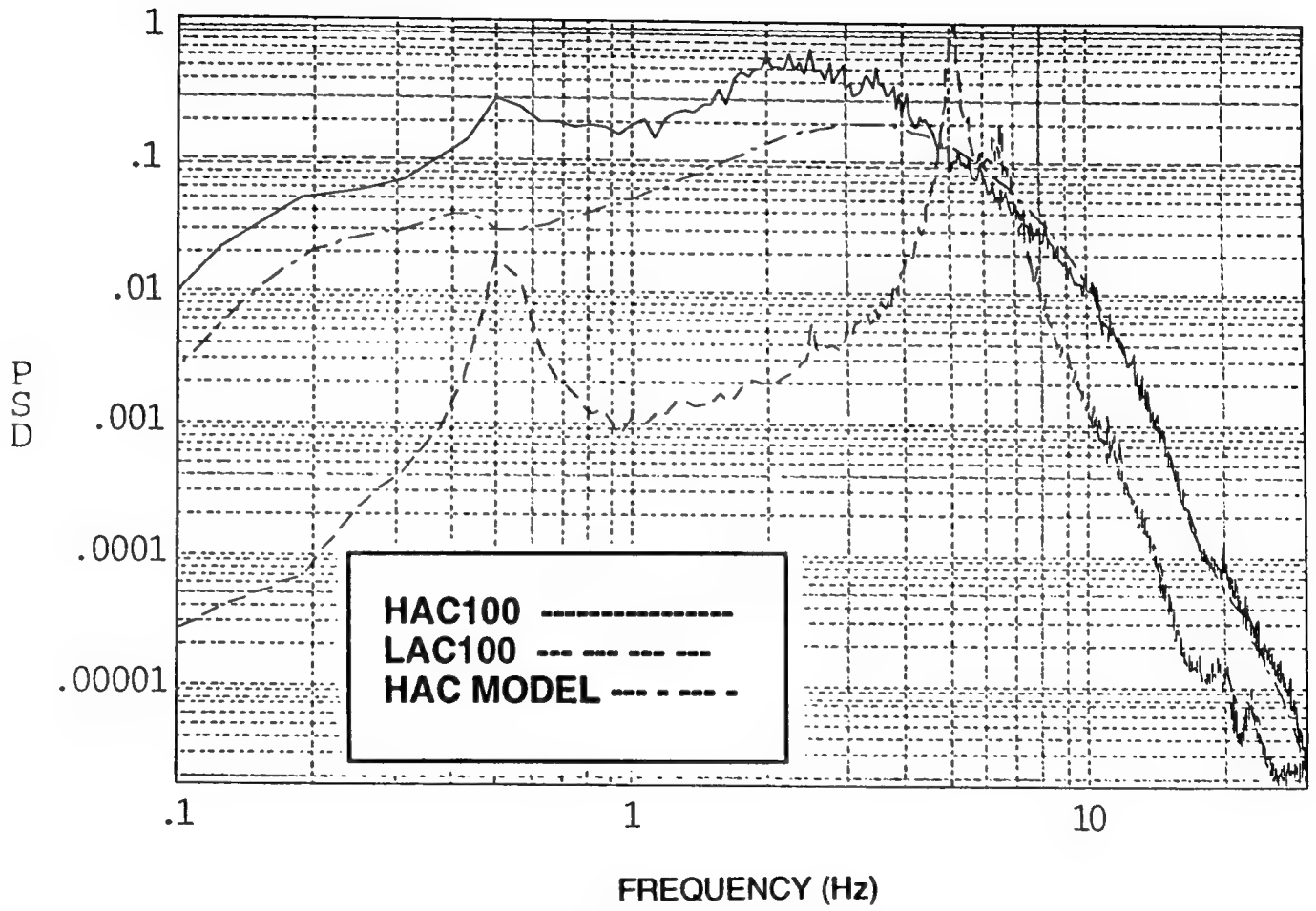

Figure A-45. Spectra of PMA 1 LVDT signal - 100-μrad caged-target LOS disturbances.

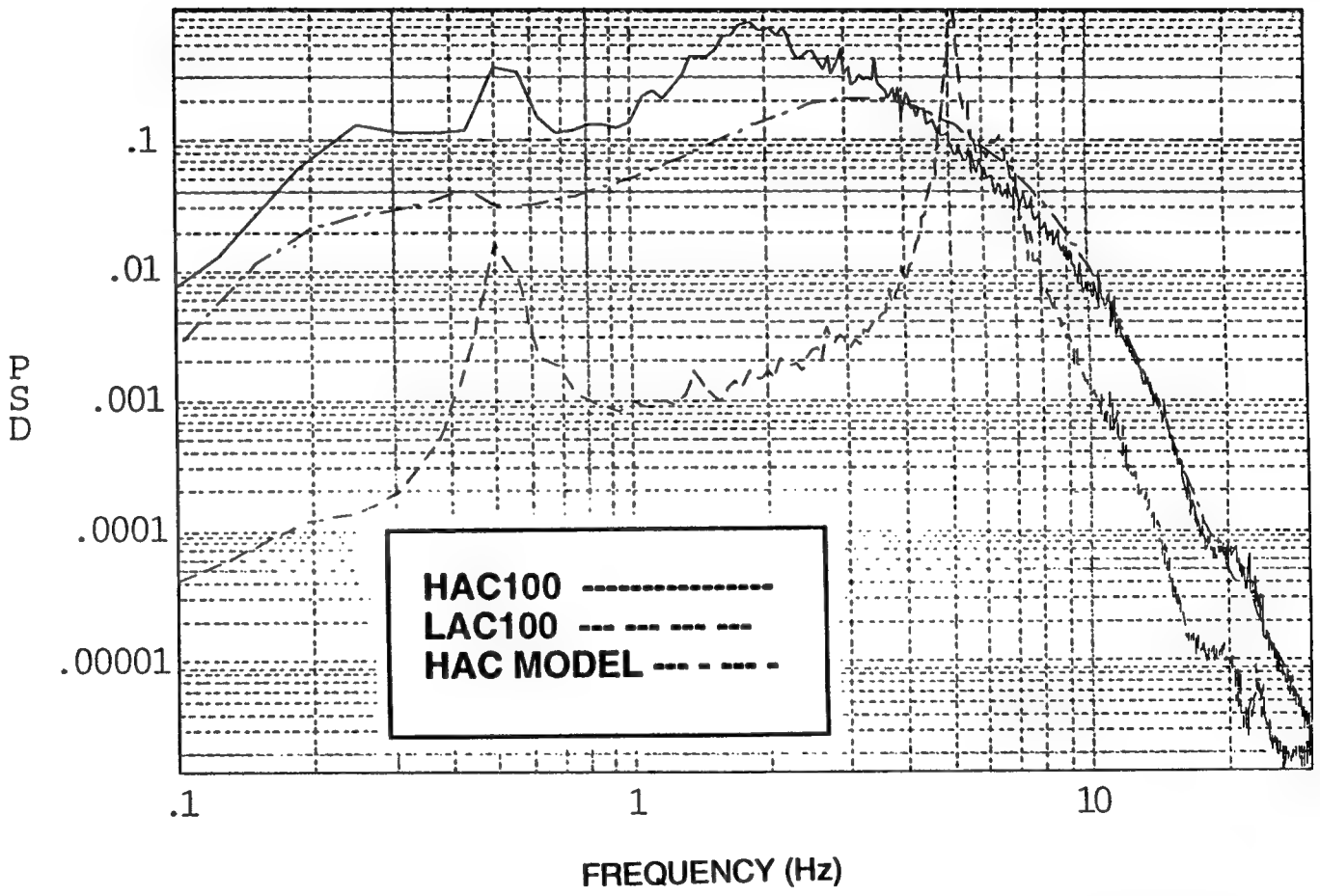

Figure A-46. Spectra of PMA 2 LVDT signal - 100-μrad caged-target LOS disturbances.

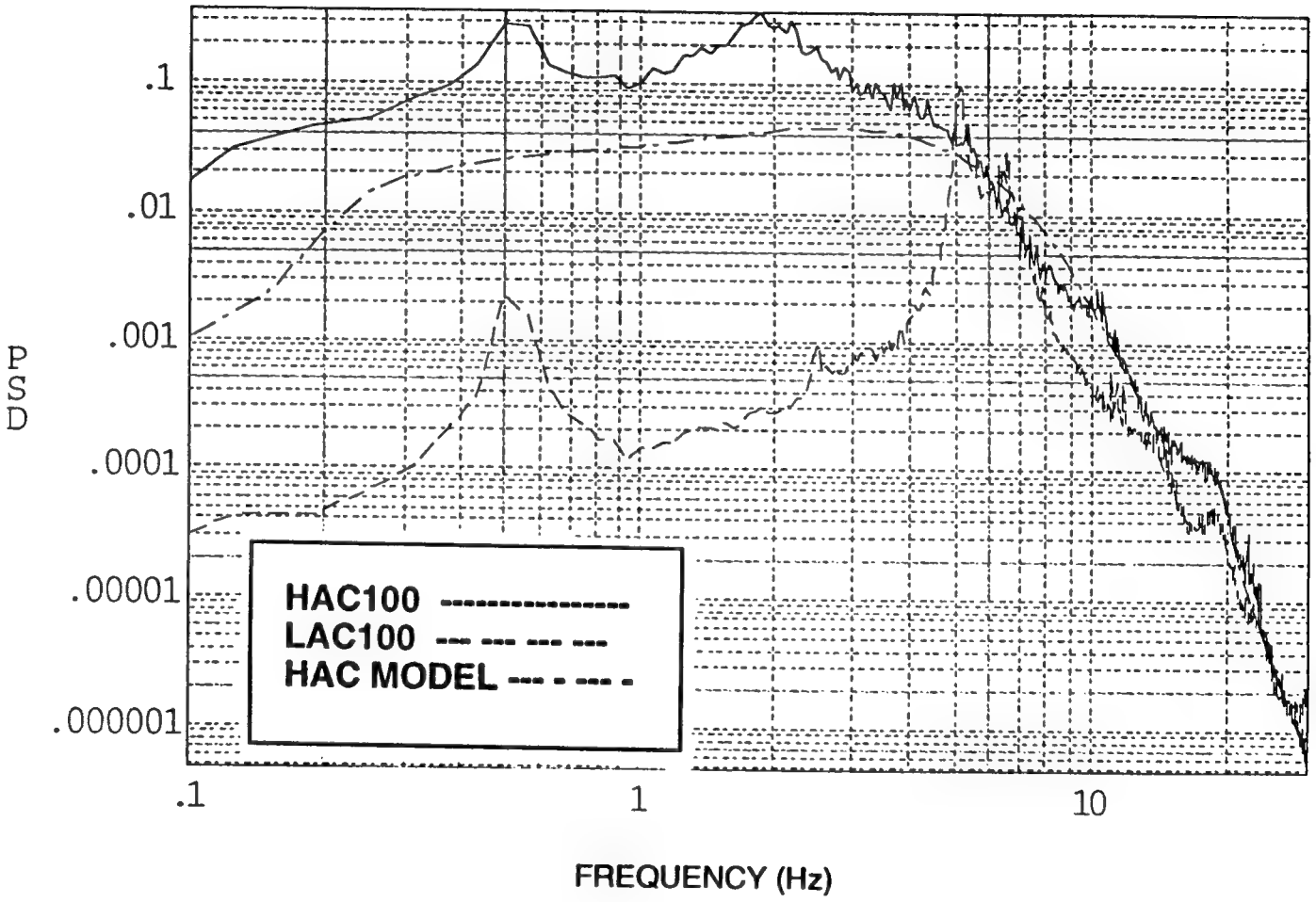

Figure A-47. Spectra of PMA 3 LVDT signal - 100-µrad caged-target LOS disturbances.

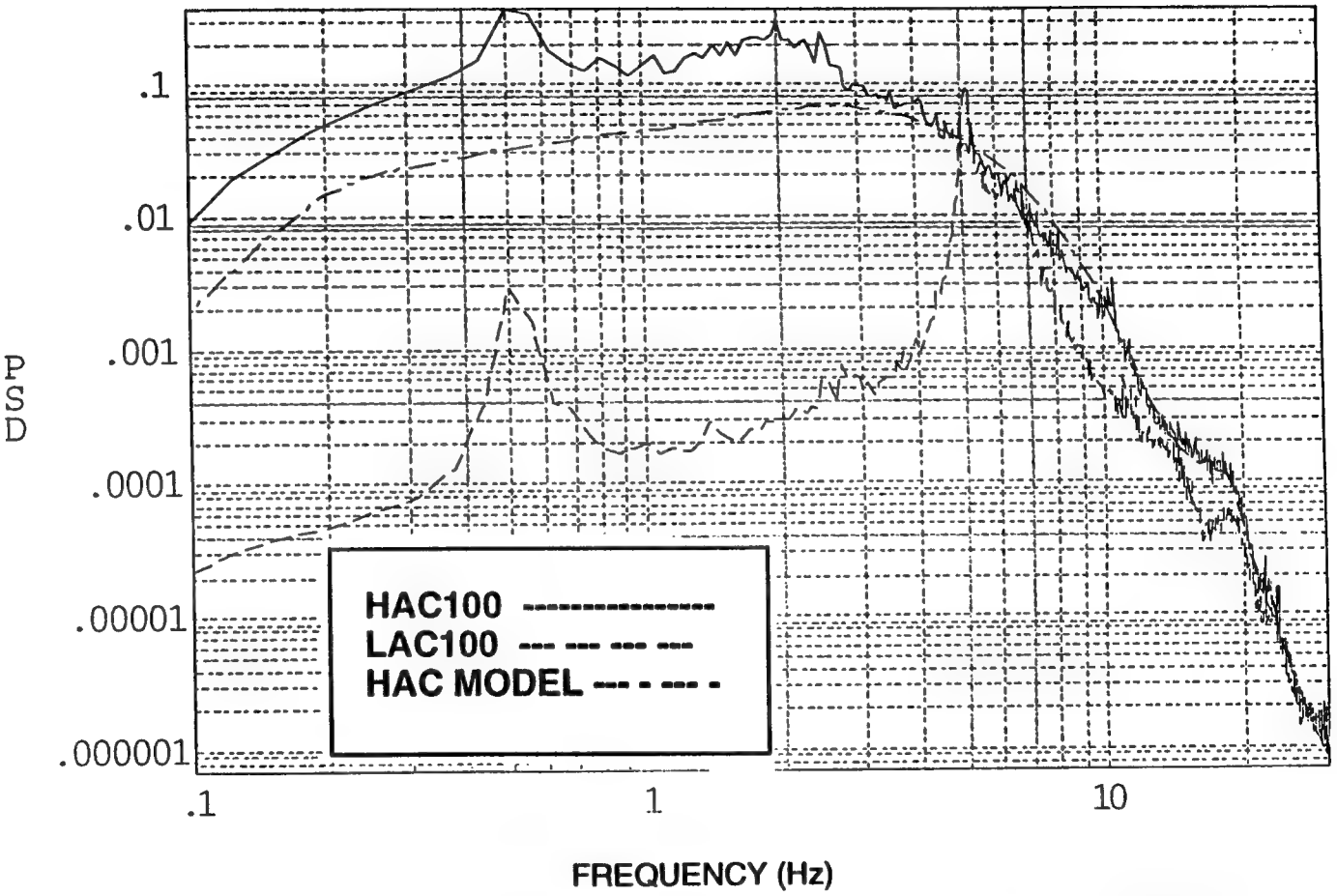

Figure A-48. Spectra of PMA 4 LVDT signal - 100-μrad caged-target LOS disturbances.

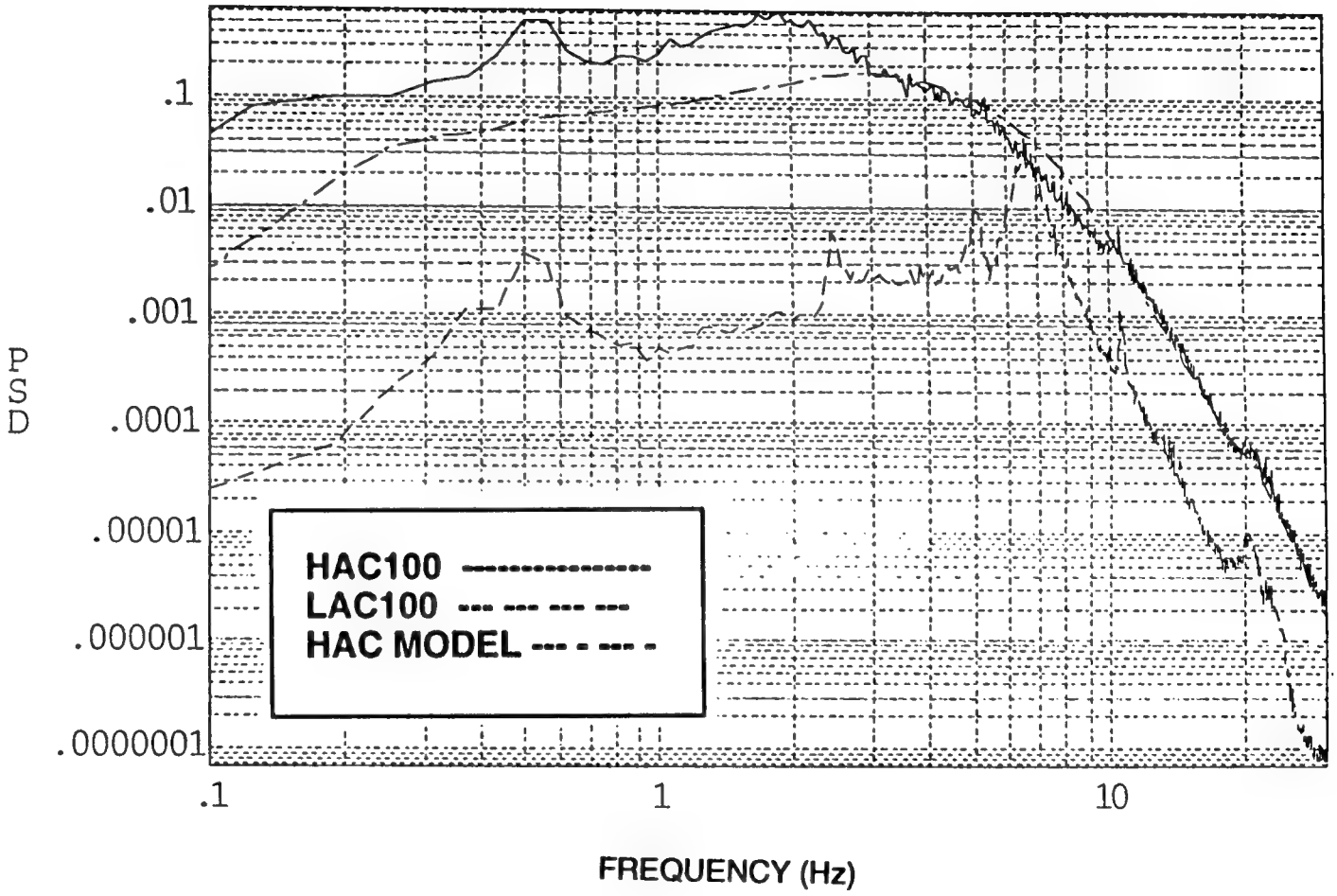

Figure A-49. Spectra of PMA 13 LVDT signal - 100-μrad caged-target LOS disturbances.

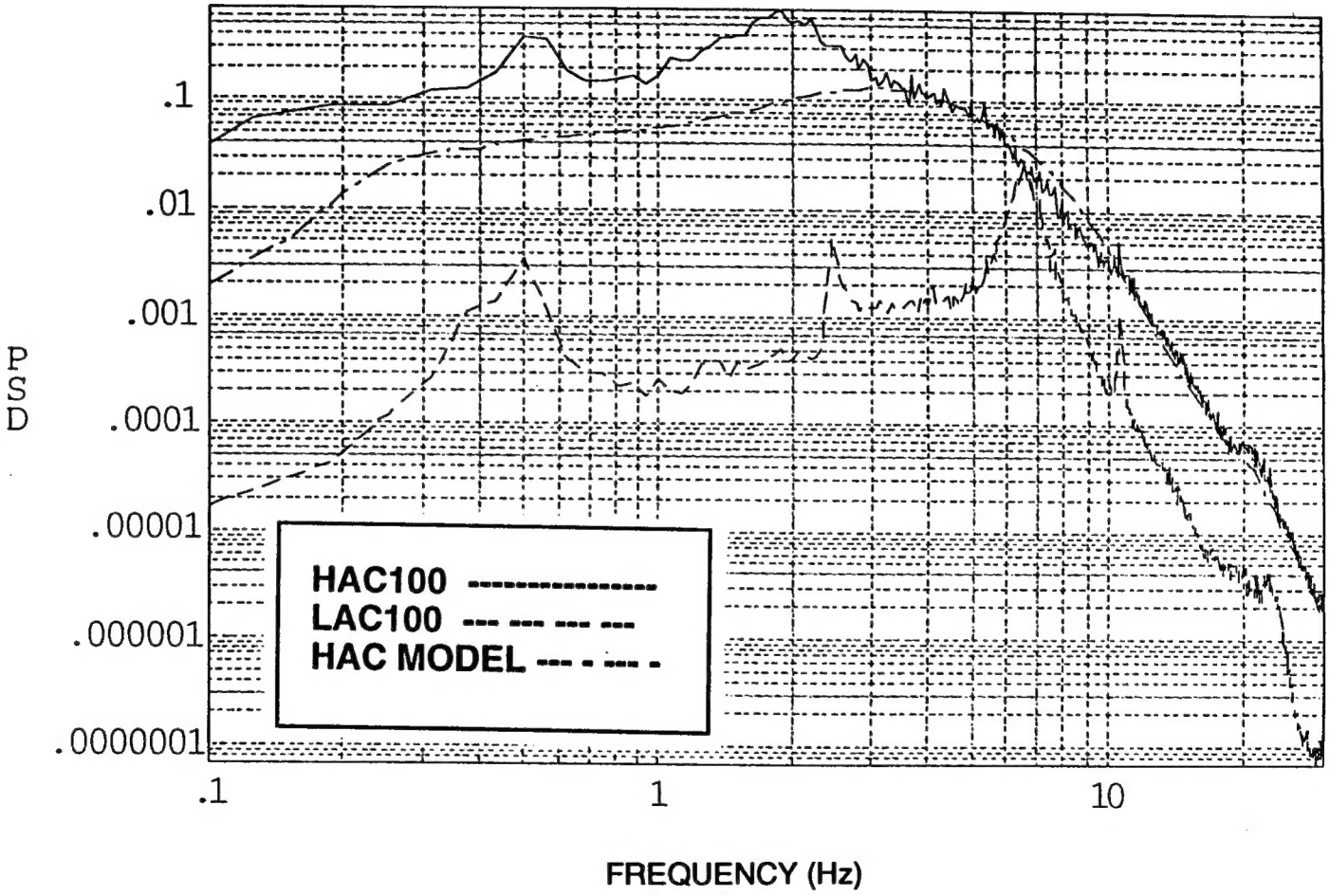

Figure A-50. Spectra of PMA 14 LVDT signal - 100-µrad caged-target LOS disturbances.

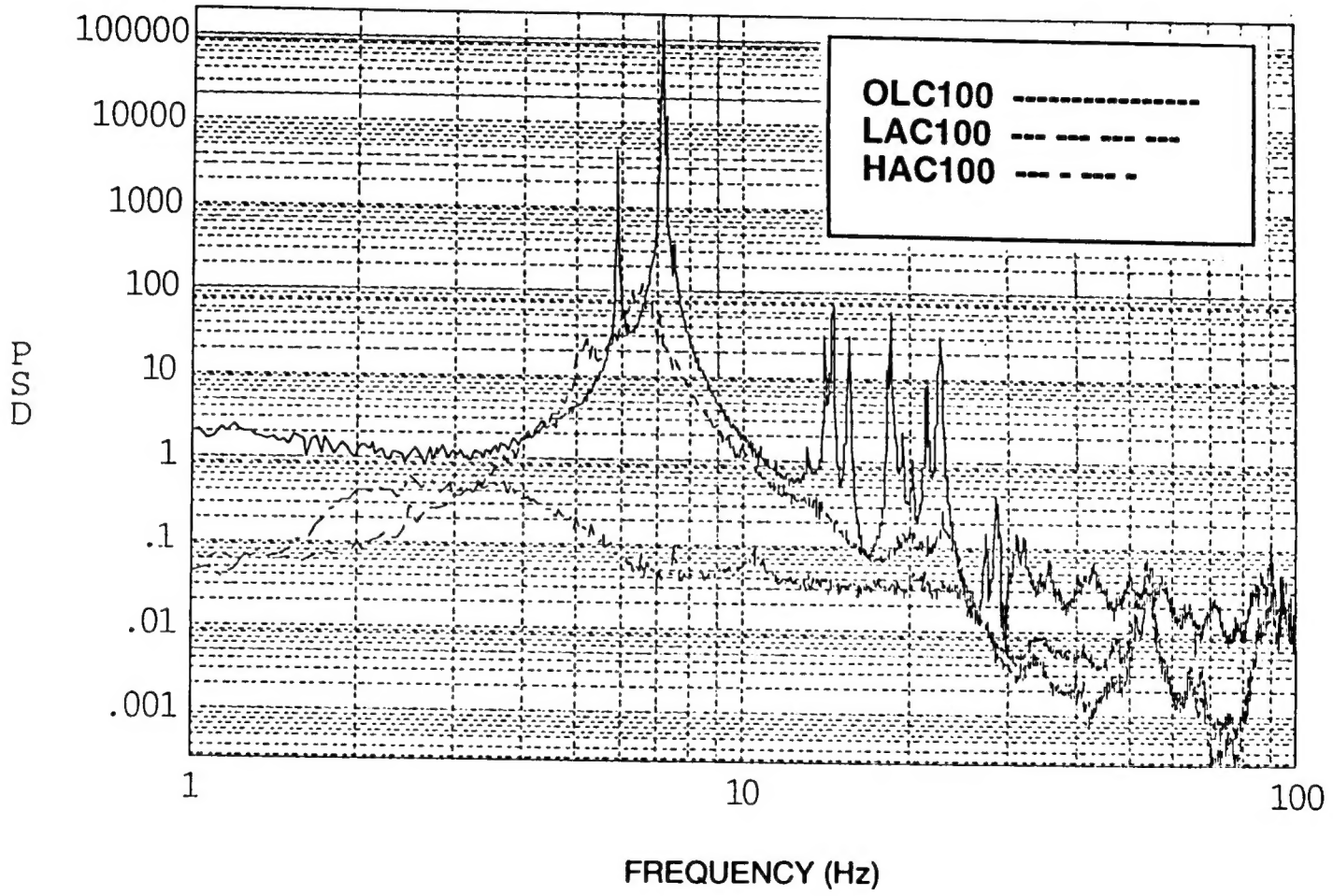

Figure A-51. Test LOS-x PSD comparisons - 100-μrad caged-target LOS disturbances.

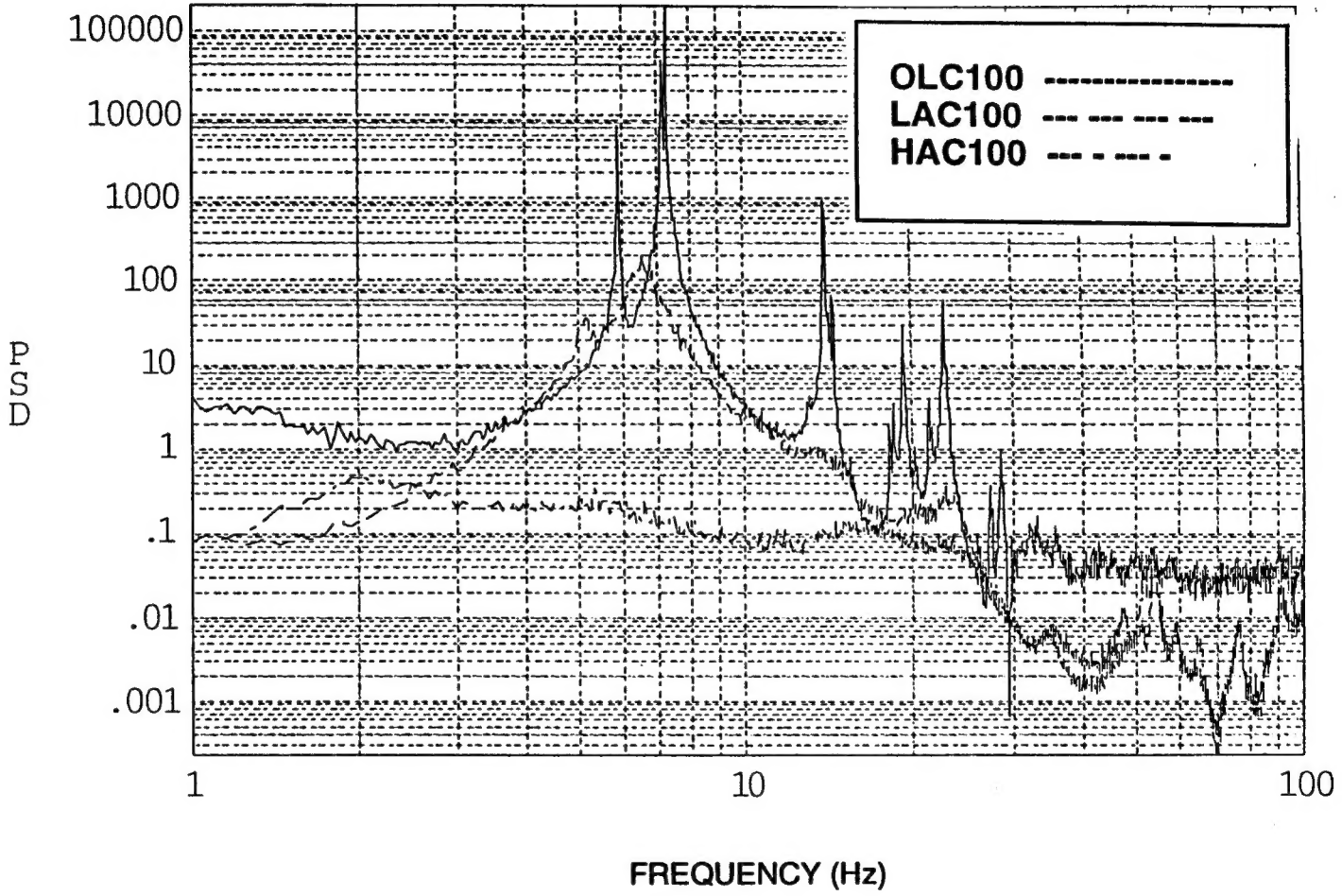

Figure A-52. Test LOS-y PSD comparisons - 100-μrad caged-target LOS disturbances.

ACRONYMS

ADS	angular differential sensor
CDR	conceptual design review
DC	direct current
FRF	frequency response function
HAC	high authority control
HP	Hewlett-Packard
LAC	low authority control
LOS	line of sight
LQG	linear quadratic Gaussian
LVDT	linear variable differential transducer
OSS	optical sensing system
PMA	proof mass actuator
PMRS	primary mirror rotation sensor
PSD	power spectral density
RMS	root-mean-square
SAVI	space active vibration isolation
SMRS	secondary mirror rotation sensor
SMTS	secondary mirror translation sensor
SPICE	space integrated controls experiment
TIM	technical interchange meeting